The development of flash tube detectors for high energy physics

J. E. Chaney

THE DEVELOPMENT OF FLASH TUBE DETECTORS

FOR

HIGH ENERGY PHYSICS

by

J.E. CHANEY, B.Sc.

A thesis submitted to the University of Durham for the Degree of Doctor of Philosophy

Being an account of work carried out at the University of Durham during the period October 1971 to September 1974.

ABSTRACT

The work reported in this thesis describes the development of a new flash tube detector particularly suited to nuclear accelerator experimentation, and specifically considers its application to the detection of high energy photons.

A flash tube detector has been developed with characteristics which permit efficient operation in a background radiation flux of about 10^5 particles/tube/second and at repetition rates of the order 1 KHz. The viability of its application to accelerator physics was investigated and verified using the DNPL e^+ accelerator beam with a chamber containing digitized flash tubes linked to a computerized data acquisition system.

Application of the device to the detection of high energy photons has also been made with the chamber, by simulating photon induced electromagnetic showers with positrons, in the energy range 0.5 - 4.0 GeV. Results from this series of experiments have shown that both energy and spatial information may be obtained from a chamber constructed with large diameter tubes and of small overall size. The energy and spatial resolution of the device have been measured as a function of energy and shown to compare favourably with more complex and expensive techniques.

Analysis of the shower data has also demonstrated that several improvements are possible. These improvements have been incorporated in the design of a new chamber capable of operating at repetition rates up to 1KHz and which should measure the energy and trajectory of incident photons with a greater precision than is possible with many conventional instruments.

CONTENTS

CHAPTER ONE

INTRODUCTION

Following the introduction of the cloud chamber by Wilson (1) in 1912, nuclear physics has experienced a rapid growth in the development of nuclear particle detecting techniques. In particular, 1928 marks a significant time in the history of electronic detectors with the advent of the Geiger-Muller counter (2). Since then a vast number of new and diverse detecting instruments have been invented. One such instrument is the neon flash tube detector, introduced by Conversi and Gozzini (3) in 1955, which has contributed significantly in the field of cosmic ray physics.

Nuclear detectors of all forms can be subdivided into three broad categories; continuously sensitive detectors like the Geiger-Muller counter, proportional counter , scintillation counter and drift chamber; non-triggerable detectors like the bubble chamber and cloud chamber; and triggerable devices such as the multielectrode spark chamber, streamer chamber and projection chamber. The flash tube may be classified in the latter group, under the general heading of electrically pulsed chambers. All detectors of this classification consist essentially of a volume of gas contained between electrodes to which an impulsive electric field is applied after the passage of an ionizing particle.

A charged particle, while traversing a gaseous volume will lose some of its energy in the form of excitation and ionization. In neon, the most commonly used gas, the total ionization produced at atmospheric pressure by a minimum ionizing particle is about 30 ion pairs cm^{-1}. Thus, the application of an intense electric field, immediately after ionization has occurred, causes free electrons created in the gas to avalanche, thereby identifying the particle

trajectory with a visible discharge.

It is the geometry of the contained gas andthe magnitude and temporal behaviour of the applied field which decides the nature of the detector. Three modes of operation have been employed; a very short high voltage pulse of a few nanoseconds allows the avalanche to grow only to the size of streamers (streamer chamber), a pulse of some ten nanoseconds duration permits a bright avalanche across the width of the gaseous volume (spark chamber), and a pulse of the order of some microseconds allows a lateral spread of the discharge through the whole gaseous volume (flash tube).

A typical flash tube detector consists of a sealed soda glass tube between 0.5cm and 2cm in diameter, up to several metres in length, and filled with a neon-helium gas mixture. Tubes are placed adjacent to each other in layers between metal electrodes. Auxilary detectors, such as plastic scintillators, are placed either side of the electrodes such that coincident signals from each detector signify the passage of an ionizing particle which can be made to trigger a pulse generator and provide an impulsive electric field. The field is applied for a sufficient time to allow the discharge to propagate along the length of the tube such that a photographic record or digitization pulse can easily be made. In this way, a stack of tubes forms an efficient track locator for ionizing particles, providing a simple and reliable device particularly suited to experiments where large sensitive volumes are required.

In comparison with spark chambers, an array of flash tubes has many features which commend it. The elemental nature of its construction gives a high multitrack efficiency which is important when the density of incident particles is large. This is one reason why the device

has been favoured by cosmic ray physicists for the study of extensive air showers. Other advantages include low cost, simplicity, reliability, low power requirements and ease of rearrangement for different detecting geometries. Adversely , the device has the disadvantages of having a poor spatial resolution, contains a large amount of interacting material and is unable to operate at high repetition rates and in a high background radiation. The latter characteristics have prevented the device being used in accelerator experiments and account for its application being limited to cosmic ray physics where the operating requirements are less stringent. In place of the flash tube, accelerator physics has favoured use of the spark chamber and the many advantages and potential applications of the device have been disregarded.

Despite the numerous investigations which have been made regarding the operation and working properties of the flash tube device (4,5) little improvement has been made to its performance until recently, when research groups working at the Frascati Accelerator Laboratory and at the University of Durham have stimulated interest in applications to accelerator physics. The purpose of this thesis is to describe the development and application of a new type of flash tube detector which is capable of operating under the more adverse conditions peculiar to accelerator experimentation.

References

1. Wilson C.T.R., Proc. Roy. Soc. 87, (1912) 277

2. Geiger, H., Muller, W., Z. Physik 29, (1928) 839.

3. Conversi M., Gozzini, A., Nuovo Cim., 2, (1955) 189.

4. Holroyd, F., Ph.D Thesis, Durham University (1971).

5. Breare, J.M., Cosmic Rays at Ground Level (1973) 191

CHAPTER TWO

PROPERTIES OF FLASH TUBES

It is necessary to begin this thesis with a brief summary of results from many investigations by other workers concerning the properties and characteristics of flash tube devices. In particular, properties and definitions of terms are given which are relevant to experimental work described in subsequent chapters.

2.1 The Discharge Mechanism

Recent work by Holroyd (1) has shown that the discharge mechanism in neon flash tubes is a combination of Townsend and streamer avalanche processes (2,3). For long high voltage pulses, discharges occur at fields as low as 1KV cm^{-1}, favouring a Townsend mechanism. For shorter pulses (0.4μs), however, much higher fields of about 5KV cm^{-1} are required before breakdown will occur. This indicates that for short high voltage pulses, when there is insufficient time for a Townsend discharge to develop, streamer breakdown will occur provided the field strength is large enough. In intermediate cases the discharge is probably a mixture of both.

Provided the electric field is applied for a sufficient time, the discharge will be propagated along the length of the tube. This can be explained in terms of the high intensity of ultraviolet photons emitted from each discharge (5) and the large photoelectric yield from soda glass (6,7) which result in a copious supply of secondary electrons to initiate further discharges along the length of the tube. By this process the discharge spreads, from the point of initial ionization, at a finite velocity. The velocity of propagation has been measured by Ayre et al (4) to be 6.7×10^{8} cm s^{-1} in the case of neon tubes filled at 2.3 atmospheres pressure.

Holroyd and Breare (8) have shown that the light emission from a tube lasts for a time of approximately 1μs, even though the applied field may exist for much longer. This implies that each avalanche quenches itself and the entire avalanche is extinguished soon after it reaches the end of the tube. The quenching is explained by charges, created by each discharge, collecting on opposite sides of the glass tube and counteracting the applied field.

2.2 Detecting Efficiency

One of the most important characteristics of the flash tube is the probability that it will register an event after an ionizing particle has passed through it. In this respect two terms have been defined; the internal efficiency, which is the probability that a tube will ignite after a particle has passed through its gaseous volume, and the layer efficiency, which is the probability of an incident particle being detected by one layer of tubes. The layer efficiency is always less than the internal efficiency and is related by a simple geometrical factor, which is the ratio of the external to the internal diameter (assuming the tubes are in contact with one another). Experimentally it is convenient and more meaningful to measure the layer efficiency.

2.2.1 Effect of the high voltage pulse magnitude

Several authors have studied the effect of varying the pulse magnitude (9,10). As expected the efficiency is low for small fields but reaches a plateau having almost 100% internal efficiency for higher fields. Figure 2.1 shows typical results.

2.2.2 Effect of the high voltage rise-time

A slowly rising pulse will sweep electrons out of the tube without imparting much energy to them and thus the discharge will extinguish itself as the electrons reach the tube wall without a

significant number of electrons having been produced to initiate further avalanches. Goxell and Wolfendale (14) have measured the efficiency for pulse rise-times up to 1.7μs. They used 6mm internal diameter tubes at 2.3 atmospheres of neon, and their results shown in Figure 2.2 give a slowly decreasing efficiency as the pulse rise-time is increased.

2.2.3 Effect of the high voltage pulse length

The length of the high voltage pulse depends on its mode of generation. A square pulse, derived from a delay line, or an exponentially decaying pulse, derived by discharging a capacitor through a resistor, are commonly used. Holroyd (1) has measured the efficiency as a function of pulse height for several pulse lengths using a CR decaying pulse. Figure 2.3 shows her results for pulses of 0.4, 4.0 and 40μs decay times. These results show that for very short pulses of 0.4μs the magnitude of the field had to exceed 7KV cm^{-1} in order to obtain a discharge, and even then it was very filamentary and did not fill the tube. For pulses of 4.0μs the tubes performed correctly and for much longer pulses the performance was only slightly improved at the low voltages.

2.2.4 Effect of the delay time of the high voltage pulse

The relationship between the efficiency and the time delay between the passage of a particle and the start of the high voltage pulse has been investigated experimentally in great detail. The interest in this parameter stems from the fact that it can be derived theoretically and a good check on the performance of a system can thus be made. Furthermore, many experiments require the use of a long time delay either to permit decision making circuits to operate or to allow particle discrimination by means of ionization loss.

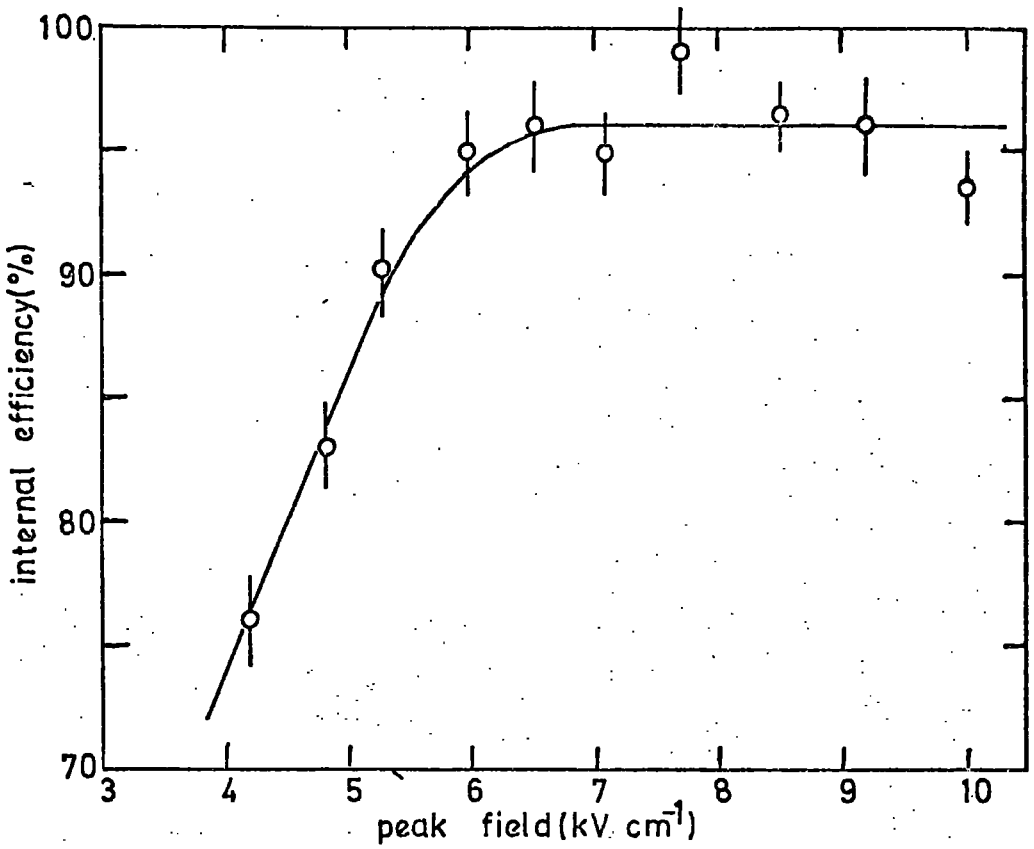

Fig 2·1 variation of internal efficiency with field strength for 0·6cm internal diameter tubes filled at 2·3 atmospheres

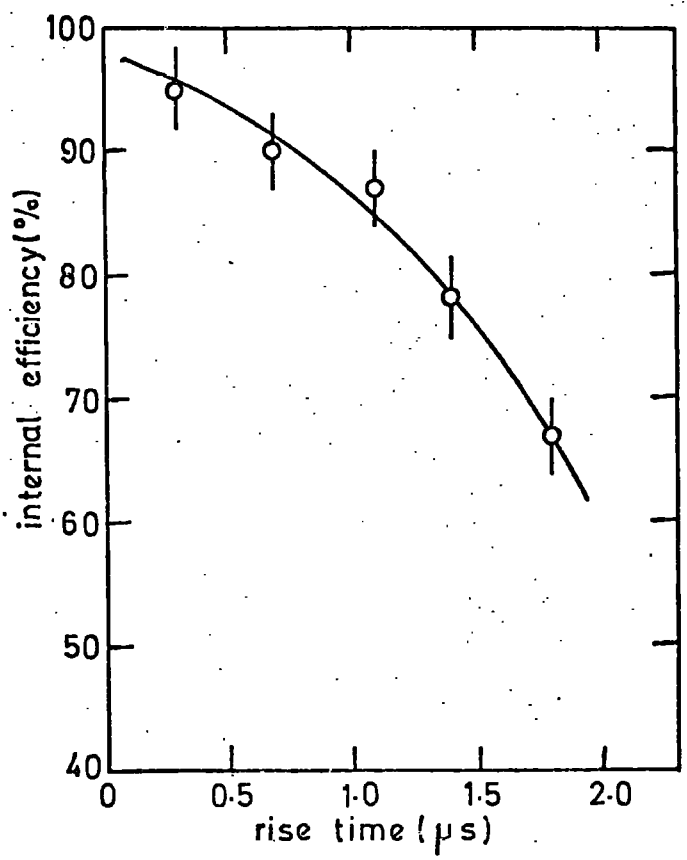

Fig 2·2 variation of internal efficiency with rise time for 0·6cm internal diameter tubes filled at 2·3 atmospheres

The efficiency of a flash tube is dependent on the number of electrons remaining in the sensitive volume when the high voltage pulse is applied. Electrons created by ionization will be lost by diffusion to the glass walls where they are captured. An accurate theory has been developed by Lloyd (11) in which the number of free electrons surviving ($\bar{n}$) at a time (t) is calculated by solving the differential diffusion equation in cylindrical geometry. The efficiency (η) at a time delay (t) is related to the probability that there are one or more electrons remaining by

$$\eta = 1 - \exp(-f\bar{n})$$

where

$$\bar{n} = 2Q \sum_{\beta} \exp\left(\frac{-\beta^2 Dt/a^2}{\beta J_1(\beta)}\right) \int J_o\left(\frac{\beta r}{a}\right) dy$$

and where D is the diffusion coefficient of the electrons, f is the probability of a discharge being formed from one electron, r is the initial position of the electron in polar coordinates, β has values in the Bessel series 2.4048, 5.5201, 8.6537, and Q.dy is the probability of an electron being produced in an element of path length dy. The relationships can be applied to any flash tube system by the use of appropriate values of D, a, Q and f. Lloyd found it convenient to plot η as a function of Dt/a^2 for ranges of the value afQ, as shown in Figure 2.4.

Holroyd and Breare (12) have used a Monte Carlo method to study the random motion of electrons initially distributed in the same manner as described by Lloyd and have obtained very similar results.

An important parameter used to describe the efficiency in terms of the delay time of the high voltage pulse is the sensitive time. This is defined as the time after the passage of a particle for the internal efficiency to fall to 50%. Flash tubes of 1.6cm internal diameter and

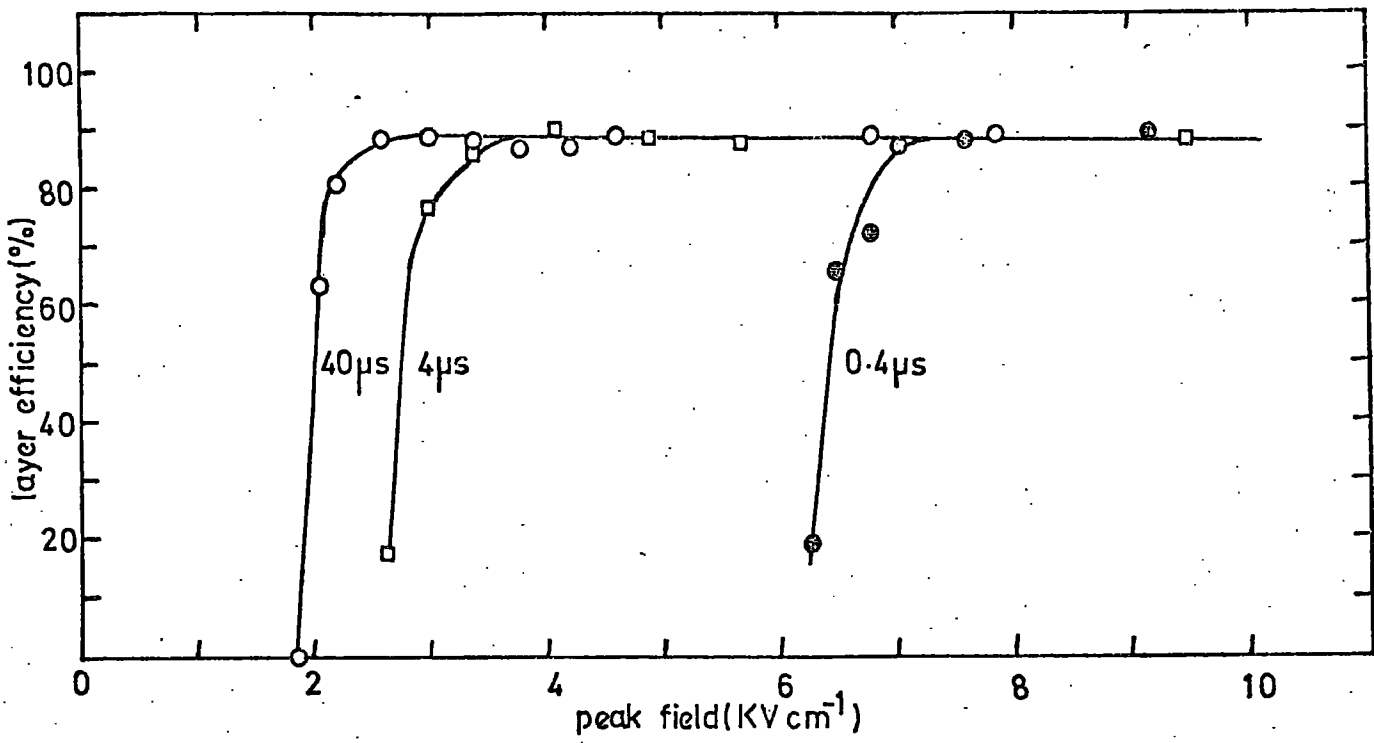

Fig 2·3 variation of efficiency with field for different pulse lengths (RC). tube internal diameter=1·6cm Ne-He pressure=600 torr

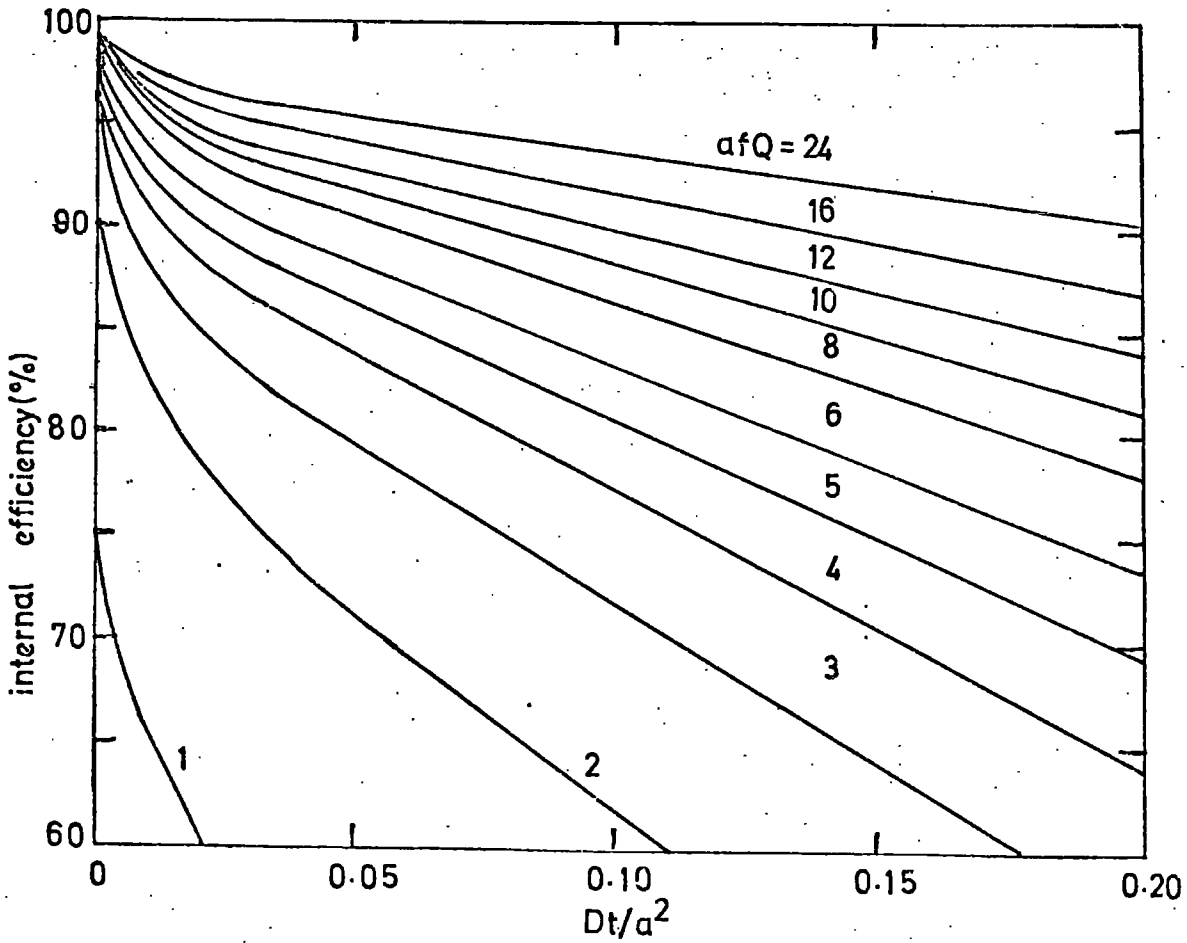

Fig 2·4 variation of efficiency with time delay calculated by the diffusion theory of Lloyd

filled at 600 torr have a sensitive time of about 100μs. This limits their operation in a background radiation to less than about 10^3 particles/tube/second. (see chapter 5).

2.2.5 Effects of the gas mixture

All successful gas fillings of flash tubes have used the noble gases or mixtures of them. Their use is associated principally with their low breakdown voltage and the copious emission of ultraviolet and visible radiation. The gas mixture in most common use is neon-helium. The large number of ion pairs produced in neon by the passage of a particle aids the formation of a discharge and gives a longer sensitive time than most other mixtures. Very little difference has been found with respect to efficiency by varying the neon to helium ratio. The most common mixture is neon (98%)-Helium (2%) although mixtures in which helium is the major component (neon(30%)-Helium(70%)) is satisfactory (13).

Unlike spark chambers, which are almost always operated at atmospheric pressure, flash tubes can be used without difficulty at various pressures; so far the pressures adopted have ranged from 200 Torr to 3 atmospheres. Below about 300 Torr the maximum efficiency attainable is found to fall(10). The reason for this is two-fold. At low pressures the number of ion pairs produced by the particle will on the average be small, thus the possibility of getting no suitably placed electron is significant. Second, the rate of avalanche build-up during the pulse will be slow, because the electron mean free path is increased, and hence the chance of the electrons being swept out without causing significant secondary ionization is increased. Investigations at high pressures up to 3 atmospheres have been conducted by Coxell and Wolfendale (14). The purpose of filling tubes at high pressure is to obtain a large number of initial ion pairs in a tube of small diameter.

Figure 2.5 shows the time delay characteristics for tubes of internal diameter 0.55cm at various pressures.

The effect of gas impurities is also an important consideration. Their effect is usually to increase the breakdown voltage of the gas, decrease the sensitive time and to make the spread of the discharge down the tube more difficult. For example, oxygen has a large cross section for electron attachment and it will readily remove electrons before and during the discharge, thereby increasing the difficulty of producing a flash. Although commercial neon does contain a small amount of oxygen, Gardener et al (15) showed that the characteristics of tubes with commercial neon were not appreciably different from tubes filled with spectroscopically pure neon.

2.2.6 Internal clearing fields

Under suitable conditions the efficiency - delay time characteristics can be predicted accurately by Lloyd's diffusion theory. In many experiments, however, anomalous results have been reported with efficiency values below the predicted value. The cause of the discrepancy has been attributed to clearing fields built up by the discharges themselves (1). The phenomenon is attributed to the high resistivity of the glass which restricts the flow of charge over the inside surface of the tube after the discharge. The unrecombined charges left on the glass surface after the discharge produce an electric field across the gaseous volume which remove electrons more rapidly than normal diffusion. Fields of a few V cm^{-1} have been calculated to last for some minutes after the discharge (1).

An efficiency-time delay curve has been measured by Breare et al (16) for a range of temperatures up to 100°C. Figure 2.6 illustrates how the effect of clearing fields decreases with decreasing glass resistivity. In general a decrease in resistivity of approximately

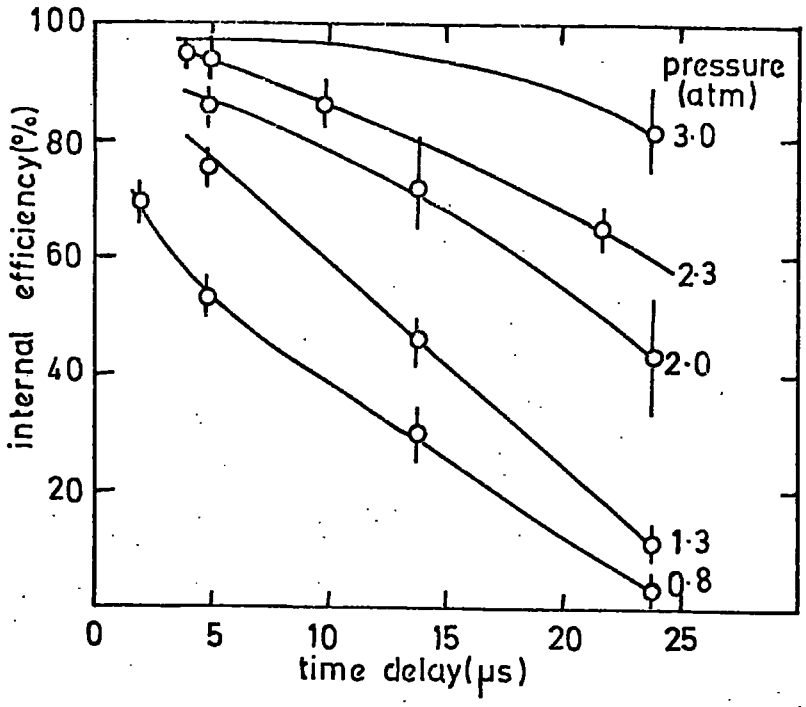

Fig 2.5 efficiency-time delay characteristics of flash tubes at different gas pressures. tube internal diameter=0.6cm. $E = 6.3\ KVcm^{-1}$

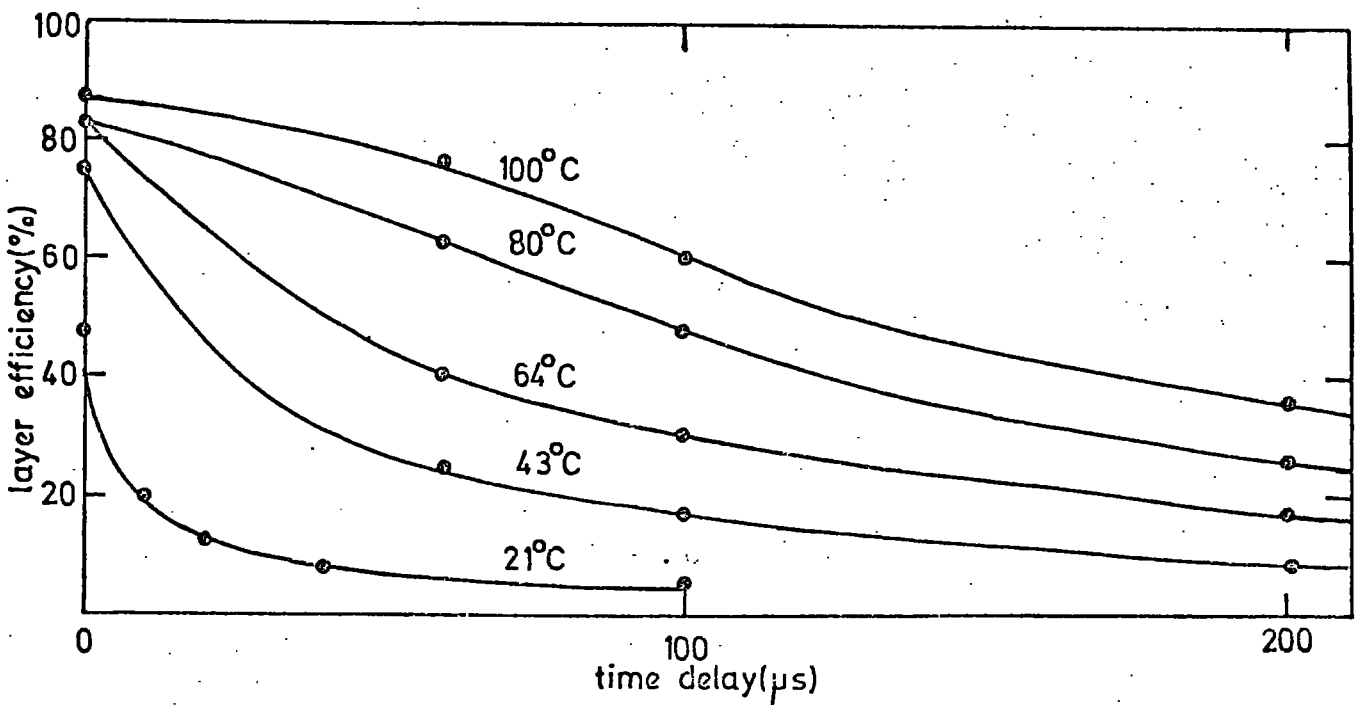

Fig 2.6 variation of efficiency with time delay at several temperatures. tube internal diameter = 1.6cm. pressure = 600 torr.

one order of magnitude occurs for a 25°C rise in temperature. Attempts to reduce the effective resistance of tubes to a suitable value with a semi-conducting coating have so far been unsuccessful.

2.3 The Recovery Time

A finite time must elapse, following the ignition of a flash tube, for it to become sensitive again and able to register further ionizing particles. Applying a second high voltage pulse before this time causes the tube to reignite, regardless of whether or not a ionizing particle had past through its sensitive volume. The recovery time is defined as the time after an ignition for the reignition probability to fall to 50%. This parameter has been measured by Gardener et al (15) who showed that it varied considerably with gas composition, being approximately 3s for pure neon, but decreasing considerably for impurity contents as small as 1 part in 50,000. Commercial flash tubes have recovery times of about 0.3s. It is this characteristic which prevents operation at high repetition rates and is partly responsible for its use being confined to cosmic ray physics.

The long recovery time is not a well understood phenomenon and is difficult to explain in terms of a simple diffusion theory. A detailed explanation and methods of overcoming the problem are discussed in Chapter 5.

References

1. Holroyd, F., Ph.D. Thesis, University of Durham (1971).

2. Townsend, J., Electrons in Gases, London: Hutchinson, (1947).

3. Raether, H., Electron Avalanches and Breakdown of Gases, Oxford: Clarendon, (1953).

4. Ayre, C.A., Thompson, M.G., Whalley, M.R., Young, E.C.M., Nuc. Inst. Meth. 103 (1972) 49.

5. Corrigan, S.J.B., von Engel A., Proc. Phys. Soc. 72 (1958) 786.

6. Harries, W.L., von Engel A, Proc. R. Soc., A222 (1954) 490.

7. Rohatgi, V.K., J. App. Phys., 28 (1957) 951.

8. Holroyd, F.W., Breare, J.M., Nuc. Inst. Meth. 100 (1972) 429.

9. Rochester, G.D., Proc. Int. Con. Cosmic Rays, Moscow (1960) 312.

10. Barsanti, G. et al., Proc. of the CERN Symposium 2 (1956) 56.

11. Lloyd, J.L., Proc. Phys. Soc. 75 (1960) 387.

12. Holroyd, F.W., Breare, J.M., Nuc. Inst. Meth. 100 (1972) 277.

13. Conversi, M., Giannoli, G., Spillantini, P., Nuovo Cim. Lett, 3 (1972) 483.

14. Coxell, H., Wolfendale, A.W., Proc. Phys. Soc. 75 (1960) 378.

15. Gardener, M., Kisdnaswamy, S., Rossie, E., Wolfendale, A.W., Proc. Phys. Soc. B70, (1957) 687.

16. Breare, J.M., Chaney, J.E., El Disouki, W., Lightfoot, J.A., Proc. Int. Con. Instrumentation for High Energy Physics, Frascati (1973) 221

CHAPTER THREE

THE CONSTRUCTION AND OPERATION OF FLASH TUBE DETECTORS.

3.1 Manufacture of flash tubes

Flash tube detectors can be manufactured within a wide range of soda glass tube sizes. The most frequently manufactured detectors are either 1.6cm internal diameter, filled at 600 torr or 0.6cm internal diameter, filled at 2.3 atmospheres. Other sizes have, however, been made from wall thicknesses between 0.01mm and 1.0mm, inside diameter between 0.5cm and 5.0cm, and lengths up to 2.5m. Careful selection of the glass is often required, where spatial accuracy is of concern, to maintain an acceptable tolerance on the outside diameter. It is also necessary that the tubes are straight. This can be achieved by controlled heating of the tube while rotating on rollers. For the manufacture of tubes at 600 torr the glass tube is filled at the required pressure and heated at the end until the excess outside pressure causes the tube to constrict and form a seal. For high pressure tubes it is necessary to fill at a low temperature in liquid nitrogen. When the tube regains room temperature the pressure reaches 2.3 atmospheres. In order to prevent ultra violet light triggering adjacent tubes in an array, it is necessary for the glass to be either painted or sleeved in an opaque material for their entire length.

Less conventional flash tube devices have been constructed from other materials. Breskin and Charpak (1) have operated very small tubes made from capillary glass of 1mm inside diameter by applying the impulsive electric field longitudinally rather than transversely with respect to the tube axes. Also flash tube devices constructed from nylon tube and honeycomb structured polypropylene have recently been

reported from the Frascati laboratory (2,3).

3.2. High Voltage Pulse Generators

Unlike spark chambers, flash tubes will operate satisfactorily even when long pulses with poor rise-times are applied. Most pulse generating systems work on the principle of discharging a capacitor across a resistance to produce a high voltage pulse with an exponential decay. The switching action may be provided by a spark gap, thyratron or hard valve. Figure 3.1 shows a basic pulsing circuit of this kind.

There are many published circuits for generating high voltage pulses with short delays and fast rise times which are suitable for flash tube arrays (4,5,6). Most systems are triggered by logic signals of a few volts or less, which must be amplified considerably in order to finally operate a spark gap or thyratron. Amplification is normally obtained with either transistor Marx generators (5,7), valves (8) or silicon- controlled rectifier circuits (6,9). The use of air gaps, rather than thyratrons as the final high voltage switch has the advantage of cheapness and simplicity. The trigertron (10), in particular, is a spark gap device of very simple construction which can be triggered by pulses of less than 1 KV amplitude. Figure 3.2 shows a trigertron constructed with a tungsten trigger electrode mounted in the earth side of the switch. This device operates satisfactorily up to 30KV and is triggered by a negative 5KV pulse. Much smaller trigger pulses can be used if a barium titanate collar is inserted around the end of the tungsten trigger electrode (4).

Recently, a new type of hydrogen thyratron, manufactured by English Electric Ltd, has provided a means of operating flash tube devices at very high repetition rates. A system built with the new thyratron and capable of switching 20KV and 1000 amps at 1KHz is described in section 8.4.

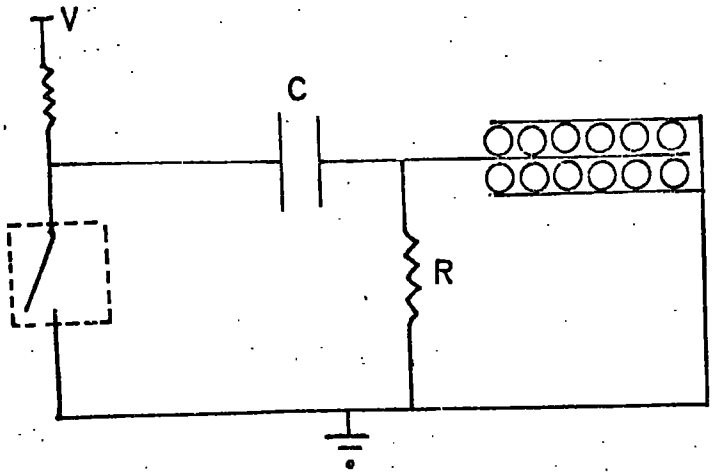

Fig 3.1 a simple flash tube pulsing circuit

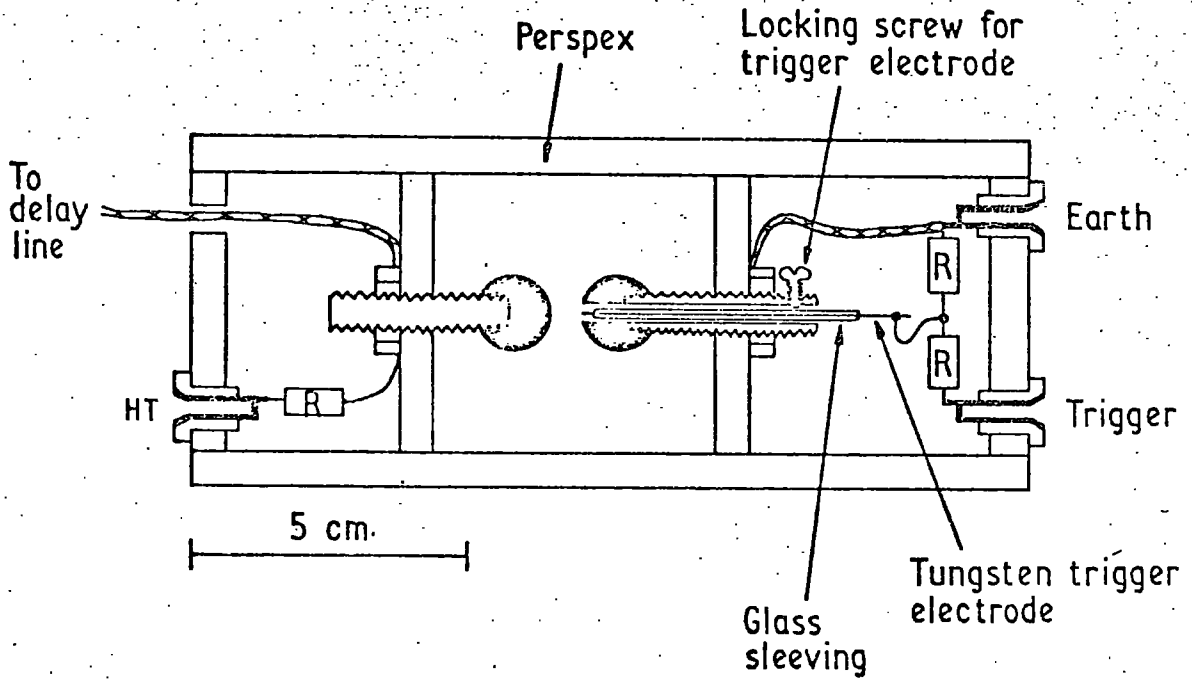

Fig 3.2 an air trigatron spark gap

3.3 Output Information

Photographic or visual techniques were first used, but several filmless techniques have been developed during the last few years as bigger arrays and higher repetition rates have been employed.

3.3.1 Photographic Method

Light emission is predominantly in the yellow-red region of the spectrum corresponding to the most intense lines of neon and helium. For photographic recording most fast red-sensitive films have been successfully tried, for example Ilford Mark V and HP3, Kodak Tri X and the very fast Kodak 2475 and 2403.

Mirror systems are often necessary with large arrays in order to reduce the angle subtended by the tubes at the camera. Such systems are normally arranged so that the optical path lengths from each group of tubes is roughly the same (11). This permits the use of a large aperture lens without loss of definition, unlike spark chambers where the lens must be stopped down so as to give a depth of focus equal to the chamber depth.

3.3.2 Light sensing method

Reines (12) has reported a technique developed for use in the South African underground neutrino experiment. This large experiment uses about 60,000 neon flash-tubes of length two metres. Because of the large area covered by the tubes photography is extremely difficult. A technique has been developed which electronically records the tubes which have flashed. The information is then displayed on a hodoscope which can be photographed more easily.

A cadmium selenide cell is placed infront of each flash tube and is connected to a silicon-controlled rectifier and associated electronics to a light bulb on the hodoscope system. The light output from the tube is detected by the cadmium selenide cell as a change in resistance of the cell. This change is detected by the silicon-controlled rectifier which consequently switches on a light bulb on the hodoscope

board. This is then photographed and scanned in the normal way.

3.3.3 The vidicon method

Harrison and Rastin (13) have developed a system in which a flash tube array is observed by a vidicon camera. A standard 405 line system is used, with the 25 frames per second producing a line scan period of 98μs. The vidicon photocathode is scanned by the electron beam in a direction parallel to the image of the flash tube layers. A pulse, which is registered when the scan of the electron beam moves across a fiducial bulb at the start of the flash tube layer, is used to gate a 2MHz timing signal. If a tube has flashed in a particular layer its coordinate is determined in terms of the signal frequency. The data from each layer of tubes are initially placed in temporary storage scalers and then transferred to a magnetic core store.

3.3.4 The Spark Tube

Bacon and Nash (14) have developed a flash tube in which sealed electrodes are added. The electrodes were 1mm wide copper strips on a thin paxolin card seperated by 1mm and running nearly the whole length of the tube. When the tube flashed, a voltage pulse was obtained from the strips owing to breakdown across the inside of the tube. They found that spurious discharges occasionally occurred between the strips but were eliminated by the addition of a quenching agent. In this case ethyl alcohol at a pressure of 30 Torr was added to neon at 1 atmosphere.

3.3.5 External probe method

Ayre and Thompson (15) have developed a very simple and effective method of determining electronically whether or not a tube has flashed. Their technique is used on the Durham University MARS spectrograph. A small probe is placed close to the end window of each flash tube. A pulse of several hundred volts can be obtained from the probe when the

tube flashes. By tapping-off from a resistor network, the pulse may be attenuated and used to drive conventional logic electronics direct, without amplifier interfacing.

The pulse is produced by capacitive coupling between the high voltage electrode and the probe when the tube ignites. During a discharge the gas becomes a conducting medium and increases the capacitive coupling such that a large pulse is transmitted to the probe. The probe pulse will thus have the same polarity and shape as the electrode pulse.

References

1. Breskin, A., Charpak, G., Nuc. Inst. Meth. 108 (1973) 27.

2. Conversi, M., Nature (Phys. Sciences) 241 (1973) 160.

3. Conversi, M., Fredericix, L., Taccetti, Q., Proc. Int. Conf. Instrumentation for High Energy Physics, Frascati (1973) 184.

4. Cronin, J.W., Bubble and Spark Chambers vol 1. New York and London: Academic Press (1967)

5. Schmitt, F. et al. Nuc. Inst. Meth, 52 (1967) 331.

6. Jung, E.A., Lewis, R.N., Nuc. Inst. Meth. 44 (1966) 224.

7. Allkofer, O.C., Knoblich, P., Kraft, E., Nuc. Inst. Meth. 47 (1967) 169.

8. Allkofer, O.C., Spark Chambers, Verlag Karl Thiemig, K.G., Munich (1969) 183.

9. Ayre, C.A., Ph.D Thesis, Durham University (1971).

10. Stubbs, R.J., Ph.D. Thesis, Durham University, (1971).

11. Hooke, J.R., Ph.D. Thesis, Durham University (1973).

12. Reines, F., Proc. R. Soc. A301 (1967) 125.

13. Harrison, D.J. and Rastin, B.C., Nuc. Inst. Meth. 77 (1970) 181.

14. Bacon, D.F., Nash, W.F., Nucl. Inst. Meth 37 (1965) 43.

15. Ayre, C.A., Thompson, M.G., Nucl. Inst. Meth. 69, (1969) 106.

CHAPTER FOUR

APPLICATIONS OF FLASH TUBE DETECTORS

4.1 Introduction

The flash tube detector has been used extensively in cosmic ray physics following its introduction by Conversi and Gozzini in 1955 (1). Since then the device has been used, in preference to spark chambers, for a vast number of cosmic ray experiments. Cosmic ray physics has favoured the use of the device because of its robustness, ease of operation, simple digitization, low cost and ability to cover large areas. Use of the device has been restricted to cosmic ray physics because of its inability to operate in a high radiation background and at high repetition rates. Nevertheless, in this field alone the device has been successfully employed for a variety of different detecting applications. Little improvement has been made to the performance of the flash tube since its introduction, but growing interest in applications to accelerator experiments has recently stimulated further investigations to produce a more satisfactory tube. The aim of this chapter is to give a brief review of past applications in cosmic ray physics and some possible fields of accelerator experimentation where the flash tube detector may be exploited.

4.2. Cosmic ray physics

Cosmic ray physics has used the flash tube technique to locate high energy cosmic ray particles in a vast number of experiments. There are five main areas of study where the flash tube detector has contributed: momentum and charge measurement using magnetic spectrographs, the structure of extensive air showers, the search for fractionally charged particles, the detection of neutrino interactions and the detection of heavy primary cosmic particles in balloon-borne experiments.

4.2.1 Magnetic Spectrographs

Large flash tube spectrographs have been developed at Durham and Nottingham Universities during the past 15 years for measuring the cosmic ray muon spectrum at sea level. These devices utilize layers of flash tubes for defining the trajectory of charged particles through a magnetic field. Spectrographs of this type normally have maximum detectable momentum (mdm) characteristics in the TeV region and large collecting areas in comparison with other devices using spark chambers, Geiger counters or cloud chambers (2).

One of the largest and most sophisticated of these devices is MARS (3), the Durham 'Magnetic Automated Research Spectrograph'. This 300 ton spectrograph has an mdm of 5.85 TeV/c and an integral Bdl value of about 8×10^6 gauss. cm. Digitized information, taken from the flash tubes by means of Ayre - Thompson probes (see section 3.3.5) is fed directly into an on-line computer.

4.2.2 Extensive Air Showers

The flash tube chamber is particularly suited to the study of extensive air showers because of its multi-track efficiency. Unlike the spark chamber, arrays of flash tubes are capable of registering multiparticle events with high efficiency over large areas.

One of the largest of these detectors is installed at Kiel (4,5) and is used to study the electron component of air shower cores. The chamber has a detecting area of $31 m^2$ and contains 180,000 flash tubes, 1cm in diameter and approximately 1cm in length. These small tubes are placed between two electrodes, one of which is transparent for photographic recording.

4.2.3 The search for Quarks

Ashton et al (6) have searched for fractionally charged particles using a large flash tube array containing more than 10,000 tubes. If

the particles exist then they should be detected by measuring their ionization density when traversing matter. As the ionization density for relativistic particles is proportional to Z^2, quarks may be distinguished from normal charged particles because they are fractionally charged as $-\frac{1}{3}e$ or $\frac{2}{3}e$ respectively. Ashton makes his flash tubes sensitive to charge by operating the chamber with a time delay between the particle passage and the application of a high voltage. Thus, fractionally charged particles are identified by having a smaller detecting efficiency than ordinary charged minimum-ionizing particles. With such a large array the efficiency can be accurately determined from a single track since about 80 tubes are expected to flash when a singly charged particle passes through, compared to about 40 tubes for a particle of e/3 charge.

4.2.4 Discrimination between particles of equal momenta

Diggory et al (7) have demonstrated the ability of flash tubes to detect differences in ionization rates caused by particles of equal momenta. The energy loss by ionization can be shown to be dependent on the mass of a particle within a certain momentum range. Diggory has measured the flash tube efficiency for cosmic ray protons and muons in the momentum range 0.1 - 10 GeV/c using a time delay between the passage of the particle and the application of the high voltage pulse of 50 or 80μs. Results of this method give distinct muon and proton curves, with variations in efficiency between 58 and 38%, which agree well with theoretical estimates.

4.2.5 The detection of heavy primary cosmic rays

Andrews et al (8) have detected primary particles of large mass using a balloon-borne flash tube array. The tubes were made sensitive to particles of high mass by delaying the high voltage pulse after an event. In this way, it is only particles of high mass which are efficiently detected. Results obtained from this experiment are in good

agreement with the theoretical efficiency curves predicted by Lloyd. Their array was digitized using the probe method of Ayre and Thompson and information of each event was transmitted to ground during the flight.

4.2.6 Neutrino Experiments

The flash tube chamber is well suited for the detection of neutrinos interactions. The small interaction cross section of neutrino particles requires large target and detecting volumes to obtain a satisfactory event rate. Experiments with cosmic ray neutrinos have taken advantage of the fact that flash tubes may be constructed in arbitrary dimensions to cover very large areas.

One of the largest of this type of experiment is in a two mile deep laboratory near Joannesburg. This experiment, developed by the Case-Wits-Irvine collaboration (9,10,11) contains 50,000 1.9cm outer diameter flash tubes 2m long.

A similar experiment, which is the result of a collaboration between groups from England, India and Japan (12) has been in operation for several years in the Kolar gold mines in Southern India at a depth of 2.316 miles.

4.3 The use of flash tubes in accelerator physics

Conventional flash tube detectors have characteristics which restrict their use to experiments where the background radiation is less than 10^4-10^3 particles/tube/second and where data is recorded at repetition rates of less than about 1 event/second. This severly limits the application of the device to accelerator work where detectors are frequently required to operate in a background radiation of 10^5 particles/second and at repetition rates in excess of 100 events/second. The unsuitability of the device under these conditions has

created a preference for using spark chambers, which has, in turn, hindered the development of tubes for accelerator work. In spite of these undesirable characteristics (discussed in detail in chapter 5), in comparison with conventional detecting techniques, the flash tube has many commendable features. The most important of these features are listed below.

(1) Arrays of tubes are simple to construct and operate.

(2) Flash tubes are inexpensive and their cost is independent of length.

(3) Arrays of almost any size and geometry may be constructed.

(4) An array may be dismantled and rearranged to be used again in a different geometry.

(5) Flash tubes do not require continued replacement of gas.

(6) The high voltage pulsing requirements are not stringent. Pulse rise-times of 0.5μs have been employed and the radiation and subsequent interference with neighbouring electronic circuits is thus considerably less than in spark chambers where rise times of 50ns or less are desirable.

(7) The elemental construction provides a flash tube device with a high multitrack efficiency at any angular inclination.

(8) A simple and inexpensive method of digitization has been developed.

Provided that the sensitive and recovery time characteristics are improved (see Chapter 5), then the flash tube detector provides a convenient and attractive technique in that class of experiments where large sensitive volumes are required, high spatial accuracy is unnecessary and the absorbing properties of the glass material are of little concern. Two main areas of nuclear research are envisaged for this device in relation to accelerator physics; the location of particles produced in rare events where large quantities of absorbing material and large

detecting volumes are required, and the detection of high energy photons where both spatial and energy measurements are necessary.

4.3.1 Charged Particle detection

An array of flash tubes used as a track locating device cannot compete against detectors such as proportional, drift and spark chambers in terms of spatial resolution. In many experiments however, the need for such high spatial accuracy is not always justified, because detectors are often employed to provide a knowledge as to whether a certain type of reaction has occurred , without the necessity of a precise trajectory determination. Such applications include the detection of rare events, where large sensitive volumes (possibly in 4_{π} geometry) are required.

A typical example of this type of experiment is the detection of neutrinos. Neutrinos, being weak interacting particles with cross sections of only about $10^{-38} cm^2$ require large target and detector volumes to give adequate detecting rates. Most neutrino experiments performed with the aid of an accelerator have utilized large spark chambers to detect the muon in the interactions:

$$\nu + n \rightarrow p + \mu^-$$

$$\nu + p \rightarrow n + \mu^+$$

Typical examples of such experiments are those which have been performed at the AGS accelerator in Brookhaven (13) and at the PS in CERN (14,15) in order to confirm the two neutrino hypothesis. The detecting arrangement at the CERN neutrino experiment consisted of 81 three electrode chambers of aluminium and 66 modular brass chambers stacked with iron and lead absorbers. The electrode area of the chambers was 160 x $100 cm^2$ and the total weight of the detector was about 75 tons. One of the main features of this device was its ability to discriminate between electrons and muons. A muon produces a straight track through the chamber, while an electron will initiate a cascade shower. By this method it was proved

that ν_e and ν_μ are different elementary particles.

Flash tubes are well suited to this type of experiment, where large sensitive volumes are required and interacting material is of advantage. Also, the flash tube chamber has a high multitrack efficiency and is thus capable of discriminating between the straight tracks of a muon and the cascade development produced by an electron.

4.3.2 Photon detection

High energy photons are normally studied by detecting the electromagnetic shower produced when a photon interacts with a heavy target material. A study of the shower development can provide a means of determining the energy and trajectory of the incident photon. The detection of photon induced showers has been done mostly with stacked assemblies consisting of either a series of detectors (scintillator or Cerenkov) interspaced with targets of a heavy material, or in homogeneous devices made of dense transparent material such as lead glass (see section 7.2).

With these types of detectors the shower information gives an energy measure only, and all spatial information needed for the determination of an incident photon trajectory is lost. In many experiments, for example, where a neutral particle decays into two photons, it is often advantageous or necessary to provide both energy and spatial information for the reconstruction of the interaction. Detectors which provide the additional spatial information normally take the form of either spark chambers sandwiched between layers of target material, with a digital read-out system to count and locate the sparks, or a series of cross scintillators coupled to photomultipliers interspaced with target material.

Spark chambers, however, have two main disadvantages: a low multi-track efficiency which reduces the energy resolution and linearity of

response; and complex digital read-out, which makes the construction of large arrays difficult and expensive. The multitrack efficiency can be improved if glass current-limited spark chambers (16,17) are used, but their operation entails even greater problems with respect to data acquisition and fast repetition rates. Detectors constructed with crossed scintillators are normally expensive and electronically complex because each scintillator element requires a photomultiplier and linear electronic circuitry.

In the past, this problem has been resolved by building hybrid systems, using spark chambers to give spatial information, and scintillator or Cerenkov detectors to provide an energy determination. But nevertheless, such systems, when built into large arrays tend to be complex and very expensive (19).

The flash tube detector may provide an alternative solution, because it has characteristics ideally suited for the detection of cascade showers. The device has a high multitrack efficiency, is simple to operate, and is easily digitized. Furthermore, due to the low cost of flash tubes, many detecting planes may be employed to give a total absorption device capable of a precise energy determination. Thus, a device of this kind has the potential of providing low cost, large area photon detection with the advantage that both the energy and trajectory of an incident photon are measured simultaneously within the same instrument.

Conversi et al (18) indicated the suitability of the flash tube chamber for measuring the energy of photons with an array installed at the Frascati (Adone) storage ring. His results show a sensitivity to the energy of electron induced showers at energies of a few hundred MeV. An investigation reported in this thesis (see chapter 7), using

the Daresbury Nuclear Physics Laboratory e^+ beam at energies of a few GeV, has demonstrated the feasibility of using a flash tube device to provide both energy and spatial information.

An estimate of the cost of a flash tube device in relation to other gamma detectors is difficult because the form of its construction will depend on resolution requirements. This will determine the tube diameter (and hense the number of tubes) and the number of detecting planes. Nevertheless, an important consideration is that the cost of covering an area with a plane of flash tubes is linearly proportional to one external dimension only because a plane is sampled in projection and the cost of a tube is independent of length. Also, the simplicity of the flash tube detector must be taken into account, for it is possible to digitize each tube without the necessity of an interfacing amplifier (see Chapter 7). With the introduction of ultra high energy accelerators, the flash tube technique may, therefore, be a convenient and inexpensive method of facilitating a gamma detector, which at such high energies is often required to be of a very large size (19).

For a comparison of costs, a calculation has been made of the expense of constructing a flash tube detector of equal size and resolution to the gamma detector proposed for the Omega project at 300 GeV at CERN (19). The proposed detector is a hybrid device in which gamma rays are detected with a matrix of lead glass blocks and several planes of spark chambers. The detector will be about 6m x 2m and contain approximately 500 lead glass elements. The cost is estimated at about SF 2.5M (1972 prices). A flash tube device of similar size, consisting of 10 modules each containing 3 planes of digitized 1cm diameter tubes would cost approximately SF 0.3M (1974 prices). These estimates include all electronics up to a computer interfacing.

4.3.3 Neutral Particle Detection

A large photon detector constructed from flash tubes may be particularly useful for measuring the position and momentum of neutral particles which decay into photons. For example, particles such as the π^o, K^o, X^o and η all have $\gamma\gamma$ decay modes.

At very high momentum, photons decay with very small opening angles, thus, in order to resolve the two cascade showers which they produce, it is necessary to position the detector at large distances downstream from the target. For example, the minimum opening angle for photons from the decay of a 10 GeV/c π^o is only 27 m.rad. (in the laboratory coordinate system). Therefore covering a sufficiently large solid angle to ensure an adequate event rate and momentum range requires a device of very large area. Flash tubes are well suited, in this respect, because they give momentum and spatial information, and are capable of being constructed into large arrays at comparatively low cost.

When both photons are detected from a neutral decay, a momentum determination may be made either from the opening angle between the decay photons or directly from information contained in the detected photon showers. Measuring the momentum of the decayed particle from the opening angle only, becomes particularly advantageous at low momentum where the opening angles are large, and the spatial resolution is good. By this method the momentum resolution is given by (19):-

$$\frac{\Delta P_o}{P_o} \simeq \frac{\Delta E_o}{E_o} = \frac{\Delta \theta_s}{\theta_s} \qquad \ldots\ldots\ldots\ldots (1)$$

where ΔP_o, ΔE_o and $\Delta\theta$ are the momentum, energy and angular resolutions respectively, P_o is the momentum of the decayed particle, E_o is the energy of the decayed particle and θ_s is the opening angle (see Figure 4.1). This

expression shows that the momentum resolution from an opening angle measurement improves with increasing opening angle. The momentum resolution obtained by considering the shower structure from each photon is given by the following expression (19,20):-

$$\frac{\Delta P_o}{P_o} \propto \frac{1}{P_o^{\frac{1}{2}}} \qquad \ldots\ldots\ldots\ldots (2)$$

In this case, the resolution improves with increasing momentum. Thus, both methods, when used together, compensate each other for losses in resolution in the upper or lower momentum ranges.

Figure 4.2 shows an example of the detecting resolution calculated by Dowell and Sloan (19) for the proposed π^o detecting system designed for use at CERN on the Omega project up to energies of 100 GeV. Although this detector is not constructed with flash tubes, the energy resolution can be expected to vary in a similar way as described by the expressions (1) and (2). The graph shows the expected momentum resolution for π^o detection using lead glass detectors with an individual photon resolution of 15% FWHM (at 1 GeV), and spark chambers to measure the opening angle with a spatial resolution of $\pm$ 1mm. The resolution is plotted for $\alpha = 90^o$ (as defined in Figure 4.1) with the detector 40m downstream from the H_2 target. The graph illustrates how the two methods compensate for one another to give a resolution which is never worse than about $\pm$ 1.0%.

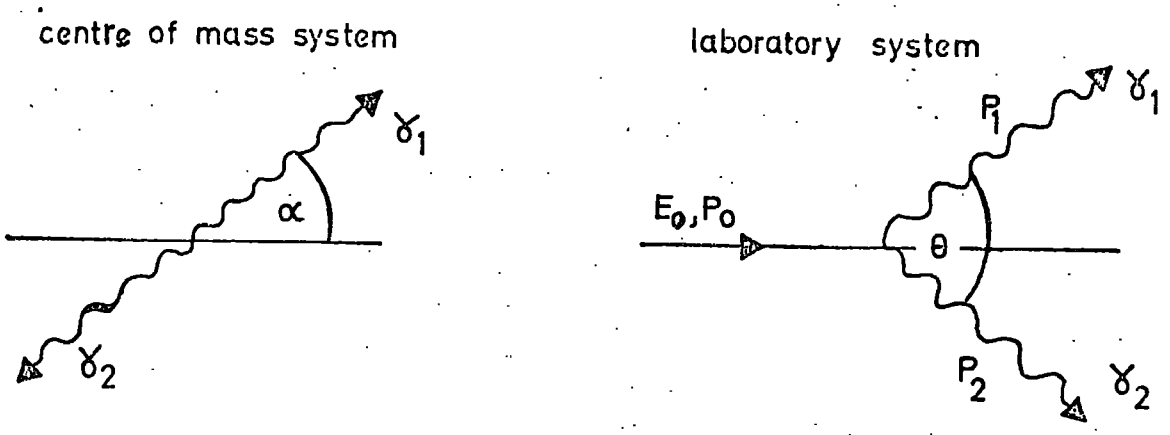

Fig 4.1 the decay of a neutral particle into two photons

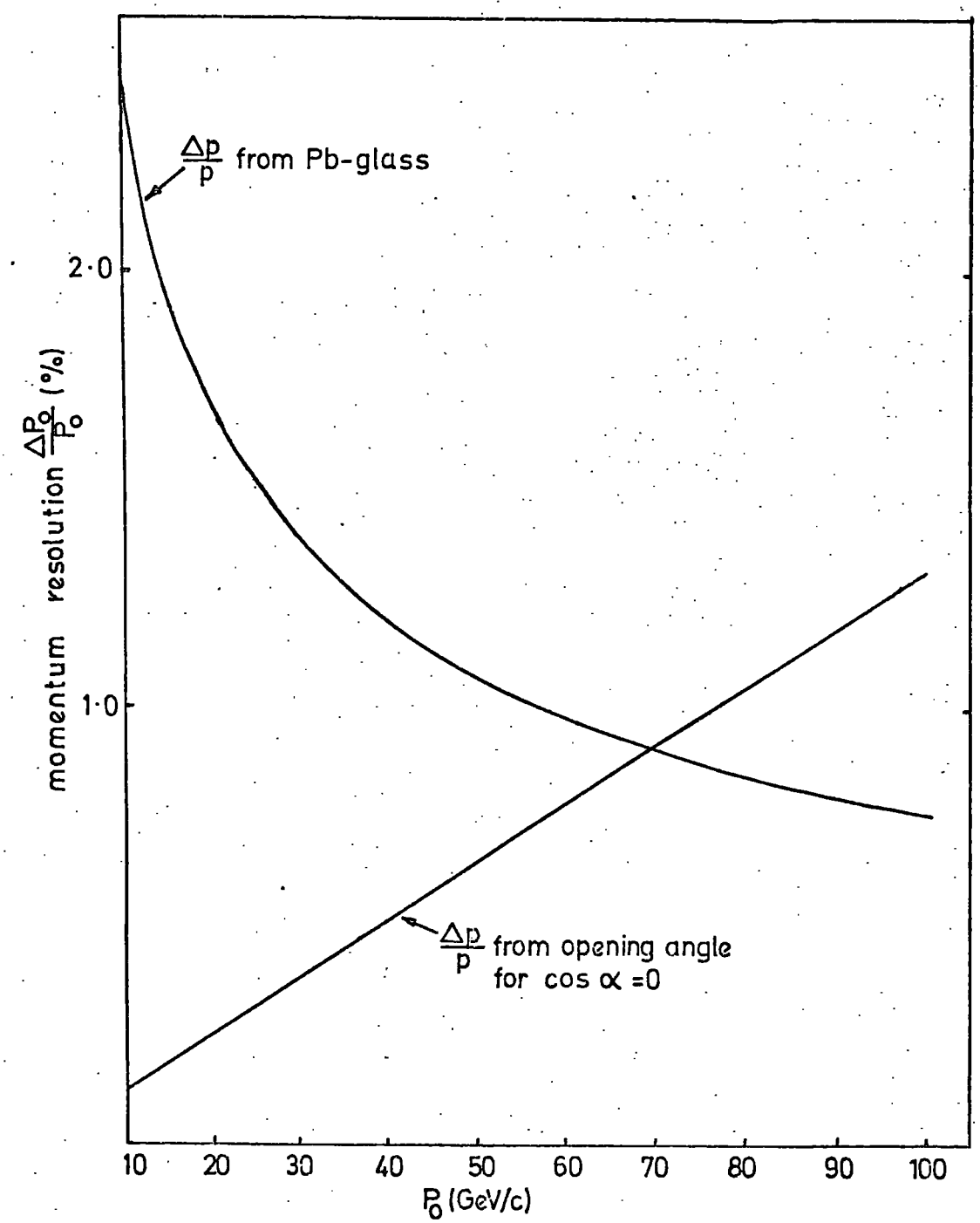

Fig 4.2 worst case errors on the π^0 momentum arising from energy and opening angle measurements

References

1. Conversi, M., Gozzini A., Nuovo Cimento 2 (1955) 189.

2. Brooke, G., et al., Proc. Phys. Soc. 80, (1962) 674.

3. Ayre, C.A., et al. Nucl. Inst. Meth., 102, (1972) 10 and 29.

4. Bohm E., Nagano M., Van Staa R., Trumper J., Proc. Int. Con. Cosmic Rays 4 (1971) 1438.

5. Samorski, M., Internal Report, Kiel, EAS 11-72 (1972).

6. Ashton, F. et al., J. Phys. A: Gen Phys. 4 (1971) 895.

7. Diggory, I.S., Earnshw, J.C., Hook, J.R., Turver, K.E., Proc. Int. Con. Cosmic Rays, Hobart, (1971) 1533.

8. Andrews D., Corydon-Peterson, O., Funch O and Rotenberg, M., Proc. Int. Con. Cosmic Rays, Hobart (1971) 1543.

9. Reines, F., CERN, Internal report 69-28 (1969) 103.

10. Meyer, B.S. et al. Phys. Rev. Rev. D1 (1970) 2229.

11. Reines, F. et al., Phys. Rev. D4, (1971) 80.

12. Menon M.G.K., et al. Proc. Roy. Soc. A301 (1967) 137.

13. Danby G., et al., Phys. Rev. Letters 9 (1962) 36.

14. Bienlein, J.K. et al., Phys. Letters 13 (1964) 80.

15. Holder, M., et al., Nuov. Cim. A57 (1968) 338.

16. Allkofer, O.C., et al Internal Report. Kiel, 020 (197).

17. Stubbs, R., Ph.D Thesis, University of Durham, (1971).

18. Conversi, M., Proc. Int. Con. Instrumentation for High Energy Physics, Frascati (1973) 126.

19. Dowell, J.D., Sloan, T., Internal Report, Birmingham University 72-06 (1972).

20. Trilling, G., Internal Report, SLAC-5-E (1962).

CHAPTER FIVE

THE DEVELOPMENT OF FLASH TUBE DETECTORS FOR ACCELERATOR PHYSICS

5.1 Introduction

The flash tube detector has characteristics which make it suited to experimental conditions where there is a small incident particle flux and low background radiation. Under these conditions the device operates efficiently ($\sim$100%) and registers very few spurious events. Unfortunately its use in accelerator experiments is made difficult by the long sensitive and recovery time characteristics which prevent operation in a high radiation background and at high repetition rates.

Little improvement has been made to these characteristics since the detector's introduction by Conversi in 1955 but interest in large area detecting systems for accelerator work has stimulated investigations to produce a more satisfactory tube. The objectives of recent work in Durham have been to produce a new Flash Tube detector which would operate in a background radiation of about 10^5 particles/tube/second and be capable of registering digitized output information at frequencies of the order of 1 KHz without deterioration in detecting efficiency. Flash tubes with these capabilities constitute a very attractive and viable detecting technique for accelerator physics experiments.

5.2 The Sensitive Time

The application of an externally applied electric clearing field is usually necessary with spark chambers working in a high background radiation environment. Spurious and background induced sparks are reduced by the removal of unwanted electrons from the sensitive volume by the continuous application of a d.c. electric field across the electrodes. The sensitive time will be equal to the mean time for

an electron to drift across the sensitive volume, and experimentally is usually defined as the time after the passage of an ionizing particle for the detecting efficiency to fall to 50%. The strength of the electric field required, will depend on the incident flux of background radiation and the maximum delay time between particle passage and the application of the high voltage pulse. D.C. fields of up to 200 V/cm are normally applied to spark chambers, reducing the sensitive time to a few μs (1,2). The sensitive time must be in the range described by the expression:-

$$T_B > T_S > T_D$$

where T_B = mean time between particles from background radiation

T_S = sensitive time

T_D = delay time of the high voltage pulse.

Another method employed to reduce the sensitive time is the admixture of electronegative gases (2). Such gases as O_2, CO_2, CCl_4, SO_2 and SF_6 are suitable additives for noble gases. SF_6 in particular, has a very high capture cross section for thermal electrons (5) and only very small quantities (1×10^{-4}%) are required to reduce the sensitive time to a few μs (6). However, the clearing field method is normally favoured because external adjustment is possible to suit different experimental conditions. This is important in the case of flash tubes where the tube is sealed and gas mixture fixed.

The sensitive time of a normal Ne-He flash tube is of the order of 100 μs (section 2.2.4) and previous attempts to apply static clearing fields which would sweep electrons to the walls of the tube have been unsuccessful. Theory and experiment predict that a field as weak as 10v/cm should remove all electrons from a 1.8cm diameter tube in about 10 μs(10), yet is has been shown that field strengths as high

as 2KV/cm have no measurable effect on the sensitive time (4). An explanation and solution to this phenomena were necessary before the device could be considered for use in high radiation background conditions.

5.2.1 Flash Tubes with a Short Sensitive Time

The failure of earlier attempts to reduce the sensitive time by the application of clearing fields is attributed to the movement of charges on the glass surface which cause the almost complete backing off of the external D.C. field. The volume resistivity of soda glass is very high and a value of $5 \times 10^{12}\ \Omega$ cm at room temperature has been measured for type S95 glass. Nevertheless it has previously been shown (7) that significant charge movement does take place. It is not clear at present whether the conduction is by sodium ion motion in the volume of the glass or by electron movement in the glass or over its surface, but rearrangement of the field lines caused by the applied clearing field is to be expected.

The use of an alternating electric field overcomes this problem provided that the frequency of the field is such that the polarity changes faster than the charges on the glass can move to counteract it. A 50Hz sinusoidal clearing field was applied between electrodes as shown in Figure 5.1. The value of capacitor C1 was chosen large enough to present a small impedance to ground for the high voltage pulse, yet small enough so as not to smooth the alternating voltage. A value of 0.1 μF was found to be a good compromise at this frequency.

Flash tube characteristics were measured using this circuit and at room temperature 50 Hz was found to be more than adequate in this respect. Figure 5.2 shows the effect of the 50 Hz sinusoidal clearing field on the efficiency versus time delay characteristics for tubes made of S95 soda glass and filled at 600 torr pressure with a 98-2

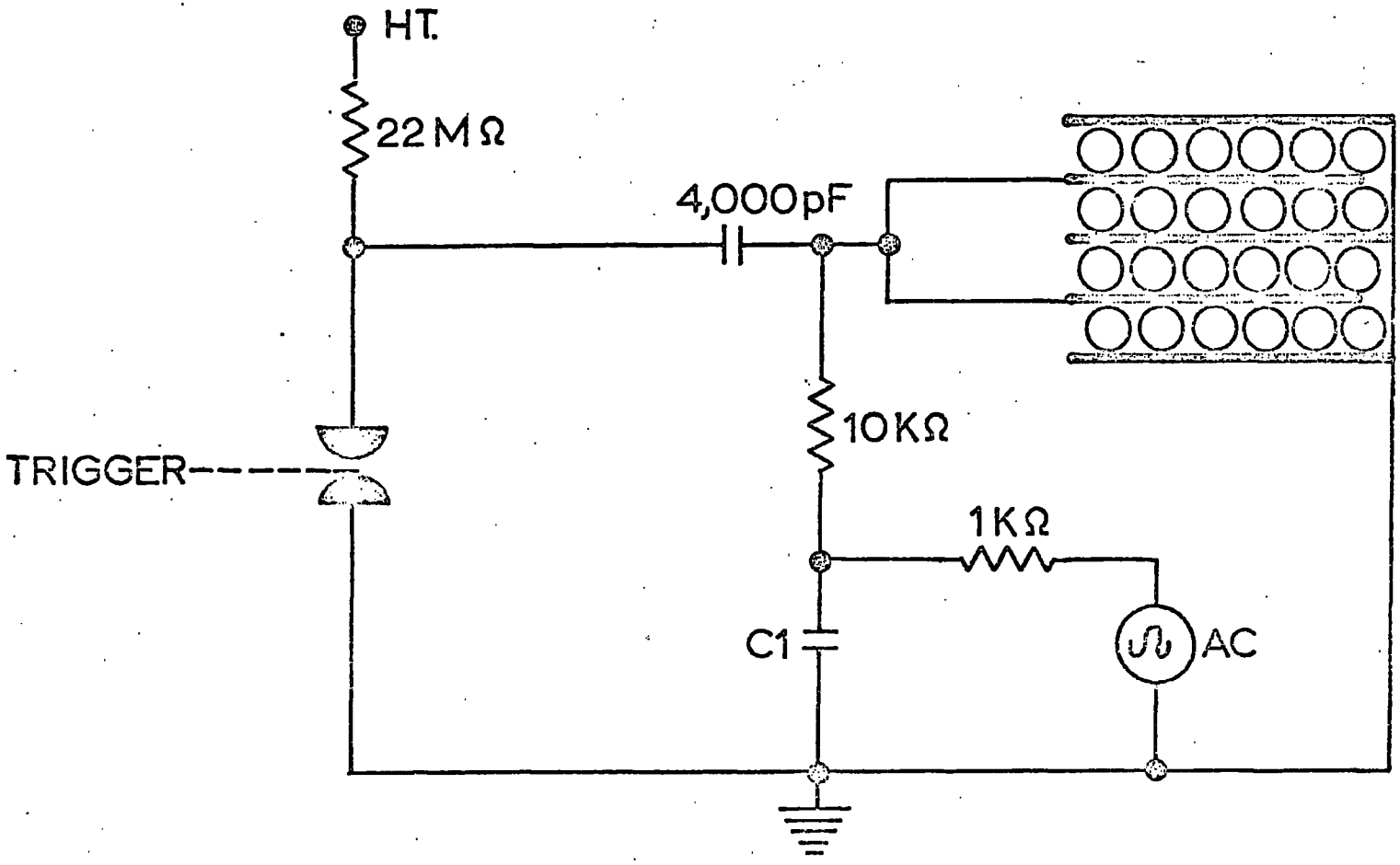

FIG. 5-1. The Pulsing circuit for use with an alternating clearing field.

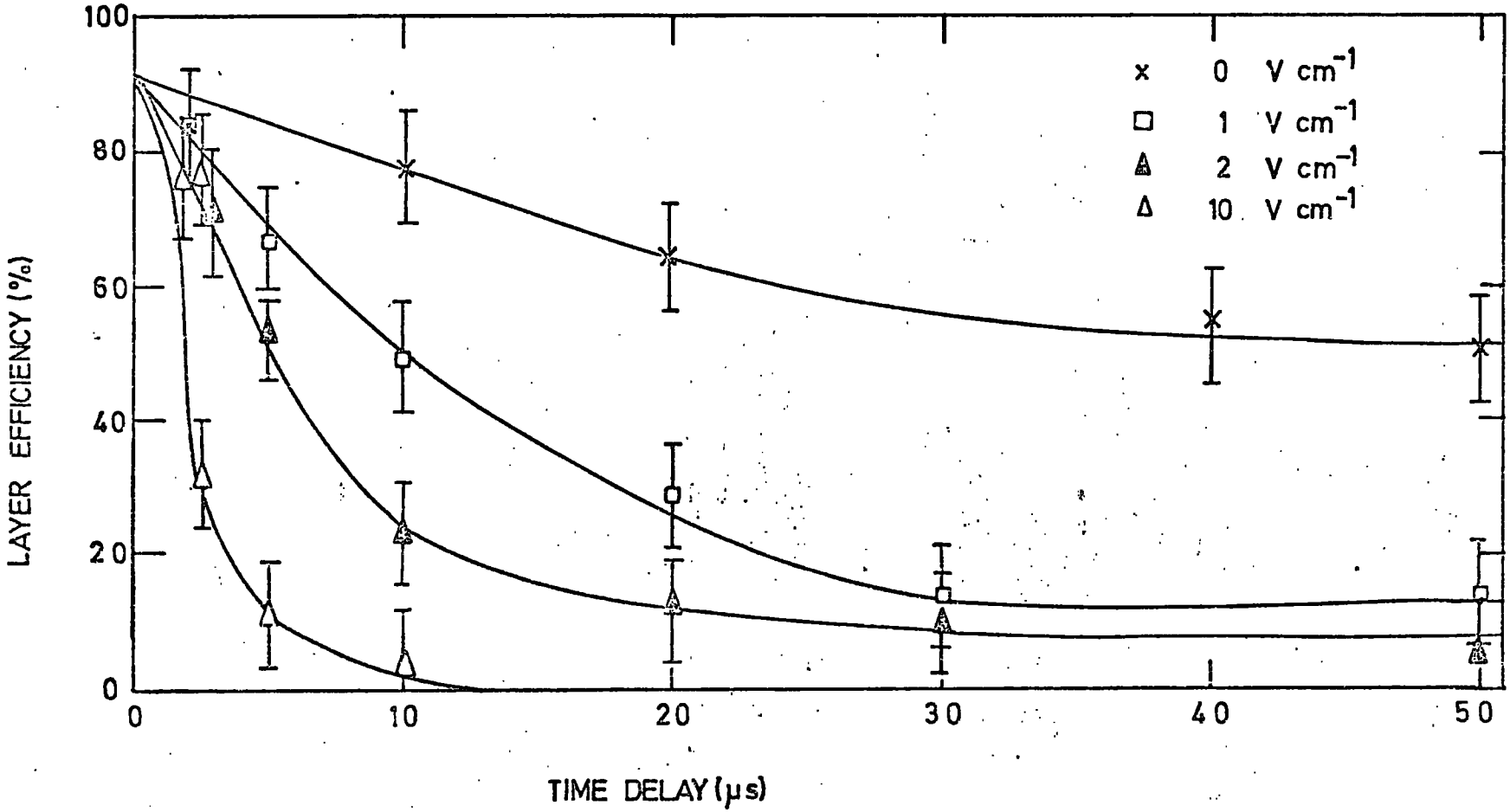

FIG. 5.2 Efficiency versus Time Delay for several Sinusoidal Clearing Fields.

Neon-Helium gas mixture. The tubes had an inside diameter of 1.6cm and a wall thickness of 1mm. It is seen that rms fields as small as 1.0v/cm have a considerable effect on the sensitive time and an rms field of 10v/cm reduces the sensitive time to approximately 2 μs. Figure 5.3 shows similar curves obtained with 0.6 cm internal diameter tubes filled with 98-2 Ne-He at 2.3 atmospheres pressure.

Comparisons can be made with Meyers results (3) of the effect of D.C. clearing fields in a 0.5cm gap spark chamber. He found a field of 18v/cm reduced the sensitive time to approximately 1.8μs, where this value is an average for the two directions of the clearing field with respect to the H.T. pulse. The main difference from Meyers results is that a long tail exists in the flash tube efficiency versus time delay characteristics for a.c. fields. This is attributed to particles passing through the system at the zero or low field part of the a.c. cycle. The problem is overcome when a square pulse of alternating direction is applied.

A reduction in the clearing field effectiveness is expected as the alternating frequency is reduced, since charges are able to move and counteract the applied field. This behaviour was observed when a square wave alternating field of variable frequency was applied to tubes at 100°C. In order to allow transmission of the higher frequency components, capacitor C1 in Figure 5.1 was replaced by one of value 0.022 μF, producing a rise time of 500μs for the leading edge of each square wave. Figure 5.4 shows the efficiency versus frequency curves for time delays of 20 and 40 μs. From these curves it is seen that charges are beginning to counteract the externally applied field at about 25 Hz, which can be thought to represent a 'cut-off' frequency dependent on the decay time for charges to become ineffective in the tube. However, the 'cut-off' frequency at room

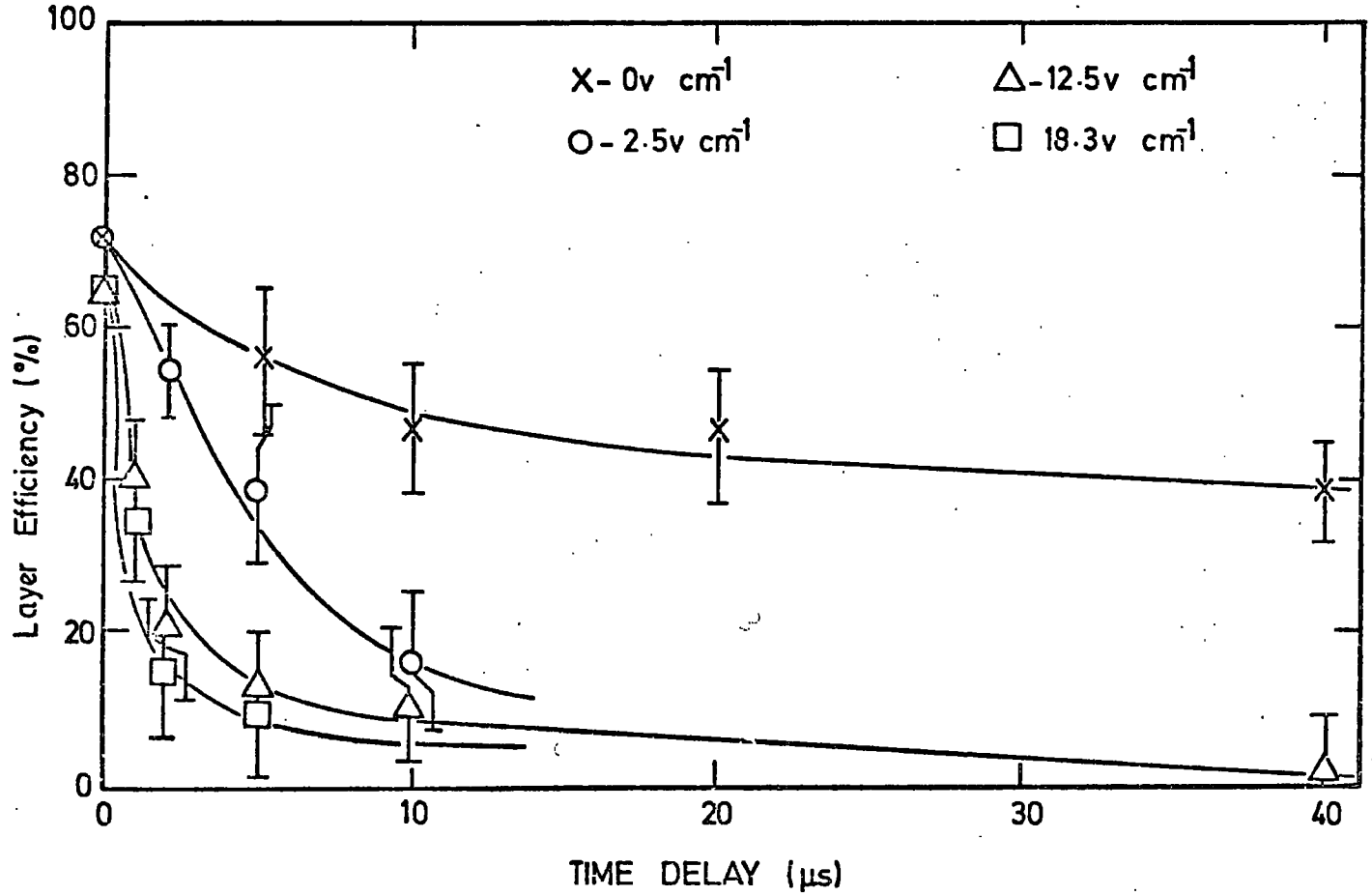

FIG. 5.3 Efficiency versus Time Delay for several Sinusoidal Clearing Fields.

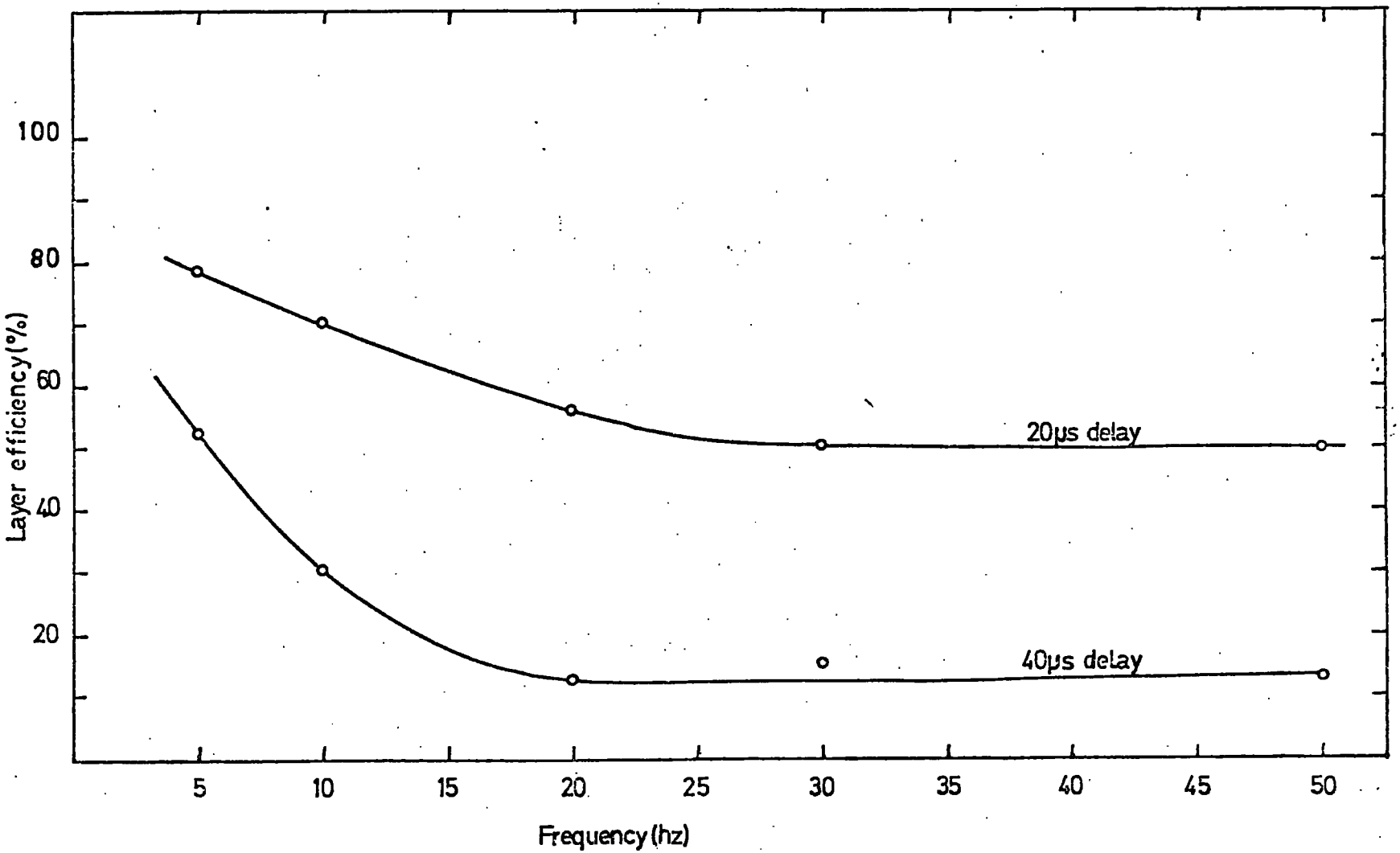

Fig. 5.4 Layer efficiency versus clearing field frequency

temperature will be much lower than this, probably of the order of 0.1 Hz, because the resistivity of glass changes by three orders of magnitude (8). A direct measurement of this frequency at room temperature was found difficult and reproducible results could not be obtained at very low frequencies. This failure may be explained by variations in surface conductivity due to contamination, which becomes significant when the glass resistivity is very high. Nevertheless, a measure of the tube decay constant was made at 100°C by investigating the dependence of efficiency on the applied clearing field frequency and a value at room temperature was induced from it. A detailed description of the method and results is given in Appendix I. The experimental results give a decay time of 61ms at 100°C with 1.9cm diameter tubes, and indicate that charge recombination is by an exponential process. At room temperature the constant may be expected to have a value three orders of magnitude larger, which would be in good agreement with experimental results of other workers using a different method (9). Their results show that internally induced clearing fields may persist for several minutes after ignition.

5.2.2 The Generation of a Square Wave Clearing Field

Two simple and reliable methods have been employed to produce an alternating square wave clearing field. The first, shown in Figure 5.5, is a 100Hz generator which is triggered directly from a mains supply via a transformer. The mains frequency is used to open and close a reed switch twice every cycle, providing a square pulse train which swings about zero volts after decoupling with a capacitor. The pulse rise time is normally of the order of 100μs for dry reed switches, although substantial improvements can be made if the wetted mercury type are used.

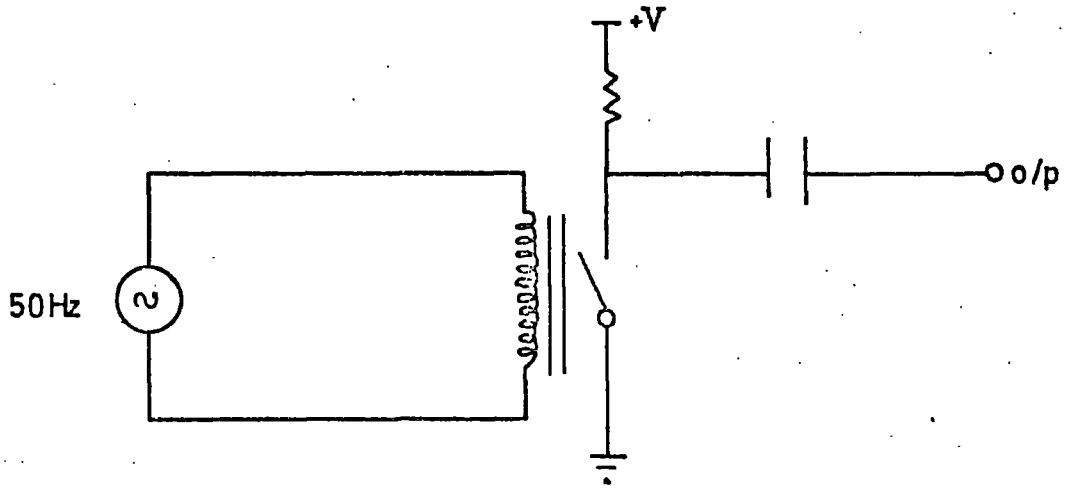

FIG. 5.5 A 100 Hz Square Wave Generator using a Reed Switch.

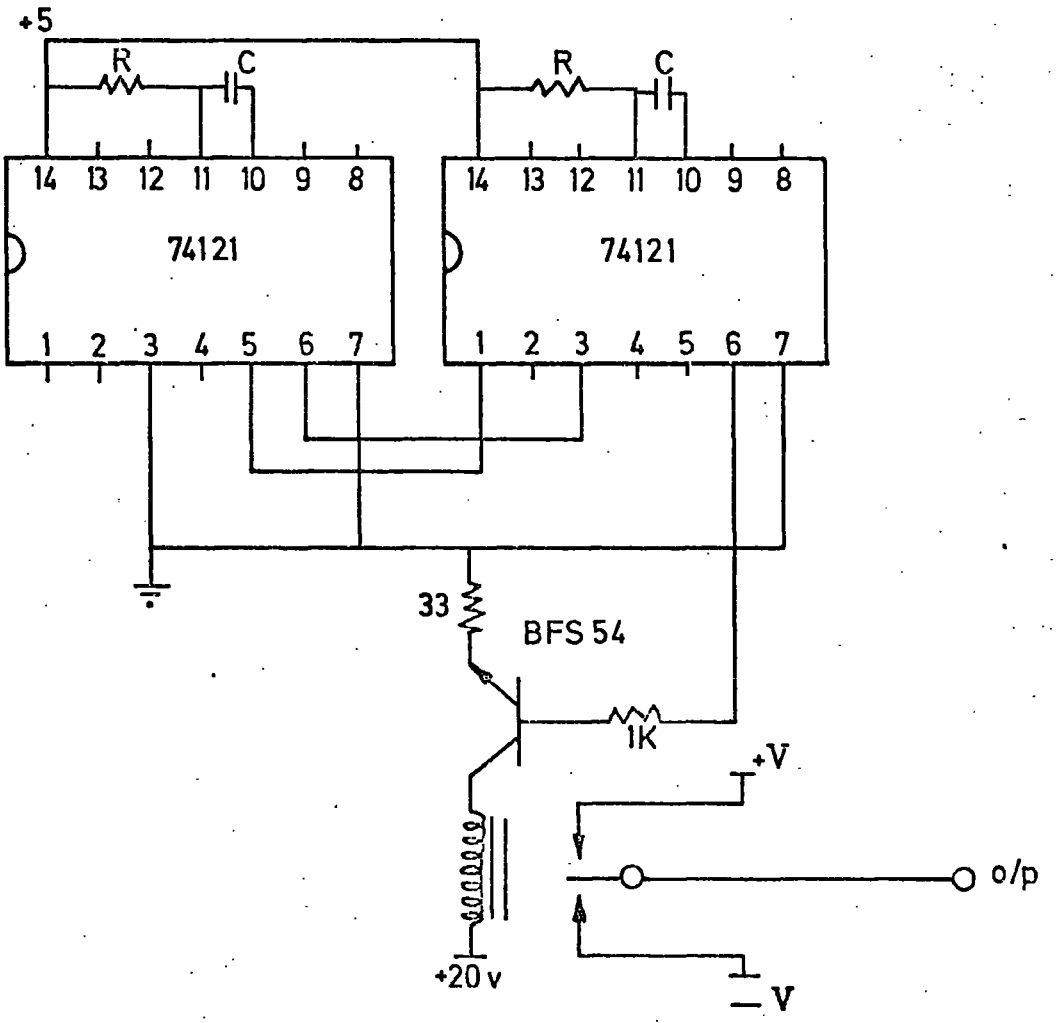

FIG. 5.6 A Variable Frequency Square Wave Generator using Monostable Flip Flops.

Figure 5.6 shows a variable frequency square wave generator which uses two monostable flip-flops coupled together to form a multivibrator with a mark-to-space ratio of 1:1. The frequency may be varied by a suitable choice of R and C. The logic output is then used to drive a bi-polar relay by means of a single transistor amplification stage.

Both types of generators have been shown to be very effective and reliable when used with the pulsing circuit shown in figure 5.1.

5.3 The Recovery Time

The recovery time of a flash tube is the time interval after an event for the tube to become sensitive again to another particle. A second high voltage pulse applied within this time causes spurious reignition. The recovery time is defined as the time after a discharge for the reignition probability to fall to 50%. A recovery time of 300 mS has been measured for 1.9 cm external diamter tubes filled with 70% Ne and 30% He at 600 Torr. Figure 5.7 shows the reignition probability plotted against the time interval between H.T. pulses for these tubes.

The phenomenon requires electrons to remain in the sensitive volume for a time after the initial discharge, and from experimental evidence this time is required to be several hundred milliseconds. If the removal of electrons is by a simple diffusion mechanism only, then the number of electrons left in the sensitive volume after a time (t) is given by the following equation for diffusion in cylindrical geometry (derived in Appendix II).

$$N(t) = 2.4\ \rho_o r_o^2\ H \exp\ (-t/T\ )$$

where T = fundamental diffusion time constant = $1/D\left[\ (2.405/r_o)^2 + (\pi/H)^2\ \right]$

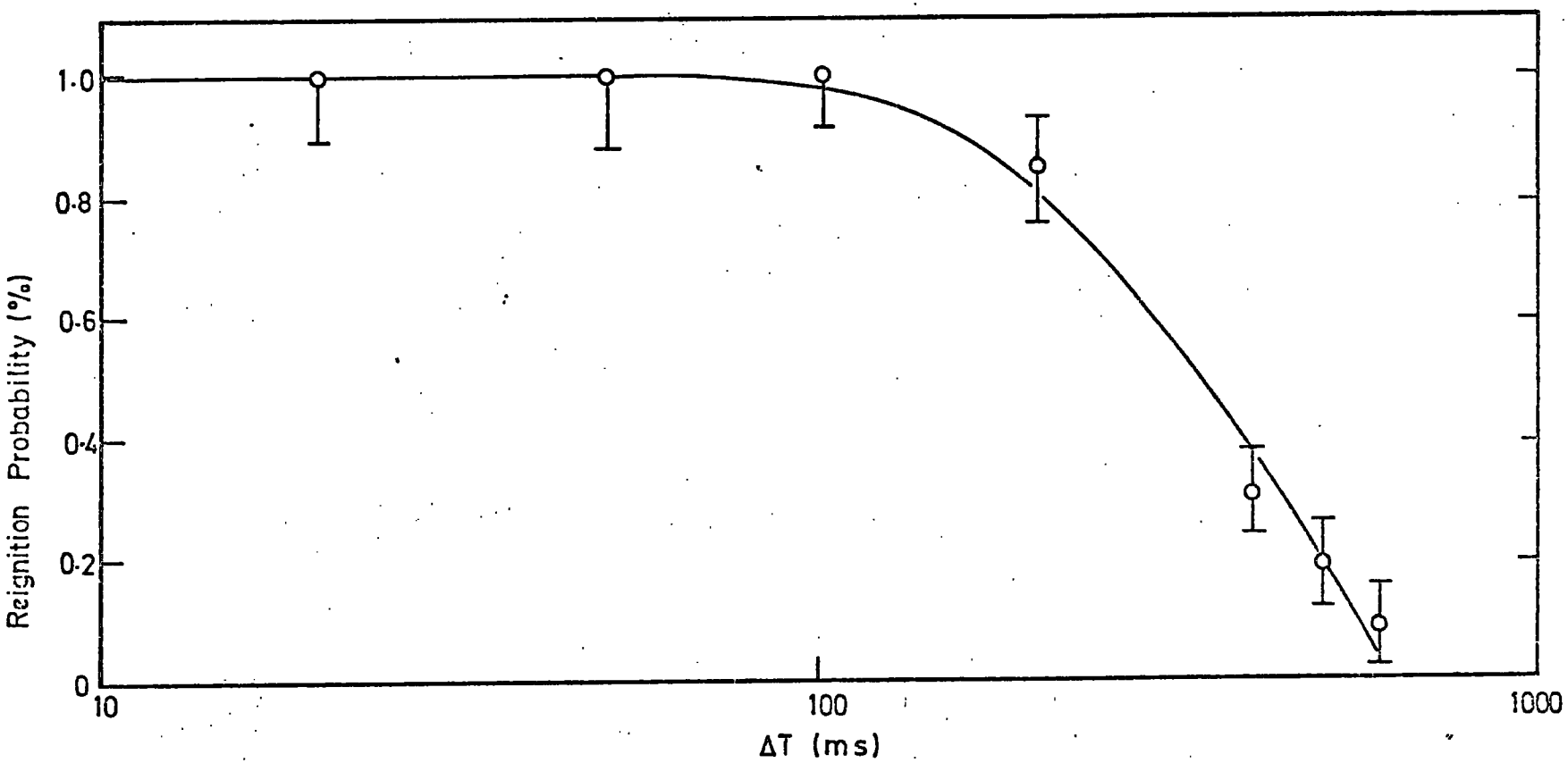

FIG. 5·7 Reignition Probability versus Time Interval between Events

ρ_o = electron density at t = 0

r_o = tube radius

H = tube length

t = time

N = number of electron in the tube at time t

From this equation the expected reignition probability may be calculated using the equation (11):

$$R(N) = 1 - \exp(-fN)$$

where R = reignition probability

f = probability of an electron producing a discharge

Taking r_o = 0.8cm, H = 50cm, D = 1800 $cm^2 s^{-1}$ and f = 0.3, the reignition probability versus time distributions were calculated and are shown in Figure 5.8 for different initial electron densities. The expected initial density is of the order of 10^{11} electrons cm^{-3} (12). It is seen that even for an initial electron density of $10^{12} cm^{-3}$ the recovery time is only a few milliseconds. If the electron density is large enough then ambipolar diffusion may make these times longer (26), but nevertheless, it is very likely that internally induced clearing fields will remove all the electrons in a very short time. For example, a field as small as 1 volt/cm will remove all electrons in approximately 50μs(10) and an externally applied sinusoidal clearing field of 200 volts/cm rms . which should remove electrons in less than 5 μs was found to reduce the recovery time only by a factor of two (see section 5.3.1).

From the above observations it is inferred that electrons created in the initial discharge do not remain in the sensitive volume for a time long enough to cause reignition. It is therefore necessary to postulate a secondary electron production process to account for the long recovery time.

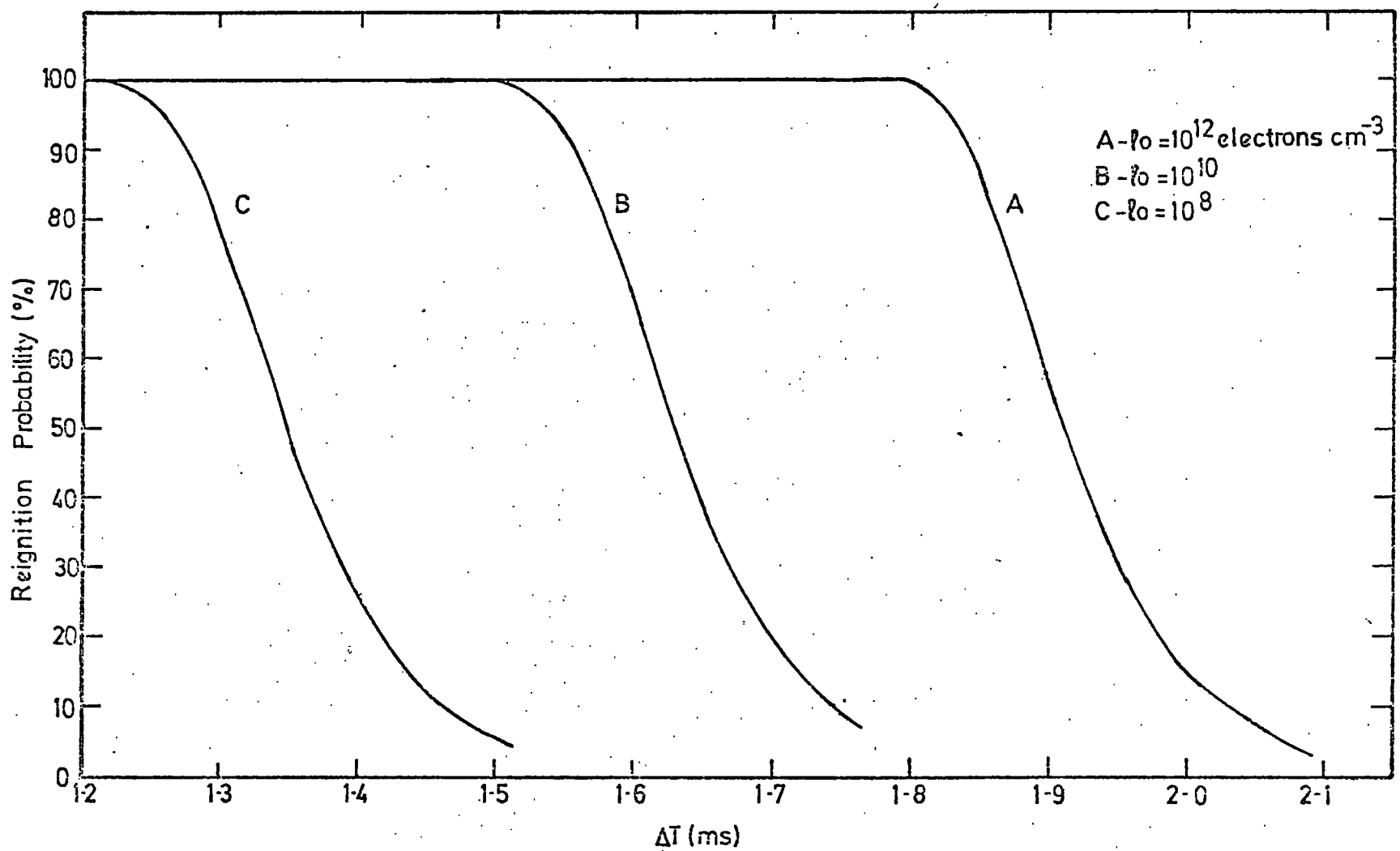

FIG. 5.8. Reignition Probability versus Time Delay calculated for electron diffusion loss only.

5.3.1 Nature of the Long Recovery Time

Many secondary electron producing mechanisms are known to exist and have been studied by other workers. These form two distinct groups; secondary effects resulting directly from interactions of ions, photons and excited states created during the discharge; and electrons produced from the surface of the glass by field emission processes. Since conventional metal electrode spark chambers filled with neon-helium mixtures are capable of operating at repetition rates in excess of 10^3 events per second (13), it is probable that the long recovery time, characteristic of flash tubes is associated, at least in part, with the glass from which the tube is made.

One possible explanation involves positive Ne ions, which have small diffusion and mobility coefficients compared to electrons, and are not removed from the sensitive volume so readily. Normal flash tube operation does not require ions to be removed from the sensitive volume because they cannot contribute to ionization at small E/P values. However, it is known that positive ions may produce secondary electrons by virtue of their potential energy when only a few angstroms from the surface of a material. This process occurs when the ionization energy is greater than twice the work function of the surface material (14). To test whether this phenomenon is relevant to flash tube reignition, a sinusoidal clearing field large enough to remove all Ne ions in one cycle was applied. The magnitude of the field was calculated from the expression

$$d = \int_0^{T/2} KE_0 \sin \omega t \; dt$$

giving $|E_0| = \pi d/KT$

where E_o = peak electric field

d = tube internal diameter

K = ion mobility

T = periodic time of the field

Using d = 1.8cm, K = 4.0 $cm^2V^{-1}S^{-1}$ and T = 20 x 10^{-3}S the calculated minimum peak field required to clear Ne ions created during the zero of the cycle, in 10mS at 50 Hz is 62.8 V cm^{-1}. In practice the times will be in the range $\frac{T}{2}$ to T, depending on the position of the ion in the tube and the magnitude of the field at the time of creation. A 200 V cm^{-1} sinusoidal field was applied to 1.8cm internal diameter tubes, and the reignition probability was measured and compared to the probability without a field. Figure 5.9 shows the reignition probability versus time between pulsing with and without the clearing field. The field reduces the recovery time only by a factor of two, indicating that the interaction of ions with the glass surface is not the dominant process responsible for secondary electrons.

Metastable atoms are also capable of releasing secondary electrons by either collisions with other gas atoms (Penning ionization) or by interaction with atoms in the surface of the glass (14). Metastable states of Ne and He are of particular concern because besides having long lifetimes (15), they are uncharged and cannot be swept from the sensitive volume by an applied electric field. According to Korff (16), metastables may cause spurious counts in Geiger tubes containing noble gases unless a small admixture of molecular gas is present to produce de-excitation. The de-excitation takes place by Penning effect, which involves an interaction between a neutral metastable and a molecule whose ionization energy is less than the excitation energy of the metastable. This results in ionization of the molecule and the release of an electron.

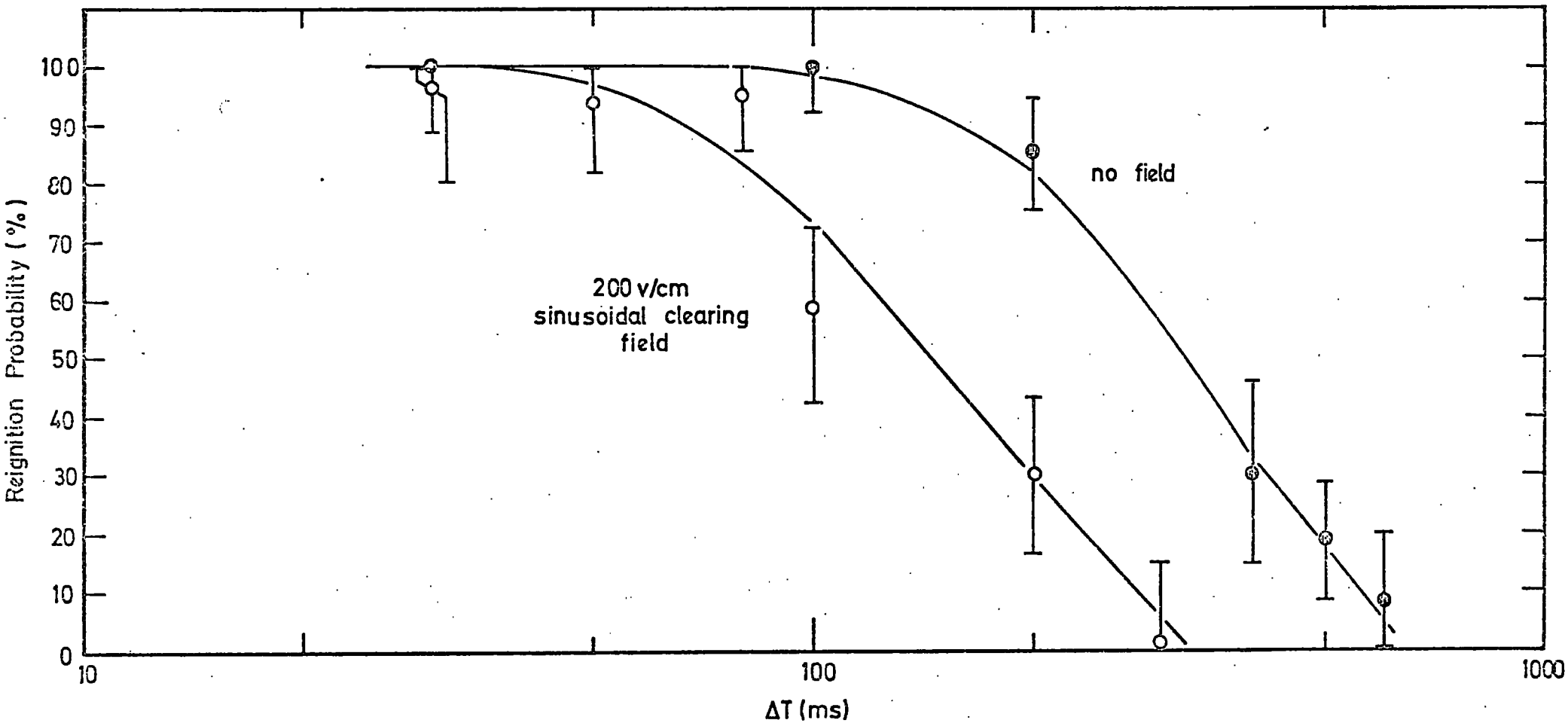

FIG. 5·9 Comparison of Recovery Time with and without Clearing Field.

$$A^* + B \rightarrow A + B^+ + e^-$$

The interaction cross-section for de-excitation of Ne metastables with gases such as CH_4, CO_2, O_2 and NH_4 are large enough (10^{-14} cm^2) for the process to occur very rapidly (15). However, measurements by other workers of the lifetimes of the $^3P_2$ and $^1P_1$ metastable states in pure neon, indicate that their influence should be of little concern for times in excess of 0.5 mS. Phelps (17) has measured the decay frequency for Ne metastables in a tube of 1.08 cm internal diamter as a function of Ne atom density. At 600 torr pressure the decay frequency is measured as 5×10^4 s^{-1} giving a mean decay time of 20 μS. If the initial metastable density is of the order of 10^{12} atoms cm^{-3} (15), then very few will remain after a few hundred microseconds if an exponential decay is assumed (17).

Photons produced in the discharge are also able to create secondary electrons by photoelectric interaction with the glass and it is this mechanism which is responsible for the spreading of the discharge along the length of the tube (18). The photoelectric quantum efficiency has been investigated by Rchatgi (19) in Ne with ultraviolet photons of 2537 A wavelength and has obtained a value of 6×10^{-4} (electrons per photon) for soda glass. A large number of secondary electrons can therefore be expected, considering that more than 10^8 photons will be produced in each discharge. Many of these photons, however, will not be directly incident on the glass surface, but will be absorbed and emitted by atoms in a diffusion-like motion for a relatively long time before being lost from the gaseous volume. This phenomena is known as resonant radiation and has been studied in detail by Holstein (21) whose theory predicts a mean lifetime of 2.6ms involving the long-lived $^3P_1$ state of Ne in a 0.8cm radius tube.

Another contributing effect may involve induced clearing fields, which remain of sufficient strength for a time after the application of the high voltage pulse to maintain localized Townsend type avalanches, which produce further ultraviolet photons and electrons until the field has decayed. Thus, a continuous flux of photons may be incident on the glass, creating secondary electrons which in turn initiate more discharges. There is experimental evidence for fields having decay times of the order of 60s (Appendix I), it is probable, therefore, that the field strength is large enough to cause Townsend avalanche after only a few hundred milliseconds. Observations by Holroyd (18) provide some evidence for the existence of weak discharges occurring at later times by showing the existence of feint sparks several microseconds after the initial discharge which were produced in a field of opposite polarity to the applied pulse.

Another possible mechanism is the charging of an insulating surface, such as glass, which can lead to thin-film emmission (20). This effect occurs when a thin layer of contaminating material deposited on an insulating surface becomes polarized by positive ions. If the electric gradient across the layer is of the order of $10^6 V\ cm^{-1}$ then secondary emission can occur. The secondary electron emission rate is found to drop when the source of ions is removed, but has been observed to persist at a non-zero value for many hours.

5.3.2 Reduction of the Recovery Time

The effect of different gas mixtures on the recovery time has been investigated with respect to the processes discussed in section 5.3.1. Gas phenomena of particular interest were electron capture, photoabsorption and metastable de-excitation. The object of this study was to find a Ne mixture which reduced the recovery time without adversely affecting the efficiency and digitization properties of the detector.

Figure 5.10 shows a schematic diagram of the gas mixing system which was designed for filling a small manifold of flash tubes with samples of different Ne mixtures. A provision was made in the design such that large quantities could be stored in a cylinder at high pressure. Consistent results could only be obtained after cleaning the tubes with concentrated HCL acid and outgassing by heating to 100°C for twenty hours until a vacuum of 10^{-3} Torr could be maintained. Two liquid nitrogen traps were included in the system one to prevent back-diffusion of rotary pump oil vapour, and the other to help remove Ne gas contaminates.

The reignition probability was measured automatically by applying two high voltage pulses after the passage of an ionizing particle and registering the flash tube discharges with a photo-multiplier. Figure 5.11 shows the circuit designed to overcome difficulties in charging a single capacitor system twice in a very short time, thus requiring a large current supply. In this circuit two capacitors are charged simultaneously and then discharged alternately after the passage of a particle, with a predetermined time interval. The time interval between pulses could be varied by a gate generator which provided a delay in one channel from the fanout. Trigertron spark gap switches were used to discharge the capacitors across a resistor R producing a high voltage pulse to the electrodes with an exponential decay constant RC. The gaps were triggered by means of two E.G.G. HV100 5 KV triggering units. The high voltage rise time and delay time after particle detection were 50 and 150 nS respectively. Output information was taken from a photomultiplier placed in line with the tube end windows such that pulses were obtained when the tube ignited. This information was then stored automatically in a scaler which

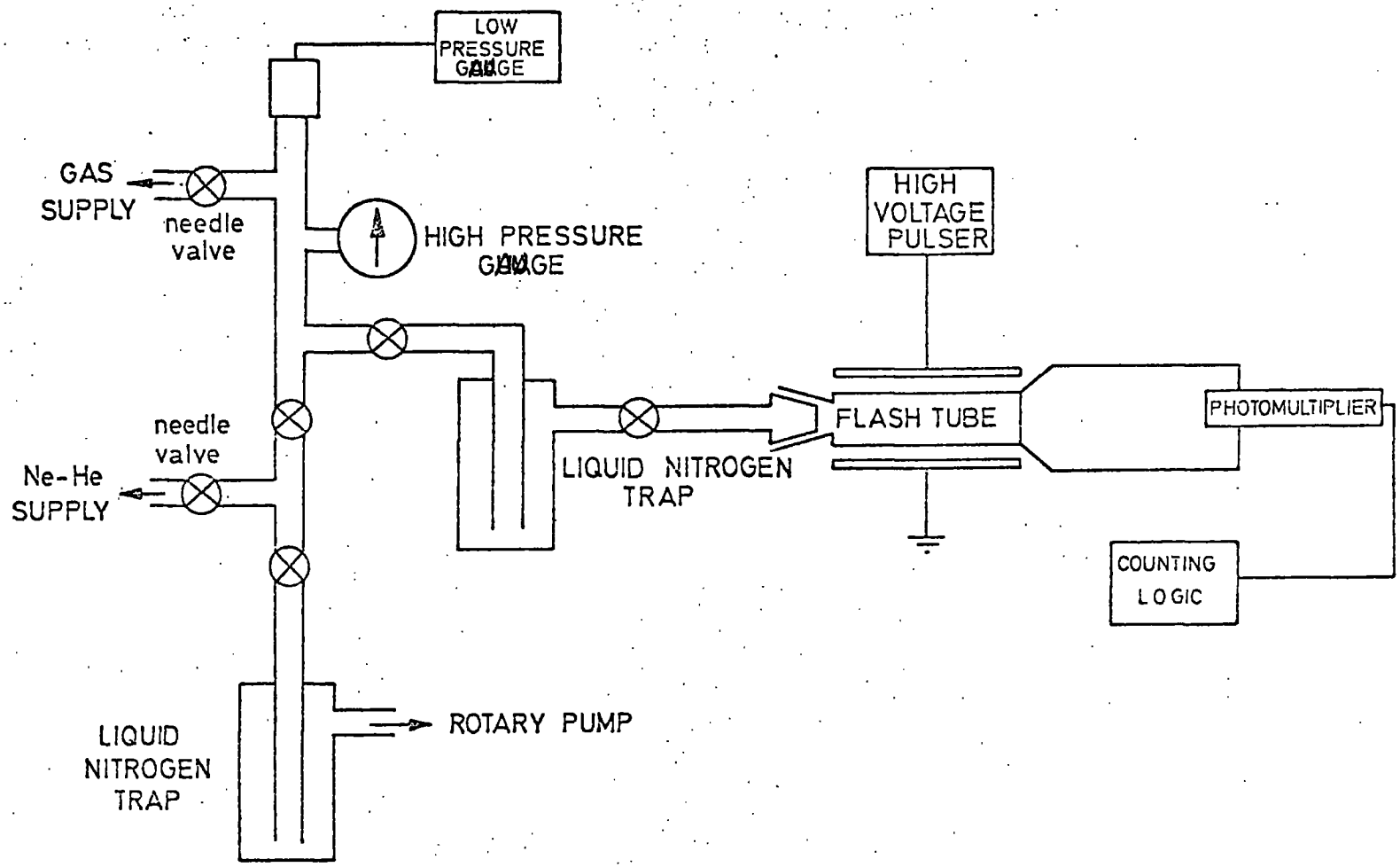

Fig 5.10 the gas mixing and testing system

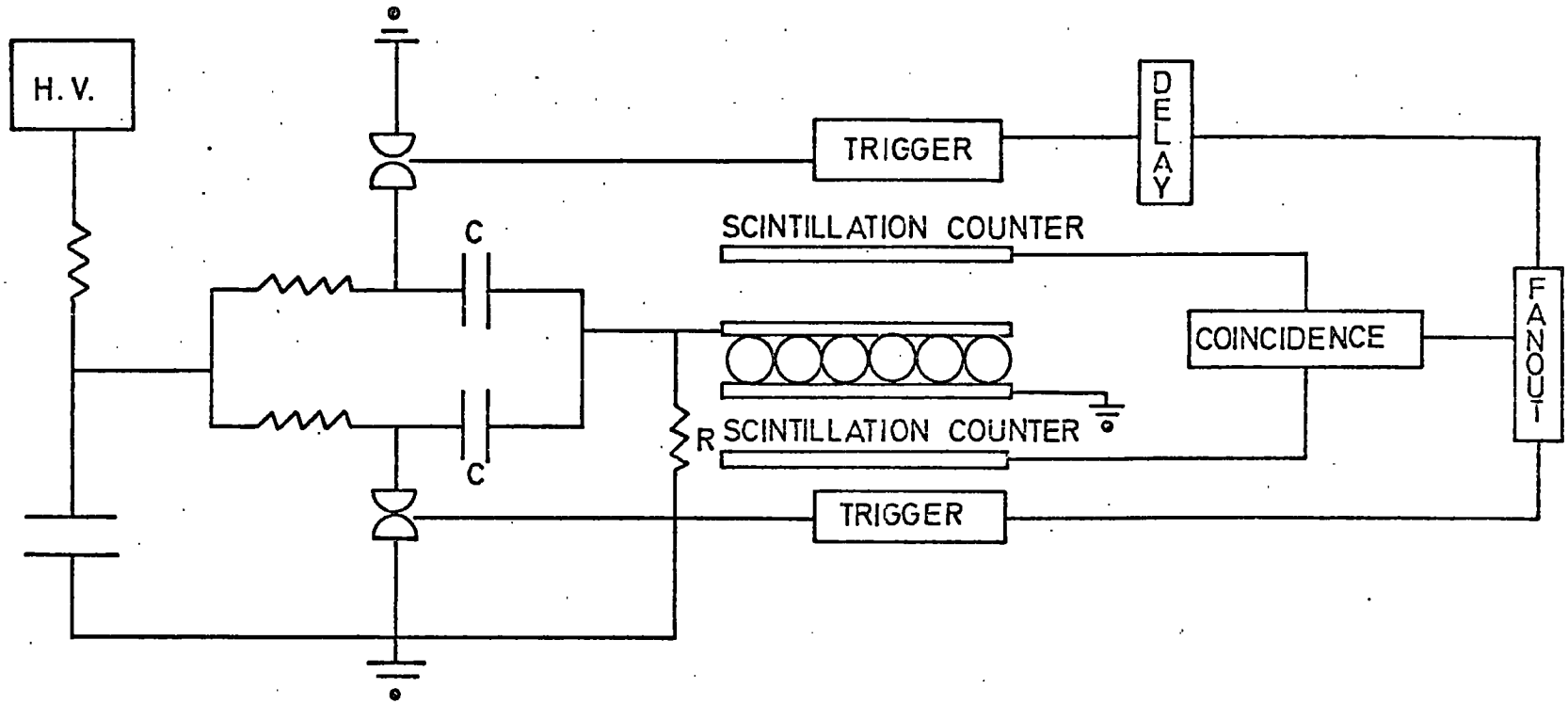

FIG. 5·11 The circuit for double pulsing using spark gaps.

recorded the number of events and the total number of tube discharges, from which the reignition probability was calculated.

Reignition probabilities have been measured for pure Ne and Ne mixtures of other gases. Measurements were first taken with very clean tubes filled with pure Ne (CP grade) to ensure the long recovery time was not a phenomenon caused by contamination in the glass or gas during manufacture. Figure 5.12 shows the reignition probability versus time interval between high voltage pulses as a function of gas pressure. The results at 600 Torr agree well with those taken with manufactured tubes, indicating that the secondary electron mechanism is intrinsic to either the glass or gas. The recovery time versus Ne pressure, obtained from these curves, is plotted in Figure 5.13 and shows a linear relationship with a negative slope. This behaviour excludes a diffusion dominated secondary emission process because the diffusion coefficient increases linearly with decreasing pressure. In terms of a metastable theory, this behaviour is to be expected for it has been shown by Phelps (17) that de-excitation at pressures above 10 Torr is due to atomic collisions and the effect of diffusion to the walls of the container is insignificant. The recovery times are, however, still two orders of magnitude too long, even at 50 Torr compared to lifetime results of other workers in very pure Ne (17), to be explained entirely by a metastable theory. The observed data may be accounted for in terms of the production of photons, created in the residual field after the initial discharge, by weak Townsend avalanches (discussed in section 5.3.1). By this mechanism the long recovery times at low pressures may be explained by considering the increase in the Townsend ionization coefficient (α). For E/P values below 10^{2} V cm^{-1} $torr^{-1}$ the coefficient is described approximately

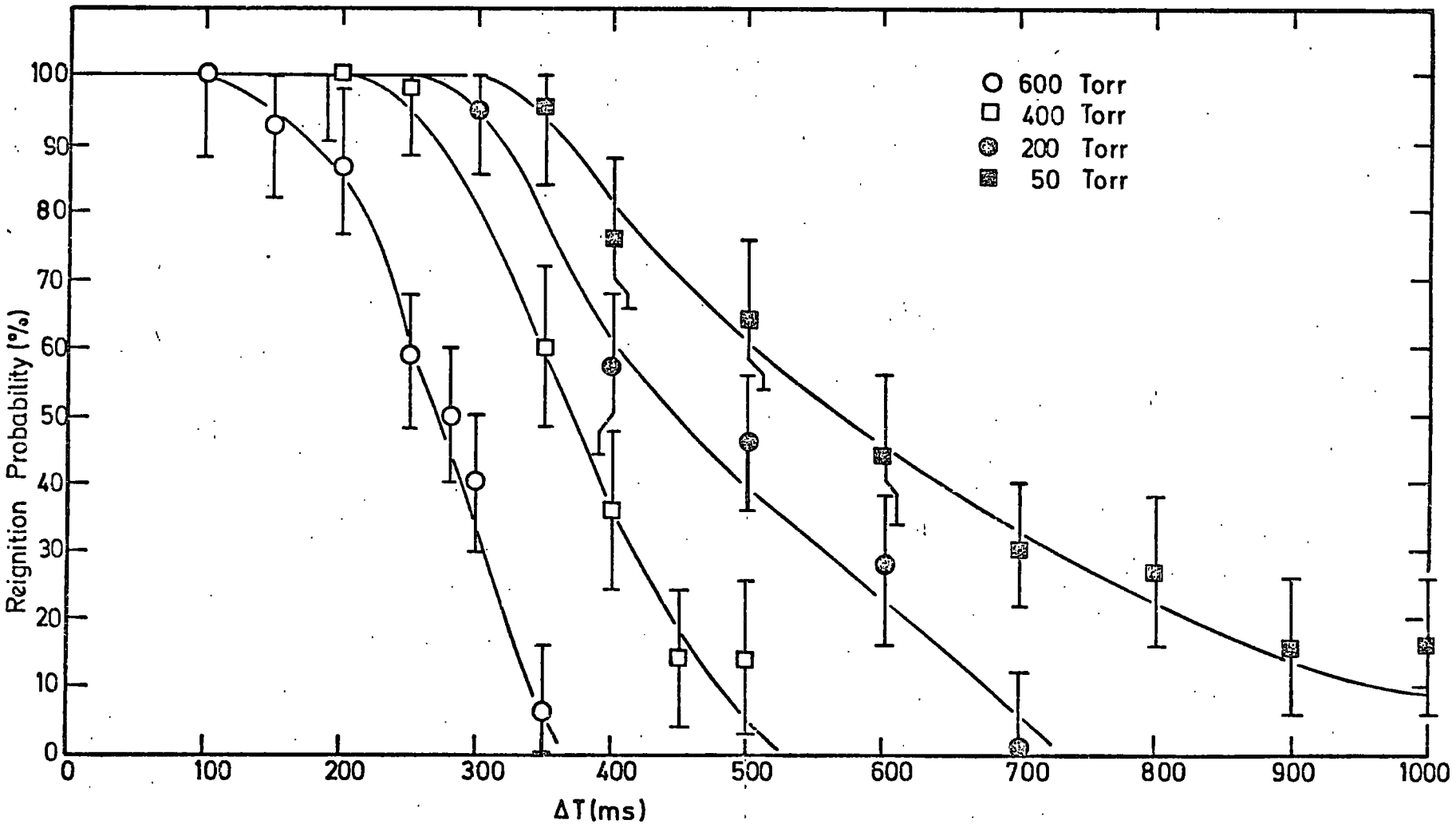

FIG. 5-12. Reignition Probability versus Time Interval for Ne.

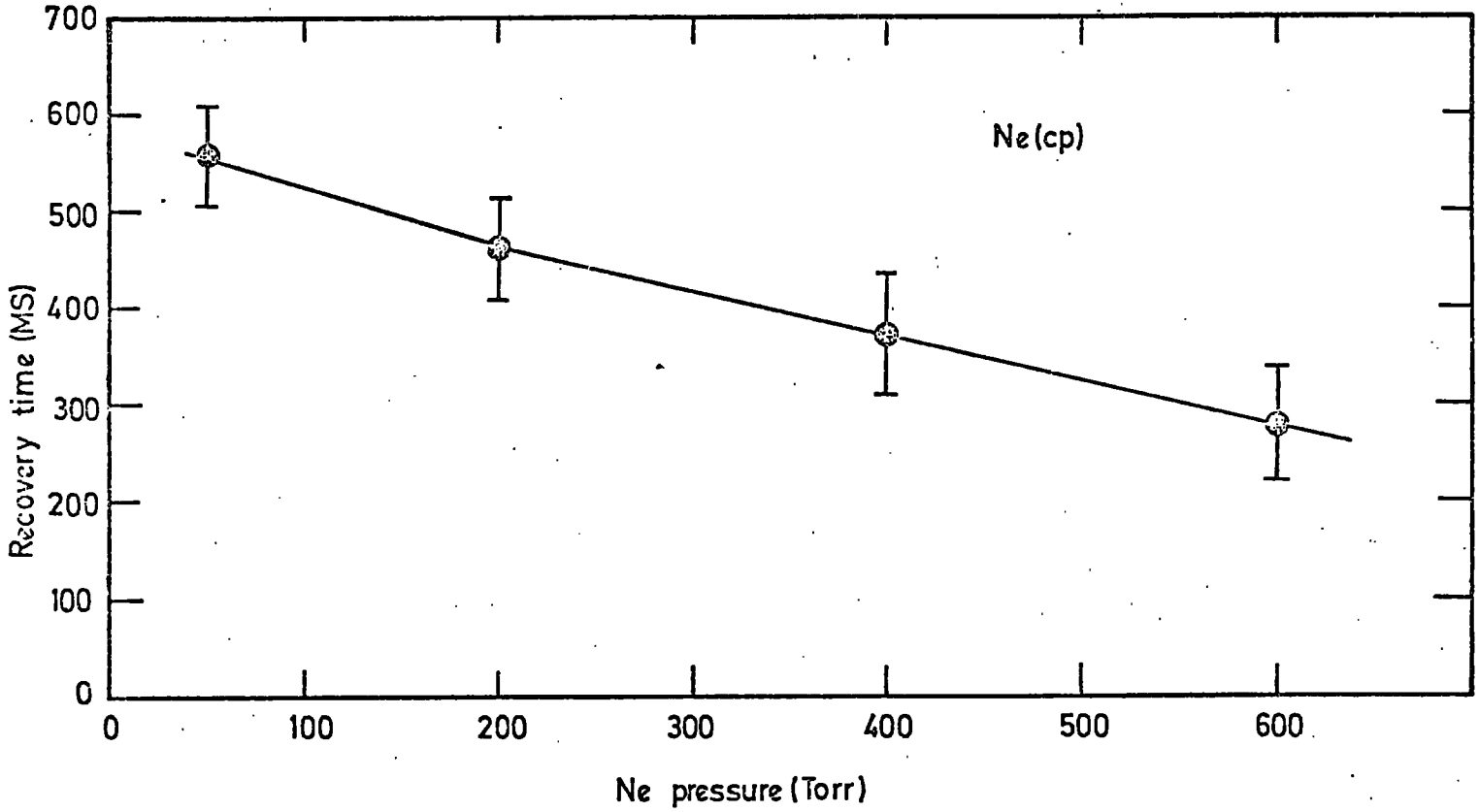

FIG. 5.13 Recovery Time versus Ne pressure

by the equation (12):-

$$\alpha/p = Ae^{-BP/E}$$

where α is the number of ionization per cm per electron

A and B are constants

E is the field strength

P is the gas pressure

Thus, an increase in the number of electrons and photons is expected with a reduction of gas pressure in the range 600 to 50 Torr.

Figure 5.14 shows the effect of mixing 0.1% of the molecular gases H_2,CO_2,O_2,C_2H_6, CH_4 and C_4H_{10} to Ne on the reignition probability versus time interval characteristics at 600 Torr. All the gases are shown to reduce the recovery time in comparison with pure Ne, but it is the organic gases which have the greatest effect, reducing the time by more than an order of magnitude. An interesting feature of these results is that the very electronegative gases of O_2 and CO_2, which are capable of removing electrons from the sensitive volume very rapidly, are not so effective as the organic gases which have relatively small electron capture cross-sections. The organic gases, however, are known to have very high and broad photoabsorption cross-section spectra (22,23) and this may be regarded as further evidence supporting the photon induced secondary electron process discussed in section 5.3.1.

The recovery time characteristics may be improved further by increasing the quantity of molecular gas. In figure 5.15 the reignition probability versus time interval is plotted for quantities of O_2 in the range 0.01 to 0.33%. For 0.33% O_2 a recovery time of about 16 ms is obtained. Increasing the amount of O_2 even further, is made difficult by virtue of its electronegativity,

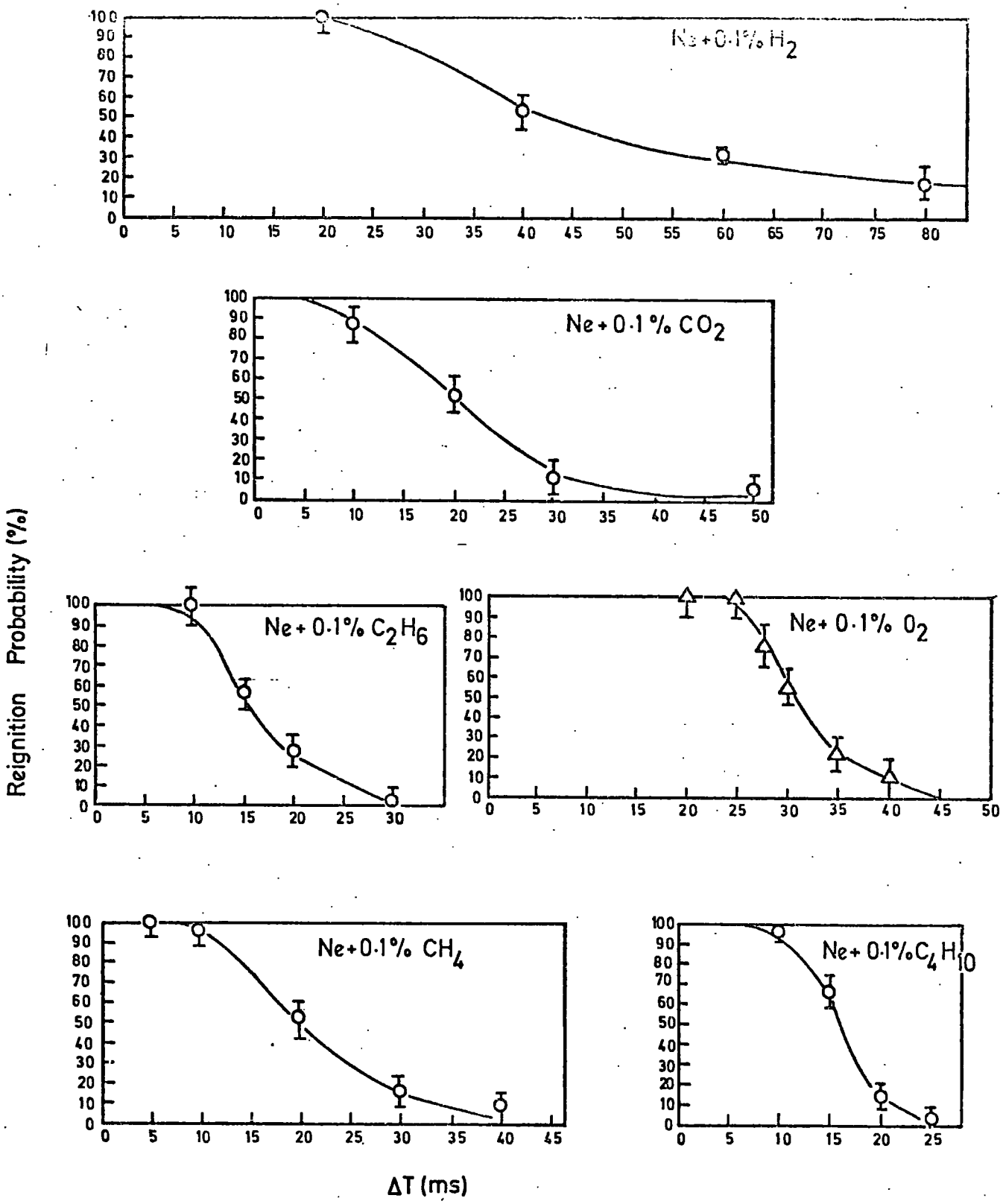

FIG. 5·14 Reignition Probability versus Time Interval for Different Gases.

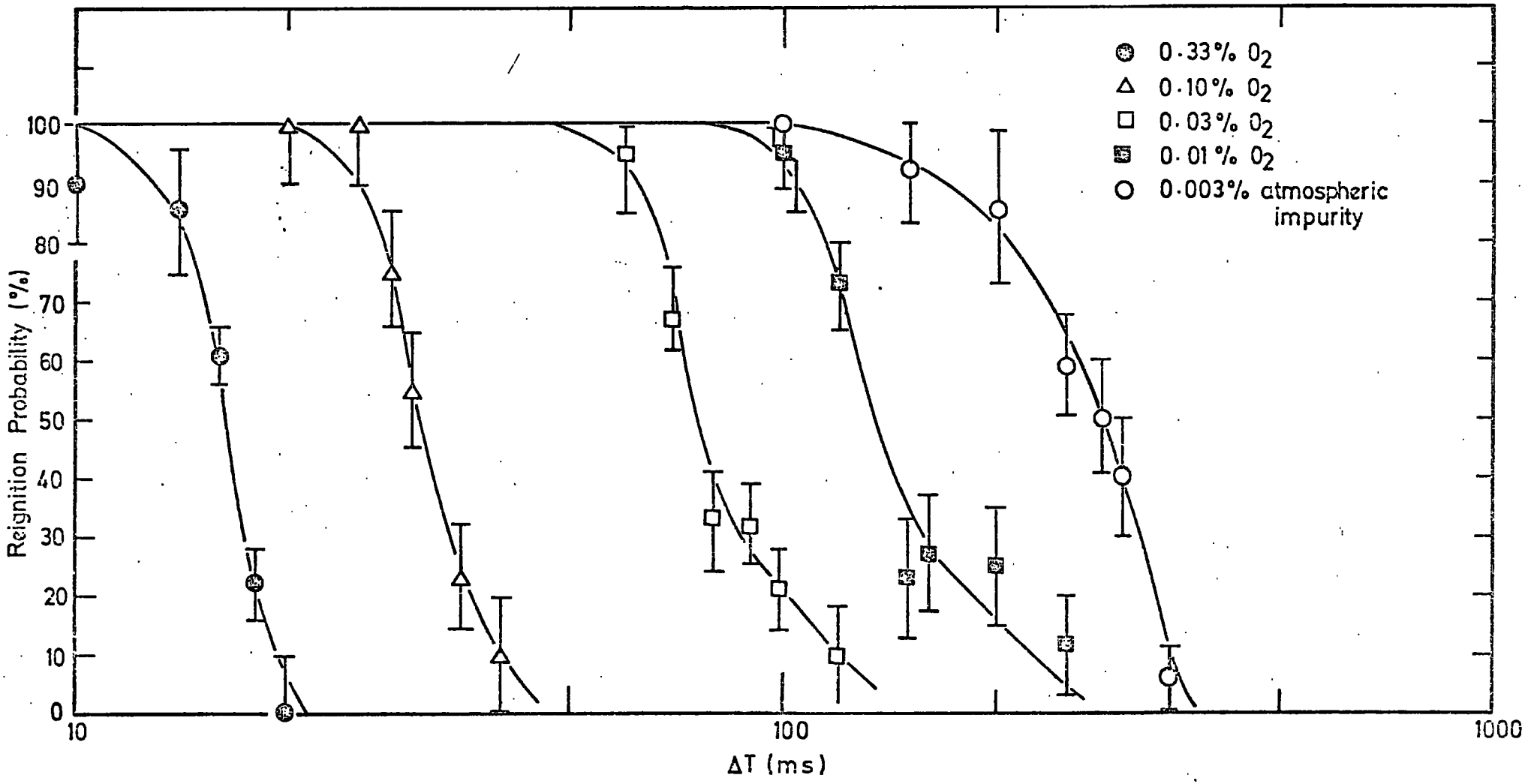

FIG.5·15 Reignition Probability versus Time interval for $N_e + O_2$

which reduces the sensitive time considerably and suppresses the spreading of the discharge along the length of the tube, making operation difficult without the use of very high field strengths. With CH_4, however, up to 2% can be added without altering the operating conditions significantly. Figure 5.16 shows the effect of increasing the quantity of CH_4. With a 1.8% mixture, a recovery time of about 4ms is obtained.

On the basis of these results, sealed flash tubes were made containing varying amounts of CH_4 at different pressures. CH_4 was chosen in preference to other organic gases because of its inexpense and availability. In Figure 5.17 the characteristics of 1.6cm internal diameter tubes, filled with Ne(70)-He(30) + 1.0% CH_4 at 600 Torr are shown. The curve is in good agreement with results shown in Figure 5.16, obtained with the gas mixing system. Smaller tubes filled with different Ne-He-CH_4 mixtures at 2.3 atmospheres, have also been investigated. Figure 5.18 shows the results obtained with 1.0, 1.5, 2.0 and 2.1% mixtures of CH_4, giving recovery times of a few ms or less (24). Tubes made from Jena 16B soda glass containing 2.0% CH_4 have the shortest recovery time ($<$0.6ms), which may be attributed to the resistivity being more than an order of magnitude lower than type S95 soda glass (8). The following table summarizes the characteristics and operating conditions of the different types of Ne-He-CH_4 tubes.

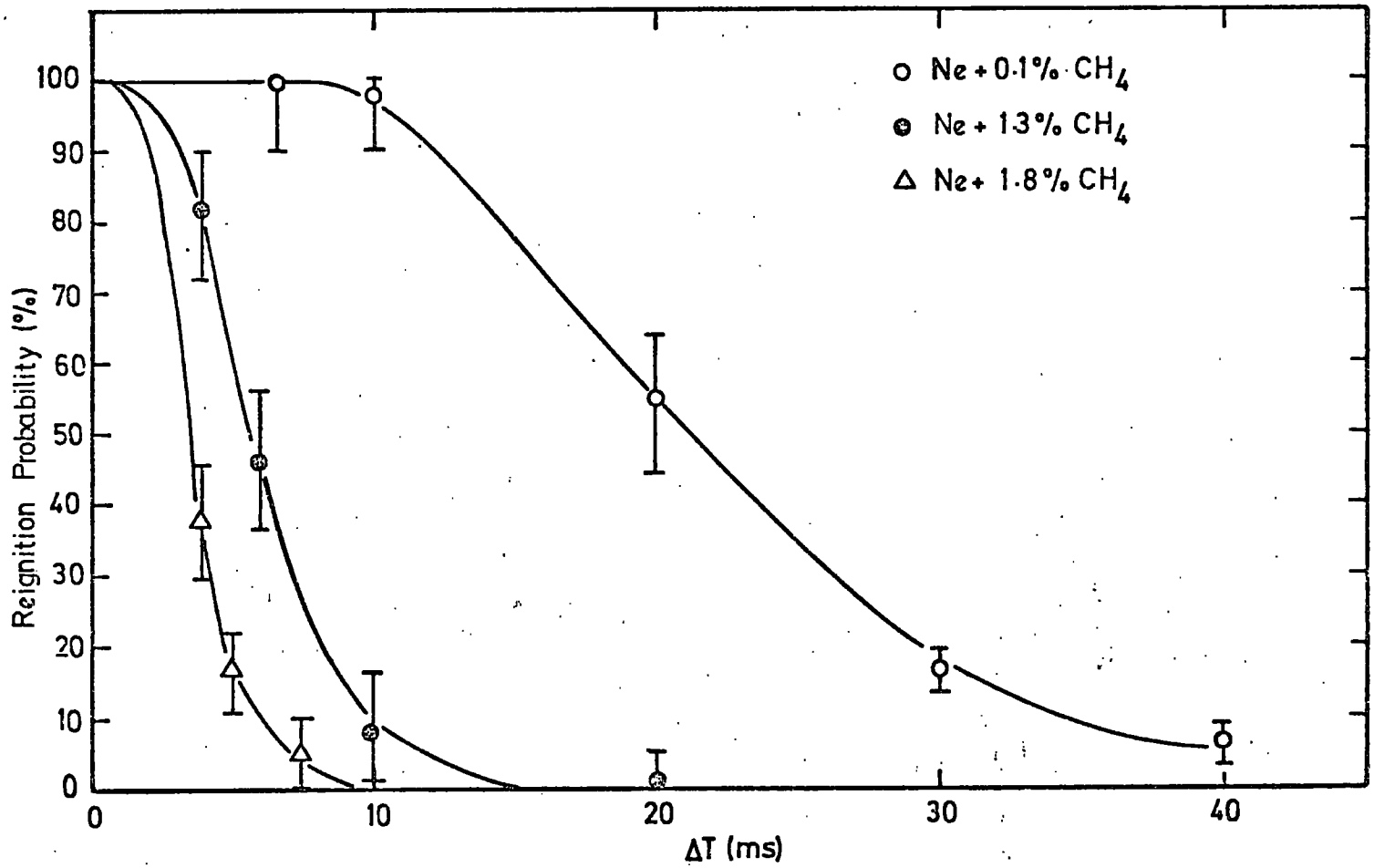

FIG. 5.16 Reignition Probability versus Time Interval for Ne + CH_4

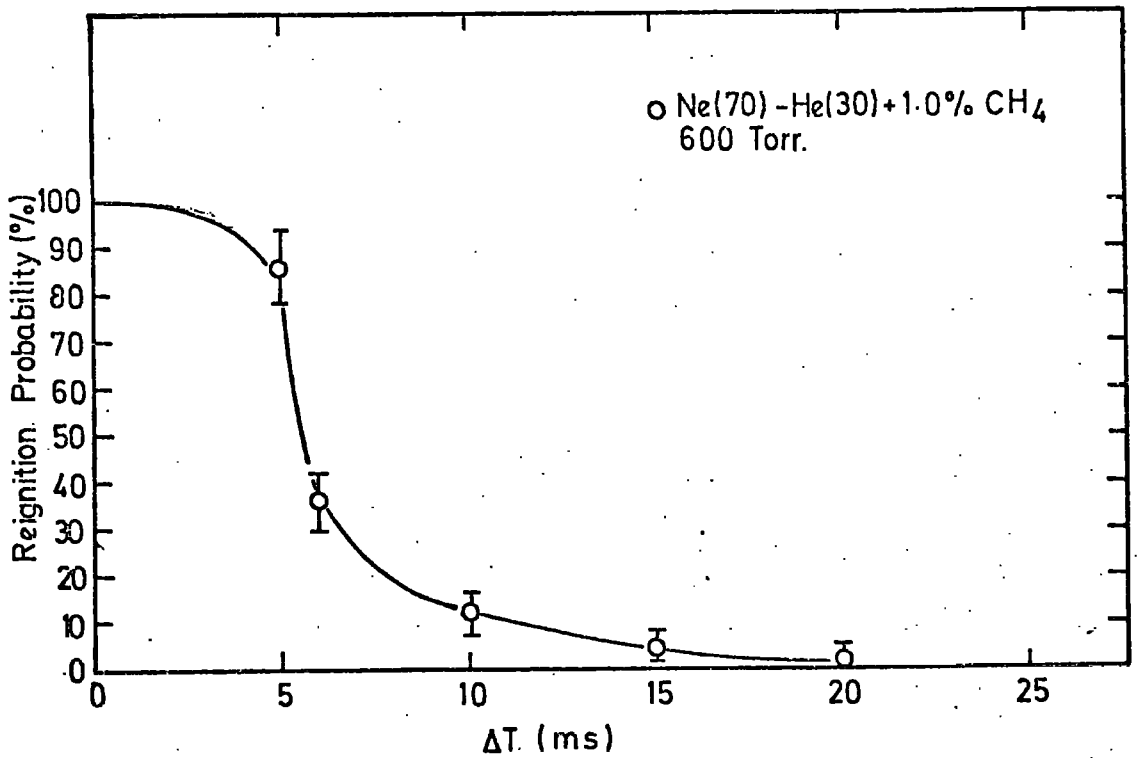

FIG. 5·17. Reignition Probability versus Time Interval for 1·6cm. internal diameter tubes filled at 600 Torr.

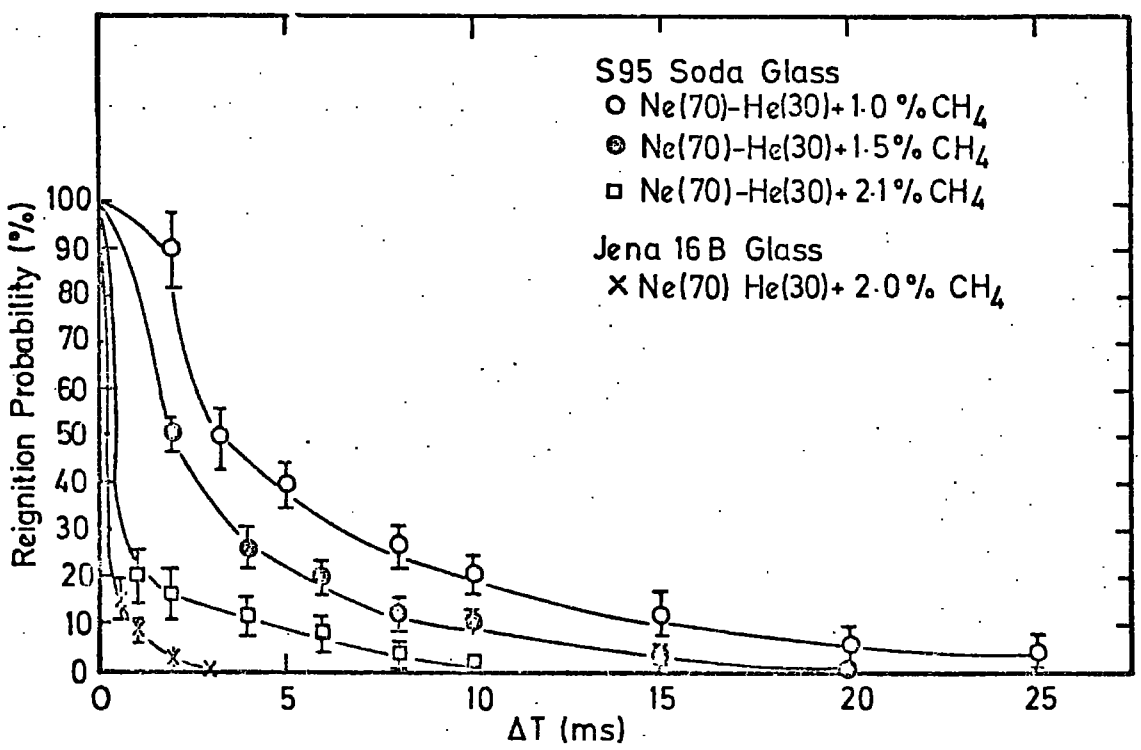

FIG. 5·18. Reignition Probability versus Time Interval for 0·6 cm. internal diameter tubes filled at 2·3 atmospheres.

% CH_4	Tube Size		Glass Type	Recovery Time	Sensitive Time	Pulsed Field	
	Int.Dia (cm)	Ext.Dia (cm)		(ms)	(μS)	Height $kVcm^{-1}$	Length (μS)
1.0	0.6	0.8	S95 Soda	3.3	1.6	10.0	2.0
1.5	"	"	"	2.0	1.4	"	1.0
2.1	"	"	"	<1.0	1.2	"	5.0
2.0	0.82	0.85	Jena 16B Soda	<0.6	1.4	11.0	5.0

5.3.3 Characteristics of Ne(70)-He(30)-CH_4 tubes

The mixing of CH_4 to Ne-He is expected to have some influence on the nature of the discharge which is propagated along the length of the tube. It was, therefore, necessary to ensure that the gas additive had no adverse effect on the working properties of the detector.

One very important consideration is that the detecting efficiency remains high for a time period greater than the delay time of the high voltage pulse. For this reason, the efficiency versus time delay was measured for tubes containing large amounts of CH_4 at high pressure. Figure 5.19 shows the efficiency measurement for high pressure tubes containing Ne(70)-He(30) + 1.0%CH_4. The layer efficiency at delays of a few hundred nanoseconds is seen to be 86% which represents an internal efficiency of 100%. The sensitive time is 1.5μs, which can, if necessary, be reduced further by the application of an alternating clearing field. The effect of a 30V (peak) cm^{-1} square wave clearing field is also shown, giving a sensitive time of 0.5μs. Sensitive time characteristics for other CH_4 mixtures were found to be almost identical to the 1.0% mixture shown in Figure 5.19. Comparison of these characteristics may be made from the table in section 5.3.2.

The efficiency is, however, dependent on the field strength, and efficient detection can only be achieved if the peak electric field is above a certain threshold value. The threshold value is obtained from Figure 5.20 where the layer efficiency is plotted as a function of peak field strength. The layer efficiency plateaus are reached at about 6 and 10 KV cm^{-1} for the low and high pressure CH_4 tubes respectively, using a pulse with an exponential decay time constant of 2 μs. These field strengths are very similar to those required for the efficient operation of normal Ne-He tubes (25,18).

Flash tubes which are capable of operation at repetition rates above 10 Hz are of little use unless automatic digitization is attainable. The effect of adding CH_4 at high pressure on the magnitude of the digitization pulse was, in this respect of concern and has been investigated for tubes of 0.6 cm internal diameter containing 2.1% CH_4 at 2.3 atmospheres. A small test system was constructed with digitization probes as shown schematically in Figure 5.21. The output from the probes was connected into a 5.6KΩ input impedance and the pulse height distribution was measured and recorded with a pulse height analyser. The results are shown in Figure 5.22, giving a spectrum of pulses of more than sufficient amplitude to drive a logic system without amplifier interfacing. The height of the pulses decay exponentially with a decay constant of 4 μs. The pulse heights could be varied by altering the distances x and d as defined in Figure 5.21, or by changing the input impedance.

5.4 Conclusion

The difficulties inherent with normal flash tube detectors for use in accelerator experiments have been investigated and their characteristics substantially improved by the use of alternating

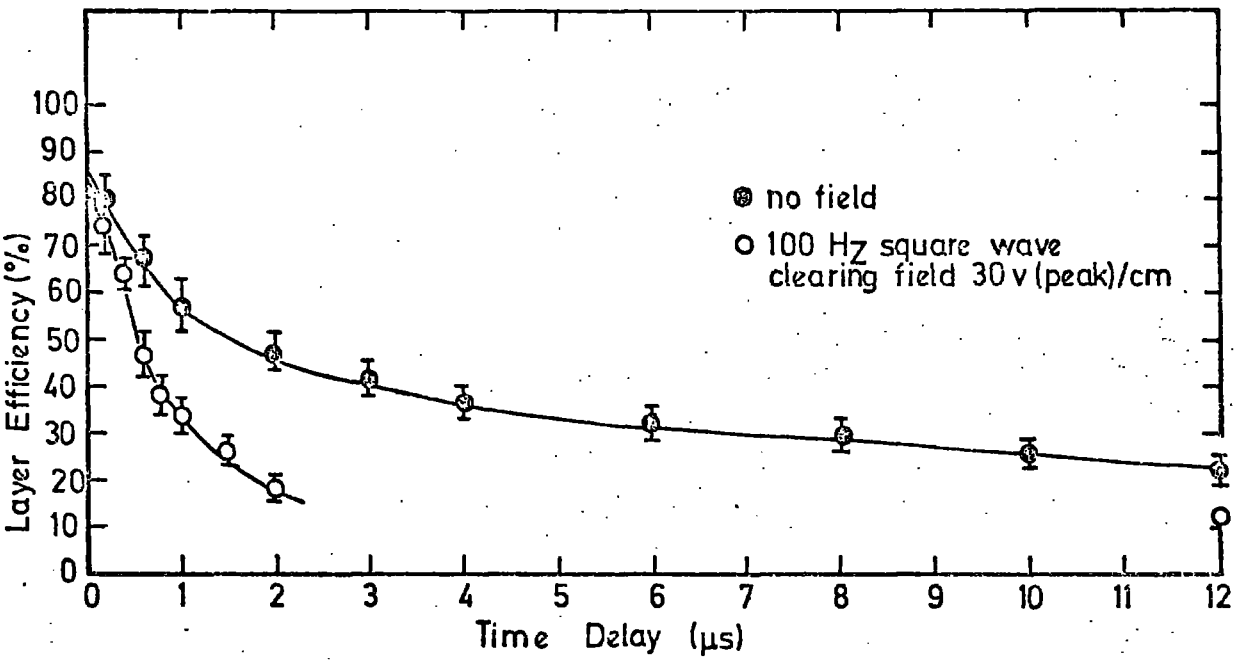

FIG. 5·19. Layer Efficiency versus Time Delay for 0·6 cm. internal diameter tubes filled with Ne (70)-He (30)+1·0% CH_4 at 2·3 atmospheres.

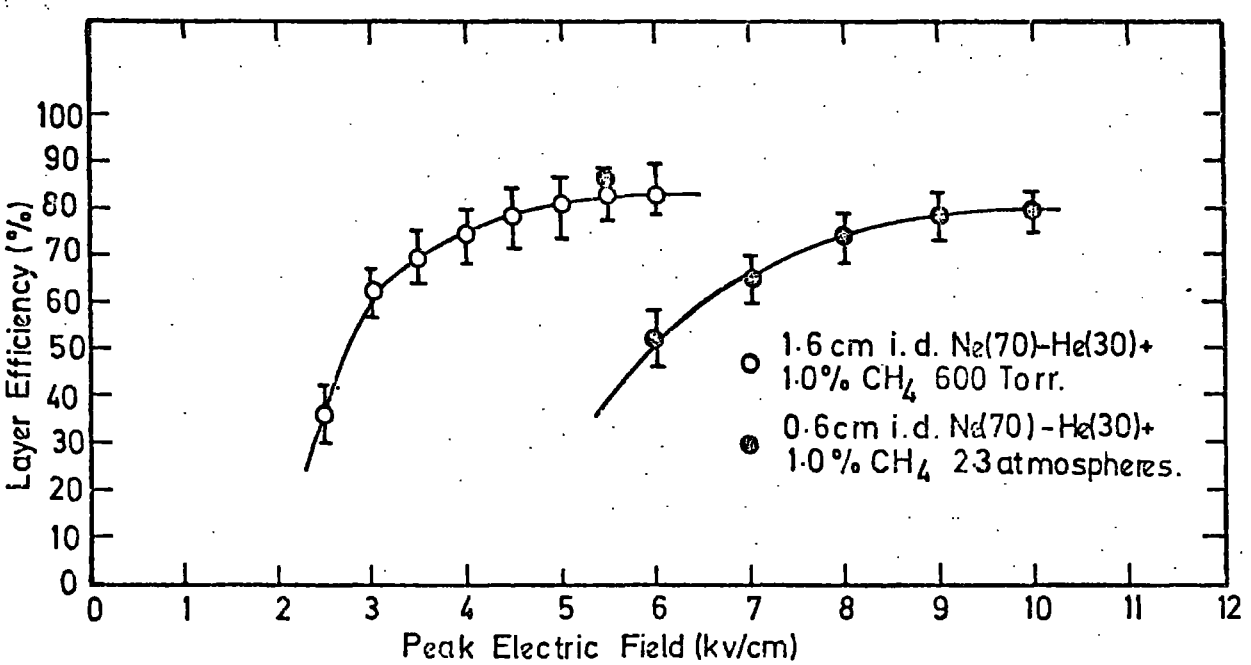

FIG. 5·20 Layer Efficiency versus Field Strength for Ne(70)-He(30)+1·0% CH_4 H.T. RC=2μs

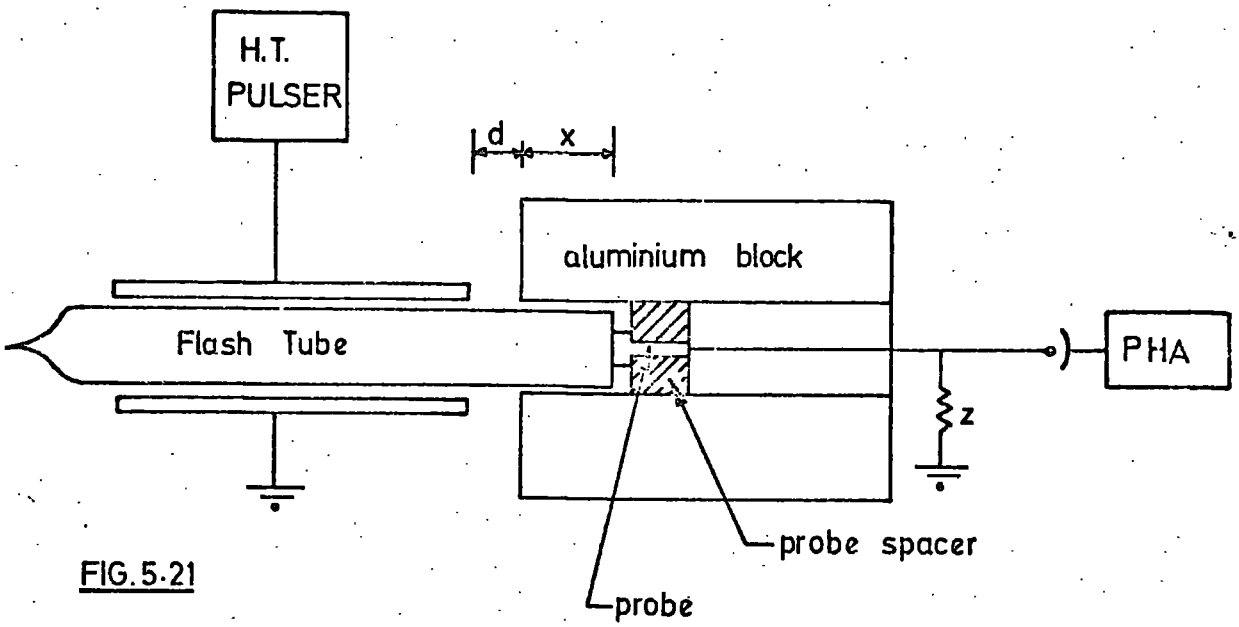

FIG. 5·21

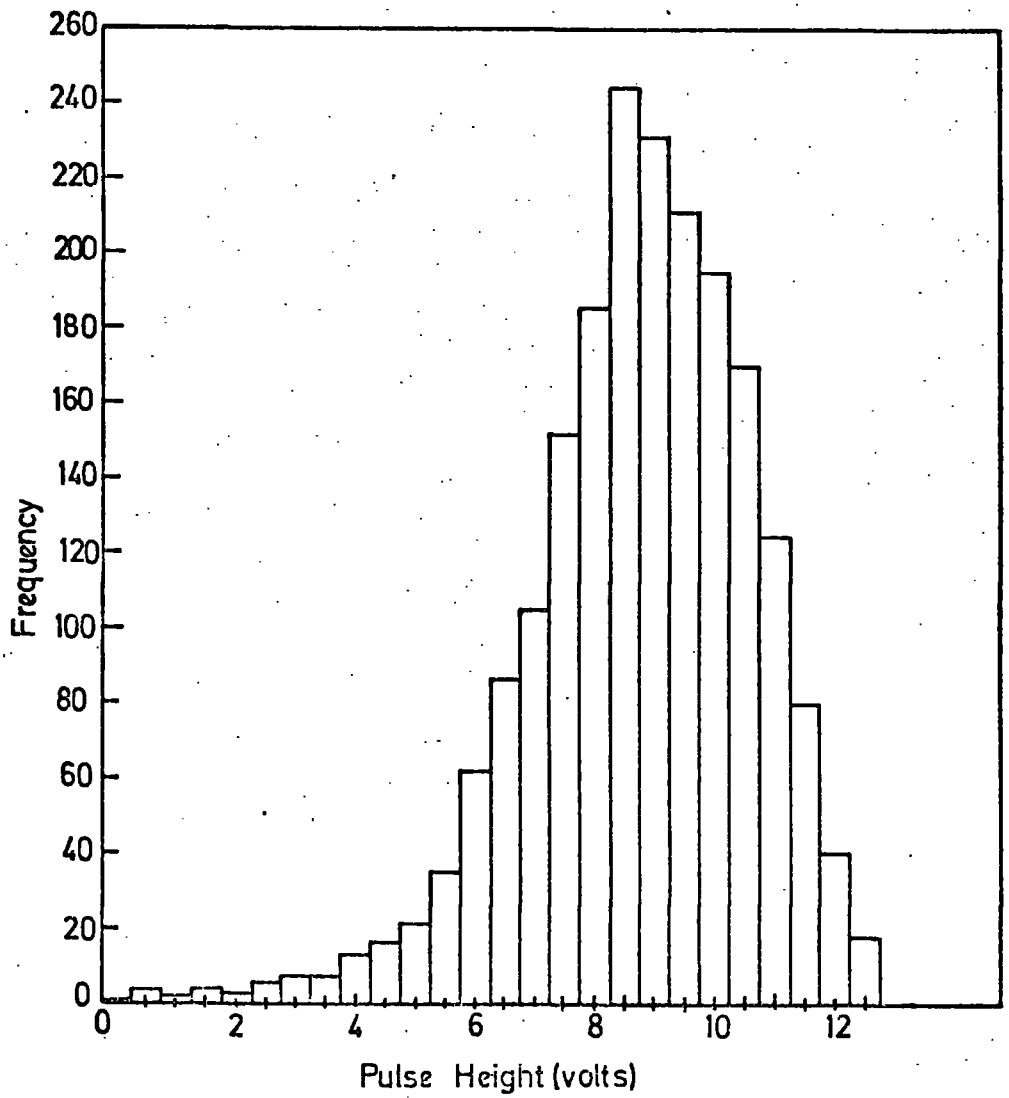

FIG. 5·22. Digitization Pulse Height Distribution for 0·6cm. I.D. tubes containing Ne(70)-He(30)+2·1% CH_4 at 2·3 atmos.
H.T. pulse = 13·8 kv/cm. RC = 5μs.
input impedence = 5·6 kΩ
x = 0·6cm. d = 1·5cm.

clearing fields and the addition of small quantities of molecular gas. Measurements of fast, short sensitive time tubes containing Ne-He-CH_4 mixtures at high pressure have indicated their suitability for operation in a background radiation intensity of 10^5 particle/tube/second and at repetition rates of about 1KHz.

It was not the purpose of this work to make a detailed study of the processes which cause undesirable characteristics in normal flash tubes, although a qualitative analysis has been given in terms of observed experimental data. No conclusive results have been drawn concerning the nature of the long recovery time, but from experimental evidence presented here, it seems very probable that the phenomenon is a result of the high resistivity of the glass, which prolongs the existence of fields inside the tube, thus maintaining weak discharges which are a source of ultraviolet photons. It is possible, that the recovery and sensitive time problems associated with normal tubes may be overcome by methods other than those described here if a low resistivity glass (semi-conducting) could be produced inexpensiviely, with sufficient mechanical strength and malleability to be formed into an envelope. No such glass with these characteristics is known to exist at present, although even if such a material was available, the need for change, in view of the simplicity of the methods described in this work for common soda glass, is hardly justified.

Measurements of the recovery time which have so far been reported, have all been obtained by pulsing the tube after the passage of a particle and then repulsing after a predetermined delay. These measurements do not, however, ensure that the tube retains its high detecting efficiency for recording the passage of a second

particle after the intial discharge. Experiments using a particle beam, were therefore necessary in this respect, before the detector could be considered acceptable for use in accelerator physics.

REFERENCES

1. Hohne, K.H., Schneider, F., CERN AR/Int. GS/63-6 (1963)
2. Schneider F., Hohne, K.H., Nucl. Inst. Meth. 20 (1963) 152
3. Meyer M.A., Nucl. Inst. Meth. 23 (1963) 277
4. Coxell H., Wolfendale, A.W., Proc. Phys. Soc. 75 (1960) 378
5. Fox R.E., Curran R.K., Phys. Rev. 92, (1953) 867
6. Brosco, G., Conversi M., Giovanni M., Nota Int. N422 Dell'Istituto de Fisia dell'Universita di Roma.
7. Holroyd F.W., Breare J.M., Nucl. Inst. Meth. 100 (1972) 429
8. Breare, J.M., Chaney J.E., Disouki W.el., Lightfoot J.A., Proc. Int. Conf. Instrumentation for High Energy Physics, Frascati (1973) 221.
9. Ashton F., Breare J.M., Holroyd F.W., Tsuji K., Wolfendale A.W., Nuovo Cimento Lettres 2 (1972) 707.
10. Phelps A.V., Pack J.L., Phys. Rev. 121, (1961) 798.
11. Lloyd J.L., Proc. Phys. Soc. 75 (1960) 387
12. von Engel A., Ionized Gases. Oxford University Press (1965) 241
13. Allkofer O.C., Spark Chambers, Verlag Karl Theimig K.G., (1969) 53
14. Hagstrum H.D., Proc. Int. Con. Phenomena in Ionized Gases (1971) 193
15. Niehans A., Proc. Int. Con. Phenomena in Ionized Gases (1971) 85
16. Korff, S.A., Electron and Nuclear Counters, Van Nostrad, (1955) 122
17. Phelps A.V., Phys. Rev. 114, (1959) 1011
18. Holroyd F.W., Ph.D Thesis, University of Durham (1971)
19. Rohatgi V.K., J. App. Phys., 28 (1957) 951.
20. Brunining H., Physics and Applications of Secondary Electron Emission, Pergamon, (1954)
21. Holstein T., Phys. Rev. 72 (1947) 1212
22. Wainfan W.C., Phys. Rev. 99, (1955) 542.
23. Walker W.C., J. Chem. Phys. 23, (1955) 1547
24. Disouki W. el., Thesis, University of Durham (in preparation)
25. Rochester, G.D., Proc. Int. Con. Cosmic Rays, Moscow (1960) 312.
26. Brosco G., Thesis, University of Rome (1972).

CHAPTER SIX

THE OPERATION OF A FLASH TUBE CHAMBER IN THE DNPL e^+ TEST BEAM.

6.1 Introduction

Digitized flash tubes containing a Ne-He-CH_4 mixture were built into a detecting array and used with the Daresbury Nuclear Physics Laboratory Accelerator e^+ test beam at energies of a few GeV. The objectives of experiments performed with this chamber were threefold:

(1) To confirm that Ne-He-CH_4 tubes operate at high repetition rates, as indicated by the laboratory results.

(2) To ensure that the detection efficiency is maintained at high repetition rates.

(3) To verify that the digitization technique is compatible with standard computer data acquisition techniques (CAMAC) without the necessity of amplifier interfacing electronics. This required the digitization pulse to remain of sufficient amplitude to drive NIM standard electronics with 50 ohm input impedance after transmission through a substantial length of connecting cable.

6.2 Experimental Arrangement

A modular flash tube chamber consisting of a total of 128 tubes was installed in the DNPL test beam experimental area such that monoenergetic positrons passed through the centre of the system. Each tube was digitized and the output information could be read and stored by a small computer after each event. Counter logic selected single particle events at predetermined repetition rates such that several thousand particle trajectories could be stored at each rate and analysed in terms of efficiency and reignition probability.

6.2.1 The DNPL e^+ Test Beam.

Elements of the DNPL test beam facility in relation to the flash tube detecting system are shown in Figure 6.1. Accelerated electrons are made to impinge on a tungsten target in magnet No. 4 either by perturbing the circulating beam with a pulsed magnetic field ('beam bump') or by simply being scattered onto it after targeting at one of the other stations round the machine ('parasitic beam'). The photon beam, resulting from Bremsstrahlung in the target, is then scrubbed of charged particles by a permanent magnet and secondary collimator. The latter allows the photon beam through to one of several conversion targets, which may be selected remotely from the control room. Electron-positron pairs are then momentum analysed by a bending magnet and fixed momentum defining slit, before emerging through a 50mm square collimator into the test beam experimental area. Monoenergetic ($\pm$ 1.0%) positrons are thus produced between 0.2 GeV/c and the maximum synchrotron operating energy at rates up to 10^4 particles per accelerator pulse (1).

Normally when the test beam is used in beam 'bump' mode only one extraction is made every 60 acceleration cycles. That is, the test beam user receives one particle pulse after every 60 main user extractions. For these experiments, however, fast repetition rates required an extraction every cycle, such that a particle beam was produced every 20mS. The problem was overcome by applying the beam 'bump' magnet pulse just before the main extraction time. With the amplitude of the beam 'bump' pulse suitably adjusted a few particles could be extracted every cycle just before acquiring peak energy in the acceleration time, without seriously perturbing the circulating beam. By this method about 10^2 particles per pulse could be extracted every 20 ms, with approximately 60% of the maximum synchrotron

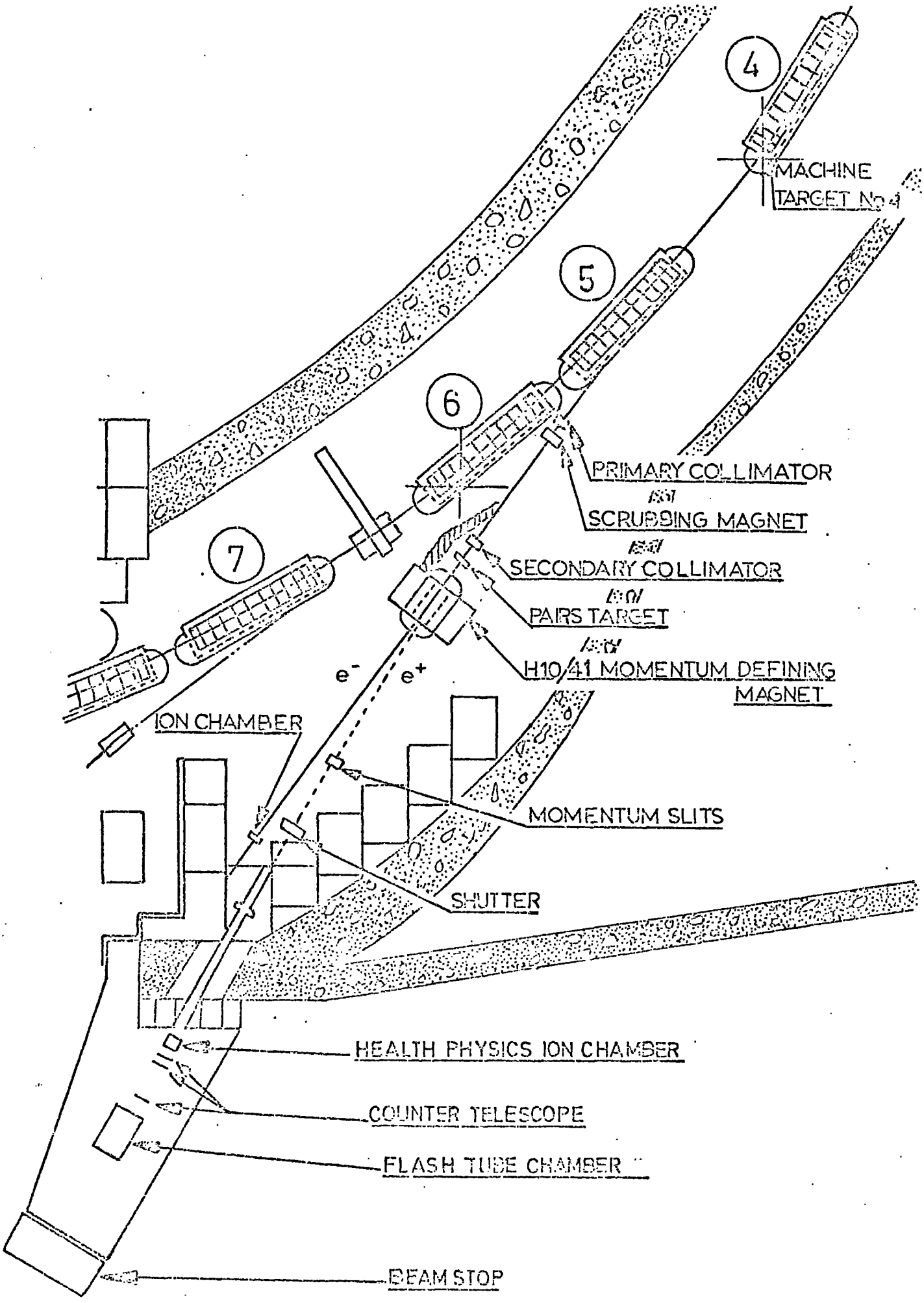

FIG. 6-1. The DNPL e^+ beam line and the Flash Tube Chamber.

operating energy. Figure 6.2 shows the temporal behaviour of the test beam 'bump' pulse in relation to the circulating beam.

6.2.2 The Flash Tube Chamber

The flash tube chamber shown in Figure 6.5, consisted of eight separate, self-contained electrode modules each containing two sets of eight 1.6cm internal diameter tubes. Each set of tubes was positioned in orthogonal X-Y planes either side of a central H.T. electrode, to give a total detecting area of 15.2 x 15.2cm. The separate electrode modules were held in position along the beam line axis by a demountable framework which allowed easy access to any individual section. A space was provided between each module for accommodating up to two radiation lengths of lead target for electromagnetic shower production experiments (discussed in Chapter 7). The tubes were made to fit closely together with digitization probes, into machined aluminium blocks, which provided a support and earth screen against electrical interference from the high voltage pulser. The aluminium blocks were machined such that the tubes were 0.1cm apart. Figure 6.3 shows a photograph of a machined block with its digitization probe assembly.

Digitized output information was obtained from each tube with a small probe made from a 6BA screw, which was placed in contact with the glass tube end window. The probes were held in a central position by perspex spacers, which were made to be a close fit in the machined hole. A 2.2KΩ resistor joined the probe to a 50Ω BNC coaxial output socket (see figure 6.3) which provided a digitization system totally shielded from external electrical interference. This was important, in view of the high voltage pulser being a distance less than a meter from the probe outputs. Figure 6.4 shows the dimensions of the H.T. electrode and probes, relative to the face of the machined

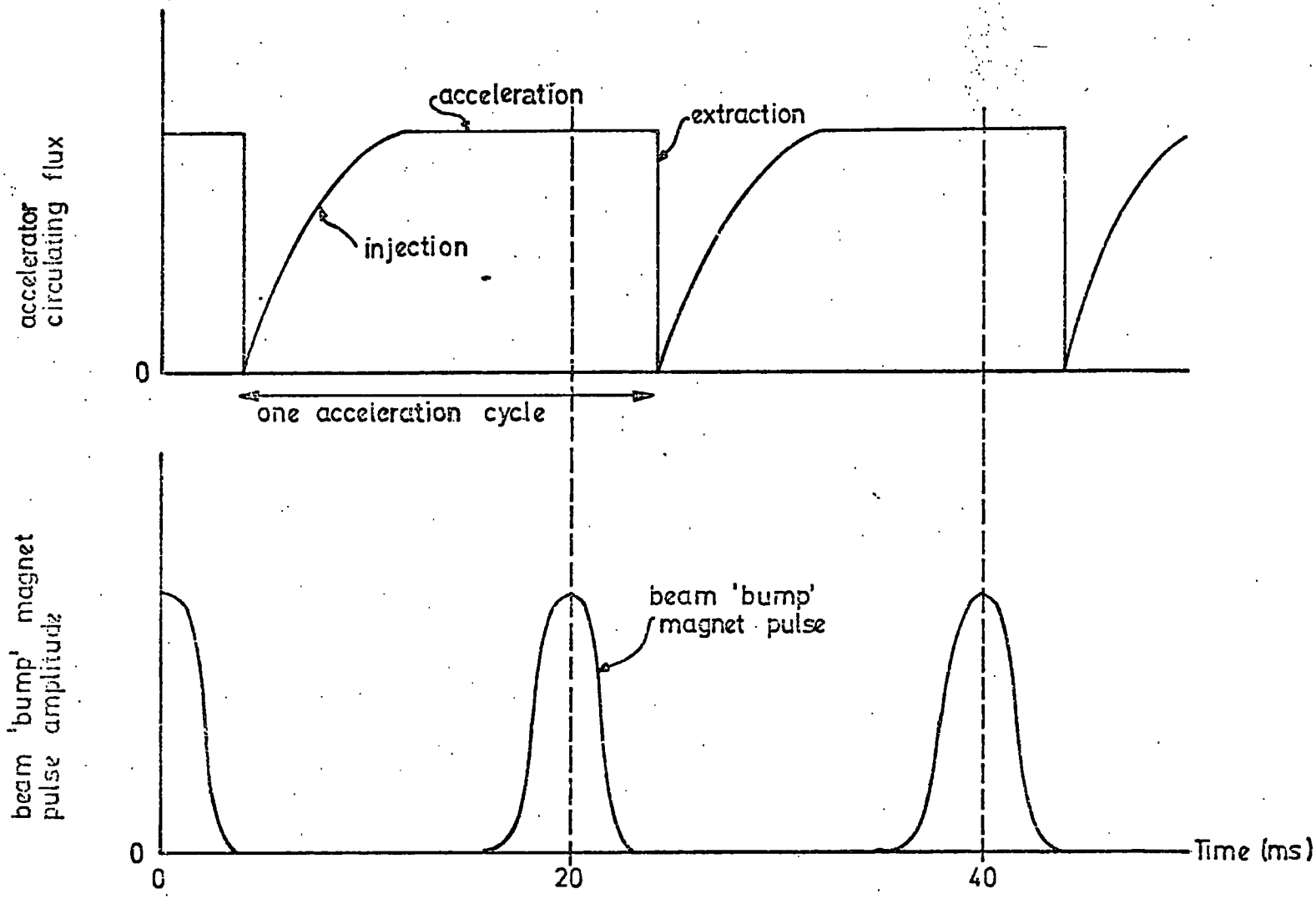

FIG. 6·2. The temporal behaviour of the beam ('bump') extraction pulse.

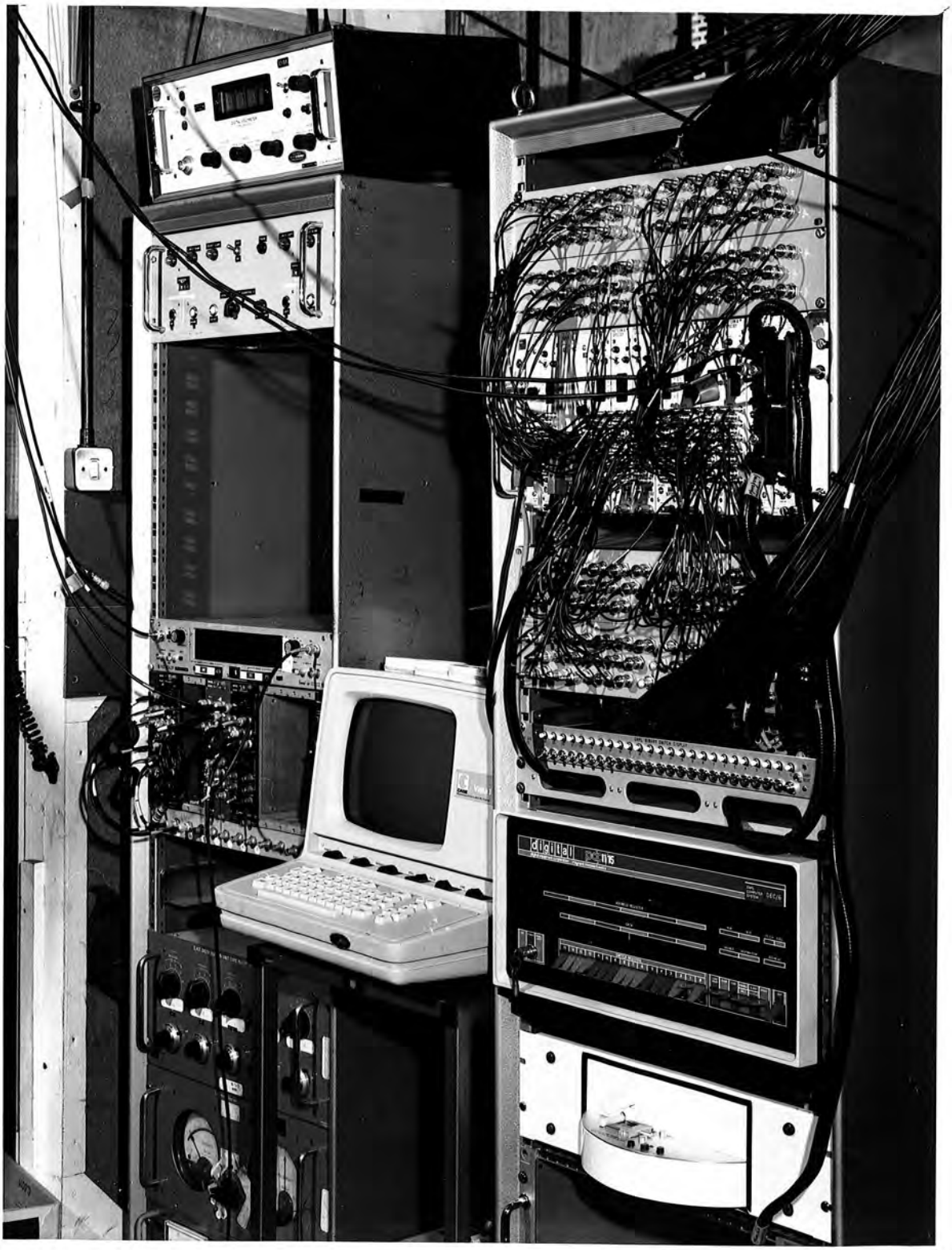

PHOTO DNPL

Fig. 6.3 The flash tube digitization probe assembly

(a)

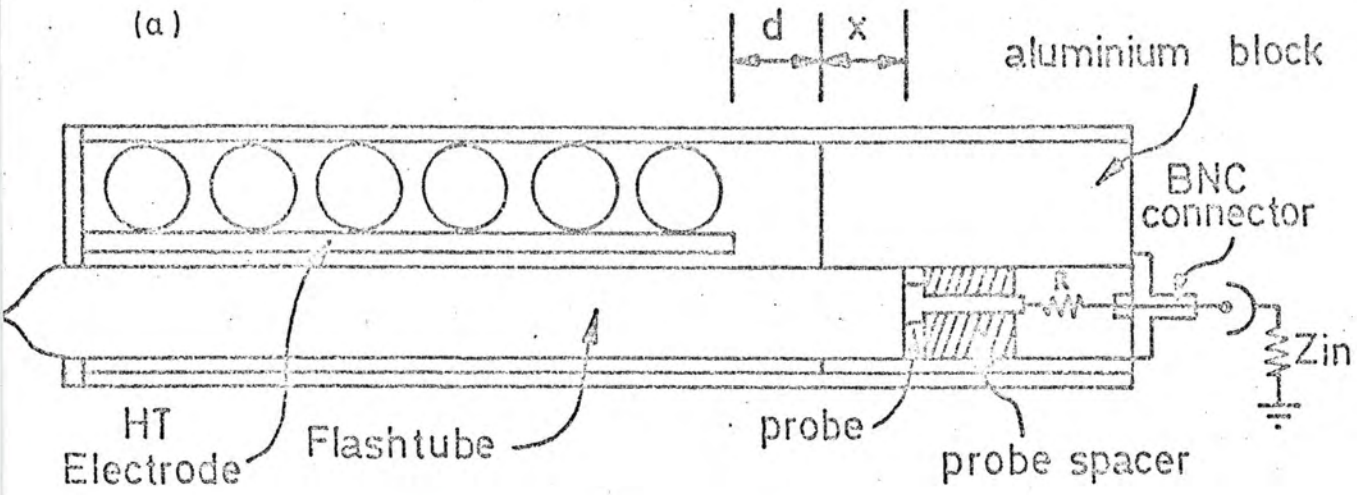

(b)

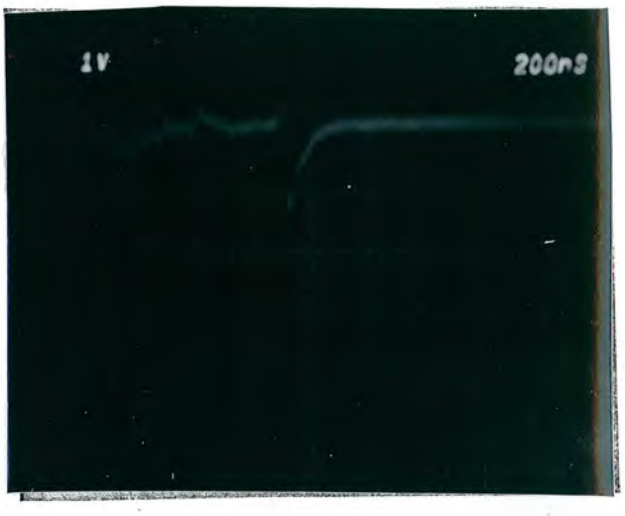

(c)

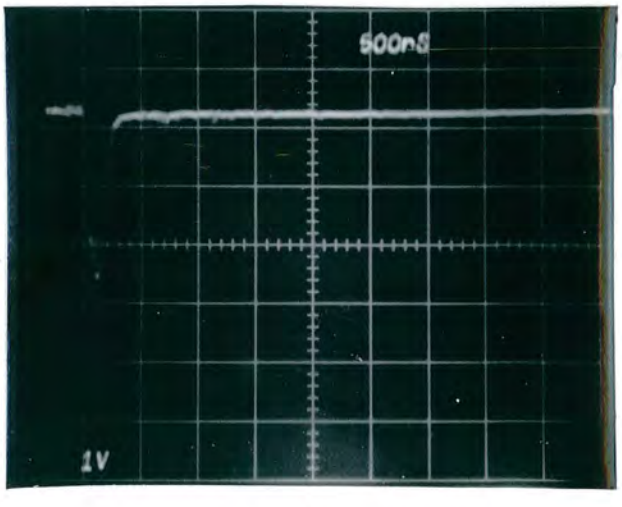

FIG. 6.4. Flash Tube Digitization.
a. the probe system
b. the digitization pulse into 50 Ω impedence
c. the light pulse observed with a photomultiplier

aluminium block, which gave an output pulse of suitable magnitude to trigger the CAMAC logic after transmission through 13ft of 50ohm coaxial cable. A digitization pulse with amplitude 1.2 volts and 100ns exponential decay time (see Figure 6.4) was obtained with d = 3.0 cm, x = 1.5cm, R = 2.2KΩ and Z_{in} = 50Ω , as defined in Figure 6.4a. Amplitude fluctuations amounted to ± 20%, which was acceptable with a CAMAC 700mV input trigger threshold level (3). Output pulses were taken from the probes through 13ft of 50 ohm doubly screened coaxial cable, without electronic amplifier interfacing, and fed directly into eight 16-bit CAMAC Pattern units (16P2007), where the information was stored in addressed registers before being read by a PDP 11 computer. Figure 6.5 shows a photograph of the complete chamber with output cables leading to the CAMAC data acquisition system.

The high voltage pulse was generated by discharging a 6000 pf capacitor across a 330 Ω resistor, thus producing a 6KV cm^{-1} peak electric field with a 2.0μs exponential decay time. The capacitor was discharged by switching a trigertron spark gap (2) driven by a EGG HV 100 pulsing unit. The total delay and rise times of the high voltage pulse were measured to be 250ns (from the scintillator coincidence) and 60ns respectively. The high voltage power supply was capable of supplying adequate current to recharge the 6000pf capacitor within the shortest cycling time of 20ms. The recharging time constant was made to be 7ms with a charging resistor of 1.2MΩ giving a maximum current drain of 10 mA. A square wave 100Hz alternating clearing field of 30v cm^{-1} was also applied to the electrodes using a reed switch as described in section 5.2.2. This produced a train of square pulses with a leading edge rise time of 100 μs.

The flash tubes were made from type S95 soda glass of 1.6cm internal diameter, 0.1 cm wall thickness, and filled with Ne(70)-He(30)

Fig. 6.5 The flash tube chamber

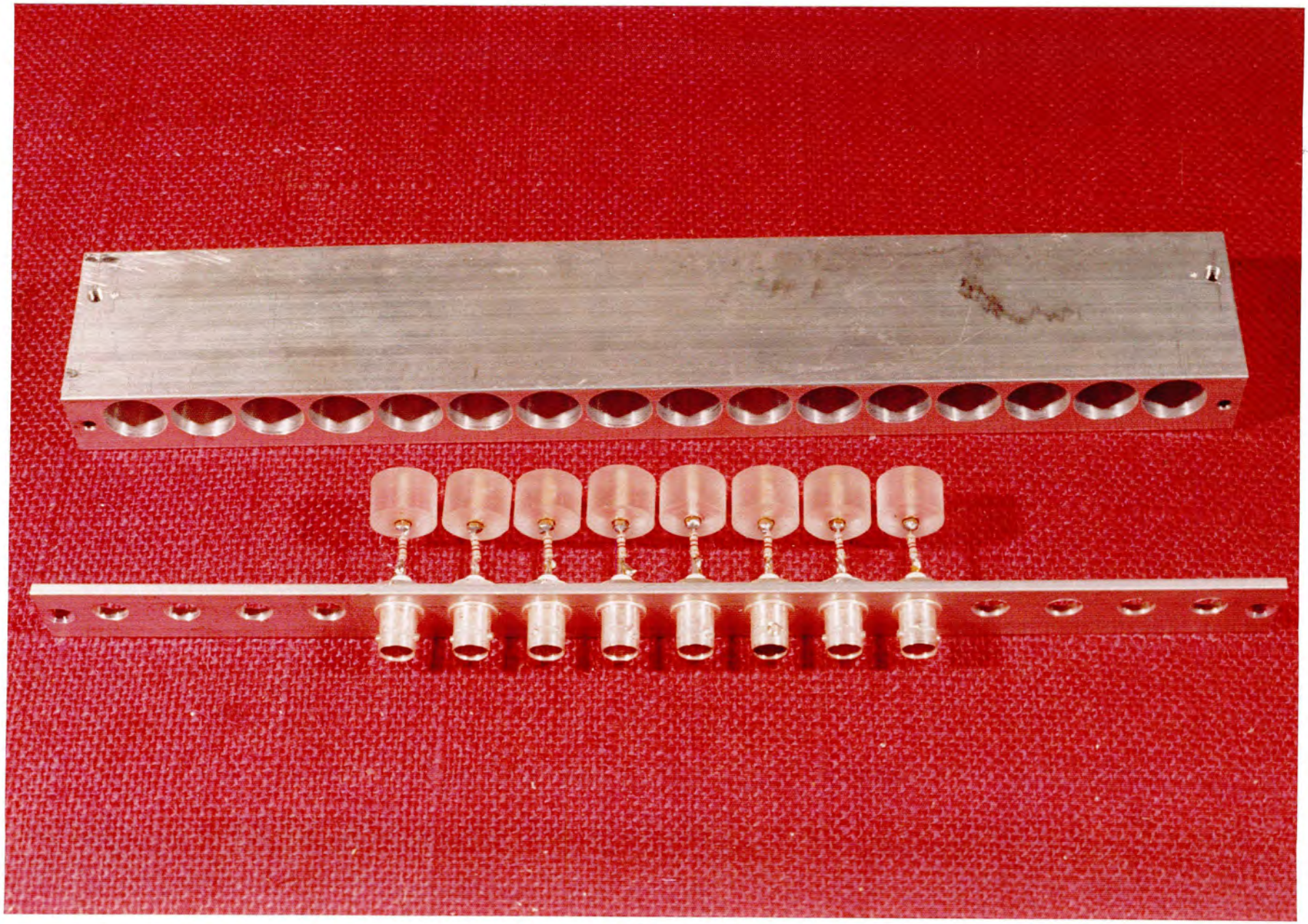

plus 1.0% methane at 600 torr pressure. The characteristics of these tubes were measured before the experiment and were found to be in agreement with measurements made with the gas mixing system, described in section 5.3.2. Figure 6.12 shows the layer efficiency versus time delay characteristics with the application of a 30v cm^{-1} square wave clearing field, giving a sensitive time of 1.0 μs and layer efficiency (at zero time delay) of 82%. Figure 6.13 shows the reignition probability versus time interval characteristics, giving a recovery time of 7ms.

6.2.3 Data Acquisition

Particle events were selected by a coincidence trigger from three beam defining scintillation detectors placed before the flash tube chamber, as shown in figure 6.6. Upon the passage of an e^+ particle, a coincidence signal was generated if certain conditions were fulfilled by a controlling logic system built with E.G.G. modular electronics. This signal was then used to trigger the high voltage pulser and provide a computer interrupt command which initialized a data processing subroutine program. The logic system, besides producing triggering signals, had five other important functions which are described below.

(1) The only particles selected were those extracted during the beam 'bump' pulse. This substantially reduced the number of spurious triggers from background radiation and ensured that the particle detection occured at the same instant in each cycle. For this purpose the extraction pulse was used to trigger Gate 2 (Figure 6.6) such that the AND was 'enabled' for a period of 2ms.

(2) Only one particle from each beam extraction in every accelerating cycle was selected. This prevented the high voltage pulser triggering on every particle within a beam

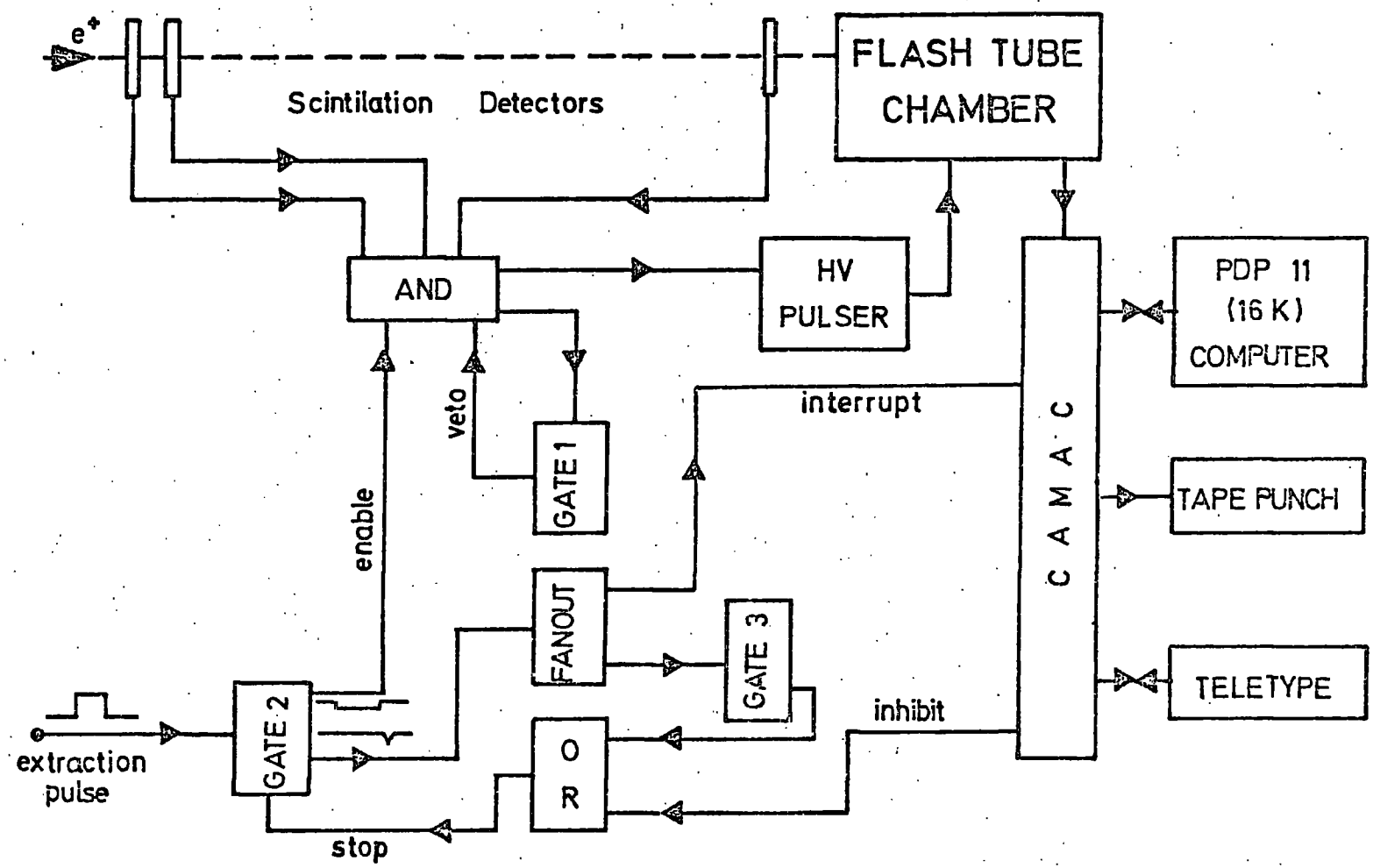

FIG. 6·6 THE DATA ACQUISITION SYSTEM

'bump' extraction period. Thus, only the first particle was recorded from each bunch of particles. This condition was achieved with Gate 1 which provided a coincidence veto pulse for a duration greater than the beam spill time after a detected event.

(3) The event repetition rate could be set to be any integral number of accelerating cycles. That is, a particle could be selected every 20, 40, 60 ....ms, etc. The rate was selected by Gate 3 which applied a stop pulse of length equivalent to a predetermined number of cycles.

(4) The CAMAC data registers were read at the end of every preset time interval regardless of particle information being present. This provided the information necessary for distinguishing whether events were consecutive or not, within the predetermined repetition rate.

(5) The pulsing system was paralysed, while the computer was processing data, by applying a 'stop' pulse to Gate 2. This pulse was generated from a CAMAC inhibit pulse via an OR gate.

Thus each event was selected by the logic system at a set repetition rate, and the trajectory data stored in eight 16-bit CAMAC storage registers (Pattern units type 16P2007). This information was read, after each event, into the memory core of a PDP 11 (16K) computer in eight 16-bit words until the core was full, where upon the system was paralysed, until all the data had been transferred to punched paper tape. In this way, 200 consecutive events could be stored in the computer at a time. The computer program was written and controlled by means of a teletype visual display terminal which could also be used to display data after collection. Figure 6.7 shows a photograph of the computer, teletype, and CAMAC. The computer

Fig. 6·7 The data acquisition system consisting of a PDP 11 computer, teletype and CAMAC electronics

PHOTO ANPL

program which controlled the CAMAC and data acquisition is described in detail in Appenix III.

6.3 Experimental Procedure

The object of this experiment was to accumulate enough particle trajectory data at known repetition rates for analysis in terms of detecting efficiency and tube recovery time.

During the preliminary tests with the chamber several data acquisition problems were encountered which had to be overcome before any reliable data could be taken. Most of these problems were a result of severe electrical interference caused by the high voltage spark gap radiating high frequency noise. This produced spurious operation of the computer and logic, although difficulties were expected, due to the high voltage pulser being not more than two meters distance from the data acquisition system. Normal operation could only be attained after taking several precautionary measures against the interference; the spark gap pulser was totally enclosed in a metal box, the computer and logic power supplies were fitted with high frequency mains filters, earth loops to and from the logic system were minimized and a heavy copper earth return lead was connected to the high voltage power supply. Similar problems were experienced in some channels of the CAMAC storage registers (Pattern units) where spurious input pulses triggered false logic levels. This was found to be caused by 'cross-talk' interference between some coaxial cables connecting the chamber outputs to the CAMAC inputs and was overcome, very simply, by replacing the cables with double screened 50Ω coaxial cable.

For the recovery time experiment is was necessary for the incident beam to be not so finely collimated that all particles passed along the same trajectory, making a reignition probability determination impossible. By selecting suitably sized coincidence scintillation

detectors and using the largest collimator aperture, it was possible for particle trajectories to be recorded at random positions across the detecting area of the chamber. Thus, the probability of consecutive tracks having the same trajectory in the chamber was minimized.

Over 700 events were recorded at each fixed repetition rate in the range 5-50 Hz, in a beam of momentum 2.0 GeV/c. Data was written directly from the computer store onto paper tape which was later transferred to magnetic disc for analysis.

6.4 Experimental Results

Computer programmes were written to analyse straight track data in terms of detecting efficiency and reignition probability using the DNPL IBM 360/165 computer.

6.4.1 Efficiency

The detecting efficiency was calculated for the chamber and each module independently, as a function of repetition rate. Figure 6.8 shows a graph of the overall chamber layer efficiency versus the time between events. From this graph it is clear that there is no deterioration in efficiency with increasing repetition rate. The layer efficiency is maintained at about 80%, which agrees well with the value of 82% which would be obtained for an internal efficiency of 100%. In Figure 6.9 the layer efficiency is plotted for each of the eight modules independently, at the fastest repetition rate of 50 Hz. Again, the layer efficiency is seen to remain high in all modules, never falling below 70%.

6.4.2 Reignition Probability

The reignition probability was measured by counting the total number of tubes which reignite from the previous event as a fraction of the total number of ignitions. Figure 6.10 shows the mean

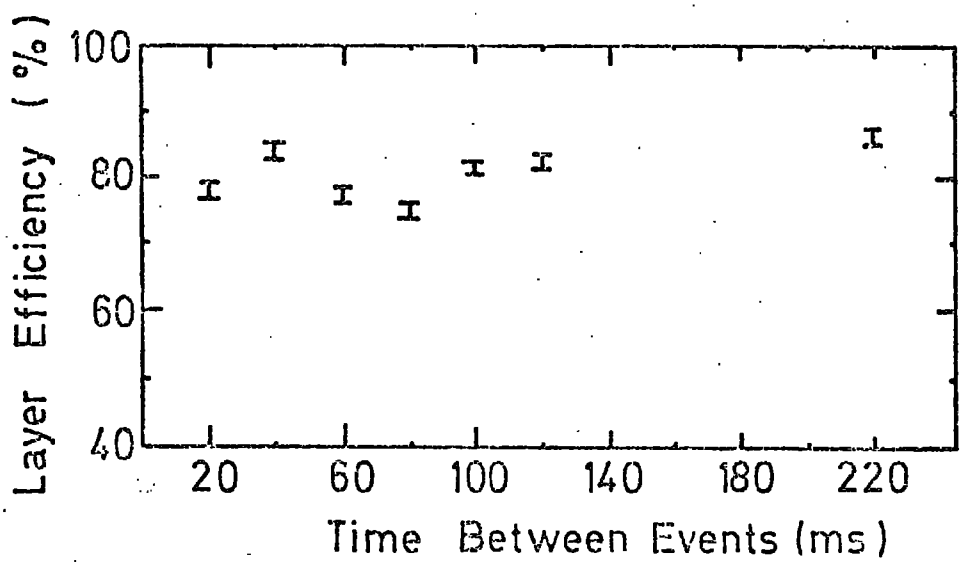

FIG. 6-8. Layer efficiency versus time between events.

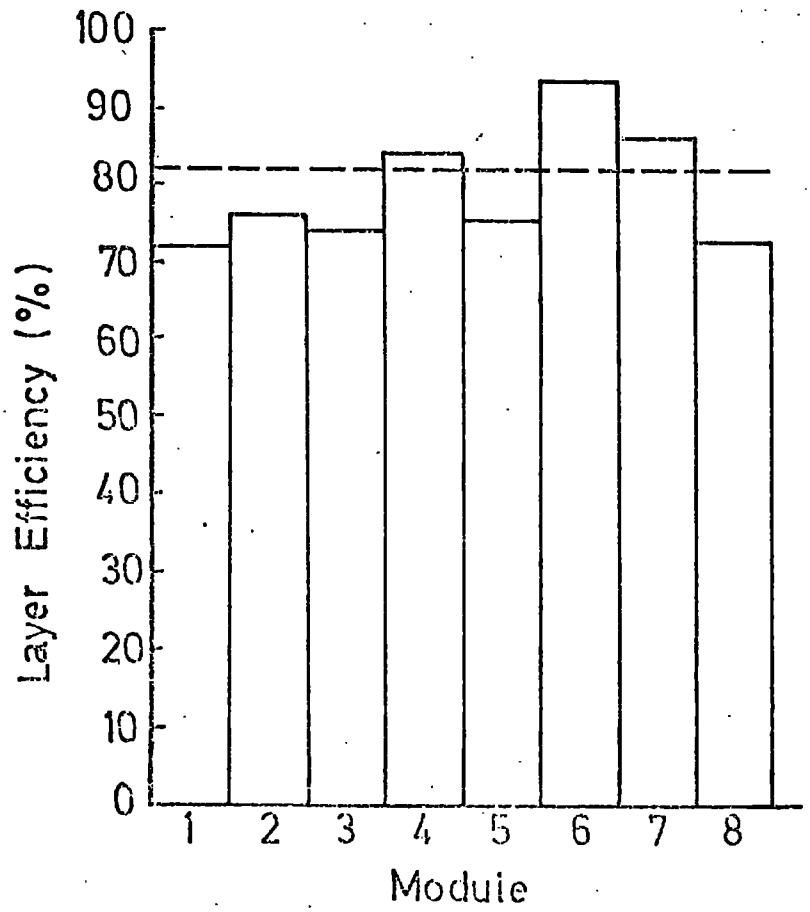

FIG. 6-9. The layer efficiency for each flash tube module at 50 Hz.

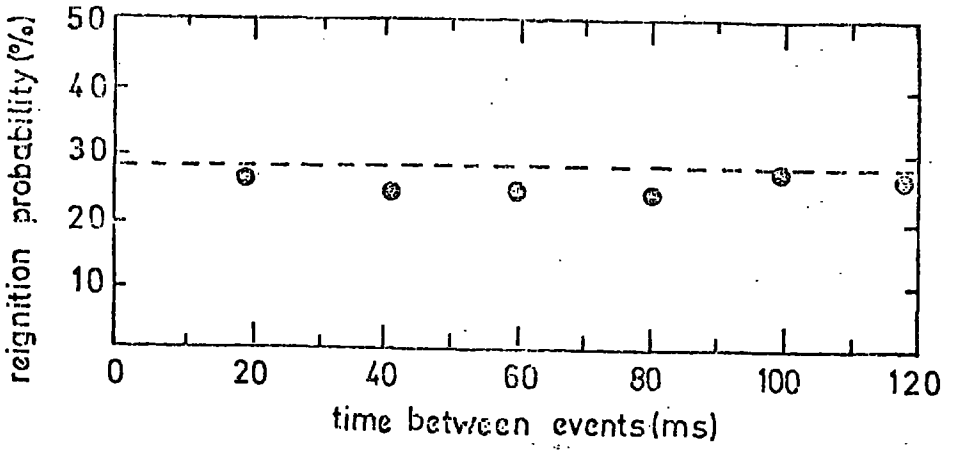

FIG. 6-10 The reignition probability versus time between events

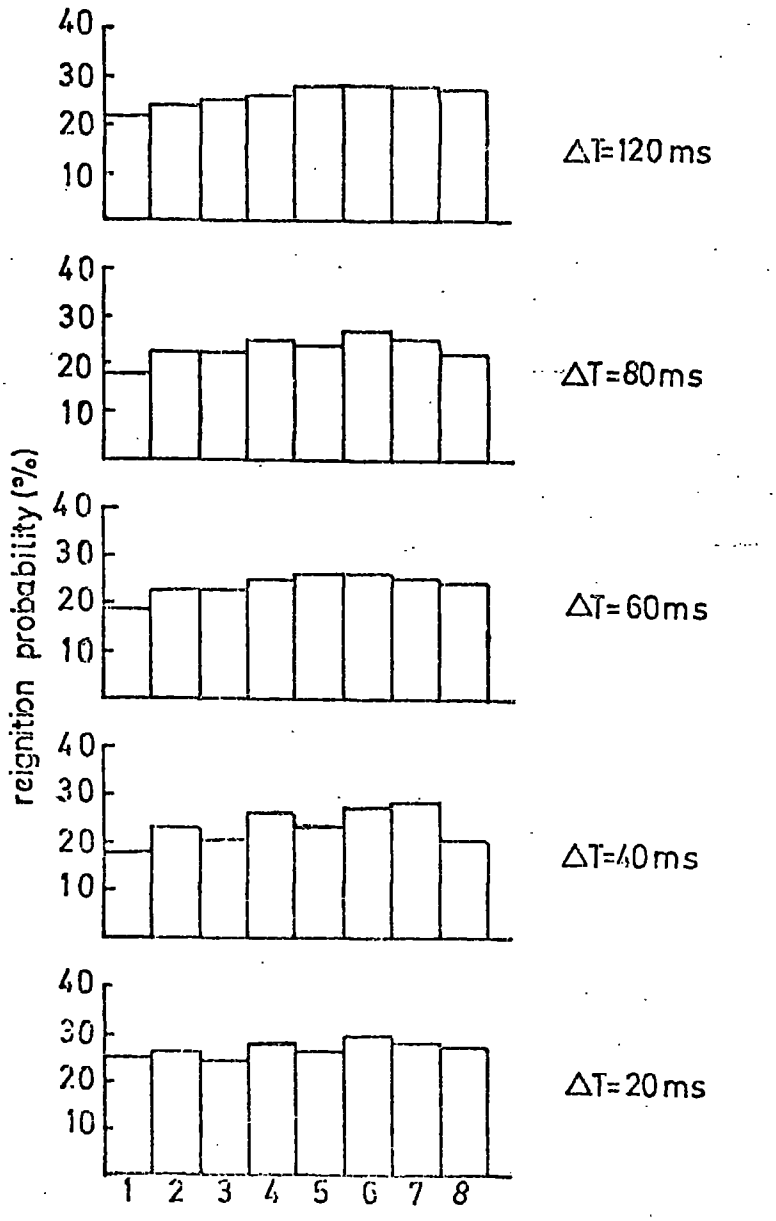

FIG. 6-11 The reignition probability for each module at different repetition rates

reignition probability of the chamber as a function of the time between events. The calculated values are seen to be constant at about 25%, there being no indication of increasing reignition probability with increasing repetition rate. The results do not give a zero reignition probability, however, because with such a small detecting area and a well collimated beam, there is a finite probability that consecutive particles will pass through the same tubes. From beam profile measurements across the plane of the tubes, this probability was calculated to be 28%, which agrees well with the measured reignition probabilities which lay around 25%. It is inferred, therefore, that the actual reignition probability is zero up to a repetition rate of at least 50Hz. In addition to the overall reignition probability, computations were made for individual modules. Figure 6.11 shows the reignition probability at five different repetition rates for each module. Again, the results are seen to be very consistent about a value of 25%.

6.4.3 Sensitive Time

No direct measure of the sensitive time, or the capability of tubes to operate in a high background radiation were possible from this data, although empirical evidence suggests that the tubes operate satisfactorily in a background of about 10^5 particles per second per tube. This was inferred from the beam characteristics where it was common for consecutive particles, in a spill of about 200 particles, to be separated by only a few microseconds, even though the total spill time was of the order of a few milliseconds. From the data analysis, however, there were no signs of multitrack events, indicating that the sensitive time is of the order of a microsecond or less, being in agreement with previous laboratory measurements using alternating clearing fields, as shown in Figure 6.12.

More than 10^6 events have been recorded during this series of experiments, using the same Ne-He-CH_4 tubes, without any measurable change in characteristics. This shows the gas mixture to be stable and that changes in the molecular properties of methane caused by ionization and dissociation during the discharge may be regarded as insignificant.

6.5 Conclusion

The results of this experiment have shown that Ne-He-CH_4 filled flash tube detectors are capable of efficiently determining the trajectory of high energy particles at repetition rates of at least 50Hz. The test beam results agree well with laboratory recovery and sensitive time measurements described in chapter 5, verifying the characteristics which are necessary for operation under accelerator conditions.

The efficiency results are particularly significant with respect to internally induced clearing fields which are known to develop in tubes of this type. Moreover, there was some justification for expecting a reduced detecting efficiency at high repetition rates based on the results of Holroyd's (4) work, which has shown that the induced clearing field strength is proportional to the repetition rate. The test beam results presented here, however, indicate that these fields have little effect, up to repetition rates of 50Hz, providing the H.T. pulse delay is sufficiently short. The H.T. pulse delay was measured to be 250nS, which is a typical delay time for pulsing systems of this purpose.

Although the repetition rate could not be increased enough to make an exact determination of the recovery time, the measurements made up to 50Hz show no deterioration in the characteristics compared

to laboratory measurements. Figure 6.13 shows the reignition probability curve as measured in the laboratory, which agrees well with the beam experiments up to 50 Hz, where the probability remained at zero. Thus, there is some confidence in accepting the validity of the laboratory measurement, which suggests that flash tubes with high concentrations of CH_4 will operate at repetition rates of about 1 KHz. The verification of this, however, requires the construction of a more sophisticated experiment, where fast data handling and high voltage pulsing problems become difficult. A description of the construction of such a system is given in detail in chapter 8.

The compatibility of the flash tube digitization technique with conventional computer data acquisition electronics was confirmed directly from the efficiency measurements. The overall detecting efficiency is dependent on the flash tube efficiency and the digitization efficiency. Therefore, the high overall detecting efficiency measured in these experiments verifies the compatibility of the technique with CAMAC electronics. Furthermore, these results have demonstrated that flash tubes may be digitized directly into a computer read-out system without the necessity of building interfacing amplifiers. This has particular significance to accelerator experiments where large area detectors are required and the cost per detecting channel is of concern.

The results presented in this chapter have ascertained the ability of the device to operate efficiently under accelerator conditions using conventional data acquisition electronics, and show that the exploitation and application of the device is possible.

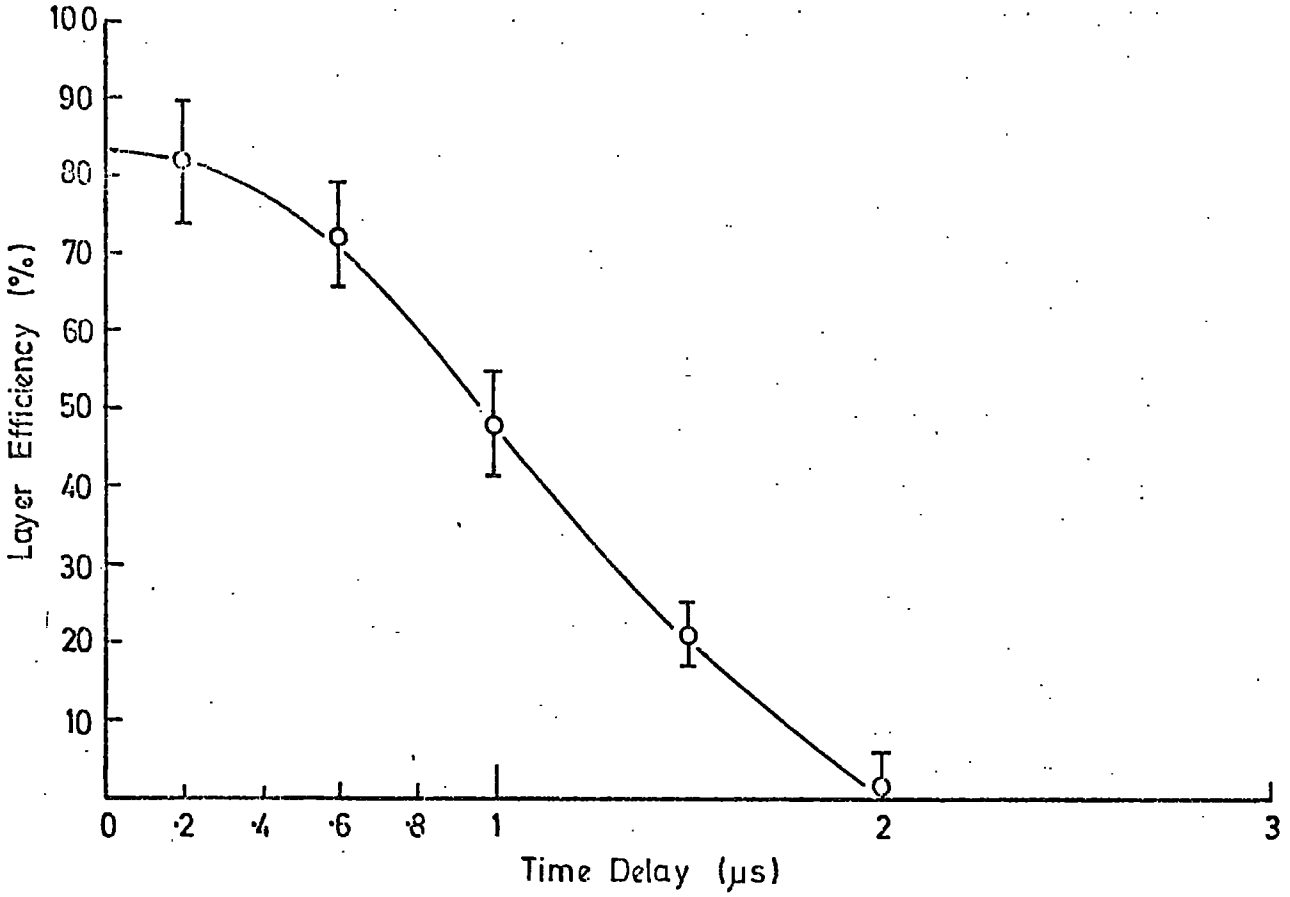

FIG. 6·12. Layer Efficiency versus Time Delay for Ne-He+1·0% CH_4 tubes with the application of a 30vcm^{-1} square wave clearing field.

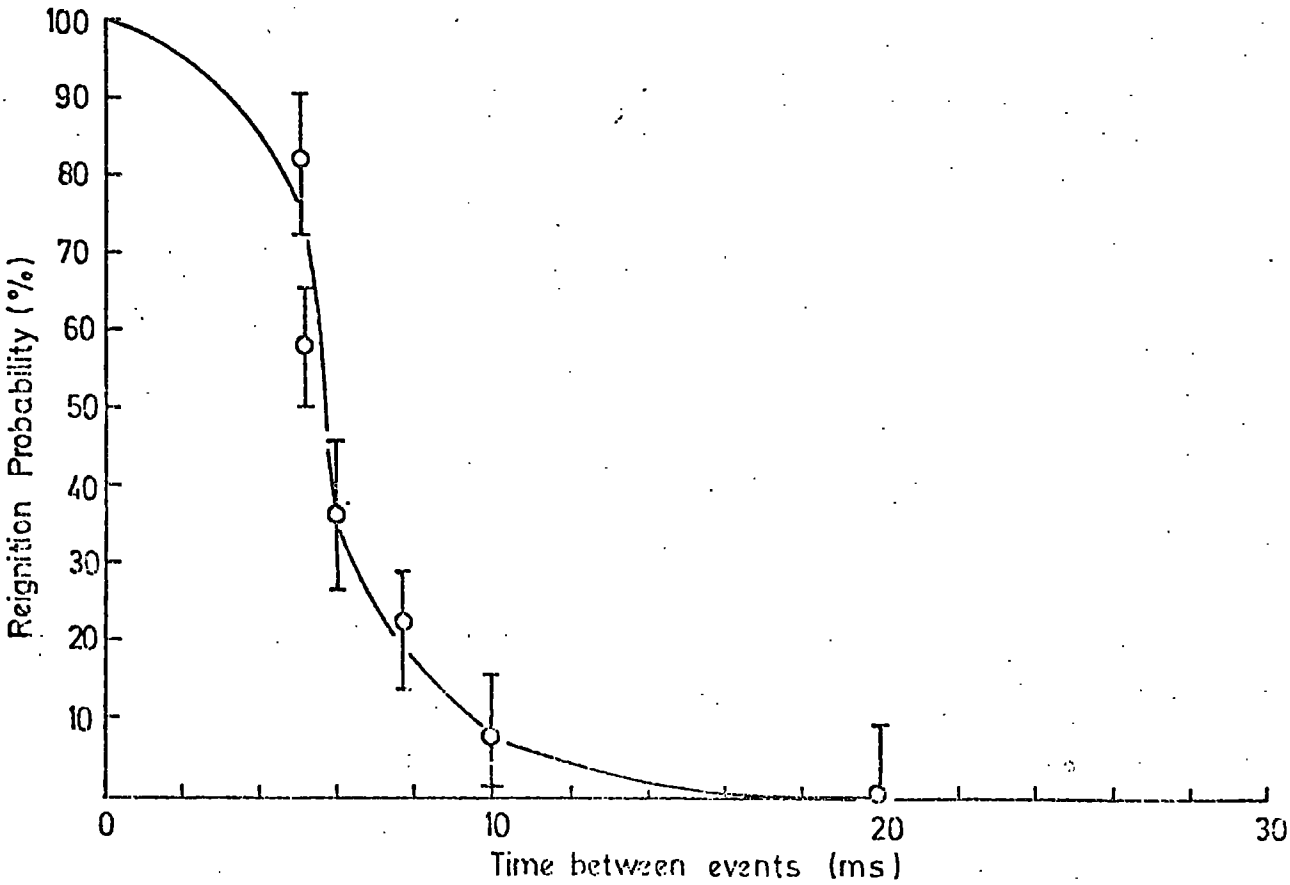

FIG. 6·13. Reignition Probability versus Time Interval for tubes containing Ne-He+1·0% CH_4.

REFERENCES

1. Thompson, D.J., Daresbury Nuclear Physics Laboratory, Internal Report, TM/70 (1972).

2. Sletten, A.M., Lewis, T.J., IEEE Monograph, 193 (1956) 54.

3. Iselin, F., CERN Internal Report, NP Camac Note 25-00(1971).

4. Holroyd, F.W., Ph.D. Thesis, University of Durham, (1971).

CHAPTER SEVEN

THE DETECTION OF HIGH ENERGY GAMMA RADIATION

7.1 Introduction

The digitised flash tube may have many potential applications in accelerator physics, but a use of particular significance is in that class of detectors which are concerned with the measurement of high energy gamma radiation. Flash tubes with short sensitive and recovery times may facilitate a large area detecting device capable of providing digitized energy and trajectory information with simplicity, reliability and low cost, in comparison with conventional gamma ray detecting techniques (see section 4.3). The purpose of this chapter is to describe a study of high energy gamma ray detection using a prototype flash tube chamber in the DNPL e^+ accelerator beam. The prime motivation behind this investigation was not to build a high resolution detector, but to demonstrate that energy and trajectory measurements of cascade showers, in the GeV region, are possible using large diameter tubes in a chamber of small overall dimensions.

A fully digitised flash tube chamber was constructed and used with the e^+ accelerator beam with the purpose of simulating photon induced electromagnetic showers at energies of a few GeV. The shower structure data was analysed and interpreted to give spatial and momentum information, from which the resolving capabilities of the device were measured. These results also provided information necessary for the construction of an improved device of larger dimensions with greater energy and spatial resolution.

7.2 The Principles of High Energy Gamma Detection

Photons of energy above a few KeV are detected by virtue of their interaction with atoms in an absorbing medium to produce electrons, positrons and secondary photons. The three main processes by which

photons lose their energy by interactions with matter are photoelectric effect, Compton effect and pair production. These processes are dominant in different ranges of the photon energy: the photoelectric effect from 0.01 MeV to 0.5 MeV, the Compton effect from 0.1 MeV to 10 MeV, and pair production starts at 1.02 MeV and increases with increasing gamma energy (1). These three interactions and their products are summarized by the following expressions:

$$\gamma + A \rightarrow A^{+} + e^{-} \qquad \text{photoelectric}$$

$$\gamma + e^{-} \rightarrow \gamma' + e^{-} \qquad \text{Compton}$$

$$\gamma + A \rightarrow A + e^{+} + e^{-} \qquad \text{pair production}$$

Detectors which determine the energy of photons are made to be sensitive to the amount of energy deposited by measuring the degree of ionization in the absorbing material. At energies below about 1 MeV semiconducting Si or Ge detectors (2,3) are used which collect free electrons created by ionization in the reverse bias depletion region inside the crystal. The collection of charge results in a potential drop across the detector giving a pulse which is proportional to the energy of the incident photon. The gas proportional counter (4) too, is used to detect low energy photons. This device relies on electron avalanche amplification in an electric field, to give a signal with magnitude proportional to the number of electron-ion pairs produced by ionization in the gas volume. For higher energies the inorganic crystal scintillation counter (5,6) is a suitable photon detecting device which utilizes a photomultiplier to produce an electronic signal from light emitted by the excitation of electrons with atoms and molecules of the crystal. Commercially available crystals will measure photon energies up to about 100 MeV, although special devices have been made which are capable of operation in the GeV region (31)

All the above mentioned detectors have an upper energy limit on their working range which is fixed by their physical size. Photons outside this range and of greater energy cause interactions which are not completely contained within the device, resulting in an output signal which is no longer a measure of the total incident energy. The problem of measuring high energy gamma radiation necessitates total absorption techniques which provide much larger amounts of interacting matter to give a signal which remains proportional to the incident energy over a sufficiently wide spectrum of gamma energy.

If the energy of the incident photon is large enough then the interaction products are capable of initiating further interactions in the absorbing material which propagate a cascade shower of particles until the energy of the individual constituents fall to a threshold value, whereupon multiplication ceases and the cascade decays (8). For energies above 10 MeV pair production is the dominant gamma conversion process, producing an electron-positron pair which rapidly lose energy in the converting material. This loss may be the result of either Bremsstrahlung or ionization. At high energies, in dense material, the loss is predominantly by Bremsstrahlung because the interaction cross section is proportional to Z^2 and increases linearly with energy, while the energy loss by ionization is proportional to Z and increases logarithmically with energy (7). The secondary photons will in turn, undergo materialization or Compton collision, giving rise to further electrons. These new electrons radiate more photons which again materialize into electrons pairs or produce Compton collision until eventually the energy of the electrons fall into the energy range where radiation losses cannot compete with collision losses and the total primary photon energy is completely dissipated in excitation and ionization of atoms. The development of the cascade shower is difficult

to predict analytically, although the process has been quantitatively described by mathematical models which depend on making several approximations (8). Monte Carlo techniques, however, are less complex, and have been used to simulate cascade shower structures (9,10,11) which are in agreement with experimental data (12,13).

The energy and trajectory of high energy photons are normally determined by studying the cascade shower development after conversion in interacting material. An energy determination is made by making the detector sensitive to the number of electrons produced in the cascade. Theoretical and experimental studies have shown that the number of cascade electrons is proportional to the incident gamma energy (9,10,11). Figure 7.1 shows the number of electrons as a function of absorber depth (expressed in radiation lengths), calculated by the Monte Carlo simulation of Messel and Crawford (9) for electron and photon induced showers of 0.5, 1.0 and 10 GeV. Total absorption methods which are normally employed to be sensitive to the number of electrons take the form of either stacked assemblies of detectors, interspaced with targets of heavy interacting material, or homogeneous Cerenkov devices of dense material such as lead glass coupled to a photomultiplier tube. All these detectors are arranged in such a way to give a signal which is proportional to the number of cascade particles.

The devices which take the form of alternate layers of detector and target, sample the cascade development, to give information which represents the number of ionizing particles at successive depths of target. This information may be added electronically to give a signal which is proportional to the incident gamma energy. Figure 7.2 shows the calculated total number of electrons expected from cascade showers of different energies by summing the electrons at 1 and 2 radiation

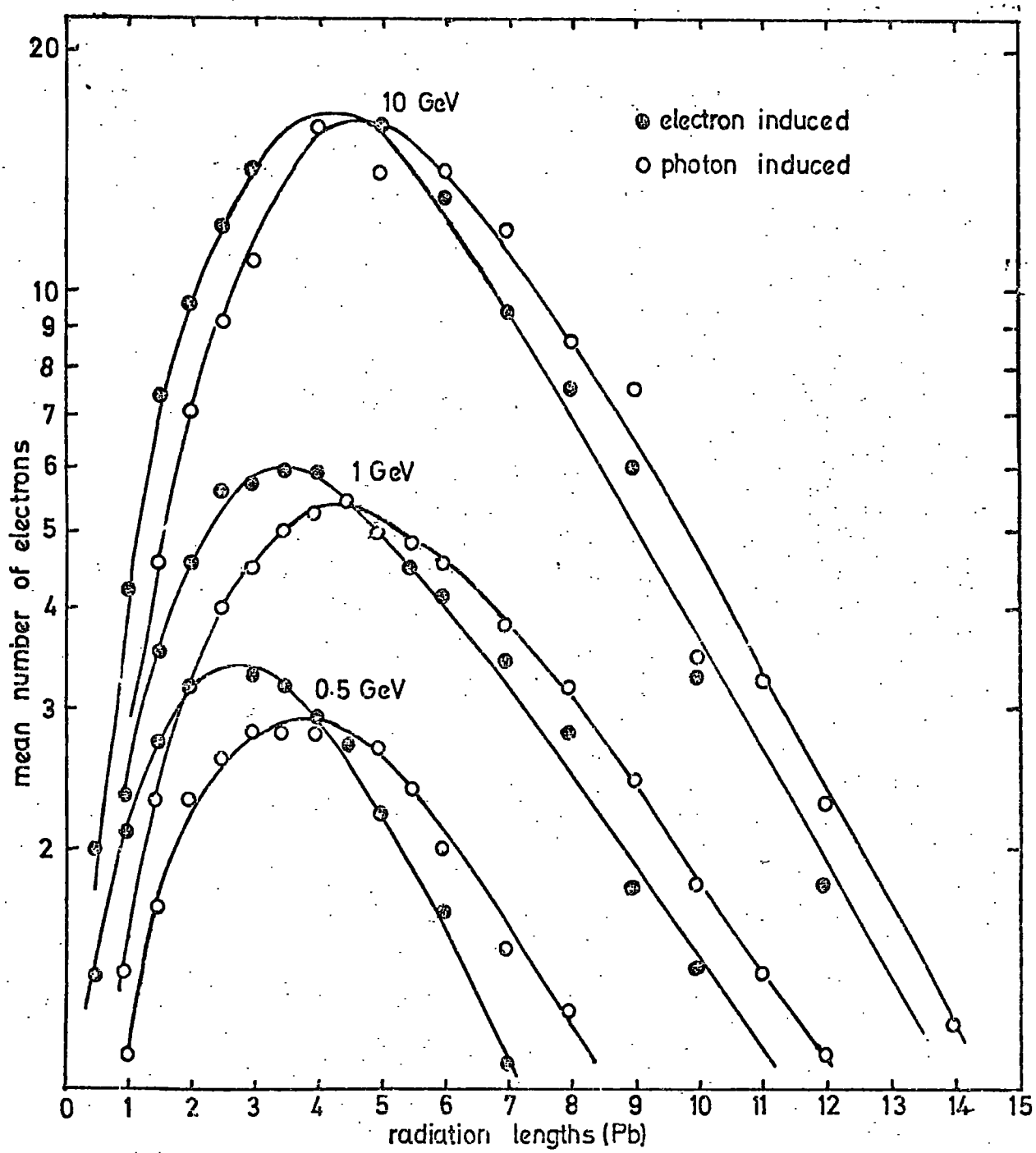

Fig 7.1 mean number of electrons produced as a function of target depth and primary energy

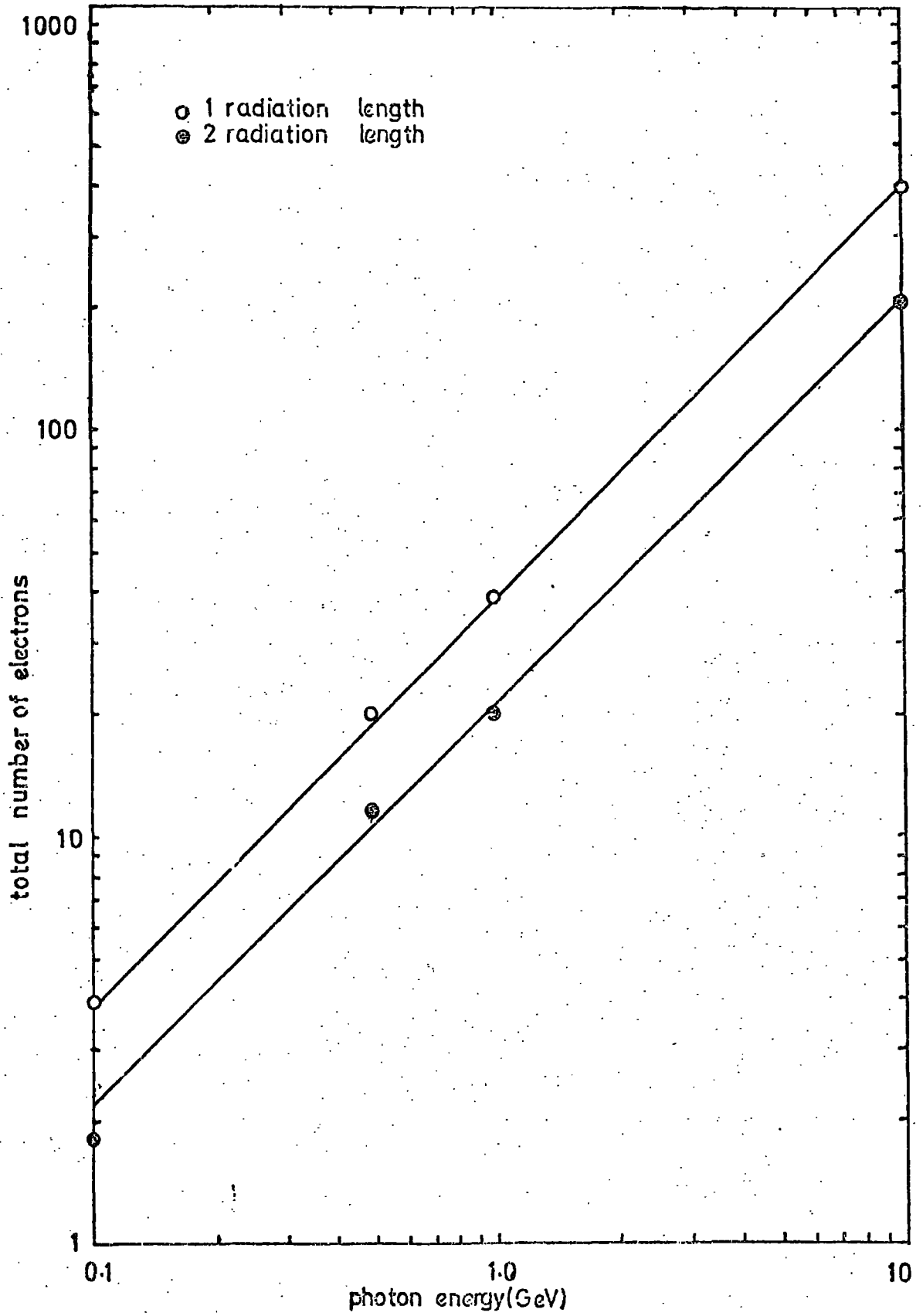

Fig. 7·2 total number of electrons expected by sampling at 1 and 2 radiation length intervals as a function of primary photon energy

length intervals in the longitudinal direction. The total number of electrons has been derived from the Monte Carlo results of Messel and Crawford (9). These results show that a linear response can be expected if the individual detecting elements are sensitive to all electrons at each stage in the cascade development. Conventional high energy gamma detectors which are based on the above working principles take the following forms:-

(1) Lead - Scintillator (14, 15, 16, 17, 18, 19)

Figure 7.3a shows a typical arrangement using an array of lead target interspaced with scintillator which is coupled to a tapered light guide and photomultiplier tube. The light from each scintillator finger is collected and fed into the photomultiplier to produce a signal proportional to the number of cascade electrons.

(2) Lead - Lucite Cerenkov (14, 20)

Lead-Lucite Cerenkov detectors are normally of similar construction to the lead-scintillator type as shown in Figure 7.3a. They consist of lead plates interleaved with lucite Cerenkov counters which are attached to a lucite light guide and photomultiplier tube. In this case, the cascade electrons produce Cerenkov light in the lucite, some of which is totally internally reflected and detected by the photomultiplier.

(3) Lead - Spark Chamber (21, 22, 23, 24, 25, 26)

Again, this system comprises of a stacked assembly of target and detector as shown in Figure 7.3b. With this type of device the gamma energy is measured by recording the number of sparks between each electrode gap. Either photographic or electronic digitization techniques using plumbicon T.V., capacitive read-out or magnetostrictive read-out may be used to count and locate the sparks. An advantage of this device is that location of the sparks provides a means of determining the cascade shower axis, from which the incident gamma trajectory may be found.

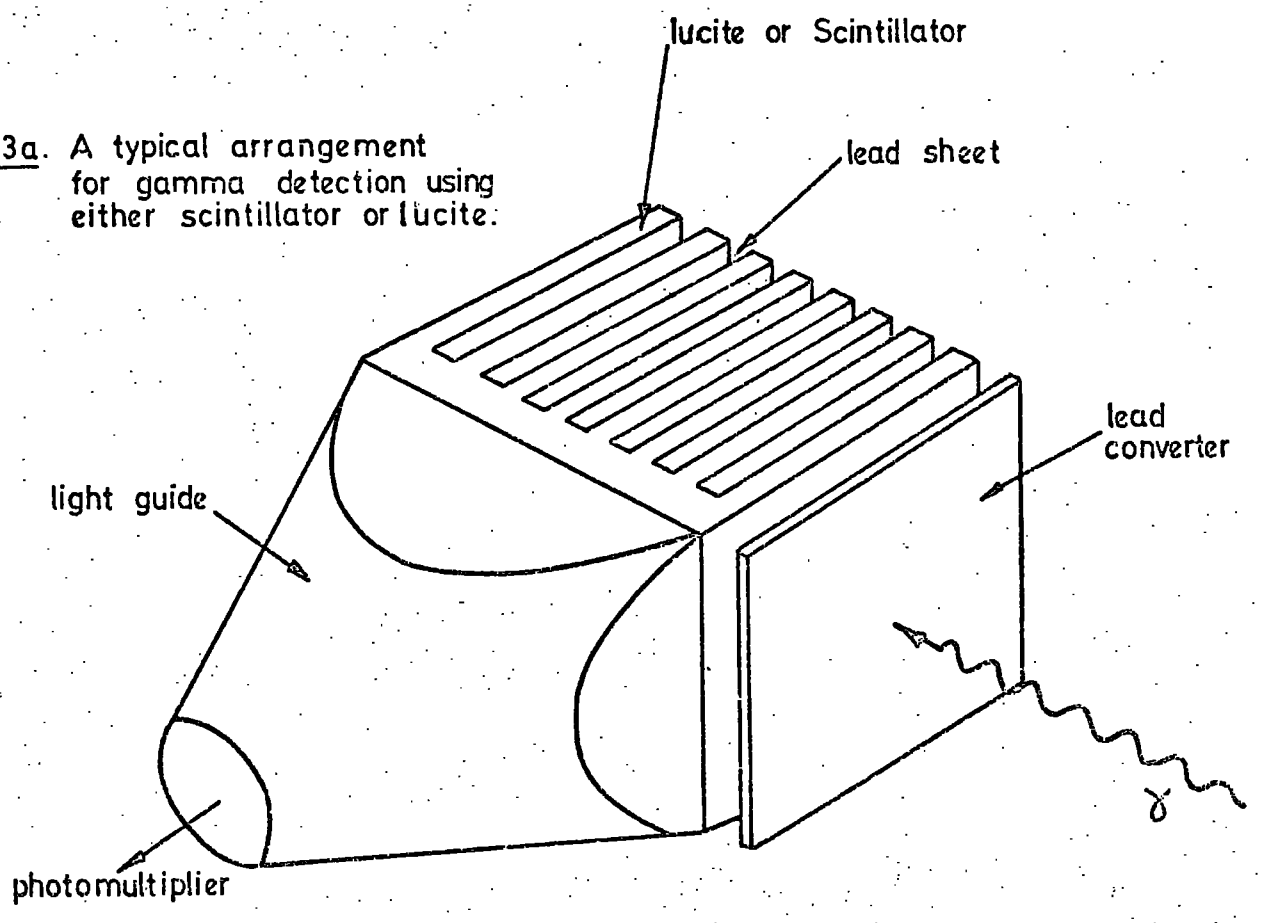

FIG. 7·3a. A typical arrangement for gamma detection using either scintillator or lucite.

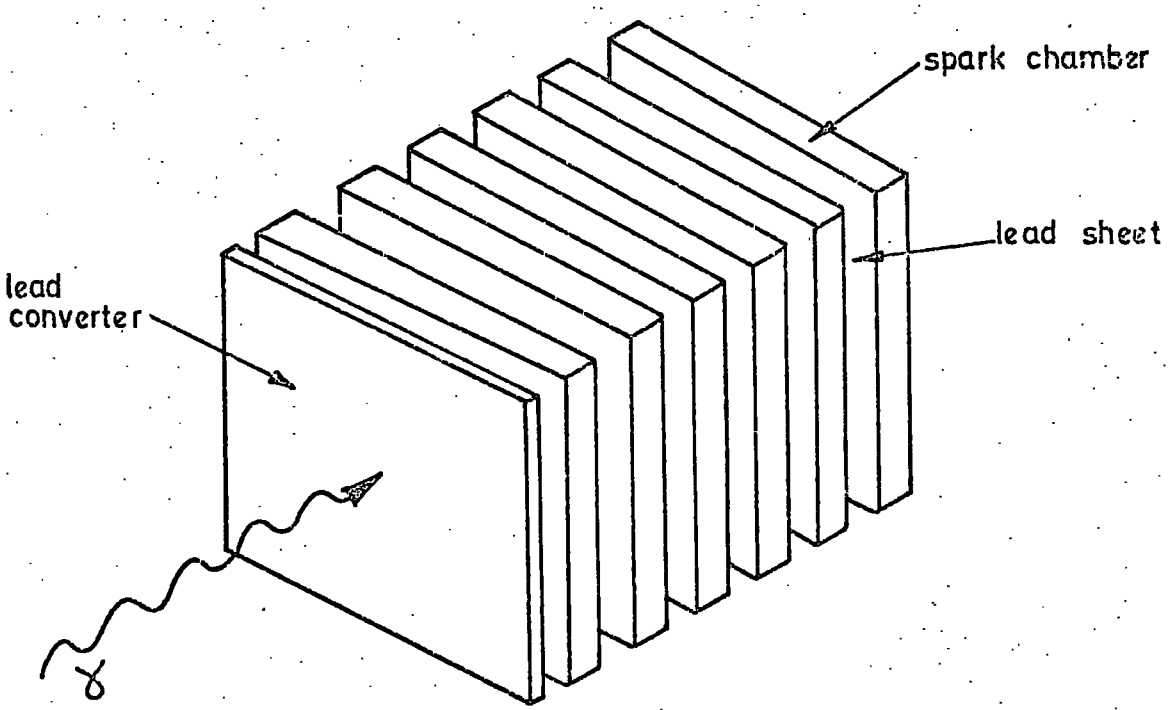

FIG. 7·3b. A typical arrangement for gamma detection using spark chambers.

(4) Lead Glass Cerenkov (27, 28, 29, 30)

The other class of gamma detectors is the homogenous Cerenkov device, which provides continuous sampling of the cascade shower by the use of a single element of high density glass ($Pb\ F_2$). This detector is usually made from a parallelepiped block of lead glass and viewed at one end by a single photomultiplier. Individual blocks can be built up into a matrix array to form a large area hodoscope which beside giving energy information can be used to give crude spatial information (29, 30).

7.3 A Study of High Energy Gamma detection using the D.N.P.L. Accelerator.

This section describes a series of experiments made on shower development in a small lead plate flash tube chamber in the energy range 0.5 to 4.0 GeV during exposure to the D.N.P.L. positron beam. The high energy positrons were used to simulate photon induced cascade showers of the same energy. Experimental (20) and theoretical (9) studies have shown there to be only small differences between photon and electron induced showers, and it is on this basis that the simulation is justified. Figure 7.1 illustrates the small discrepency expected between photon and electron showers for the number of cascade electrons produced as a function of absorber depth.

The flash tube chamber was constructed on the total absorption detecting principle described in section 7.2. where the shower development is sampled after fixed intervals of interacting target. The chamber was thus arranged, such that a series of flash tubes, positioned in lateral planes relative to the incident beam, were interspaced with interacting lead target. The tubes were contained in electrode modules and arranged such that the cascade could be sampled in two orthogonal planes. This provided two measures of the number of ionizing particles at each successive target interval, and allowed the incident positron trajectory to be studied in two dimensions.

The cascade shower data recorded from the device in this configuration was analysed to provide information concerning the detectors ability to measure both the energy and trajectory of the incoming particle. The resolution of the device, with respect to energy and trajectory determination has been measured as a function of the incident energy with two different thicknesses of interacting lead between detecting planes.

7.3.1 Experimental Arrangement

The flash tube chamber consisted of eight seperate electrode modules each containing two sets of eight 1.6cm internal diameter tubes with digitization probes. A detailed description of the electrode modules, flash tubes, digitization probes and high voltage pulsing electronics is given in section 6.2.2. Figure 6.5 shows a photograph of the chamber, mounted in its framework and complete with output cables leading to the CAMAC data acquisition system. The framework which held the electrode modules together was designed to provide a space before each module for accomodating up to 2 radiation lengths of lead target. In this configuration the chamber had an overall depth of 63 cm, with 5.4 cm between each detecting plane, and a detecting area of 15.2 cm x 15.2 cm.

Incident positrons were selected by a coincidence trigger from three small beam defining scintillators placed before the chamber. Figure 7.4 shows a schematic diagram of the scintillation detectors with controlling logic (E.G.G. modular electronics) which generated a signal to trigger the high voltage pulse and data control subroutine in the computer after a coincidence event. The logic, besides producing triggering signals, had several other important functions which are described below.

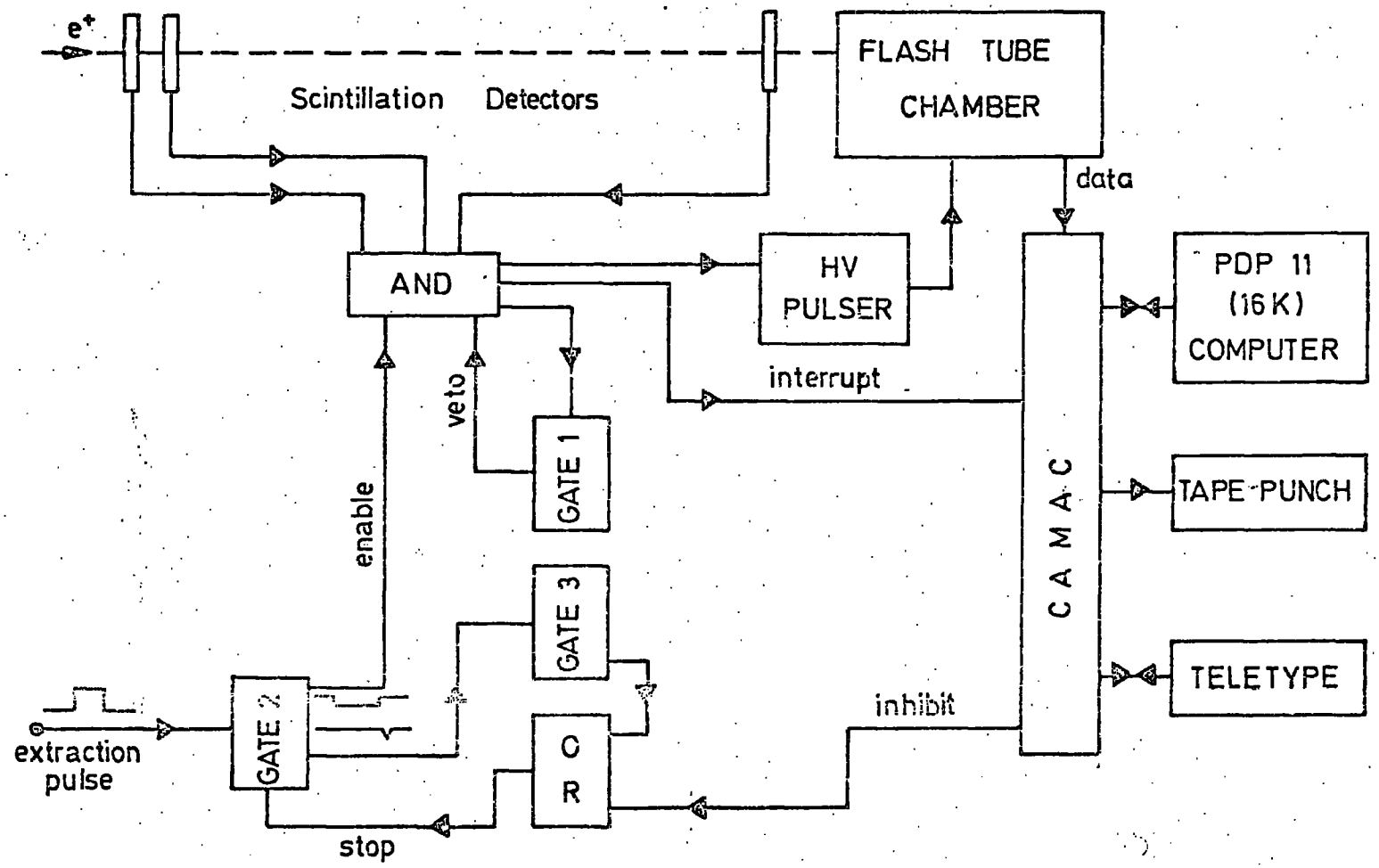

FIG. 7.4. The data acquisition system.

(1) Spurious showers resulting from background particles were reduced by ensuring that events were only selected during the beam extraction time. For this purpose the magnet extraction pulse was used to trigger Gate 2 (Figure 7.4) such that the coincidence AND was 'enabled' during the extraction time (2ms) only.

(2) Cascade showers resulting from multiparticle interactions were prevented by selecting only one positron in each beam extraction. This condition was achieved with Gate 1 which provided a coincidence Veto pulse for a duration greater than the beam spill time, thus ensuring that only the first particle was recorded from each bunch of particles.

(3) The event repetition rate could be set to be any integral number of accelerating cycles. That is, a particle could be selected every 20, 40, 60 ... ms, etc. The rate was selected by Gate 3 which applied a 'stop' pulse of length equivalent to a predetermined number of cycles.

(4) The pulsing system was paralysed while the computer was processing data by applying a 'stop' pulse to Gate 2. This was generated from the CAMAC inhibit pulse via an OR gate.

The data from each cascade shower was thus stored, consecutively, into addressed CAMAC registers (Pattern units, type 16P007) in eight 16-bit words. This data was then read, after each event, into the memory core of a PDP 11 (16K) computer until the core was full, whereupon the system was paralysed, for a sufficient time to allow the data to be transferred to magnetic disc for analysis. The computer program which controlled the CAMAC and data acquisition is described in detail in Appendix III.

7.3.2 Energy Measurements

Gamma-ray cascade showers were simulated by monoenergetic (±1%) positrons in the momentum range 0.5 to 4.0 GeV/c with 1.0 and 2.0 radiation lengths of lead target interspaced between electrode modules. Target material was positioned before all but the first module, which was used to define the trajectory of the incident particle for spatial analysis. Over 2500 showers were generated at each momentum to give enough statistical data for the characteristics of the device to be measured. The shower data was processed and analysed using the DNPL 370/165 computer.

Data from the flash tube chamber has been analysed with regard to the total number of flash tube ignitions as a function of the incident positron momentum. The total number of flash tube ignitions is representative of the total number of ionizing particles, which has been shown to be proportional to the incident particle energy (see section 7.2). This number does not, however, represent a direct measure of the energy, for it will vary from one device to another, according to the detectors geometry and size. As a consequence, it is necessary for all devices which work on the principle of shower sampling, to be calibrated in a beam of known energy. Figure 7.5 and 7.6 show the frequency distributions for the number of flash tube ignitions at different momenta with 1.0 and 2.0 radiation lengths of lead target. These results are seen to be symmetrically distributed about their maxima, except for the 4.0 GeV/c results (Figure 7.6) which were subject to a background, due to low energy beam contamination. From the distributions the calibration curve of the mean total number of tube ignitions as a function of incident positron momentum was determined, as is shown in Figure 7.7. The curves show the device

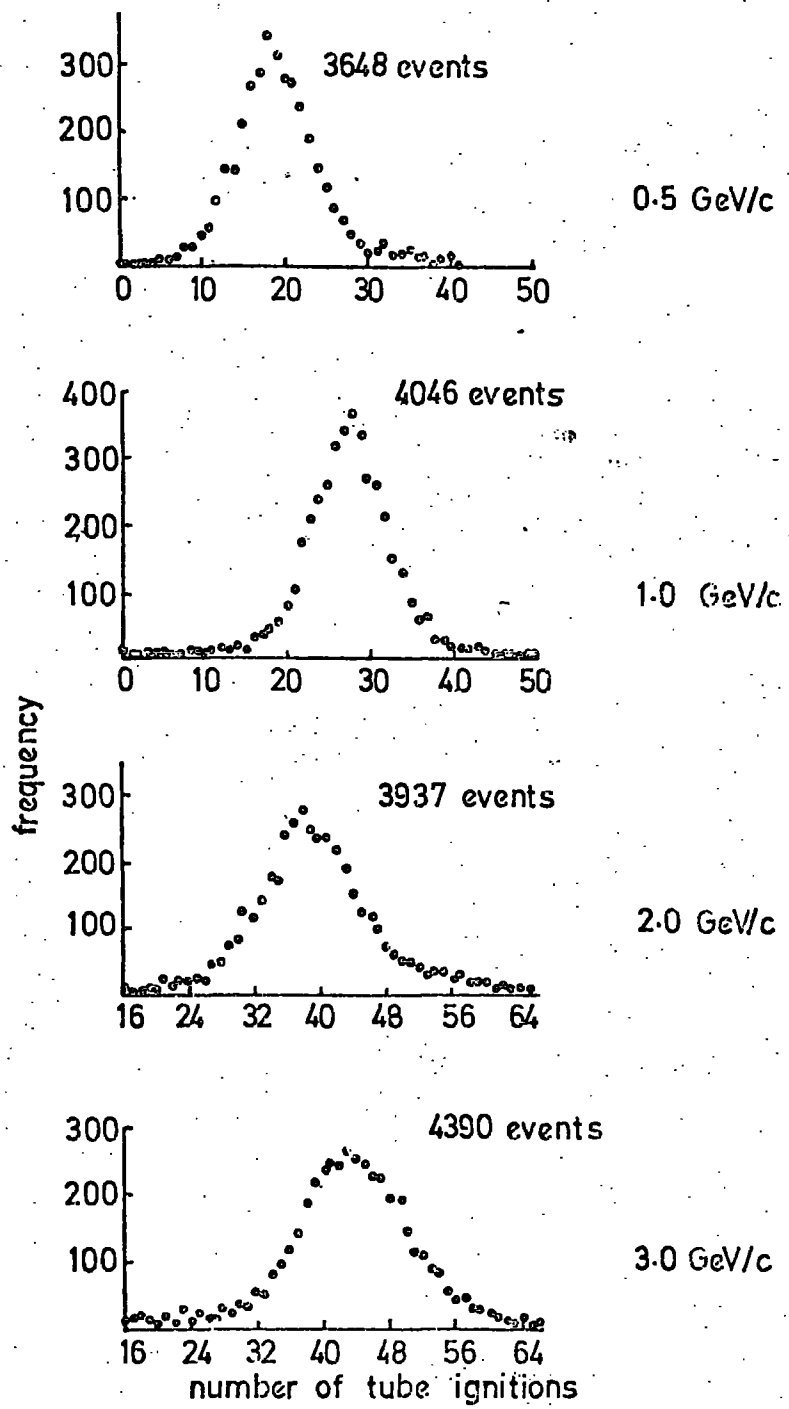

Fig 7.5 frequency distributions of the total number of tube ignitions with 1·0 radiation length of lead between modules

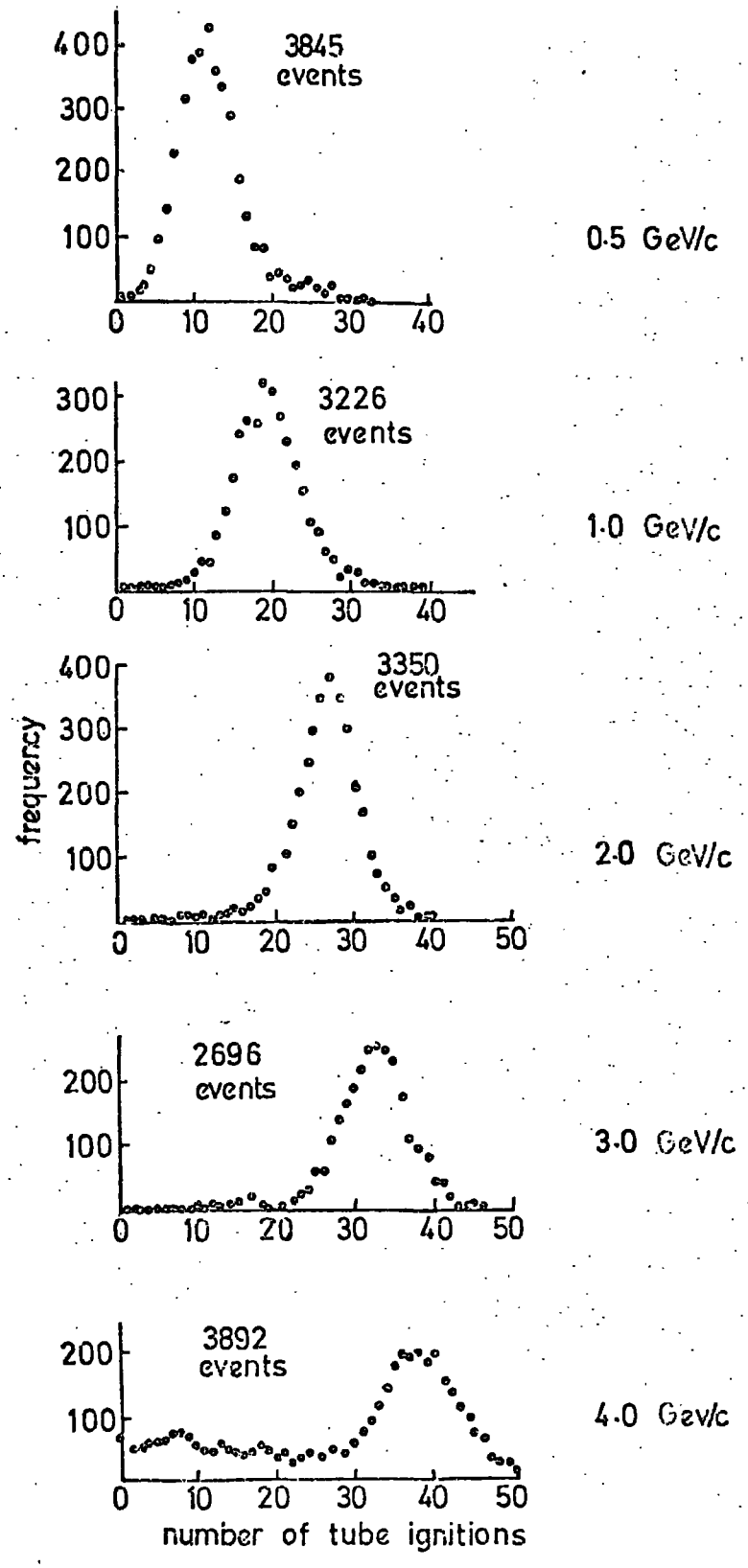

Fig 7.6 frequency distributions of the total number of tube ignitions with 2.0 radiation lengths of lead between modules

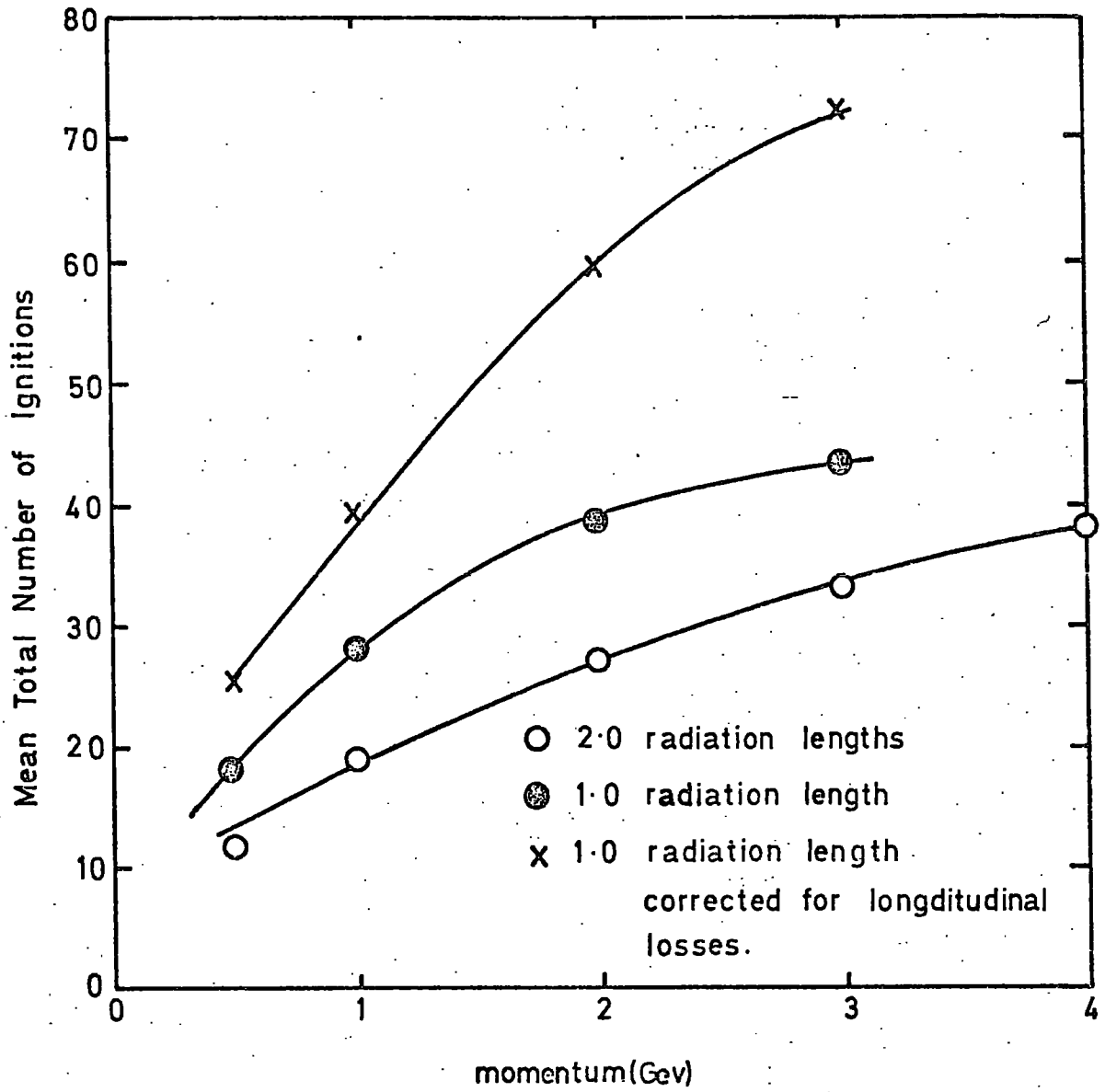

FIG. 7·7 Mean total number of tubes igniting versus positron energy.

to be sensitive to momentum, although the response is seen to depart from the linear relationship predicted by the theoretical work described in section 7.2. Data obtained with the 2.0 radiation lengths, of target give the best approximation to a linear function, but deviations from a straight line are still seen to occur, particularly at high momentum values. Non-linearity in the 1.0 radiation length data is more pronounced, the discrepancies being evident at even lower momentum values. The deviations from the straight line predicted by theory are attributed to the cascade shower spreading further than the dimensions of the chamber and the failure of the device to resolve individual electrons in high density showers. Thus, greater deviations may be expected with increasing energy, where less than the predicted number of flash tube ignitions will occur, due to particle leakage and tube insensitivity.

Longitudinal leakage is evident from Figure 7.8 where the mean number of tube ignitions is plotted for each module in the X-plane. With only 1.0 radiation length of lead between modules there is a significant number of flash tube ignitions in the last module after a total of 7.0 radiation lengths at all momenta. Figure 7.9 shows the same data, but with the average number of ignitions plotted against thickness of target material expressed in radiation lengths. These results give good agreement between the 1.0 and 2.0 radiation length data, and qualitatively the functions describe the behaviour expected from theory for the number of electrons; a linear rise at the beginning, a flat maxima, and an exponential absorption tail. Again, the results show the loss due to particle leakage in the longitudinal direction is severe in the case of the 1.0 radiation length data. Consequently, the momentum sensitivity curve obtained with 1.0 radiation length of lead, shown in Figure 7.7 is expected to have a much greater slope than

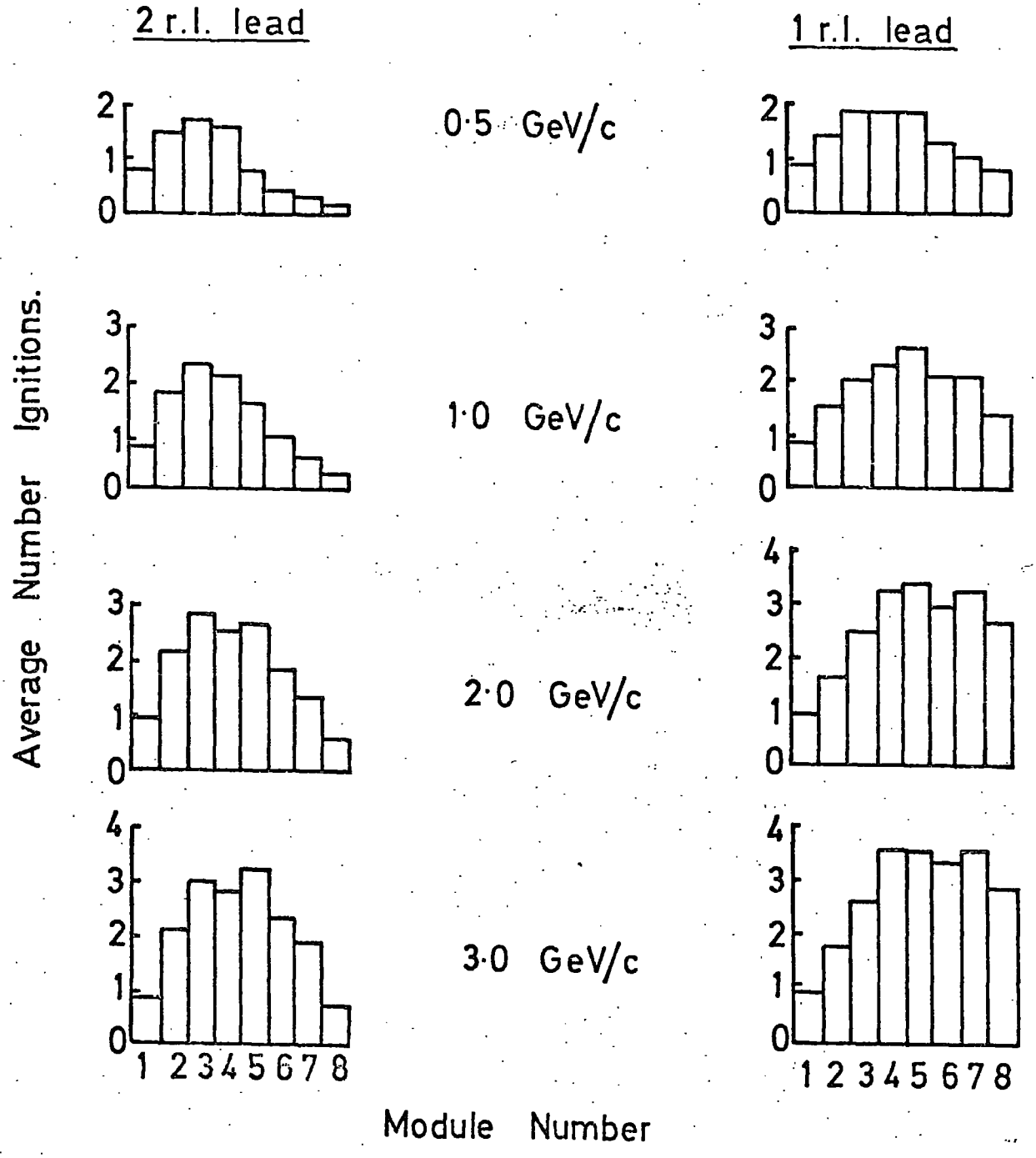

FIG. 7·8 The average number of ignitions for each module at different momenta.

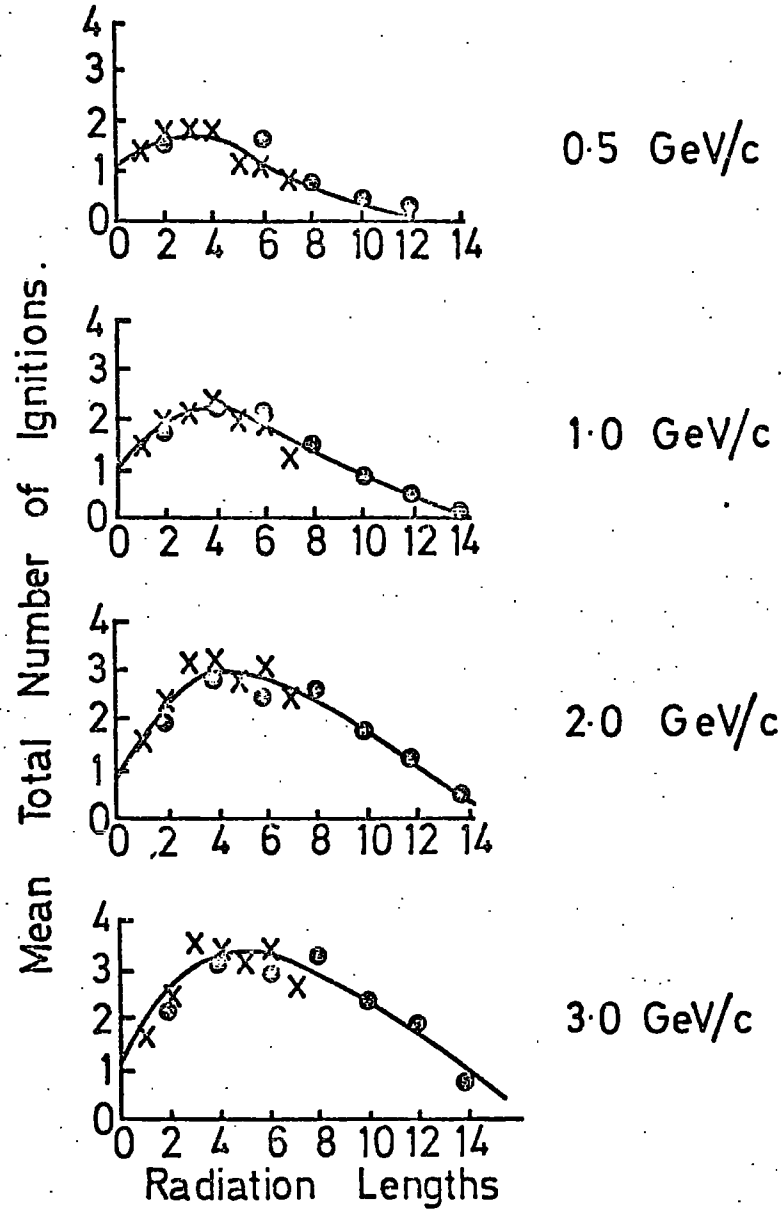

x Data from 1·0 r.l. between modules.

● " " 2·0 " " "

FIG.7·9 Mean total number of ignitions versus thickness of lead target at different momenta.

that measured, as a result of the very large losses. Results corrected for this loss are also plotted in Figure 7.7, where the total number of tube ignitions is calculated by integrating the 2.0 radiation length curve over 14 radiation lengths. This new curve is more linear and is in better agreement with the Monte Carlo results shown in Figure 7.2, where the number of electrons increases approximately twofold by halving the target thickness.

Shower leakage in the lateral direction also contributes to non-linearities in the sensitivity of the device. Figure 7.10 shows the electron probability profiles plotted for each module at 3.0 GeV in the X-plane. These results show that lateral leakage is not so severe compared to longitudinal leakage at higher momenta, although a contribution is evident.

The individual electron sensitivity is an important characteristic with respect to linearity and energy resolution and is partly responsible for the observed departures from theoretical predictions. With large 1.6cm internal diameter tubes a poor electron sensitivity must be expected, especially as the shower is sampled in projection. A measure of this sensitivity was obtained by comparing the Monte Carlo simulated results of Messel and Crawford (9) with the flash tube results at 0.5 and 1.0 GeV/c, assuming an electron energy detection threshold of 1.0 MeV. Figure 7.11 shows the results of this comparison, the individual electron sensitivity being plotted as a function of the mean total number of electrons expected in any flash tube detecting plane. The results show an inverse correlation between sensitivity and the total number of electrons produced. Consequently, a deterioration of linearity, caused by insensitivity to individual electrons is to be expected when the energy increases and the number of electrons becomes large. The following table gives the overall

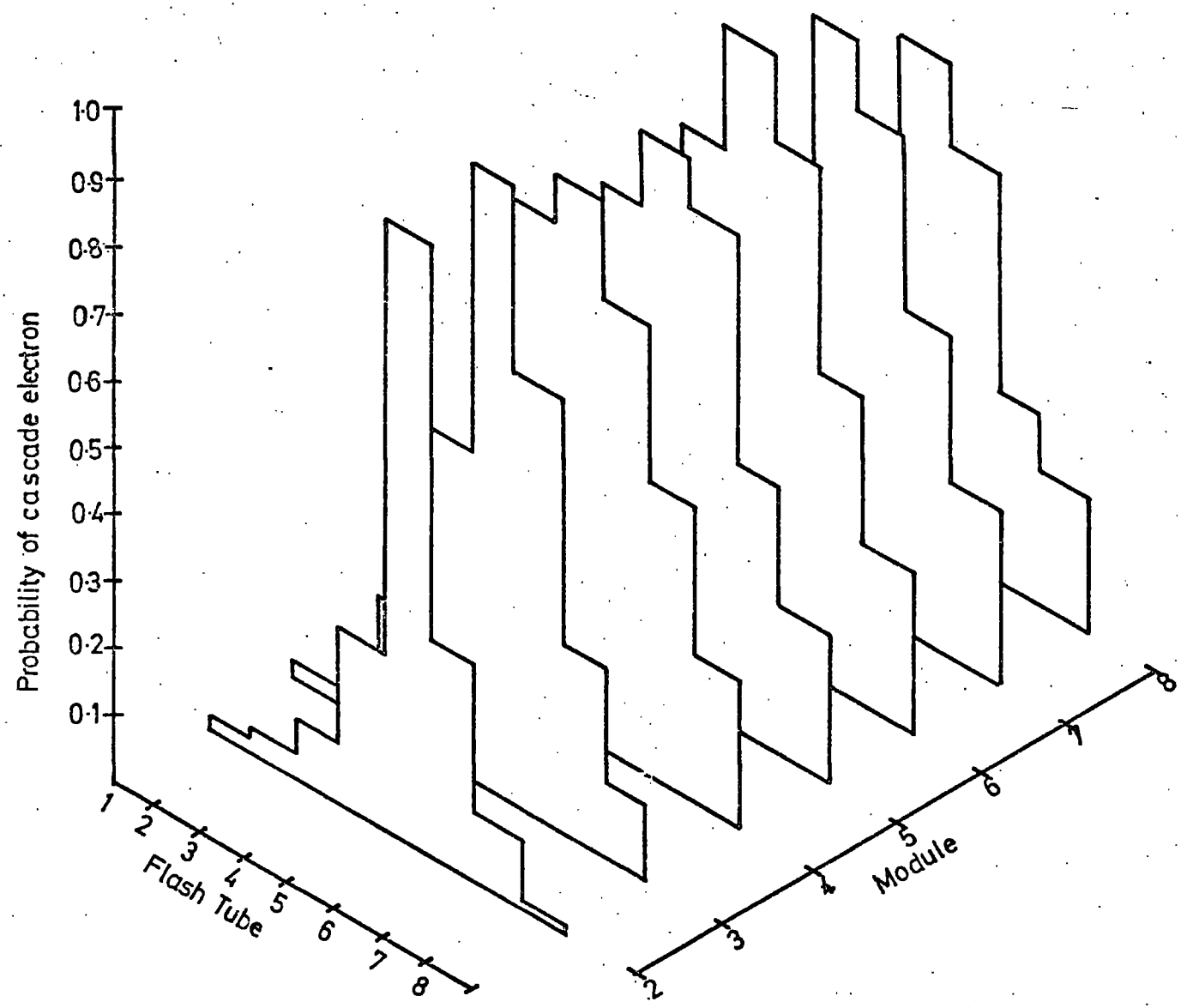

Fig 7·10 electron shower profile for 3·0 GeV/c positrons with 1·0r.l. of lead between modules

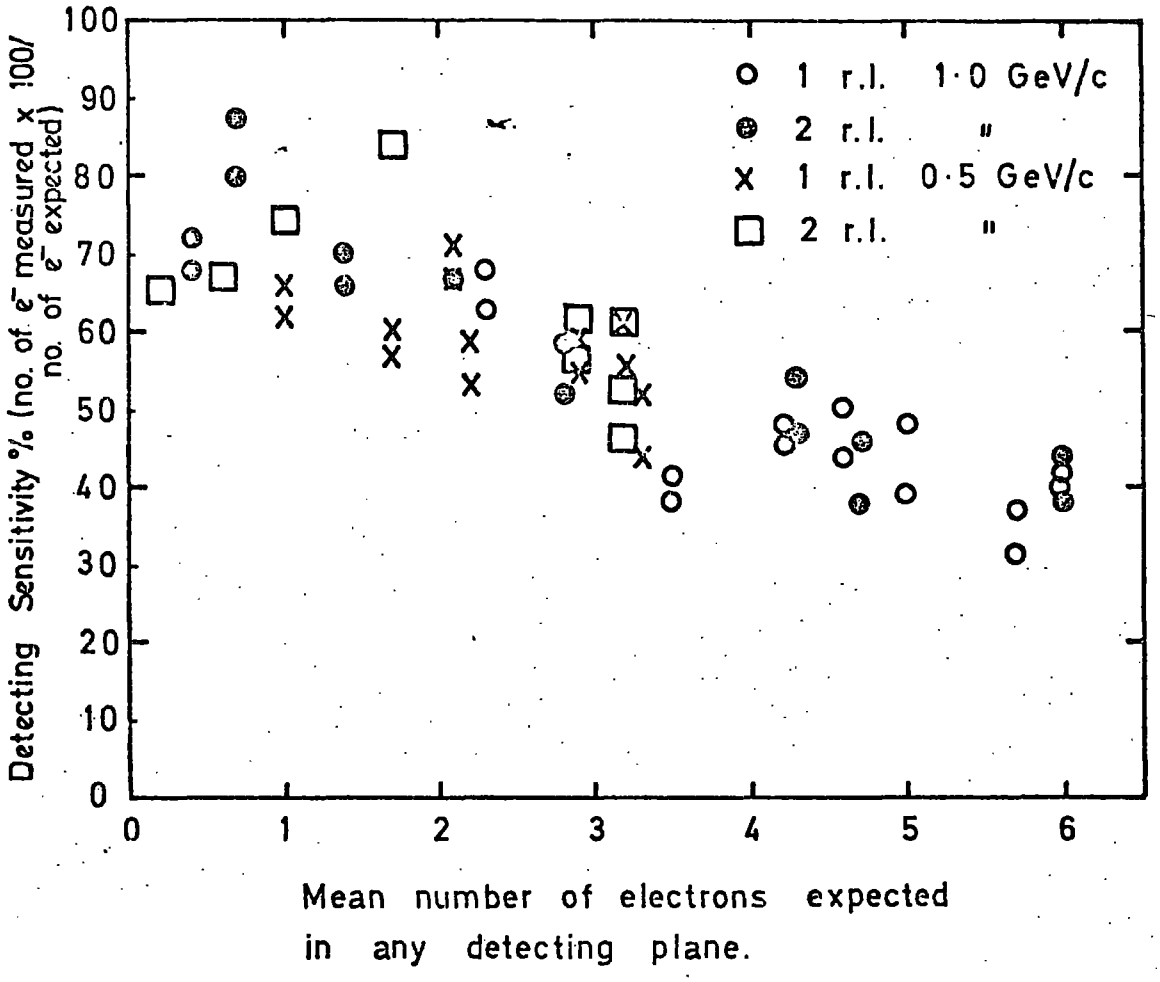

FIG. 7·11 Electron sensitivity versus number of produced electrons.

sensitivity, measured by comparing the average total number of electrons in the shower expected theoretically (9), with the average total number of observed flash tube ignitions.

GeV/c	Radiation Lengths	Number of electrons	Number of F.T. Ignitions	Sensitivity (%)
0.5	1.0	16.7	9.7	58.1
0.5	2.0	10.0	6.4	63.9
1.0	1.0	31.4	13.4	42.8
1.0	2.0	20.2	9.8	48.7

Improvements to the electron sensitivity may be made by decreasing the flash tube diameter or increasing the distance between the lead target and detecting planes. The latter is normally restricted by limitations on the physical size of the chamber, and from this series of experiments the increase in distance between target and detecting plane required to make a significant difference in the sensitivity is shown to be large. Measurements on the numbers of tube ignitions as a function of lead thickness for the 1.0 and 2.0 radiation length data agree well (see Figure 7.9), indicating that spaces greatly in excess of 5.4 cm (the distance between detecting planes) are required to give any substantial improvement. This is also evident from Figure 7.11, where the electron sensitivity plotted against electron number for both the 1.0 and 2.0 radiation length data approximates to the same function. Nevertheless, chambers constructed with smaller diameter tubes are expected to give an increased sensitivity, and the effect of increasing the target-detecting plane distance by a relatively small amount should give a measurable improvement.

The energy resolution is characterized by the full width of the frequency distribution (Figures 7.5 and 7.6) at the half maximum,

ΔE over E. By this definition and from theoretical considerations, the resolution should improve as $1/\sqrt{E}$, assuming the frequency distributions are of Poisson type and the number of cascade electrons increase linearly with energy. Figure 7.12 shows the resolution of the flash tube chamber plotted against momentum for both the 1.0 and 2.0 radiation length data, giving 36 and 47% (FWHM) respectively, at 1.0 GeV/c. The resolution is seen to improve roughly as $1/\sqrt{E}$, but deviates at higher momenta when shower leakage and insensitivity to individual electrons becomes significant. At low momenta the resolution is substantially improved by using only 1.0 radiation length of target, but decreases crossing the 2.0 radiation length curve, due to excessive longitudinal leakage.

Deterioration in resolution usually results from two sources; statistical fluctuations in the shower development, and measuring errors caused by inherent properties of the detectors themselves. Large fluctuations in the numbers of detected electrons in any plane can be expected because the mean total number of electrons at any target thickness (see Figure 7.1) is small for incident energies of a few GeV. Improvements in resolution should be expected, therefore, if the shower is sampled at more frequent intervals by decreasing the thickness of target and increasing the number of detecting planes. In practice, however, the amount of sampling is usually restricted by the overall size of the chamber, and a compromise must normally be made between resolution and the number of detecting planes. A detailed and qualitative study of the variations in the resolution as a function of the number of target-detecting planes was not made during this series of experiments and little work has been reported by other authors (32). Nevertheless, from the experimental results shown in Figure 7.12 the resolution is seen to improve by about 20% by halving the target thickness from 2.0

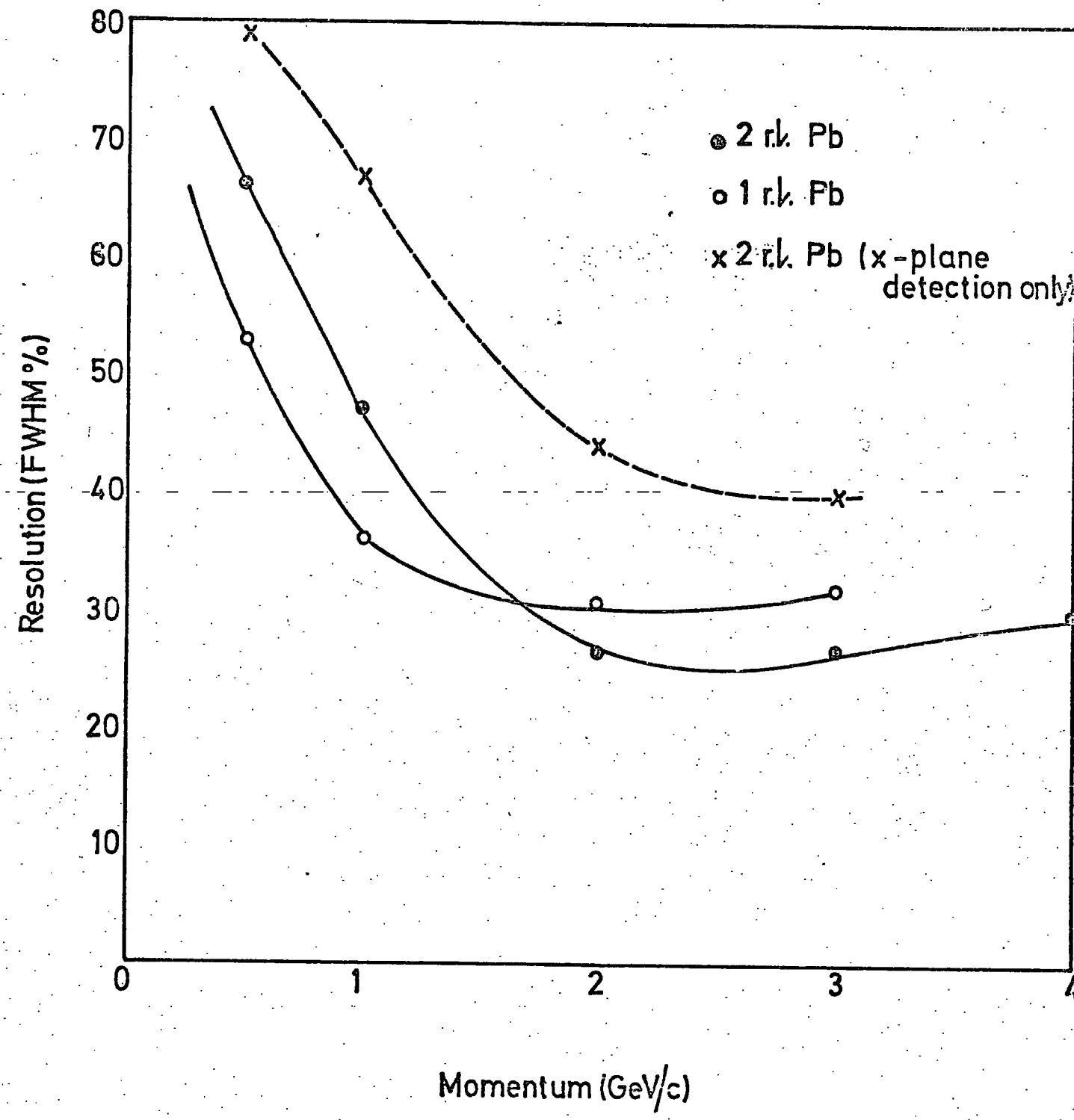

Fig 7·12 Resolution versus Momentum

to 1.0 radiation lengths. A more thorough investigation is necessary in this respect, either experimentally or by Monte Carlo simulation, such that the detecting geometry may be optimized.

Detecting planes which do not always give a true measure of the number of cascade electrons also contribute to a deterioration in resolution. This occurs with detectors like flash tubes, which often measure less electrons than are actually created, because they sample the cascade in projection and have a limited ability to detect single electrons by virtue of their size. Thus, a measure in one plane will always be dependent on the spatial structure of the shower which will vary from one event to the next. This situation will be improved by decreasing the tube radius, to help minimize the probability of detecting more than one electron in each tube, and by sampling the shower in several different projections. The latter method requires adjacent layers of flash tubes placed after each target, which sample the shower in different planes. This method gives a measure of the total number of electrons which is less susceptable to detecting fluctuations. A measure of the increase in resolution obtained by this method can be seen in Figure 7.12 where a third resolution curve is plotted for data obtained with only one layer of flash tubes after each target, instead of the two orthogonal layers, which in comparison gives a much improved resolution curve. The gain in resolution is of the order of 30%.

7.3.3. Spatial Measurements

The spatial accuracy of a gamma-ray detector is not an easy quantity to measure because it will depend as much on the method used to analyse the data in determining a trajectory, as the properties of the detector itself. A gamma-ray trajectory is normally determined by locating the axis of the cascade shower, which is on average, symmetrically distributed around the original direction of the initiating particle.

The determination may be made by a visual estimate, in the case of a photographic recording (33, 34), or by an analytical method using the shower coordinates. Visual methods have the disadvantage of being subject to errors of judgement and are not usually compatible with fast electronic experiments where large quantities of data are collected. Analytical methods, however, are not always simple if the best resolution is to be obtained, because the axis of any individual shower is not a well defined parameter in terms of the coordinates of its cascade particles, which vary statistically about a mean shape.

It is the purpose of this section to describe a method of shower axis location which optimizes the coordinate data from the flash tube chamber, and to compare the results with trajectories of incident positrons.

If it is assumed that a shower spreads isotropically about its core, then the axis may be determined by calculating the 'centre of gravity' in each detecting plane. The centres may be found, very simply, by calculating the following expression for each detector module.

$$y_i = \sum_{j=1}^{N} x_{ij}/n_i \qquad \ldots\ldots\ldots\ldots\ldots\ldots (1)$$

where y_i is the coordinate of the shower centre in the ith module

x_{ij} is the coordinate of the jth ignited flash tube in the ith module

n_i is the total number of ignited tubes in the ith module

N is the total number of tubes in a module.

In this way, coordinate points may be found in each plane along the length of the shower, which represent a series of axial determinations. From these points a straight line may be fitted to give the trajectory of the incident particle.

This method is not, however, entirely satisfactory because it assumes that electrons are produced uniformly about the axis and does not take account of statistical variations which occur from one shower

to another. Electrons which are produced at large lateral and longitudinal distances are more susceptible to fluctuations in position, thus more weight should be placed on information at the beginning and interior of the shower than at the edges and rear, where absorption and large angle multiple scattering has occurred. Consequently, it is advantageous to weight the data in the lateral direction, during the determination of the shower centres in each plane, and in the longitudinal direction, when the individual points are fitted to a straight line.

Weighting in the lateral direction was achieved by using a weighting function of similar form to the mean lateral shower distribution in a given plane. The distribution of shower particles, observed in projection, may be represented by a Gaussian function (35), from which a weighting factor for each of the shower defining tubes was obtained. The weighting function is described by the following expression:

$$W_{ij}(y_{ij}) = e^{-\phi^2_{ij}} \qquad \text{..... (ii)}$$

where

$$\phi_{ij} = \frac{y_{ij} - y_o - x_i \tan\theta}{\Delta y_i / \cos\theta} \qquad \text{..... (iii)}$$

and $W_{ij}(y_{ij})$ is the weighting factor given to the jth tube in the ith module.

y_{ij} is the coordinate of the jth tube in the ith module from a defined axis

y_o is the distance of the shower axis apex from a defined axis.

Δy_i is a quantity representing the mean spread of the shower in the module

x_i is the distance of the ith module from a defined axis

θ is the angle between the shower axis and the x axis

For particles at normal incidence ($\theta = 0$) equation (iii) simplifies to

$$\phi_{ij} = \frac{y_{ij} - y_o}{\Delta y_i} \qquad \text{.....(iv)}$$

In this series of experiments equation (iv) was used because the beam was known to be normal to the chamber to within $\pm 2.4^{o}$.
These parameters are given more clearly in Figure 7.13 which shows a shower and its defining coordinates. Using the above method a flash tube, distant from the shower axis, carries less weight than those close to the core. Thus, a electron which is not associated with the main core of the shower is weighted such that its contribution leads to a comparitively small error in the determination of the shower centre.

Fitting this data to a straight line, to give the axis, also requires weighting, because information obtained from the first detecting modules is more reliable than that from the last modules, where the shower has undergone absorption and mutiple scattering. Figure 7.14 shows the development of a 0.5 GeV/c shower, clearly illustrating the increasing spread of particles in the lateral direction.

For the purpose of weighting, a factor was determined for each module at different momenta, which was a measure of the information content in each detecting plane. The weighting factors were made equal to $1/\sigma$ where σ is the standard deviation of the distribution of fluctuations of the calculated shower centres about the real centres in each detecting plane. This was found by measuring the frequency of differences between the calculated shower centre (using equation (i)) and the real centre, for several thousand events at each energy. The real shower centres were found from the first detecting module which contained no lead, and was used to locate the trajectory of the incident particle. By this method, the projected particle trajectory was assumed to represent the shower axis with the knowledge that the incident beam was parallel to better than $\pm 0.4^{o}$ (36). The values of the standard deviation , calculated by the above method, are given in the following tables.

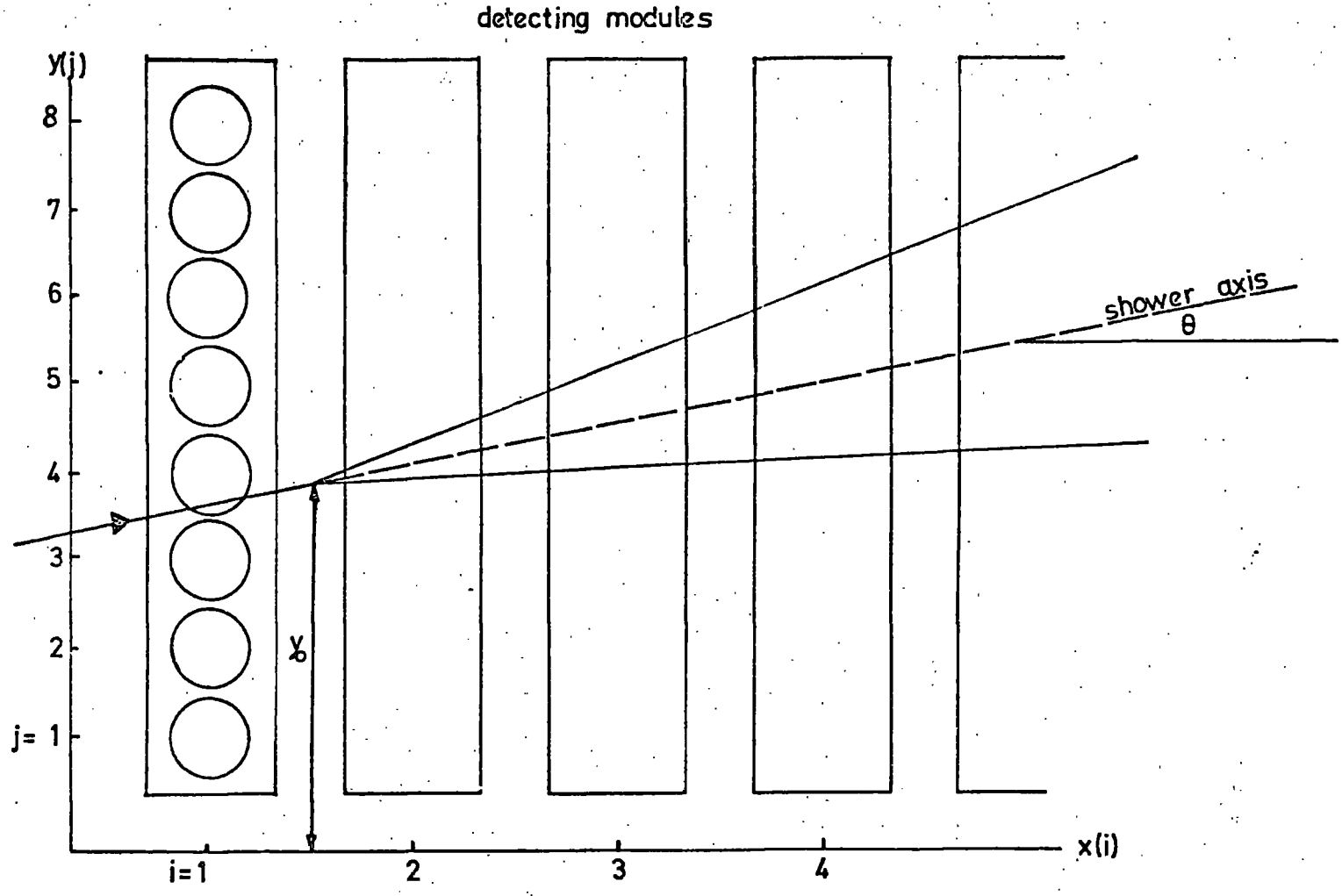

Fig 7-13 the shower defining coordinate system

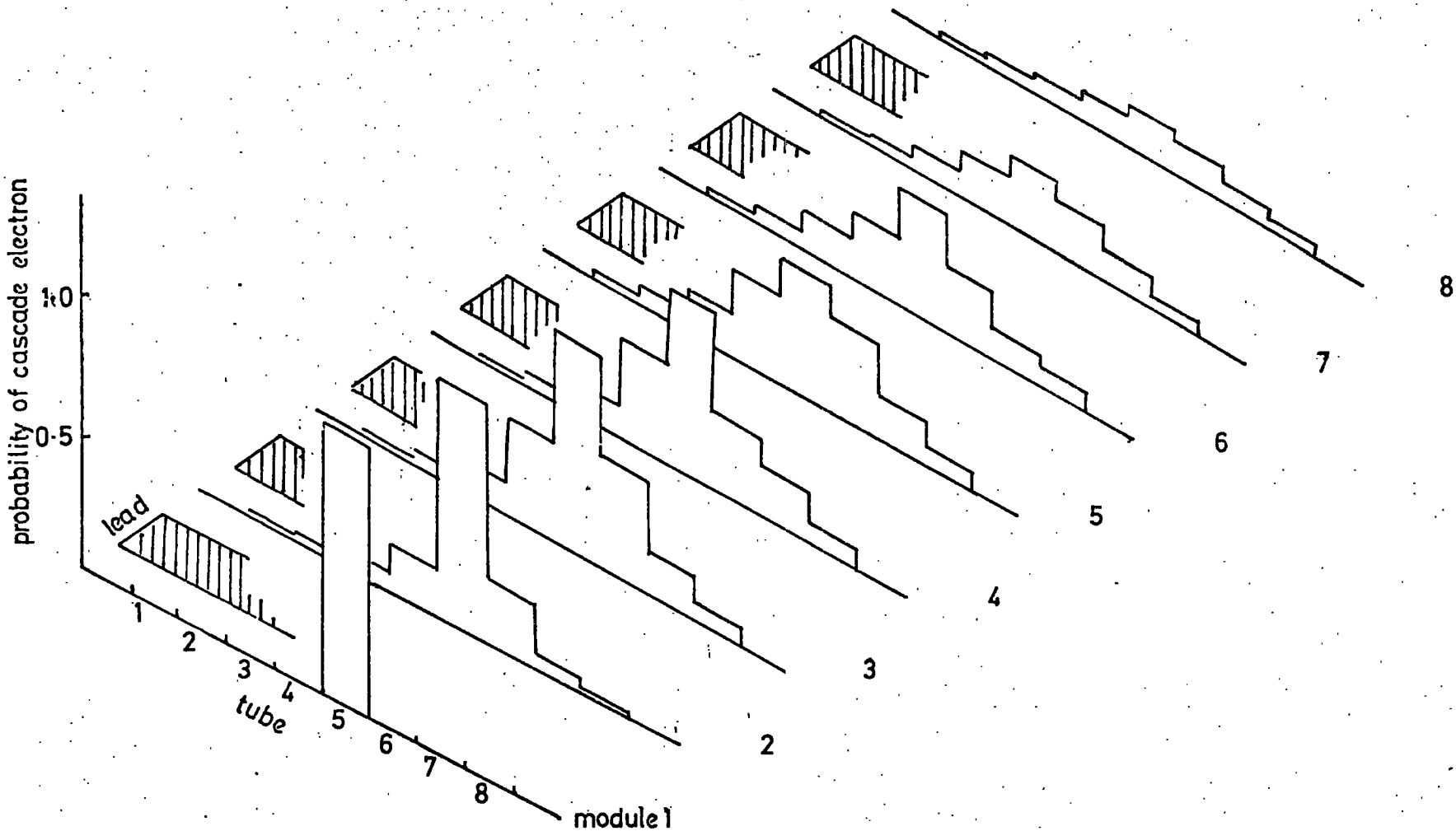

Fig 7·14 electron shower profile for 0·5 GeV/c positrons with 1·0 r.l. of lead between modules

One radiation length of lead target

standard deviation (cm)

E(GeV)	module 2	3	4	5	6	7	8
0.5	1.03	1.20	1.77	2.48	3.64	4.94	8.68
1.0	1.03	1.09	1.29	1.63	2.01	3.01	5.04
2.0	1.01	1.02	1.09	1.25	2.09	2.09	4.08
3.0	1.05	1.13	1.10	1.13	1.62	1.62	3.13

Two radiation length of lead target

standard deviation (cm)

E(GeV)	module 2	3	4	5	6	7	8
0.5	1.11	1.26	1.35	1.59	2.11	2.22	2.63
1.0	1.09	1.10	1.19	1.24	1.41	1.61	2.14
2.0	1.23	1.27	1.32	1.29	1.39	1.42	1.63
3.0	1.29	1.28	1.30	1.27	1.35	1.33	1.61

The tables clearly show an increase in spatial fluctuations at low energies and in detecting planes furthest from the shower apex. These measurements provide the weighting factor $(1/\sigma)$, used in the least squares fit of the shower centres, and the value of Δy_i in equation (iii) for weighting data in the lateral direction. The standard deviation could be used to represent Δy_i because it is an effective measure of the lateral spread of the shower in a plane. The justification for doing this can be seen from the example shown in Figure 7.15 where the shower profiles (normalized) are compared with their weighting functions, described by equation (ii) using the appropriate standard deviation. The Gaussian weighting functions are seen to be an acceptable approximation to the measured profiles in each plane.

The shower axis was calculated by an iteritive process using the described weighting functions. The calculation required the use of a computer which determined the axis by executing the following procedure:

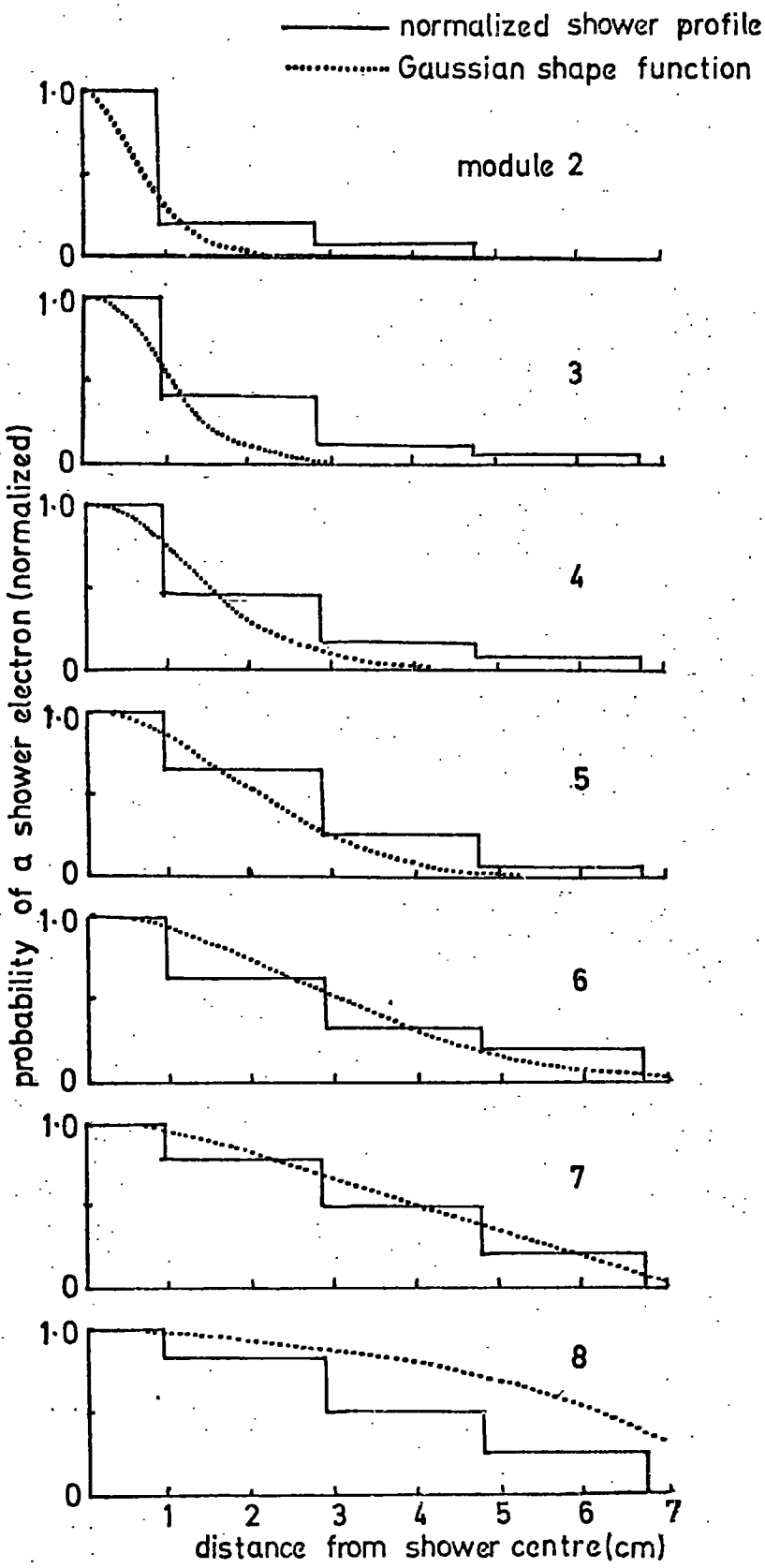

Fig 7.15 normalized shower profiles at 0.5 GeV/c with 1.0 r.l. of lead compared with Gaussian shape functions

(1) An initial estimate of the shower centres was obtained by calculating the 'centre of gravity' in each module using equation (i).

(2) A straight line, representing the axis, was determined from the shower centres by a weighted least squares fit using the weighting factor $1/\sigma$.

(3) The flash tube data in each module was weighted laterally about the determined axis using equation (ii).

(4) A new 'centre of gravity' was determined for each module using the weighted data.

(5) A straight line, representing the axis, was determined from the new centres by a weighted least squares fit using the weighting factor $1/\sigma$.

(6) Redetermination of the axis was continued, by weighting about the previous determined axis, until convergence was obtained.

Convergence to a constant value was normally obtained after about five iterations.

A measure of the accuracy of axis location was made by comparing the calculated axis with the real axis. The real axis could be determined from the position of the incident particle in the first flash tube module, with the knowledge that the beam was parallel to better than $\pm$ 0.4^{o} (measured with an array of high precision drift chambers (36)). Two parameters were measured from each event to determine the angular and spatial resolution; the angle of the shower axis relative to the X-plane, and the deviation of the position of the calculated shower apex from the true apex which was located by flash tubes in the first module. Figure 7.16 defines the angle (θ) and the apex deviation (Δ) measured for each event.

The necessity for weighting the data is illustrated by figure 7.17 and 7.18 which show the frequency distributions for the apex deviation

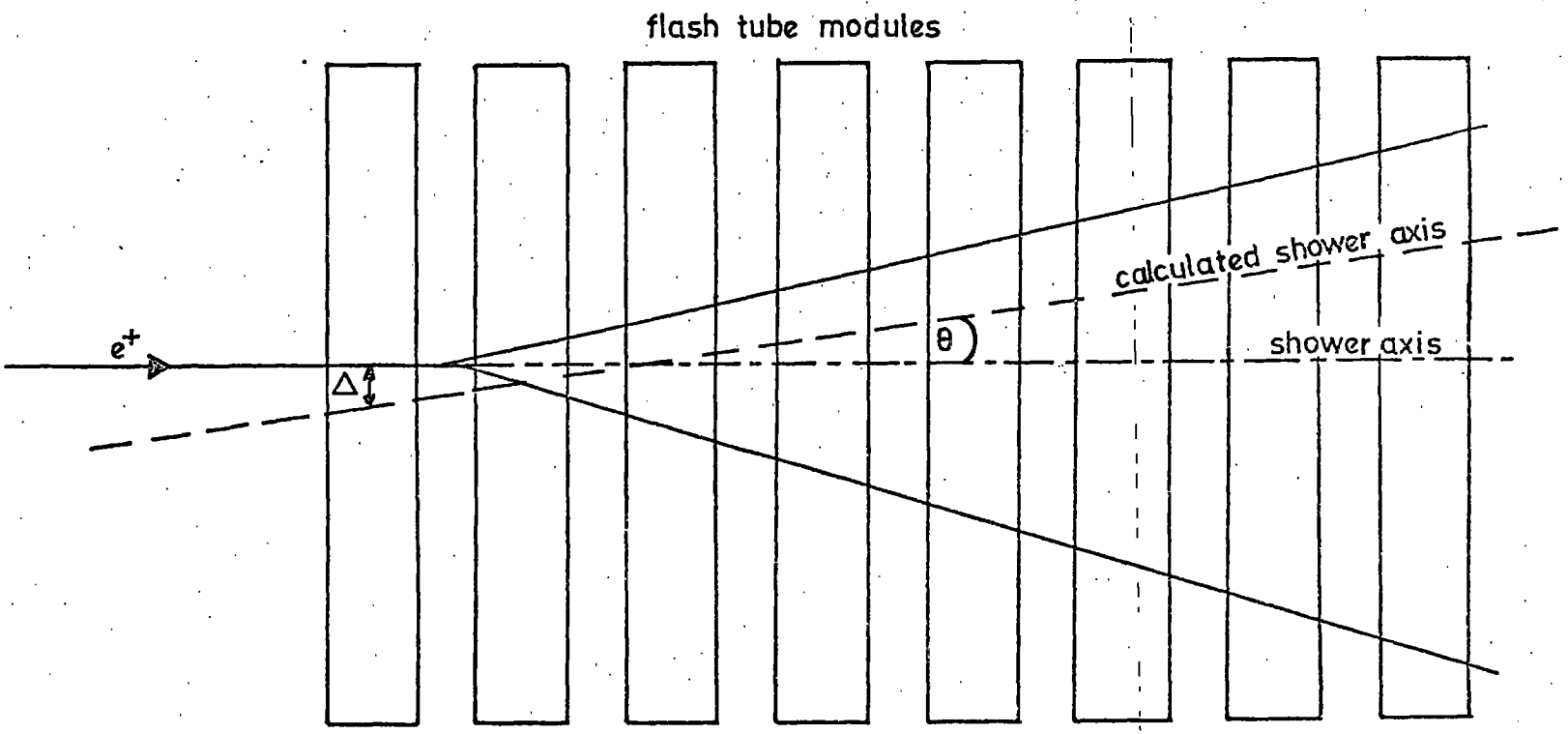

Fig 7.16 the shower apex deviation (Δ) and shower axis angle (θ)

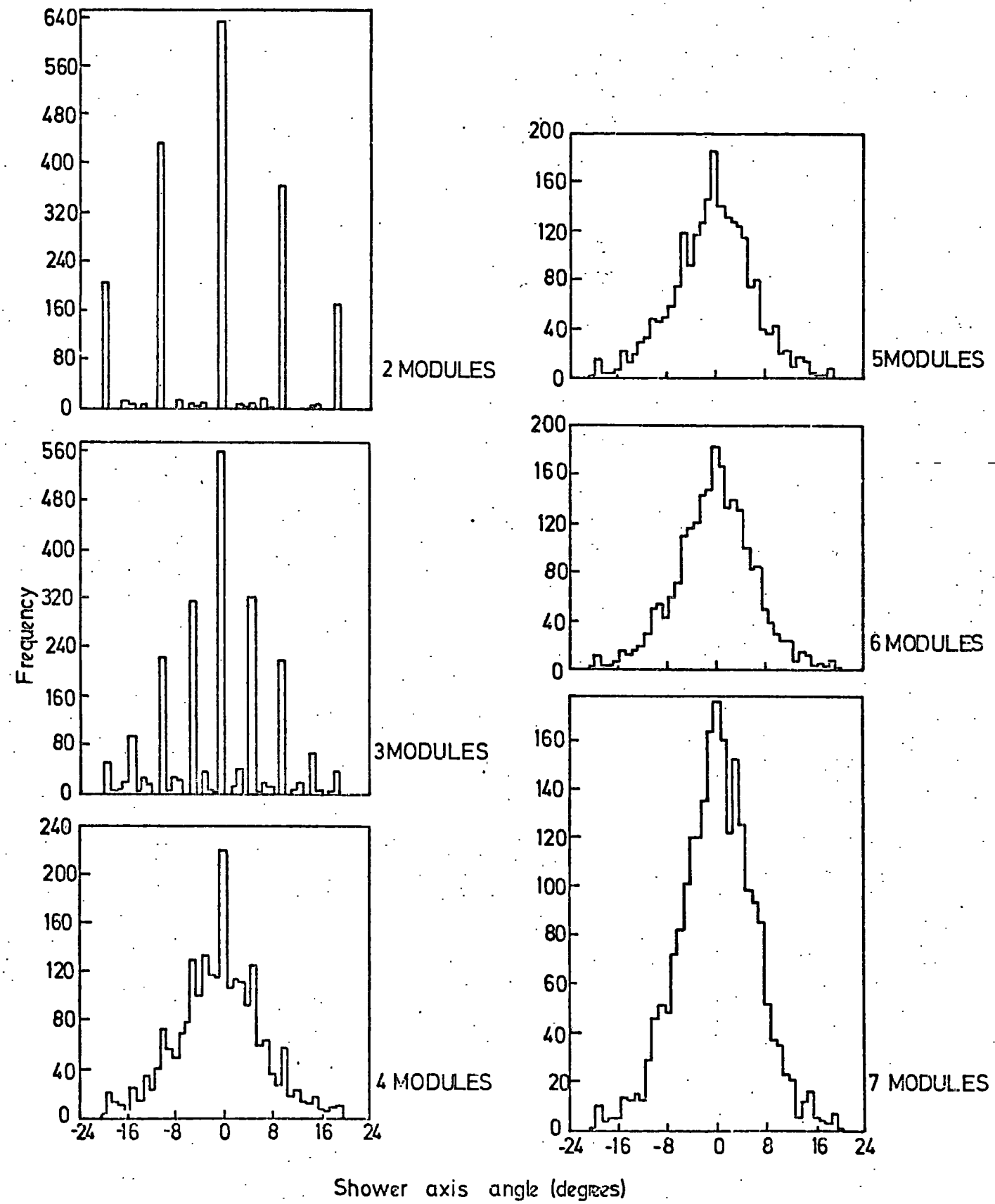

FIG. 7.17. Shower axis angle measurement using different number of modules for 1 GeV/c positrons with 2 radiation lengths of lead target.

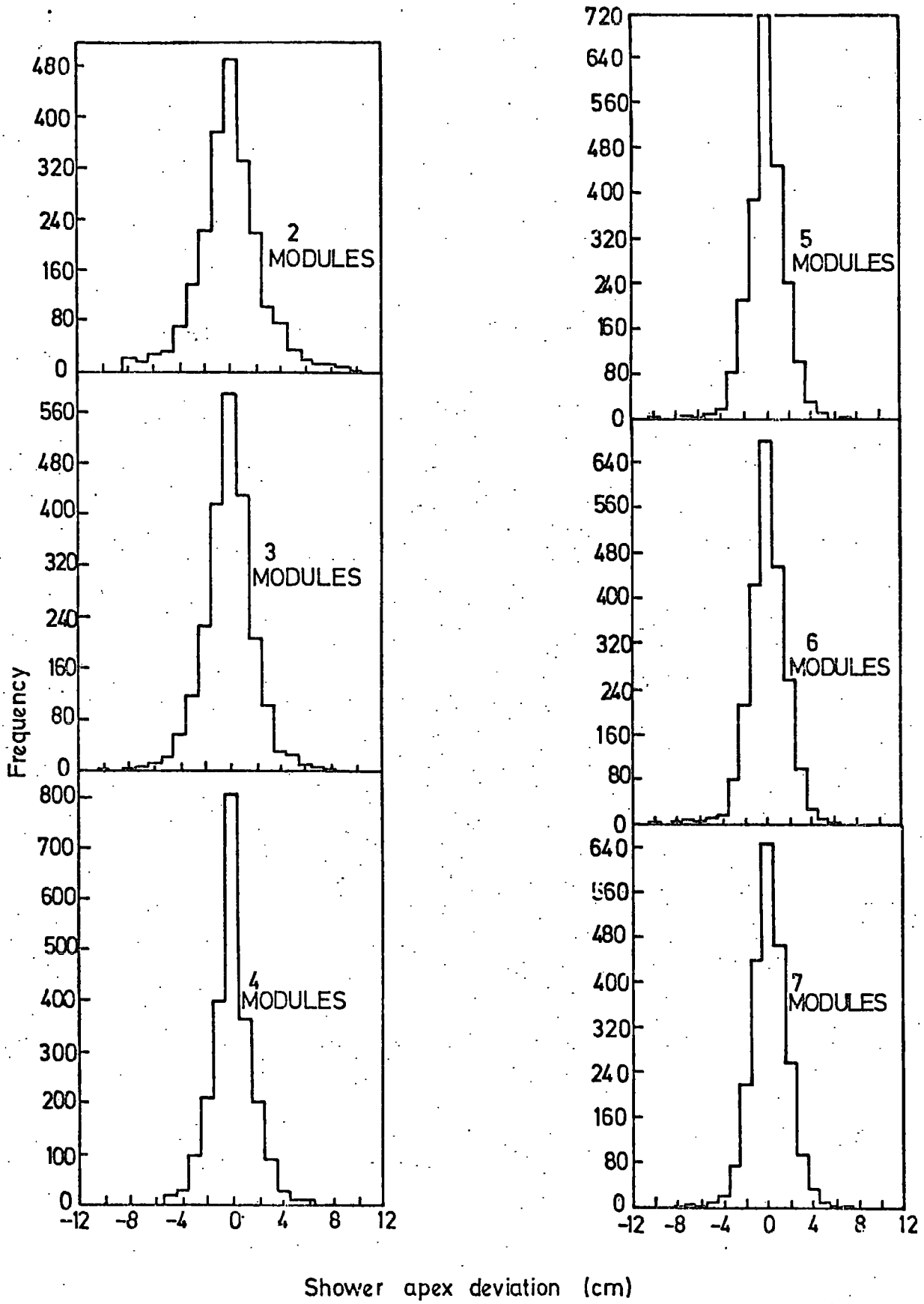

FIG. 7·18. Shower apex deviation using different numbers of modules for 1·0 GeV/c positrons with 2 radiation lengths of lead target.

(Δ) and the shower axis angle (θ), plotted using different numbers of detecting modules at 1.0 GeV/c. A gain in resolution is obtained as the number of detecting modules is increased to four. Increasing the number still further provides no additional contribution to the spatial or angular resolution, in fact the FWHM measurement indicates a deterioration. This may be expected because a large fluctuation in the determined shower centre from the real centre, which frequently occurs in the last few modules, will cause a loss of precision if all the centres are given equal weight. Moreover, if several large fluctuations occur, a severe discrepency from the true axis can be expected for an unweighted least squares fit.

Shower data was analysed using both the simple 'centre of gravity' and the weighted-iterative method. Figures 7.19, 7.20, 7.21 and 7.22 show the frequency distributions for the shower axis angle and the apex deviation, analysed from over 3000 events at each energy with 1.0 and 2.0 radiation lengths of target between modules. Each figure compares the results calculated using the weighted iterative method with the unweighted method of analysis. The results from both methods give a resolution (angular and spatial), characterized by the width of the distributions, which improves with increasing energy and decreasing quantity of lead target. This may be expected because a greater number of detected shower particles will produce a 'centre of gravity' determination which is less susceptible to statistical fluctuations about a mean position.

In each case, a comparison of the two sets of distributions show that a substantial improvement in resolution may be gained by using the weighted iterative method of analysis. The following table summarizes the resolution in terms of the full width measured at the half maximum (FWHM) for both the apex deviation and the shower axis angle.

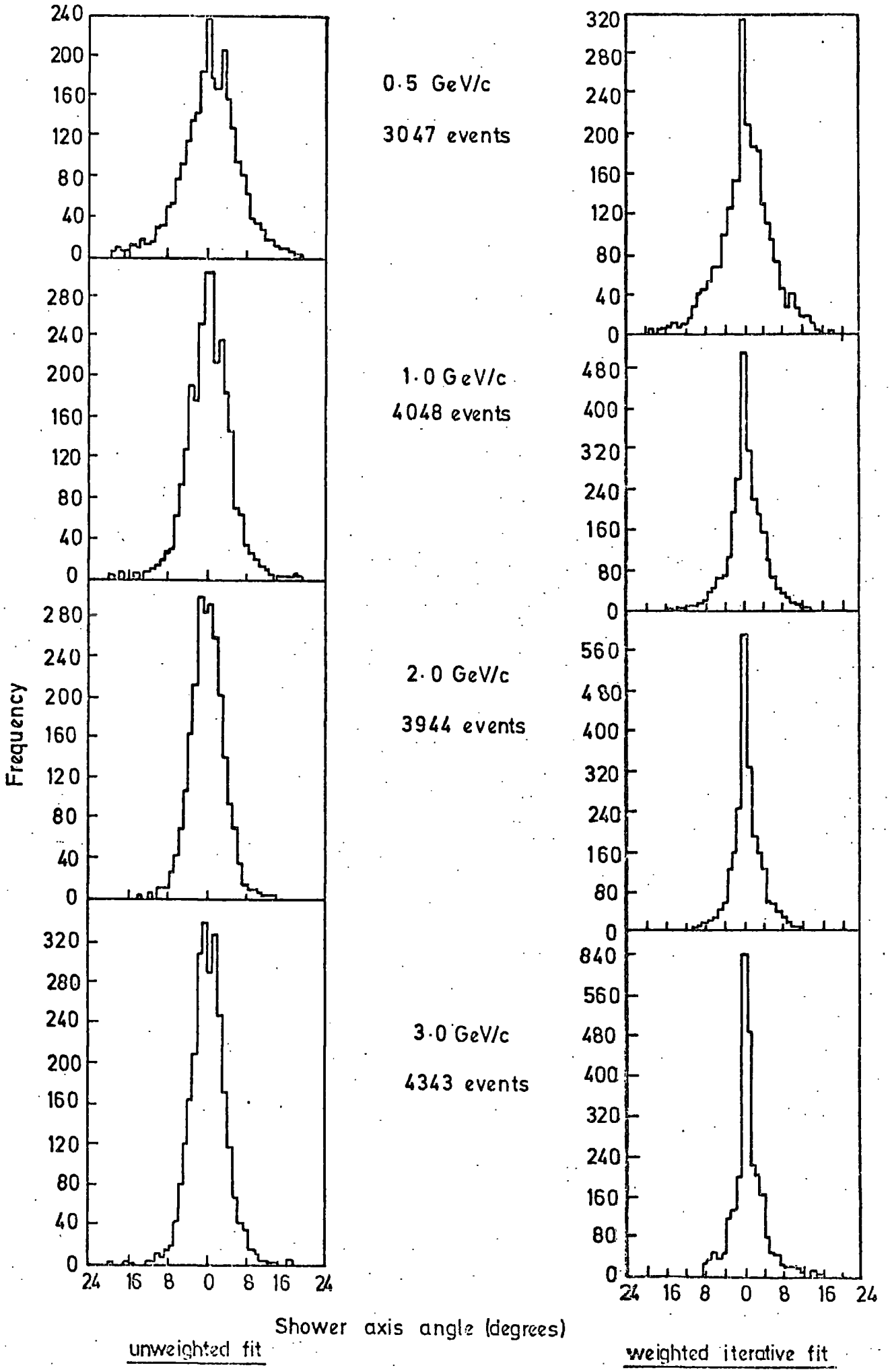

FIG. 7·19. Frequency distribution for the shower axis angle calculated by an unweighted and weighted iterative fit from 1·0 radiation length data.

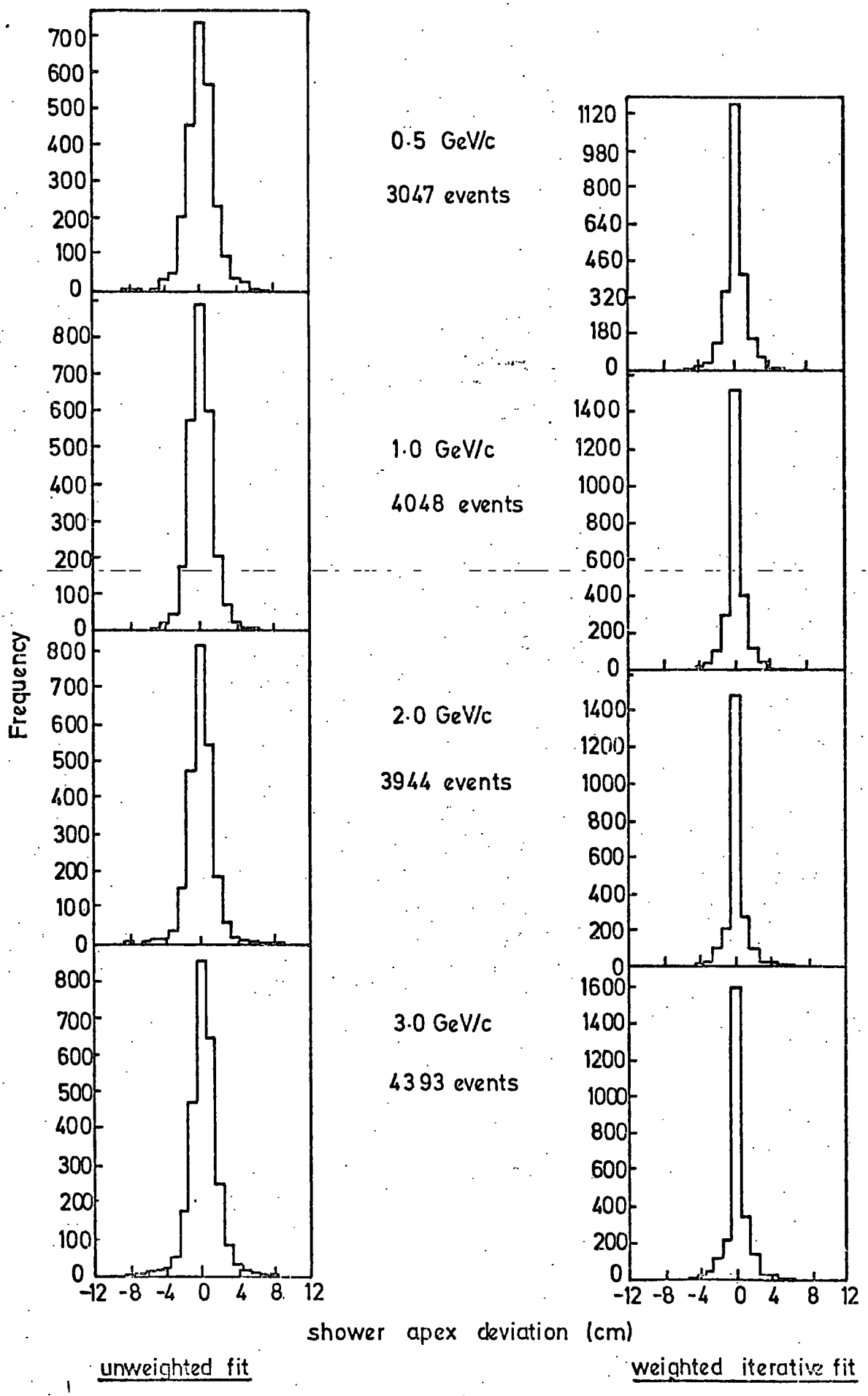

FIG. 7·20 Frequency distribution for the shower axis deviation calculated by an unweighted and weighted iterative fit from 1·0 radiation length data.

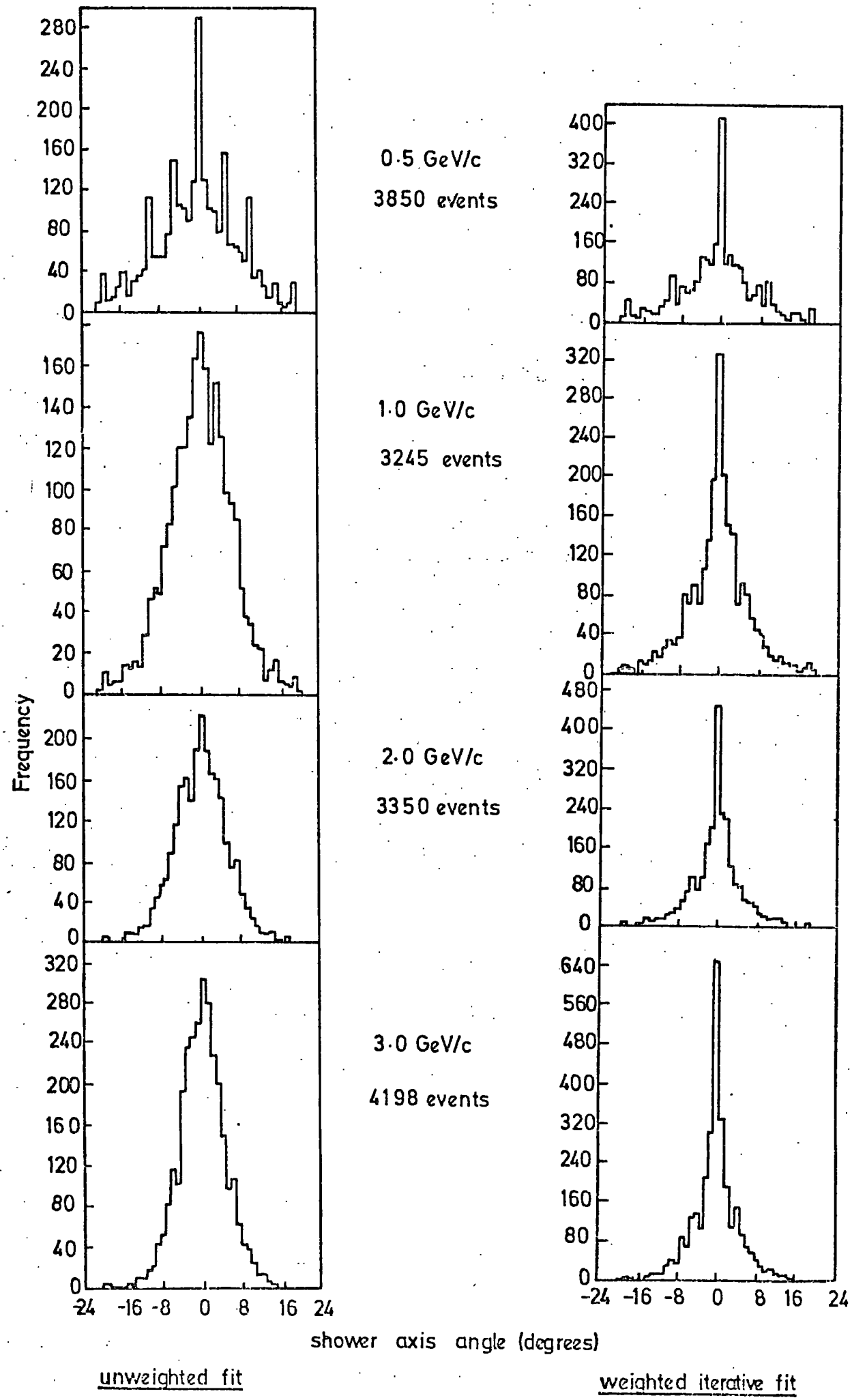

FIG. 7·21. Frequency distribution for the shower axis angle calculated by an unweighted and weighted iterative fit from 2·0 radiation length data.

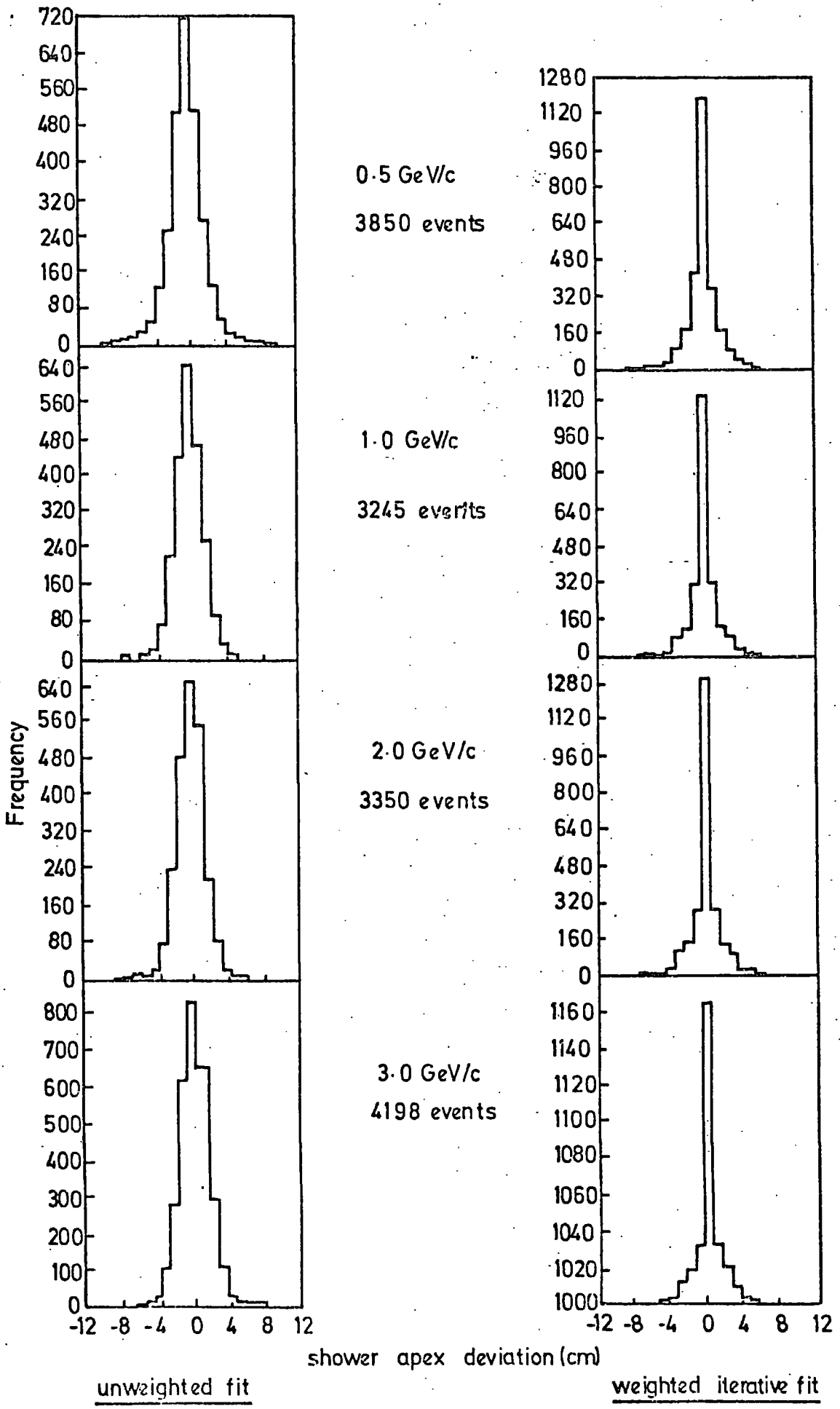

FIG. 7·22. Frequency distribution for the shower axis deviation calculated by an unweighted and weighted iterative fit from 2·0 radiation length data.

		Unweighted Fit		Weighted-iterative Fit	
	E(GeV)	Apex dev. FWHM(cm)	Angle FWHM (degrees)	Apex dev. FWHM(cm)	Angle FWHM (degrees)
2 r.l. of lead target	0.5	3.0	12.0	1.0	1.0
	1.0	3.0	13.0	1.0	3.0
	2.0	3.0	10.0	1.0	2.0
	3.0	3.0	8.0	1.0	2.0
1 r.l. of lead target	0.5	3.0	9.0	1.0	4.0
	1.0	3.0	8.0	1.0	2.0
	2.0	3.0	7.0	1.0	2.0
	3.0	3.0	8.0	1.0	2.0

From the table it is clear that the weighted-iterative method has had a considerable effect, the FWHM resolution increasing by a factor of about 3 or 4 in each case.

Although the FWHM resolution measurement provides a rough means of comparison, due to the form of the distributions in this instance, the measurement is not a very meaningful quantity. The weighted-iterative fit distributions are non-Gaussian in shape, and the FWHM measurement is often only one bin-width wide. Decreasing the bin width, for the apex deviation distribution, to less than 1 cm was not justified because the position of the incident particle could only be determined to $\pm$ 0.8cm ($\pm$ a tube radius).

A more informative method of measuring the resolving capabilities of the device, especially when the distributions are non-Gaussian, is to calculate the proportion of events which have been determined to within a fixed error. The following tables shows the percentage of results which lay between $\pm$ 0.5cm and $\pm$ 1.5cm for the apex deviation, and $\pm$ 1.5^{o} and $\pm$ 2.5^{o} for the shower axis angle using the unweighted and weighted-iterative method.

		% data laying between fixed error limits							
		Unweighted fit				Weighted-Iterative fit			
		Apex dev.		Angle		Apex dev.		Angle	
	E(GeV)	± 0.5 cm	± 1.5 cm	$\pm 1.5^{\circ}$	$\pm 2.5^{\circ}$	± 0.5 cm	± 1.5 cm	$\pm 1.5^{\circ}$	$\pm 2.5^{\circ}$
2 r.l. of lead target	0.5	26.5	64.2	20.5	35.1	44.4	73.4	35.7	44.1
	1.0	28.2	67.8	21.9	44.0	49.8	77.6	31.6	55.0
	2.0	27.3	71.1	25.0	51.3	54.2	78.0	36.8	62.2
	3.0	28.2	71.2	28.4	51.2	55.7	76.6	43.0	63.6
1 r.l. of lead target	0.5	33.9	71.5	20.0	50.9	58.3	79.7	40.1	54.3
	1.0	30.1	64.4	24.3	63.9	48.0	85.2	37.7	69.4
	2.0	34.9	78.4	37.5	73.3	63.6	84.5	49.9	82.1
	3.0	32.7	75.1	35.6	70.0	61.2	82.3	50.5	75.8

Again, these results show that the weighted-iterative fit gives considerable improvement; 70-90% more spatial data lies between ± 0.5cm and 30-80% more angular data lies between $\pm 1.5^{\circ}$. The best results were obtained at 3.0 GeV using 1.0 radiation length of lead target where 61.2 and 50.5% of data lies between $\pm$ 0.5cm and $\pm 1.5^{\circ}$ respectively Using the criterion that the resolution represents the width of the distribution containing 70% of the data, which in the case of a Gaussian distribution defines the FWHM, the resolution of the flash tube chamber can be determined approximately from the table above. This gives a spatial resolution between $\pm$ 0.5 and $\pm$ 1.5cm, and an angular resolution of the order $\pm 2.5^{\circ}$, using the weighted-iterative results. It should be noted, however, that the accuracy of location of the incident particle ($\pm$0.8cm) lies within the spatial resolution range, thus the percentage values given in the above table should be larger than those recorded. It is possible, therefore, that the spatial resolution is better than $\pm$ 0.8cm, that is $\pm$ a tube radius.

7.4 Comparison with other methods

The spatial and angular resolution of the prototype-flash tube chamber compares favourably with conventional gamma ray detecting techniques described in section 7.2. In the visual class of detectors, which normally consist of spark chambers interspaced with lead target, the energy resolution compares very well indeed, infact, in the 0-3GeV range the flash tube results are superior to those obtained with the best spark chamber devices of the current-limited type. In Figure 7.23 the resolution is plotted as a function of energy for different spark chamber devices, giving a comparison between this work and the work of Bauer (26) and Agrinier (21), using metal spark chambers, and Allkofer (25) using glass current-limited spark chambers. Also, an overall comparison between the different types of gamma detecting devices is made in Figure 7.24, where the resolution range of each type is plotted as function of energy. From this diagram the flash tube energy resolution is seen to lie between the highest resolving spark chamber devices and the poorest resolving scintillation/ Cerenkov sandwich devices.

A more valid comparison can be made if detectors of a different type are compared in the same accelerator beam to prevent discrepencies arising from beam contamination. Figure 7.25 shows the flash tube resolution measurements compared to results obtained with a total absorption lead glass Cerenkov device in the DNPL e^+ accelerator beam (37). These results show the Cerenkov detector to be only marginally better than the flash tube chamber, at energies in the range 1-2 GeV This is surprising, considering other reported resolution measurements made with Cerenkov devices which give much higher values (see Figure

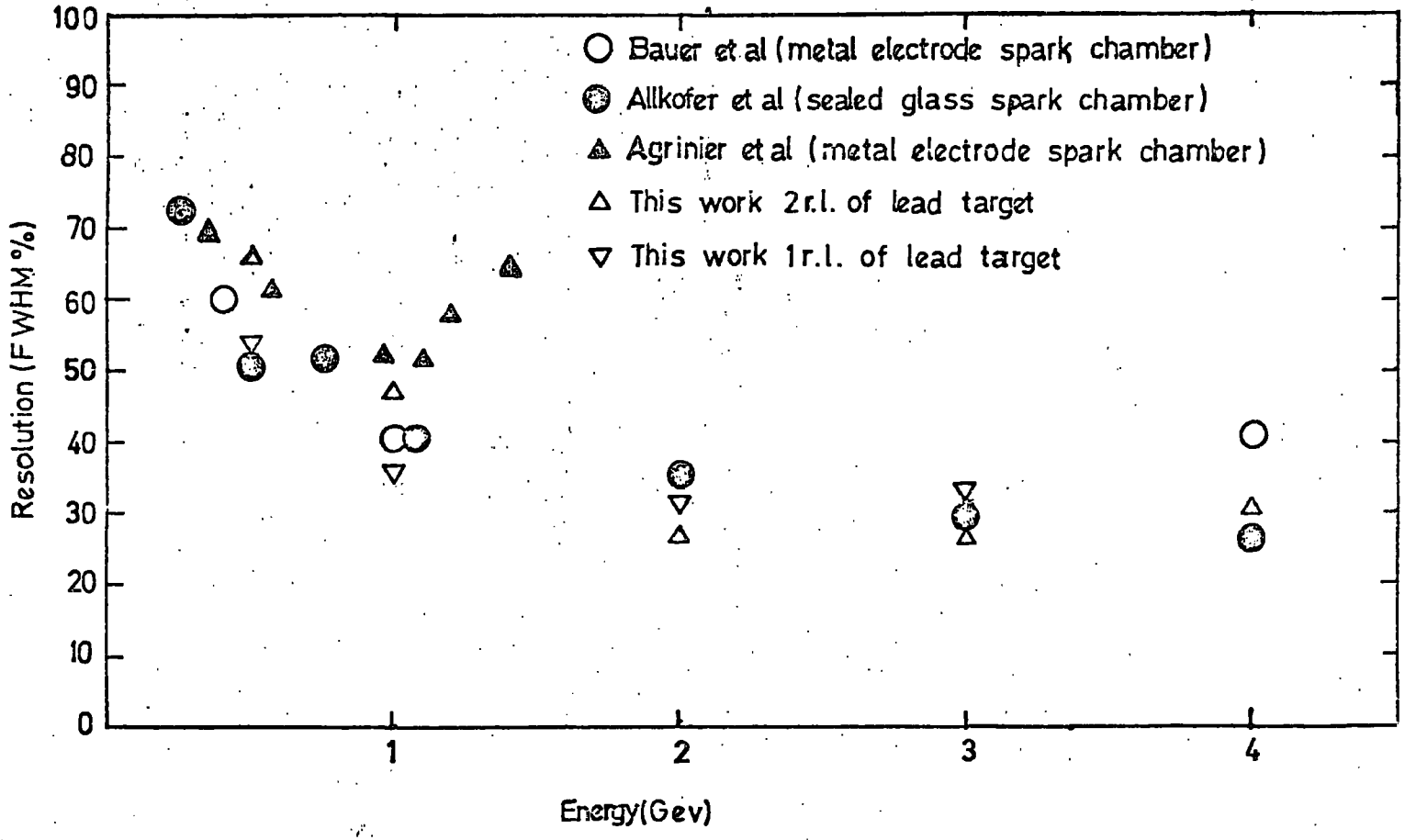

FIG 7·23 A comparison of resolution with spark chamber devices

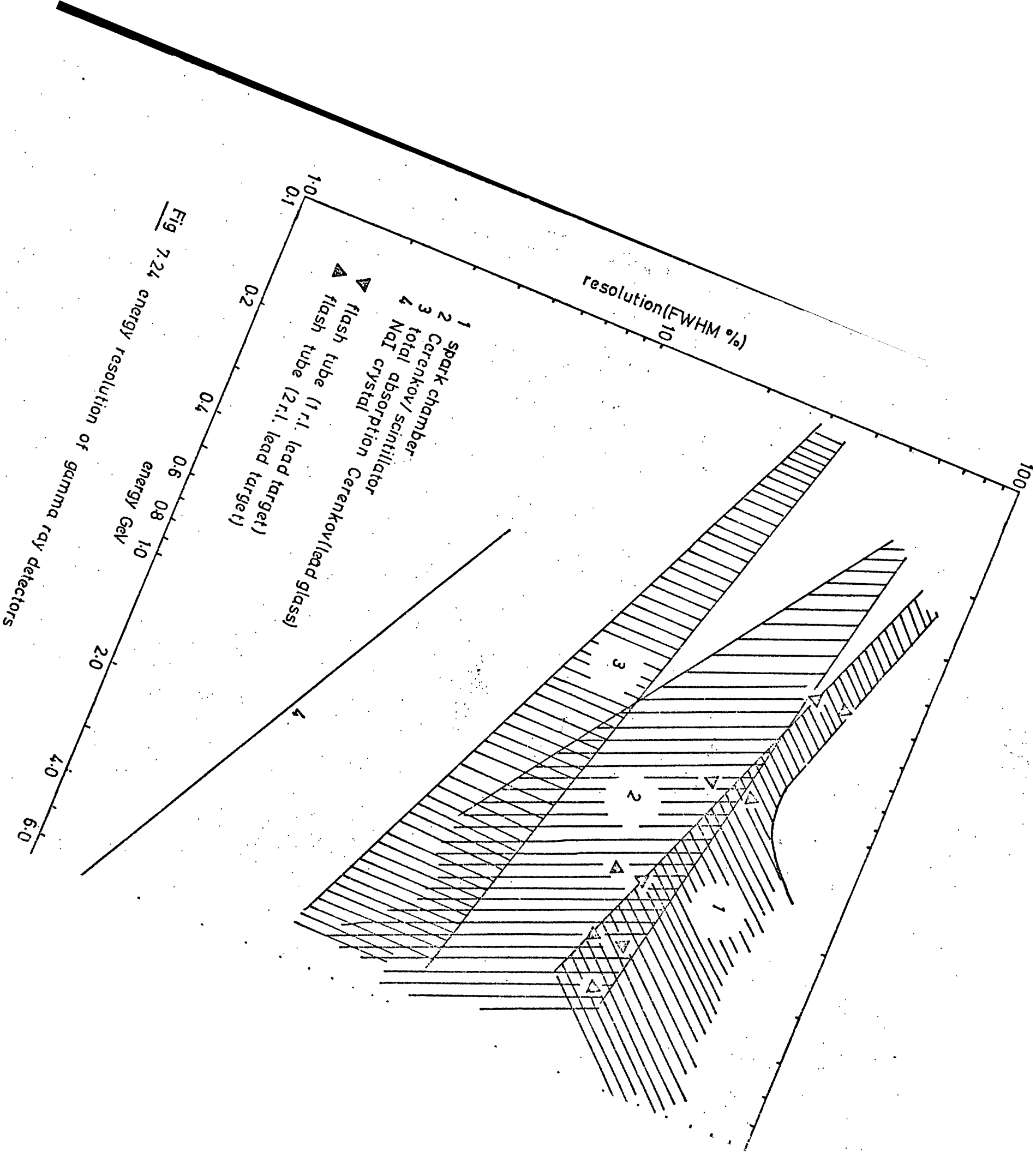

Fig 7.24 energy resolution of gamma ray detectors

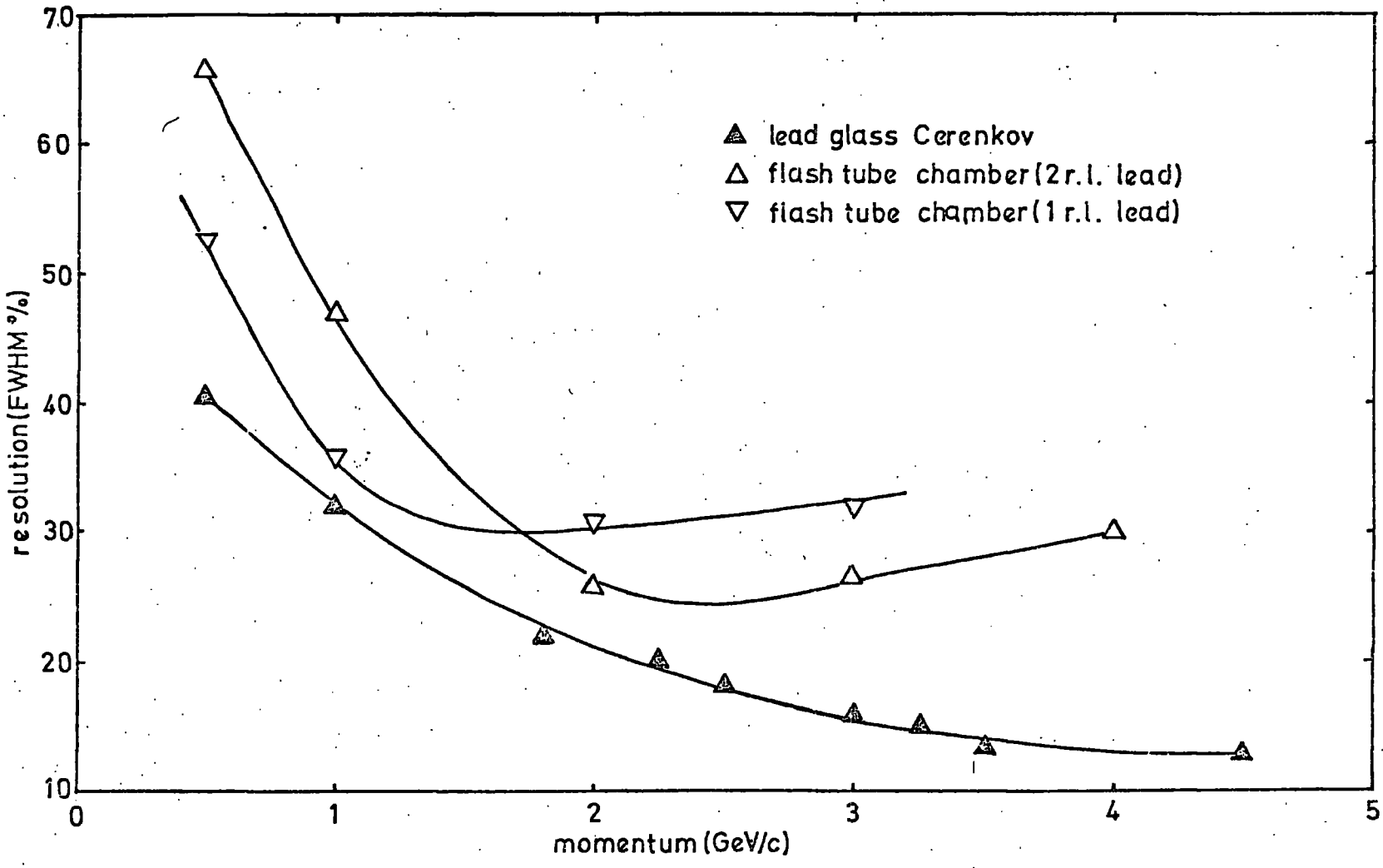

Fig 7.25 flash tube chamber and lead glass detector resolution measured in the DNPL e+ beam

7.24). An explanation may be that the beam purity is less than the quoted design figure of ± 1% which is almost impossible to measure experimentally. Alternatively, the low value may be caused by an inherent feature of the detecting system which gives an inferior resolving power compared to other Cerenkov devices, but nevertheless, this result does throw some doubt on the quoted resolution of the beam energy.

A comparison of the spatial and angular resolution of the flash tube chamber with other devices is made difficult by the lack of reported work by other authors. Except for the very sophisiticated and expensive cross scintillation sandwich detectors, which some claim to have a spatial accuracy of ± 0.2cm (28), spark chambers are the only other type of device which have been used to give accurate spatial information. Bauer (26) has studied the accuracy by which the shower axis may be measured from metal spark chamber data using electrons at 4.6GeV. This study has shown that the angle may be determined to an accuracy of about $\pm 0.7^{o}$ by a visual and analytical method. If the flash tube angular resolution is taken as $\pm 2^{o}$ (FWHM) then the spark chamber results of Bauer are only a factor of about three better.

7.5. Conclusion

The results presented in this chapter have demonstrated the feasibility of using flash tubes as a high energy gamma ray detector. Experiments with the positron beam at DNPL have verified the usefulness of the device under accelerator conditions and have shown its capability as a high energy photon detector having both spatial and energy resolution comparable with conventional detecting techniques and at a fraction of their cost (see section 4.3). In particular, the measurements have shown that

flash tubes may facilitate a large area detecting device, capable of providing digitized energy and trajectory information with simplicity and reliability, for the detection of neutral particles which decay into photons.

The results obtained in this series of experiments have shown the resolution of the device to be comparable, and in some cases superior to, spark chamber devices, which is encouraging, as the flash tube detector was a first attempt of very simple construction and used large diameter flash tubes. An improved design, which should have an energy and spatial resolution in excess of spark chamber devices, has been designed and constructed on the basis of the information gained from the prototype detector. This device is constructed from smaller diameter tubes and is expected to operate at repetition rates of the order of 1 KHz. The successful operation of the device at very high repetition rates would illustrate the potential and compatibility of the flash tube chamber for use with other fast data acquisition detecting systems.

References

1. Davisson, C.M., Evens, R.D., Revs. Mod. Phys. 24 (1952) 79

2. McKay, K.G., Phys. Rev. 84 (1951) 829

3. Friedland, S.S., Mayer, J.W., Wiggins, J.S., Nucleonics 18 (1960) 2

4. Korff, S.A., Electron and Nuclear Counters, Van Nostrand (1955).

5. Garlick, G.F.G., Prog. Nucl. Phys., 2 (1952) 51.

6. Siegbahn, K., Alpha-Beta-and Gamma-ray Spectroscopy, New York: Interscience Publishers Inc., (1965).

7. Heitler, W., The Quantum Theory of Radiation, New York: Oxford University Press (1944).

8. Rossi, B., High Energy Particles, Prentice-Hall Inc., (1952).

9. Messel, H., Crawford, D.F., Electron-Photon Shower Distribution Function, Pergamon Press (1970).

10. Volkel, V., Internal Report DESY, 65/6 (1965).

11. Volkel, V., Internal Report DESY, 67/16 (1967).

12. Tom, H., Phys. Rev. 136 (1964) B447

13. Heusch, C.A., Prescott, C.Y., Phys. Rev. 135 (1964) B773

14. Heusch C.A., Proc. Int. Conf. Electron and Photon Interactions at High Energies, Hamburg, (1965) 408.

15. Muller, D., Phys. Rev. 5 (1972) 2677.

16. Zichichi, A., Proc. Int. Con. Instrumentation for High Energy Physics, Frascati, 1973 565.

17. Pugh, G.E., Frisch, P.H., Gomez, R., Rev. Sc. Inst. 25 (1954) 1124.

18. Homma, S., Kiruchi, R., Kitagaki, T., Rev. Sc. Inst. 35 (1964) 506.

19. Backenstoss, G., Hyams, B.D., Knop, G., Stierlin, V., Nuc. Inst. Meth. 20 (1963) 294.

20. McFarlane, W.K., Rothe, K.W., Wadlinger, E.A., Nuc.Inst. Meth, 91 (1971) 85.

21. Agrinier, B., Koechlin, Y., Parlier, B., Boella, G., Degle, G., Dilworth, L., Scarsi, L., Sironi, G., Il. Nuovo Cimento 36 (1965) 1077.

22. Faissner, H., Proc. Int. Con. Instrumentation for High Energy Physics, CERN (1962).

23. Faissner, H., Ferrero, F., Ghani, A., Krienen, F., Novey, T.B., Reinharz, M., Nucl. Inst. Meth. 20 (1963) 161.

24. Kajikawa, R., J. Phys. Soc. Jap. 18 (1963) 1365.

25. Allkofer, O.C., Dau, W.D., Grupen, C., Pischke, J., Stamm, W., Vhr, R., Internal Report, University of Kiel, Germany 020 (1973).

26. Bauer, A., Brocking, D., Faissner, H., Karl, H., Kohmstedt, H., Stein, J., Proc. Int. Con. Electron and Photon Interactions at High Energies, Hamburg, (1965) 401.

27. Blumenfeld, B.I., Lederman, L.M., Cool, R.L., Segler, S.L., Nuc. Inst. Meth. 97 (1971) 427.

28. Hemmi, Y., Nuc. Inst. Meth. 56 (1967) 213.

29. Lewis, R., Luckey, D., Vglum, J., Proc. Int. Con. Electron and Photon Interactions at High Energies, Hamburg, (1965) 424.

30. Daresbury Laboratory, Annual Report (1973) 106.

31. Hofstadter, R., Proc. Int. Con. Instrumentation for High Energy Physics, Frascati, (1973) 362.

32. Luckey, D., Proc. Int. Con. Electron and Photon Interactions at High Energies, Hamburg, (1965) 397.

33. Faissner, M., et al., Phys. Lett, 11 (1964) 178.

34. Bienlien, J.K., et al., Phys. Lett, 13 (1964) 80.

35. Franzinetti, C., Gerber, H.J., Internal Report. CERN NPA 64-10 (1964)

36. Browell, R., Short, K.A., Private Communication, University of Durham.

37. Thompson, D.J., Daresbury Nuclear Physics Laboratory, Internal Report TM/70.

38. CERN Courier, No.3, Vol. 14, March 1974. 83.

CHAPTER EIGHT

THE DESIGN AND CONSTRUCTION OF A FAST, HIGH RESOLUTION FLASH TUBE CHAMBER FOR FUTURE EXPERIMENTS WITH GAMMA RADIATION

8.1 Introduction

As a result of the experiments described in chapters 6 and 7, several improvements to the original flash tube chamber became apparent. This chapter describes the design of a new chamber, at present under construction, which incorporates these improvements, and is capable of operating at repetition rates of about 1KHz. The device is expected to locate and measure the energy of incident photons with a greater precision than was possible with the prototype chamber. Furthermore, the detector has been designed with the requirements of a nuclear physics experiment in mind, and consists of a single integral unit containing a fast high voltage pulsing system and data acquisition logic for an on-line computer link.

A flash tube chamber capable of recording shower data at rates of 1KHz requires several design features different from the prototype device. The flash tubes, high voltage pulsing system and data acquisition had to be redesigned in this respect. In addition, experimental results obtained with the prototype chamber have shown that energy resolution and linearity of response is dependent on several geometrical properties such as the diameter of the flash tubes, the thickness of lead target between detecting planes and the overall lateral and longitudinal size. Thus, on the basis of these results, the new chamber is being constructed with several structural improvements. These improvements are listed below.

(1) The detecting efficiency is increased by using thinner walled glass tube, and the individual electron sensitivity and spatial accuracy is improved by decreasing the diameter of the tube.

(2) The number of detecting modules is increased such that the thickness of target between planes can be reduced without excessive longitudinal leakage. In this way, the shower can be sampled at a greater number of target intervals.

(3) The width and breadth of the chamber is increased to minimize lateral shower leakage.

8.2. Mechanical Construction

The flash tube chamber was designed as a modular system, and in many respects is similar to the prototype device. Twelve modular elements containing planes of flash tube detectors are mounted inside an electrically shielded enclosure together with data acquisition electronics and a high voltage pulsing system.

Each module contains two sets of 32 flash tubes positioned in orthogonal X-Y planes either side of a central H.T. electrode. The tubes and digitization probes are contained in machined aluminium blocks which also act as spacers for the outer earth electrodes. In order to maximize the detecting efficiency, the holes, in which the tubes fit were machined as closely together as possible. Holes of 0.91cm diameter were machined 0.04cm apart, to give an overall detecting area of 30.4 x 30.4 cm^2. Figure 8.1 shows a photograph of four modular assemblies complete with data acquisition circuits and output leads.

The chamber fits together in a steel framework such that a space is provided before each module for accommodating up to three radiation lengths of lead target. In this geometry there is a distance of 3.75cm between each detecting plane giving an overall chamber depth of 45.0cm. The framework was designed to support the chamber with the machined blocks as its base and both sets of tubes positioned at 45° to the

Fig 8·1 four flash tube modular assemblies complete with data acquisition logic circuitry

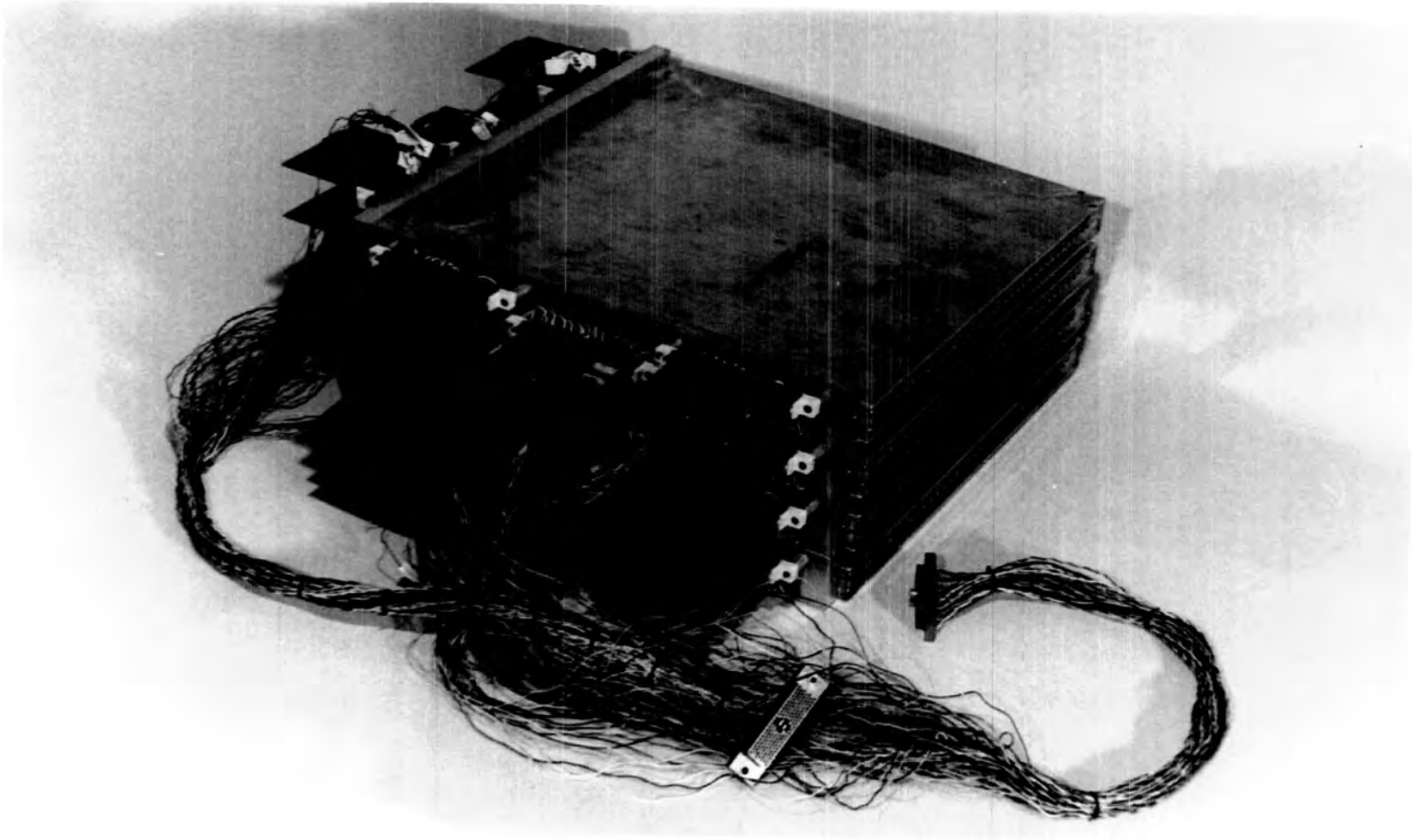

horizontal. This ensures that the flash tube end windows are always held in contact with the digitization probes by their own weight. The framework also provides a means of electrically shielding the device with aluminium sheet, which is fixed to the frame as a number of detachable panels. Shielding is necessary because of the severe high frequency noise generated by the pulsing system. Figure 8.2 shows a photograph of the chamber mounted in its framework with some of the aluminium side panels removed.

8.3 Flash Tubes

Flash tubes were selected which had characteristics suitable for operation at repetition rates of about 1KHz. Tubes made from Jena soda glass and filled with a gas mixture of Ne(70)-He(30) + 2% CH_4 at 2.3 atmospheres pressure were chosen for this purpose. These tubes have a recovery time of less than 0.6ms and a sensitive time of 1.4μs (see section 5.3.2). The glass envelope was manufactured (1) from Jena 16B glass with an internal diameter of 0.82 cm and a wall thickness of 0.03cm. A thin wall thickness was selected to minimize the amount of 'dead' space in the chamber, yet strong enough not to be fragile. With the tubes mounted in the chamber the detecting efficiency (detecting area/total area) is 86%. The diameter of the tubes was chosen as a compromise between cost and detecting sensitivity. The sensitivity could be increased further, by using even smaller diameter tubes, but this, in turn, increases the size and complexity of the device. Using 0.82 cm diameter, the chamber contains 768 tubes, each one being coupled to a data acquisition memory circuit.

8.4 The High Voltage Pulsing System

Most forms of electrically pulsed chambers use the principle of discharging a capacitor across a resistor to give a high voltage pulse

Fig 8.2 the flash tube chamber

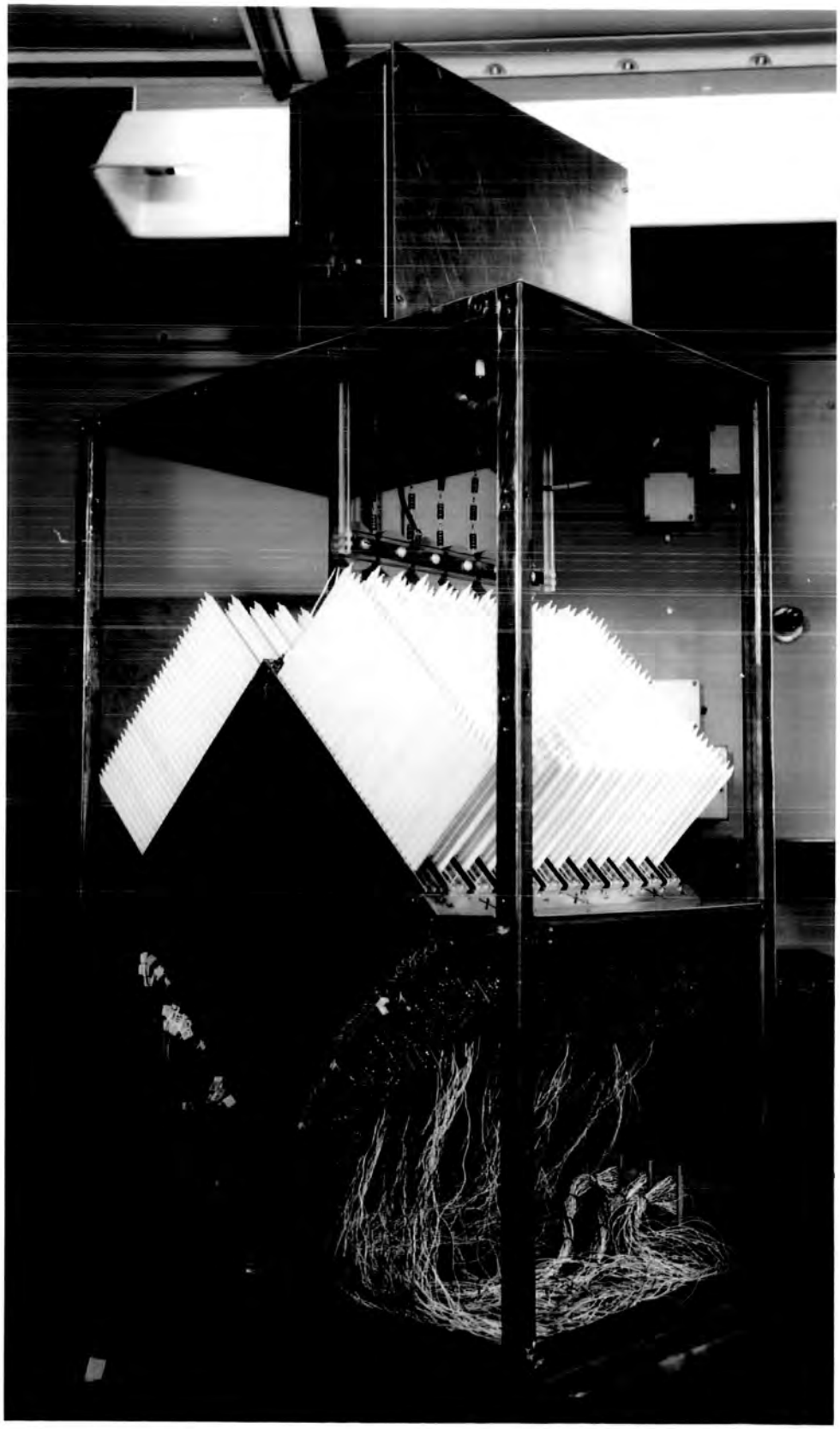

with an exponential decay. In the case of flash tubes, spark gaps are normally used as a means of switching the high voltage. Air spark gaps of the type used with the prototype chamber (see section 6.2.2), although capable of switching large currents and voltages, have a limited life between adjustments and are unable to operate at frequencies more than about 100 Hz. Pressurized nitrogen spark gaps are capable of higher repetition rates, but have the disadvantage of requiring a pressurized gas system, and they too need periodic adjustment. Classical valve thyratrons may also be used, but these have the disadvantage of long delays times and require large amounts of power for efficient triggering.

These problems were overcome with a pulsing system designed around a new type of hydrogen thyratron made from a ceramic material and of coaxial construction (2). The hydrogen thyratron, type CX 1157 is manufactured by English Electric Ltd and is capable of switching high voltages (20 KV) and currents (1000A) at frequencies up to about 1KHz. Figure 8.3. shows the circuit diagram of the system. The circuit is made up of three seperate amplification stages, using a ceramic hydrogen thyratron, a xenon thyratron and a transistor working in avalanche mode.

The ceramic hydrogen thyratron is of a coaxial tetrode structure giving an inherently low inductance. The first grid has a positive characteristic with respect to the cathode and the second grid a negative characteristic with respect to the first grid. To obtain maximum switching speed with low power, the first grid is biased positive with respect to the cathode such that it conducts about 60mA and maintains ionization between itself and the cathode. The second grid when pulsed positively, performs a gating action on the plasma between the first grid

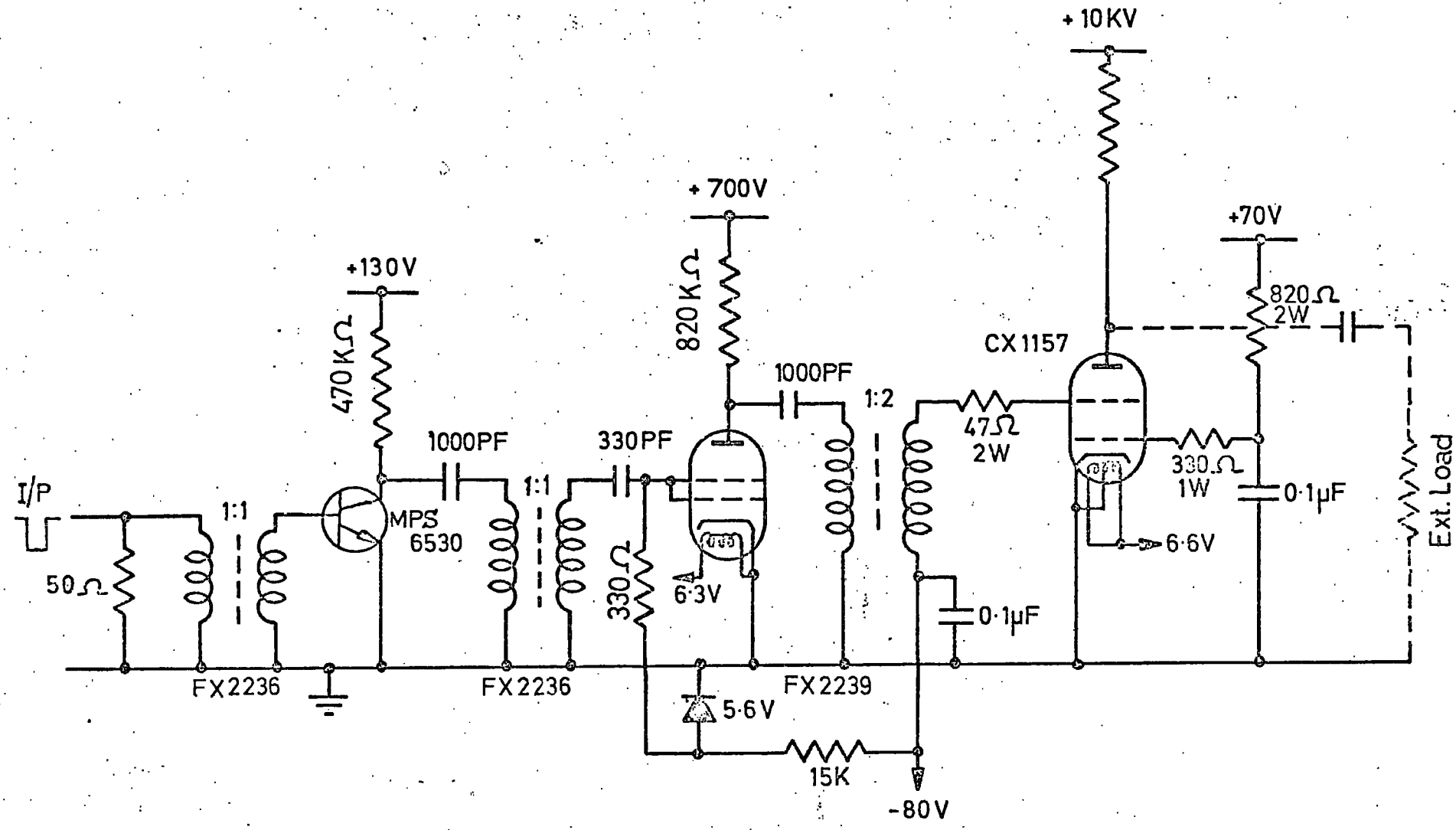

Fig 8.3 the high voltage pulsing system

and the cathode, producing a very rapid switching action to the anode. In this mode the thyratron is capable of switching 20KV with a rise time of less than 15ns into small capacitive and inductive loads.

A small Xenon thyratron (Mullard type 2021 W) is used for amplification and as a buffer between the hydrogen thyratron and the transistor input stage. Fast switching is achieved by connecting the grids together and biasing them positive at +5v. In this way a 500v output pulse with a 10ns rise time is produced. The output pulse is inverted, using a Mullard Ferroxcube (type FX 2239) pulse transformer with a turns ration of 1:2, before being fed to the second grid of the hydrogen thyratron. The xenon thyratron also acts as a buffer stage, by preventing large pulses returning from the hydrogen thyratron grid and destroying the input transistor.

The input stage was designed to provide fast triggering from a NIM type pulse of 700mV amplitude. The NIM pulse, after inversion with a pulse transformer, is used to drive a single transistor (type MPS 6530) working in avalanche mode. High voltage silicon transistors of this type are able to operate similarly to thyratrons, the transistor junction avalanching after triggering and conducting large currents for a short time. The rise time of the avalanche breakdown current can be short, and in this circuit the transistor switches 100v in about 2ns. Again, this pulse is inverted after decoupling with a Ferroxcube pulse transformer before being fed to the grid of the xenon thyratron.

The circuit as a whole, is capable of switching up to 20KV into chambers of at least 10,000 pf with a rise time of 40ns and total delay of 47ns. The flash tube chamber has a total capacity of about 2500 pf and requires the discharging of six 3000 pf capacitors to give a pulse of amplitude equal to 94% of the supply voltage. The pulsing system

can be seen in Figure 8.2 in a screened enclosure above the chamber.

8.5 Data Acquisition

The size of the new flash tube chamber required the construction of a data acquisition system which would provide a temporary memory store for flash tube information before being read by a computer. The large number of flash tubes contained in this device made the use of CAMAC storage registers (pattern units) with connecting cables physically impractical. Instead, a TTL memory logic system was designed which linked with CAMAC input registers to provide a means of temporarily storing addressed data before being processed by an on-line computer.

Digitized output information is obtained from each flash tube with a small probe placed in contact with the glass tube end window. The probes are held in a central position by perspex formers glued into the machined holes supporting the flash tubes. The dimensions of the HT electrode and probes relative to the face of the machined aluminium block were chosen to give output pulses of magnitude greater than the memory logic input threshold of 3v. A digitization pulse with an amplitude of about 8v and decay time of 1μs is used to drive TTL logic with d = 1.5cm, x = 0.6cm (defined in Figure 6.4a) and a peak applied field of 12KV/cm. Amplitude fluctuations amount to about ± 20%, which is acceptable with a TTL threshold of 3v.

The flash tube digitization pulse is used to change and set a voltage level representing a logical '1' to a logical '0', using TTL integrated circuits. Figure 8.4 shows the logic circuit used to store information from one flash tube. A cross-coupled NAND gate provides a 'latching' action when the input is changed from a logical '0' to a logical '1' level. Thus, a negative input pulse from a flash tube causes the output, normally

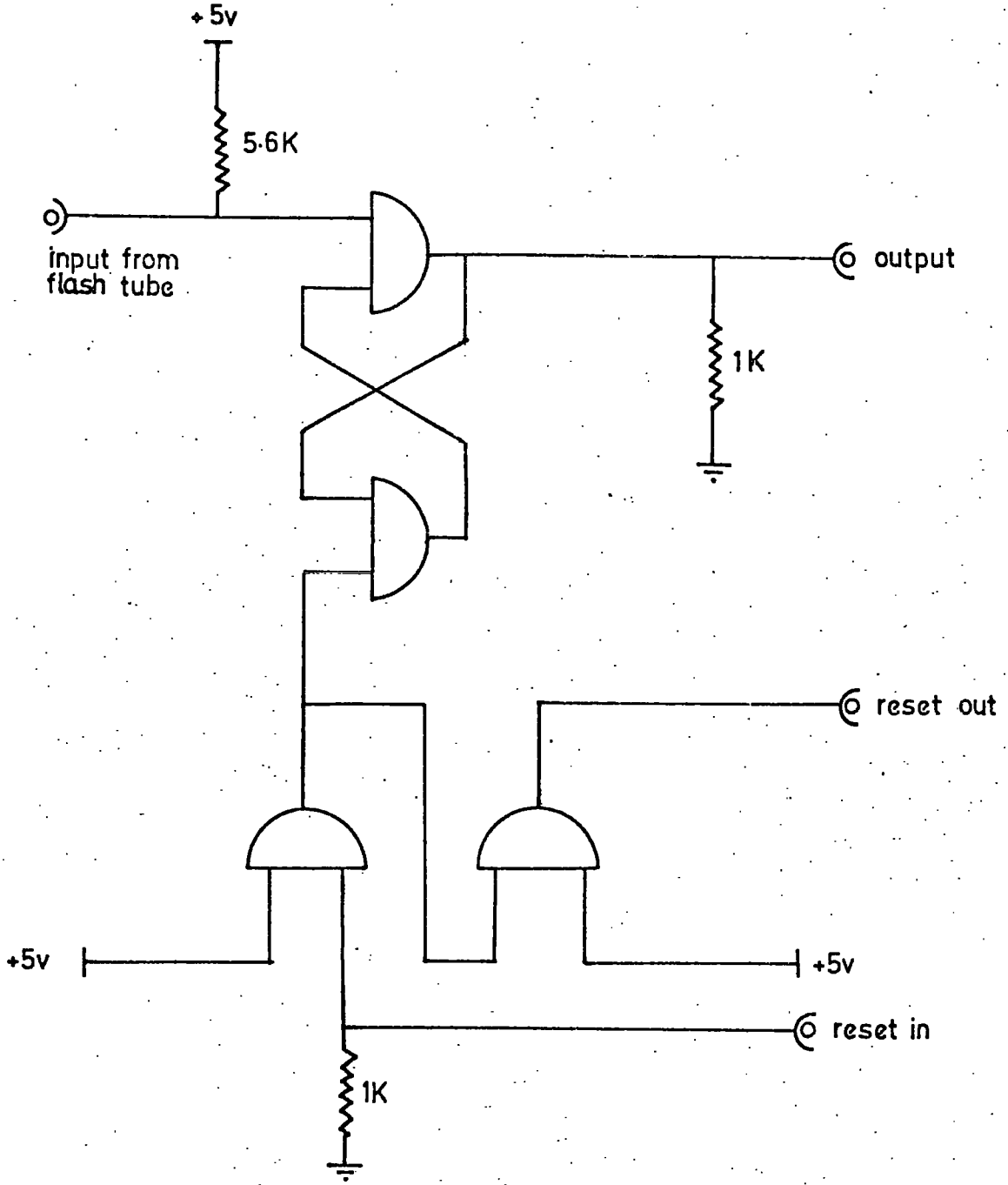

Fig. 8·4 The memory logic for one flash tube detector

set to a logical '1' to invert, where it remains until the cross-coupled NAND gate receives a reset pulse. The reset is obtained by a NAND buffer gate, (see Figure 8.4) driven by a CAMAC output unit to provide a logical '1' level at the latch reset input. This pulse is inverted by another NAND gate to give an output pulse for resetting other circuits.

The circuits are mounted on printed circuit boards, each one containing two sextuple set-reset latches (type 74118) and one dual 4-input positive NAND buffer (type 7440), to give 72 12-bit storage registers. Figure 8.5 shows the circuit diagram of each 12-bit register board with numbered pin connections. The circuit boards are held in 32-way edge connectors fixed to the sides of the chamber as shown in Figure 8.1. The logic circuitry requires a total current of about 10amps when all 768 latches are in the logical '0' state.

The output of each cross-coupled NAND gate is relayed in parallel to three 256-bit input CAMAC registers (type EC 221) by means of six 132-way EMIHUS cables. Thus, after an event, the data can be processed in the PDP 11 computer after being read serially from each of the CAMAC registers. After all the addressed registers have been read the memory logic may be reset by means of a CAMAC output level unit (type EC 316), which initiates the NAND buffer gates connected to each memory 'latch' reset.

8.6 Conclusion

The flash tube chamber described in this chapter is proposed for testing in a series of experiments, similar to those described in Chapter 6 and 7, using the DNPL e^+ beam. The device will be linked on line, to an IBM 370/165 computer via a small 16K PDP 11 computer, programmed to transmit blocks of data continuously at high repetition rates. By this method the chamber will be able to operate at repetition

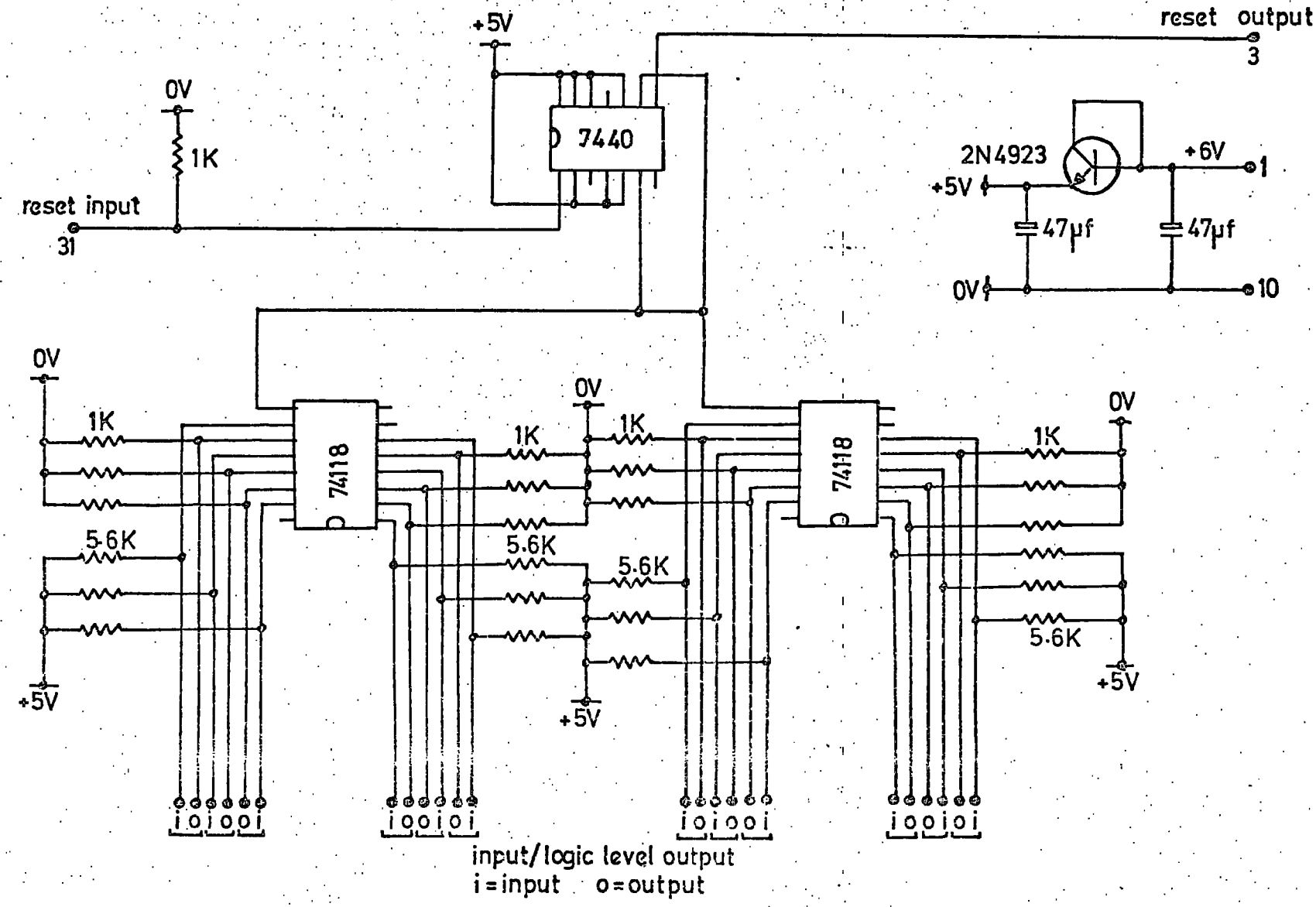

Fig 8·5 12-bit memory register

rates up to 1KHz. Some experiments which could be carried out with this detector are described in chapter 9.

References

1. The flash tubes were manufactured by International Research and Development Co. Ltd., Newcastle-upon-Tyne.

2. This device was initially developed by the author and P. Davidson at the Rutherford Laboratory, and is now marketed commercially by Hivotronics Ltd.

CHAPTER NINE

FUTURE WORK WITH GAMMA RAY DETECTORS

9.1 Introduction

The content of this chapter is intended to give a brief summary of experimental work envisaged for flash tube gamma chambers in the near future. Several experiments and ideas relevant to gamma detection are discussed together with some of the problems which may be encountered. The chapter is divided into two sections: proposed experiments using the new flash tube chamber described in the previous chapter, and other work which may help to improve the detecting properties of flash tube gamma chambers.

9.2. Experimental work using the flash tube chamber

Results obtained from the first series of experiments using the prototype chamber have stimulated interest in a further investigation using a larger chamber in the DNPL e^+ accelerator beam. Experiments proposed for this device are intended to fulfill two main objectives. First, to verify that the device will operate at repetition rates compatible with the requirements of most particle physics experiments. Second, to determine how accurately a gamma ray may be located and its energy measured. In addition to this, a detailed study of shower detection using different chamber geometries is possible. Such a study should give information necessary for the optimization of the chamber geometry and methods by which the resolution may be improved.

9.2.1 High Repetition Rates

The flash tube chamber was designed for operation up to about 1KHz. Testing the device at these frequencies in the DNPL e^+ beam is not, however, so readily accomplished. Two problems are evident; producing particles in the frequency range 50 - 1000Hz from an

accelerator whose cycling time is 50 Hz, and handling large quantities of data at high repetition rates with an on-line computer.

In order to ensure that the flash tubes will operate satisfactorily without reignition it is necessary to operate the device in a beam of particles at a known repetition rate (see section 6.2.1). The DNPL accelerator produces a beam spill of about 2ms duration every 20ms. Thus, under normal operation particles may be extracted either from consecutive spills, giving a maximum frequency of 50 Hz, or within one beam spill, giving a minimum frequency of about 500 Hz. This does not give a satisfactory range of frequencies in which to work, the range 50-500 Hz being unobtainable.

The problem may be overcome by using both the 'parasitic' and beam 'bump' methods (1) of particle extraction (see section 6.2.1). The signal from a detected particle extracted using the beam 'bump' is made to open a gate for a predetermined time (say 50μs) after a suitable delay. The gating pulse can then be used to 'enable' the detection of a second particle which arrives 'parasitically' within that time. In this way, any frequency may be selected by chosing the appropriate gating delay. The finite probability that a particle will not arrive in this time means that a gating pulse length will need to be chosen as a compromise between event rate and frequency precision.

The second main problem is that of data acquisition. Although the chamber is able to operate at 1 KHz, reading and storing all the data onto magnetic disk is impossible by normal methods using a conventional CAMAC/PDP 11 computer system linked to the DNPL 360/165 computer (2). Normally, data from an event is read into the PDP 11 computer from CAMAC and is then sent as a 'block' down a link into a buffer store before being written onto magnetic disk. The buffer

store, is, however, unable to contend with the frequency of data required from this experiment, where at 1KHz, 48 16-bit words are transmitted every 1ms.

This problem may be solved by storing pairs of consecutive events and then transmitting both sets of data in one block. In this way, data is relayed to the buffer store only once every 20ms (the cycling time of the accelerator). Working in this mode, the frequency is limited only by the operating speed of the CAMAC and PDP 11 computer. If the PDP 11 computer is programmed in a low level language (machine code) then it should be capable of handling data at frequencies in excess of 1KHz.

9.2.2. Energy and Spatial Measurements

Experimental results obtained with the prototype device have shown that energy and spatial resolution is dependent on several geometrical characteristics of the chamber. In view of these results, a similar but more extensive investigation is suggested. The energy and spatial resolution should be measured as a function of incident energy, lead target thickness and target-detecting plane spacing.

In addition to the conventional method of measuring the energy, that is by counting the number of shower particles, spatial information of the shower may provide a means of measurement. If the numbers of detected electrons are large enough then a curve may be fitted to the shower profile, the function of which is dependent on the incident energy (see Figure 7.1). This method, does not, however, provide a direct energy measure, but requires computer analysis. In this respect, the method is incompatible with an experiment which requires fast digitized energy information. Alternatively, a separate energy determination could be made from each module independently from which

a weighted mean value could be calculated. Such a method is only feasible if the numbers of detected particles in each plane are large enough not to cause serious statistical fluctuations. It is unlikely, on this basis, that the method would give an improvement in resolution for energies below a few GeV where the number of shower particles are small.

Spatial measurements from the prototype device indicate that the spatial resolution could be better than $\pm$ a tube radius, therefore an improved method of locating the position of the incident particle should be employed. A multiwire proportional chamber or drift chamber, placed in front of the chamber, could be used to this effect, although the simplest method is to use three plastic scintillation telescope detectors connected in $A\bar{B}C$ mode, with the centre one having a small aperture through it.

9.3. Other Work

9.3.1 Fast decision making logic

In many nuclear physics experiments it is often necessary or advantageous to have a fast electronic system which is able to decide whether an event is of interest. This may be important in those experiments which search for rare interactions and require the detection of many thousands of events. An electronic system which is capable of determining whether an event is constrained within predetermined parameters can thus prevent the accumulation of vast quantities of unwanted data. In the case of a flash tube gamma chamber, a system which could discriminate between events of different incident gamma energy before the data is read or processed in a computer, would be particularly useful. Two different electronic systems are suggested which may prove to be valuable in this respect; a fast digital circuit which counts the total number of ignited

flash tubes, and an optical system using a photomultiplier and fibre optics to integrate the light pulses from each flash tube to give an electrical pulse of amplitude proportional to the number of ignited tubes.

A fast digital circuit could be devised, using TTL logic, to count and compare the total number of ignited flash tubes with a predetermined upper and lower limit representing the required energy range. If the number of ignitions lies within this range then an interrupt signal can be generated which allows the data to be processed and stored in the computer. The ignited tubes may be counted by a series of shift registers, each one being connected in parallel to the memory 'latch' (see section 8.5) of each flash tube. The data may then be counted by shifting the stored logic levels through each shift register into a binary counting circuit. A train of pulses to drive the shift registers would need to be generated by an oscillator circuit, the frequency being chosen such that all the data is counted within a sufficiently short time period. The data may be counted with decade counters which are coupled to BCD binary-to-decimal converters for comparing the total number with two preset variable numbers which define the energy range.

The other suggested method, is an analogue technique, which in comparison with the above method, will give a fast response but at the expense of some loss in resolution. This method utilizes lengths of plastic light transmitting fibres (fibre optics) which optically couple each flash tube to a single photomultiplier. An aperture fitted across the face of the photomultiplier can be adjusted in size until the output pulse height is proportional to the total number of flash tube ignitions. This signal may then be fed into a discrimination

circuit to select pulses of the required magnitude.

9.3.2 Monte Carlo Simulations

A quantitative analysis of shower development within a detector, based on a theoretical model, is made difficult because of the non-homogeneity of absorbing material in the device and the large number of possible interactions between cascade particles and absorbing material. The use of Monte Carlo techniques, however, may overcome this difficulty by simulating individual showers by random interaction generation and a knowledge of the interaction cross-sections as a function of incident energy and absorbing material. Shower simulation in a homogeneous media has been proved feasible (3) and has shown good agreement with experimental results (4,5). It is not unreasonable, therefore, to assume that similar computations can be performed for nonhomogeneous systems which might constitute a flash tube chamber. Such calculations will probably require more computing time, but will not, necessarily, be more complex. Several simplifying and time saving approximations could be used; for example the chamber construction could be approximated to a series of lead-air gaps, the glass tube and aluminium electrode material being ignored.

Computer simulations of this type would be of particular value for aiding the design of flash tube chambers. A Monte Carlo computer program, versatile enough to cope with varying geometrical parameters, could be used to optimize the chamber detecting geometry in terms of target thickness, distance between detecting planes, number of detecting planes, flash tube diameter and lateral dimensions. Other methods of measuring the incident energy and trajectory may be tested using simulated data too, without having to install a chamber in an accelerator beam.

9.3.3 Experiments with Photons

All the experiments described in previous chapters have used electron or positron beams to simulate gamma induced showers. The use of a charged particle beam is advantageous because the position and momentum of individual particles are easily determined with conventional auxilary detectors. Nevertheless, similar experiments using gamma rays of known energy and trajectory would be valuable for comparison, and would give some measure of discrepency for the determined energy and spatial resolution.

Experiments of this kind would necessitate the use of a tagged photon beam where gamma rays are produced from the bremsstralung interaction of electrons with a target. The energy of a photon, produced by this method, is calculated by measuring the difference between the incident and scattered electron energy using two bending magnets and multiwire proportional chambers (6). A beam of photons, produced in this way, will not be monoenergetic, therefore the kinematic information from the proportional chambers will need to be stored together with the flash tube data after each event.

Triggering the flash tube chamber on photons will require a scintillation detection system different from that used with charged particles. Photons will not trigger a plastic scintillator coincidence arrangement, therefore the photon will need to be detected after its interaction with target material in the chamber. A large plastic scintillator counter placed before the chamber and connected in anticoincidence with scintillation counters placed inside the chamber will ensure that the device is triggered by neutral particles only.

References

1. Rousseau, M., (DNPL) Private Communucation.

2. Peatfield, A., (DNPL) Private Communucation

3. Messle, H., Crawford, P.F., Electron-Photon shower Distribution Function, Pergamon Press (1970)

4. Tom. H., Phys. Rev. 136, (1964) B447

5. Hensch, C.A., Prescott, C.Y., Phys. Rev. 135, (1964) B773.

6. Annual Report, DNPL 1973, 39.

CHAPTER TEN

CONCLUSION

Accelerator experimentation has been responsible for the rapid development of a wide range of particle detectors and has produced many new forms of track locating instruments. The development of the electrically pulsed detectors, in particular, has been intensified by the advent of the electronic counter experiment. One exception in this category is the flash tube, which despite its many advantages and potential applications has been limited to cosmic ray physics by undesirable operating characteristics. The work reported in this thesis has described the development of a new type of flash tube which has overcome these difficulties and has characteristics similar to other electrically pulsed detectors.

Two parameters have been of principle concern: the sensitive time which is required to be short for operating in a flux of background radiation, and the recovery time which becomes important when data is required at fast repetition rates. These parameters have been substantially improved by the application of an alternating electric clearing field and the use of special gas mixtures to give characteristics in excess of the requirements of many accelerator experiments. By these methods the sensitive time has been reduced by a factor of approximately 10^{-2} to a few microseconds and the recovery time by a factor of approximately 10^{-3} to a millisecond or less. Experiments using the DNPL accelerator have helped verify their suitability for operating under accelerator conditions and have shown the device capable of efficient detection to frequencies of at least 50Hz. Furthermore, the digitization technique has been shown to be compatible with conventional computer data acquisition systems without the necessity of amplifier interfacing electronics.

The objective of this work was not to develop a device which completely supercedes other detectors; its aim instead was to complement them with a specialized device, and show where its properties can be exploited to best affect. In comparison with other electronically pulsed chambers the flash tube has three features which commend it: large sensitive volumes can be constructed at low cost, digitization is simple and inexpensive, and due to its elemental structure it has a high multitrack efficiency. In view of these properties and the future needs of high energy physics, the device has been investigated as a means of detecting high energy photons. Results from this study have verified the usefulness of the device for measuring the energy and trajectory of photons, and indicate that very large flash tube chambers can be built with superior resolution and at a fraction of the cost of conventional techniques. Experiments using the prototype device with the DNPL accelerator e^+ beam gave an energy resolution at 1 GeV/c of $\pm$ 18% (FWHM) and angular resolution of about $\pm 2^{o}$. These results are encouraging because despite the device being constructed with large diameter tubes and of small overall dimensions, the resolutions are superior to those obtained with many conventional methods of detection.

Information gained from experiments with the prototype chamber have enabled a larger version to be built with smaller diameter tubes which should give an improved energy and spatial resolution and be capable of operation at repetition rates up to 1KHz. Successful operation of the chamber at this frequency would illustrate the potential of the device for most large gamma detecting systems envisaged in the near future at high energies. The new chamber is due to be installed in the DNPL e^+ beam early in 1975.

APPENDIX I

MEASUREMENT OF THE DECAY TIME OF INTERNAL CLEARING FIELDS IN 1.9cm DIAMETER FLASH TUBES

Internally produced clearing fields are the result of charges being separated during the application of the impulsive electric field and remaining on the glass surface for a finite time. The field will decay by the conduction of charges either across the glass surface or through the glass volume with a time constant which depends on the resistivity of the glass and the capacitance of the flash tube. A measurement of this time constant was made possible by investigating the dependency of the detecting efficiency upon the frequency of an externally applied clearing field.

The field produced inside a flash tube will not follow the perfect square wave form of an externally applied field, but instead will decay due to the tubes intrinsic capacity. The effective clearing field is thus reduced, particularly when low frequencies are used. Figure A1 shows the external square wave field and the decayed field produced inside the tube. The diagram also shows the effective square wave field, which is defined to give the same detecting efficiency as the applied field.

For the same detecting efficiency the effective square wave field must remove an equal number of electrons in one period as the internal field. This leads to the condition:-

$$\int_0^T U\,dt = U_E T \qquad \text{.....1}$$

where U is the velocity of electrons in neon

U_E is the effective constant velocity of electrons in neon

T is the half period (defined in Figure A1)

now, for electrons $U = K \left(\frac{X}{p}\right)^{\frac{1}{2}}$

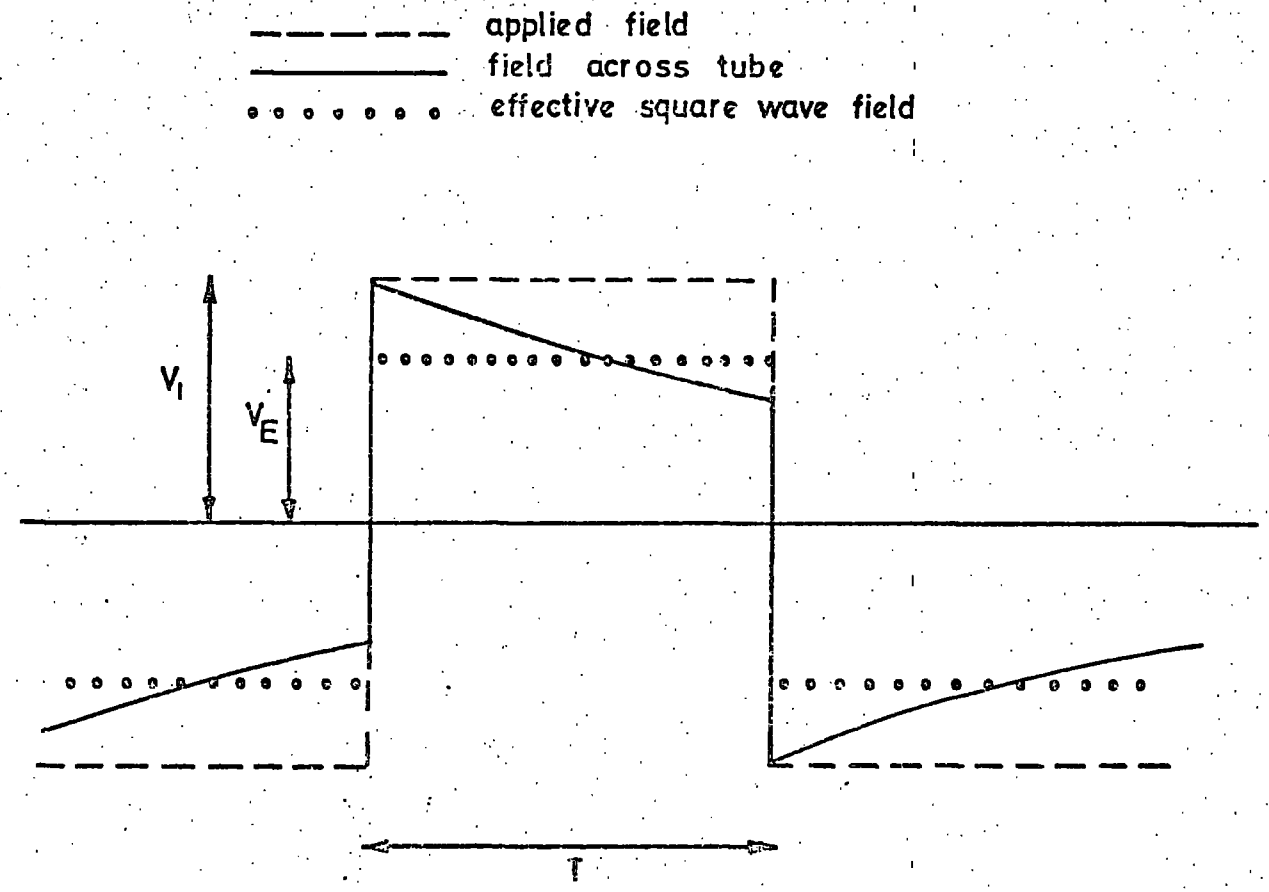

FIG. A1. Attenuation of the applied square wave clearing field.

and $$X = \frac{V}{d}$$

where K is the electron mobility

X is the field strength

P is the gas pressure

V is the voltage

d is the tube internal diameter

thus, for constant P and d

$$U = AV^{\frac{1}{2}} \qquad \ldots\ldots\ldots \quad 2$$

where A is a constant

substituting (2) in (1) gives

$$\int_0^T AV^{\frac{1}{2}}\, dt = AV_E^{\frac{1}{2}}T \qquad \ldots\ldots\ldots \quad 3$$

If it is assumed that the field inside the tube decays exponentially then

$$V = V_1 e^{-t/\tau} \qquad \ldots\ldots\ldots \quad 4$$

where τ is the expontential decay constant

substituting (4) in (3) gives

$$\int_0^T (V_1 e^{-t/\tau})^{\frac{1}{2}}\, dt = V_E^{\frac{1}{2}}T$$

therefore $$V_E^{\frac{1}{2}} = \frac{2V_1^{\frac{1}{2}}\tau}{T}(1 - e^{-T/2\tau}) \ldots\ldots \quad 5$$

Also, for a square wave field of high frequency (where $T \ll \tau$) which gives the same detecting efficiency as the effective square wave field of low frequency (where $T \gtrsim \tau$) we may write

$$X_o = X_E$$

and for constant d and P

$$V_o = V_E$$

where X_o is the strength of the high frequency field

X_E is the effective strength of the low frequency applied field

V_o is the applied voltage of the high frequency field.

therefore from (5), for the same detecting efficiency we have

$$V_o^{\frac{1}{2}} = V_E^{\frac{1}{2}} = \frac{2V_1^{\frac{1}{2}}\tau}{T}\left(1 - e^{-T/2\tau}\right) \quad \ldots\ldots\ldots 6$$

Thus, a plot of $(\frac{V_o}{V_1})^{\frac{1}{2}}$ against $(\frac{2\tau}{T})$ gives a universal curve for all frequencies and field magnitudes.

Figure A2 shows the efficiency versus clearing field frequency measured for a 2.9v(peak) cm^{-1} square wave field at 100°C. These results show that the field is transmitted for frequencies greater than about 20Hz without significant attenuation. This graph was used to provide values of T in equation (6). Figure A3 shows the variation of efficiency with clearing field strength for a square field of 50Hz at 100°C. This graph was used to provide the values of V_o in equation (6).

Figure A4 shows the theoretical curve of $(\frac{V_o}{V_1})^{\frac{1}{2}}$ versus $\frac{2\tau}{T}$ and the experimental points using values taken from Figures A2 and A3. A good fit to the theoretical curve is found by taking the decay constant of a flash tube τ = 61mS. The agreement between theory and experiment would indicate that the assumption that the field decays by an exponential mechanism is justified.

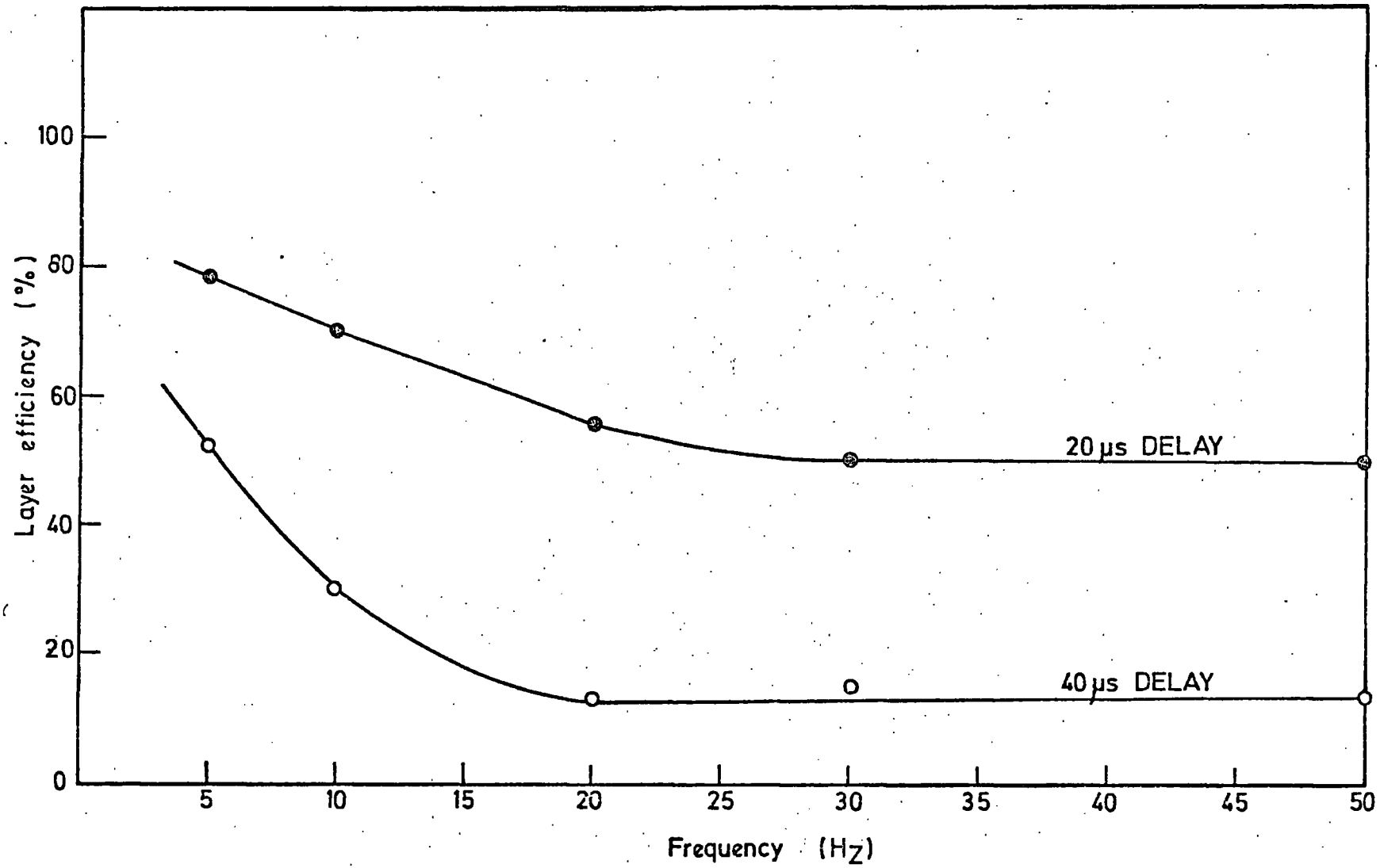

FIG. A2. The effect of the clearing field frequency on the detecting efficiency for a 2·9v (peak) cm^{-1} square wave field at 100°C.

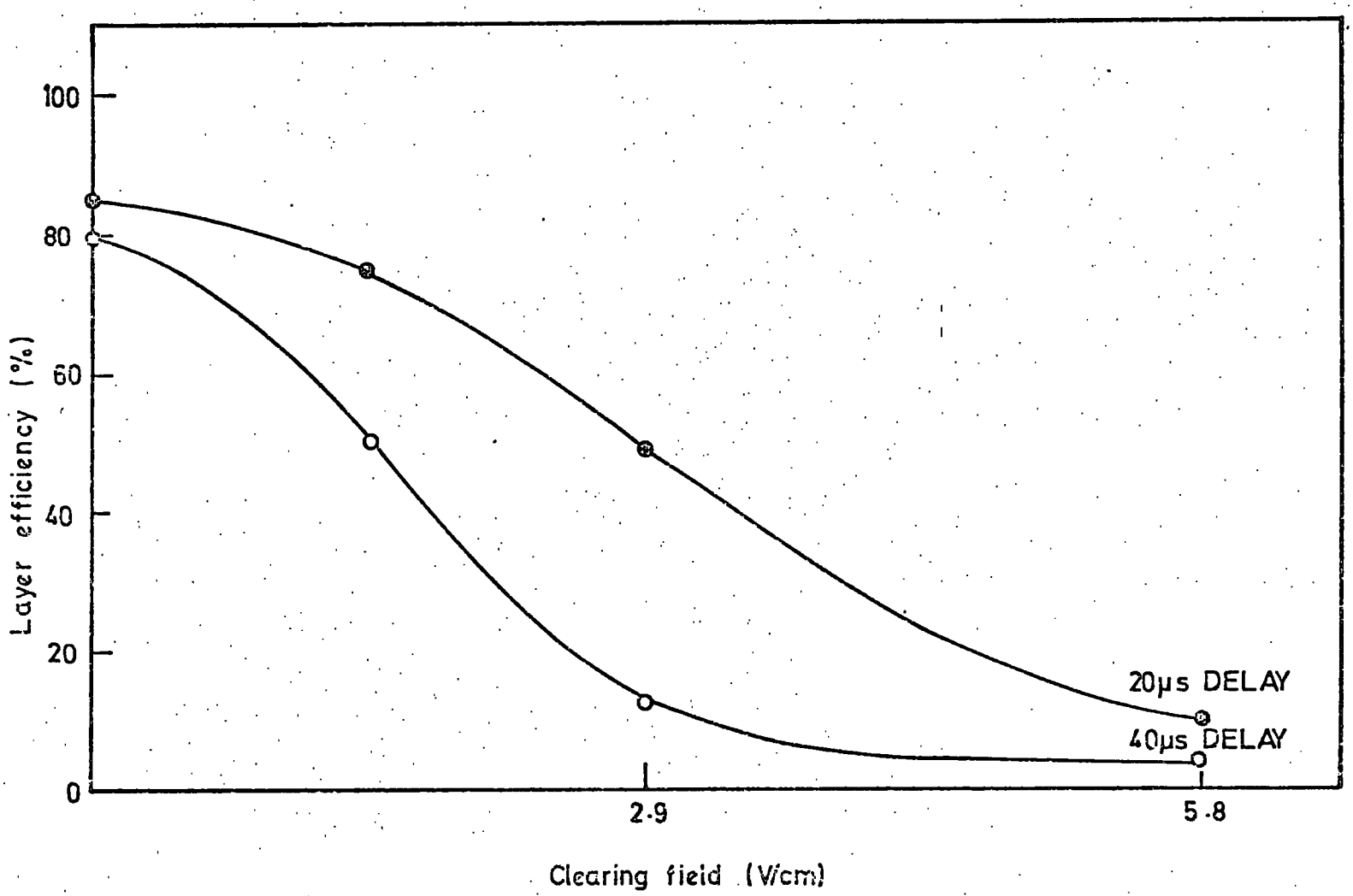

FIG. A3. The effect of the field strength on the detecting efficiency for a 50 H_Z square wave at 100° C.

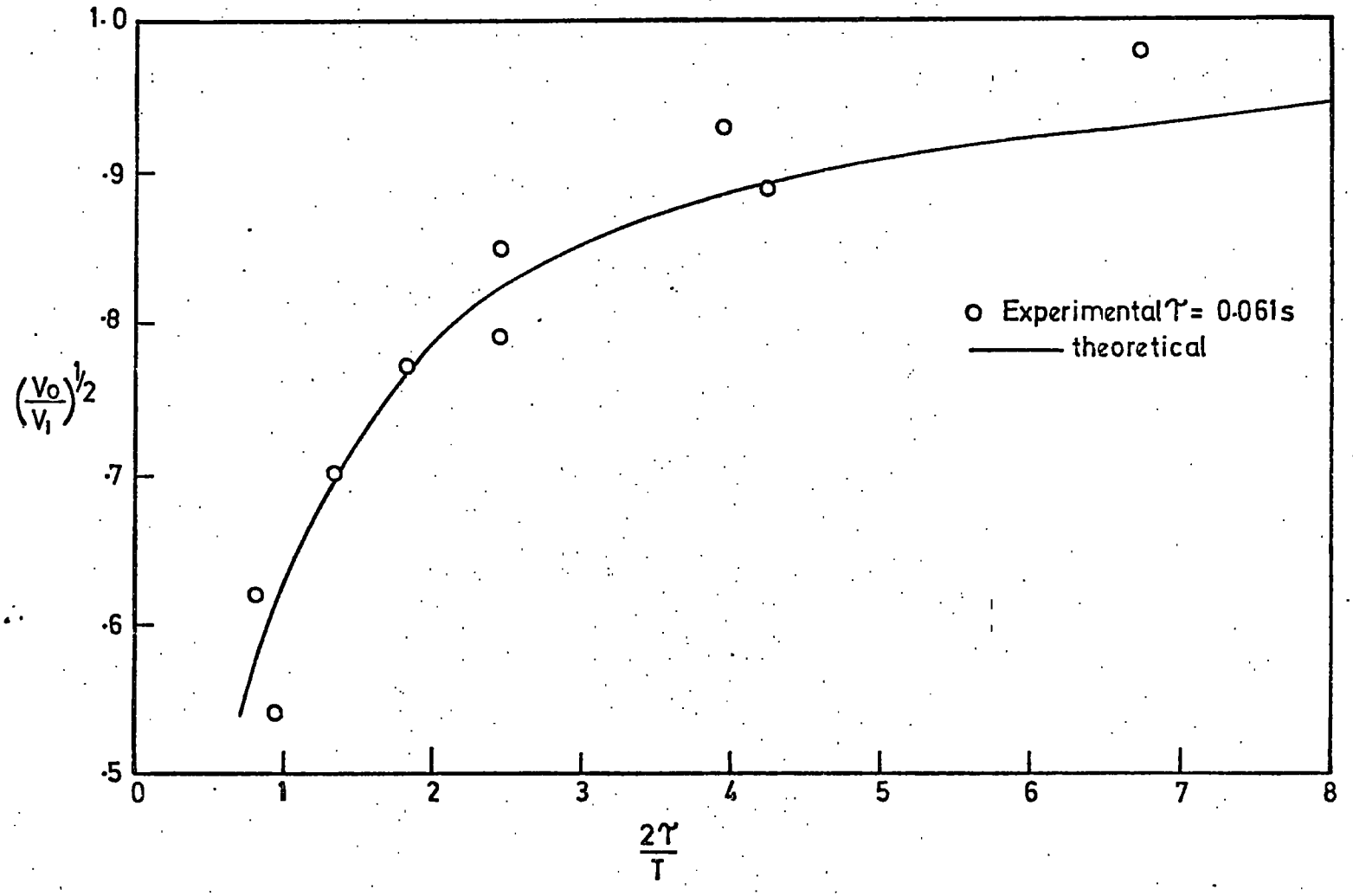

FIG. A4. Comparison of experimental data with theory for a tube decay constant of 61 ms.

APPENDIX II

CALCULATION OF THE NUMBER OF PARTICLES REMAINING IN A CYLINDRICAL CAVITY WHEN DIFFUSION IS THE ONLY REMOVAL MECHANISM

The diffusion of an ensemble of particles in a closed system is described by the diffusion equation

$$\nabla^2\rho + \frac{\rho}{D\tau} = 0 \quad \ldots\ldots\ldots\ldots (1)$$

where ρ is the density of particles at a point

D is the diffusion coefficient

τ is a time constant describing the decay.

The solution for ρ is an eigenvalue problem whose solution depends on the geometry of the container and appropriate boundary conditions. For a cylindrical cavity of radius r_o and height H the equation becomes

$$\frac{\partial^2\rho}{\partial r^2} + \frac{1}{r}\frac{\partial\rho}{\partial r} + \frac{1}{r^2}\frac{\partial\rho}{\partial\theta^2} + \frac{\partial^2\rho}{\partial Z^2} + \frac{\rho}{D\tau} = 0$$

Assuming symmetry about the axis and no dependence on the azimuth angle θ this reduces to

$$\frac{\partial^2\rho}{\partial r^2} + \frac{1}{r}\frac{\partial\rho}{\partial r} + \frac{\partial^2\rho}{\partial Z^2} + \frac{\rho}{D\tau} = 0$$

By the separation of variables and applying the boundary conditions $\rho = 0$ for $r = 0$ and $Z = \pm H/2$, the solution is given by

$$\rho(r,z,t) = \sum_{i=1}^{\infty}\sum_{j=1}^{\infty} G_{ij}\, Jo(\alpha_i r)\cos\frac{(2j-1)\pi z}{H}\exp\left(-\frac{t}{\tau_{ij}}\right) \ldots (2)$$

where Jo is the zero order Bessel function

$\alpha_i r_o$ is the ith root of Jo

and the decay time is given by

$$\tau_{ij} = 1/D\left[\alpha_i^2 + ((2_j-1)\pi/H)^2 \right] \qquad \ldots\ldots\ldots\ldots (3)$$

Equation (2) shows the diffusion to be represented by a cos function in the longitudinal direction and a Bessel function in the radial direction. This solution can be simplified if all decay modes except the fundamental are neglected. Thus, equation (2) becomes

$$\rho(r,z,t) = \rho_o (r,z,t)\, Jo \left(\frac{2.405r}{r_o} \right) \cos \frac{\pi Z}{H} \exp \left(- \frac{t}{\tau_{11}} \right) \ldots (4)$$

and from (3)

$$\tau_{11} = 1/D\left[\left(\frac{2.405}{r_o}\right)^2 + \left(\frac{\pi}{H}\right)^2 \right] \qquad \ldots\ldots\ldots\ldots\ldots (5)$$

The number of particles dN at a time t in any element volume dV inside the cylinder is given by

$$dN(r,z,t) = \rho(r,z,t)\, r d\theta . dr . dz .$$

and if the simplifying assumption is made that at $t = 0$, $\rho_o(x,z,t)$ is a constant, then from (4)

$$dN(r,z,t) = \rho_o J_o \left(\frac{2.405r}{r_o}\right) \cos \frac{\pi z}{H} \exp \left(- \frac{t}{\tau_{11}} \right) r d\theta . dr . dz .$$

thus the total number of particles at a given time is given by

$$N(t) = 2\rho_o \int_o^{H/2} \int_o^{r_o} \int_o^{2\pi} J_o \left(\frac{2.405r}{r_o} \right) \cos \frac{\pi Z}{H} \exp \left(- \frac{t}{\tau_{11}} \right) r d\theta . dr . dz$$

giving

$$N(t) = 2.4\rho_o r_o^2 H \exp \left\{ -tD \left[\left(\frac{2.405}{r_o}\right)^2 + \left(\frac{\pi}{H}\right)^2 \right] \right\}$$

A P P E N D I X III

THE DATA ACQUISITION PROGRAM

The program controlling the PDP 11 (16K) computer and CAMAC electronics had five main functions:-

(1) to read data from the eight 16 bit memory registers (Pattern units type 16P 2007).

(2) to store the data after each event in the computer memory core.

(3) to disable all active CAMAC electronics until the data had been processed by the computer.

(4) to display the data before being transferred to paper tape.

(5) to transfer the data to paper tape when the computer core store was full.

Figure A5 shows a schematic diagram of the data acquistion giving the most important elements of the CAMAC system. Pulses from each flash tube were used to set voltage levels in Pattern units (type 16P 2007) during a time determined by a gating signal. A binary number register was also included to label each set of data with a predetermined number. This number was read before each block of data. The data contained in the Pattern units and binary number register was read into the computer core store upon receipt of an interrupt signal generated by external triggering logic. Consecutive events were stored until the computer core store was full, whereupon the system was paralaysed and the data displayed on a 'Vista' teletype terminal before being transferred to paper tape.

A computer program was written to perform the above process in the CAT II language (a modified form of the BASIC computer language developed at DNPL). Figure A6 shows a flow diagram describing the program.

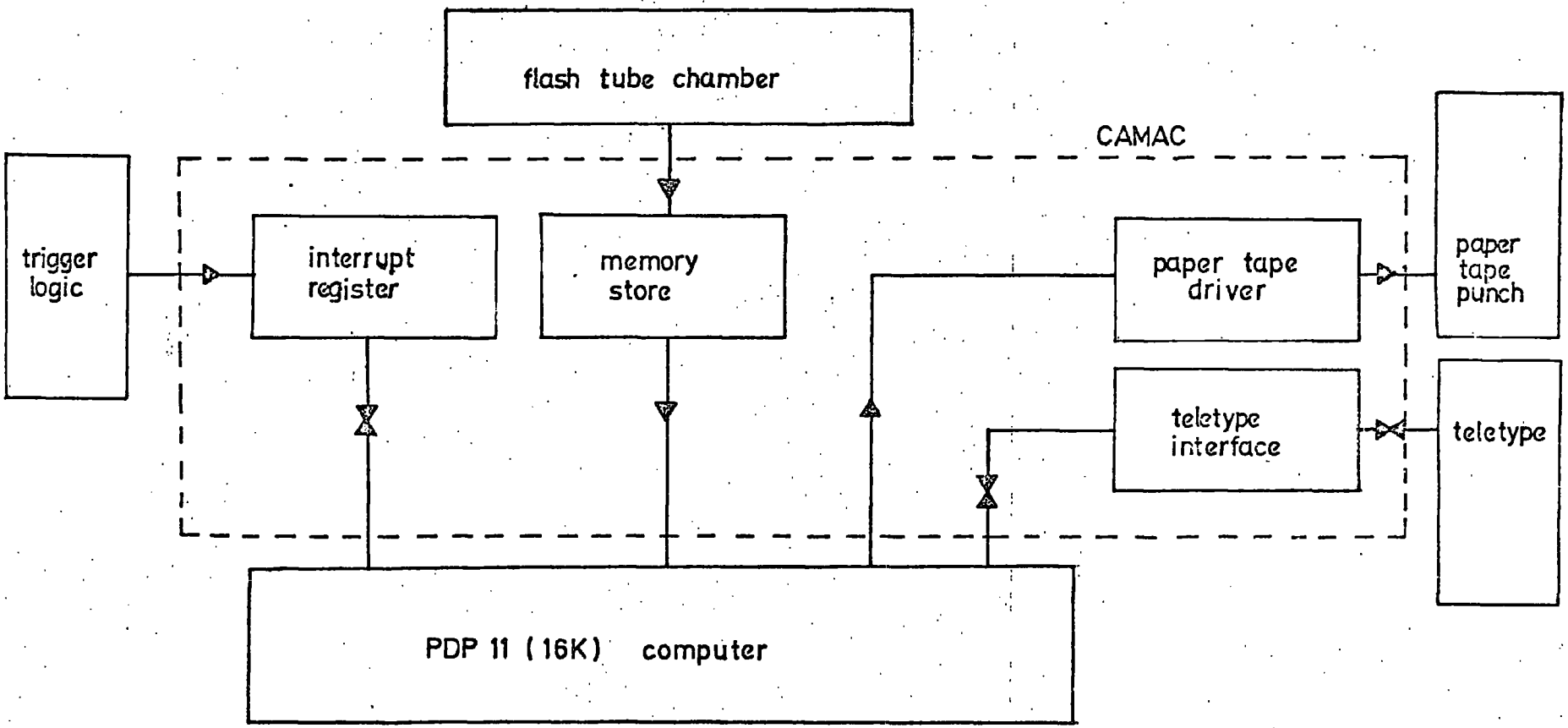

Fig. A5 schematic diagram of the computer/CAMAC system

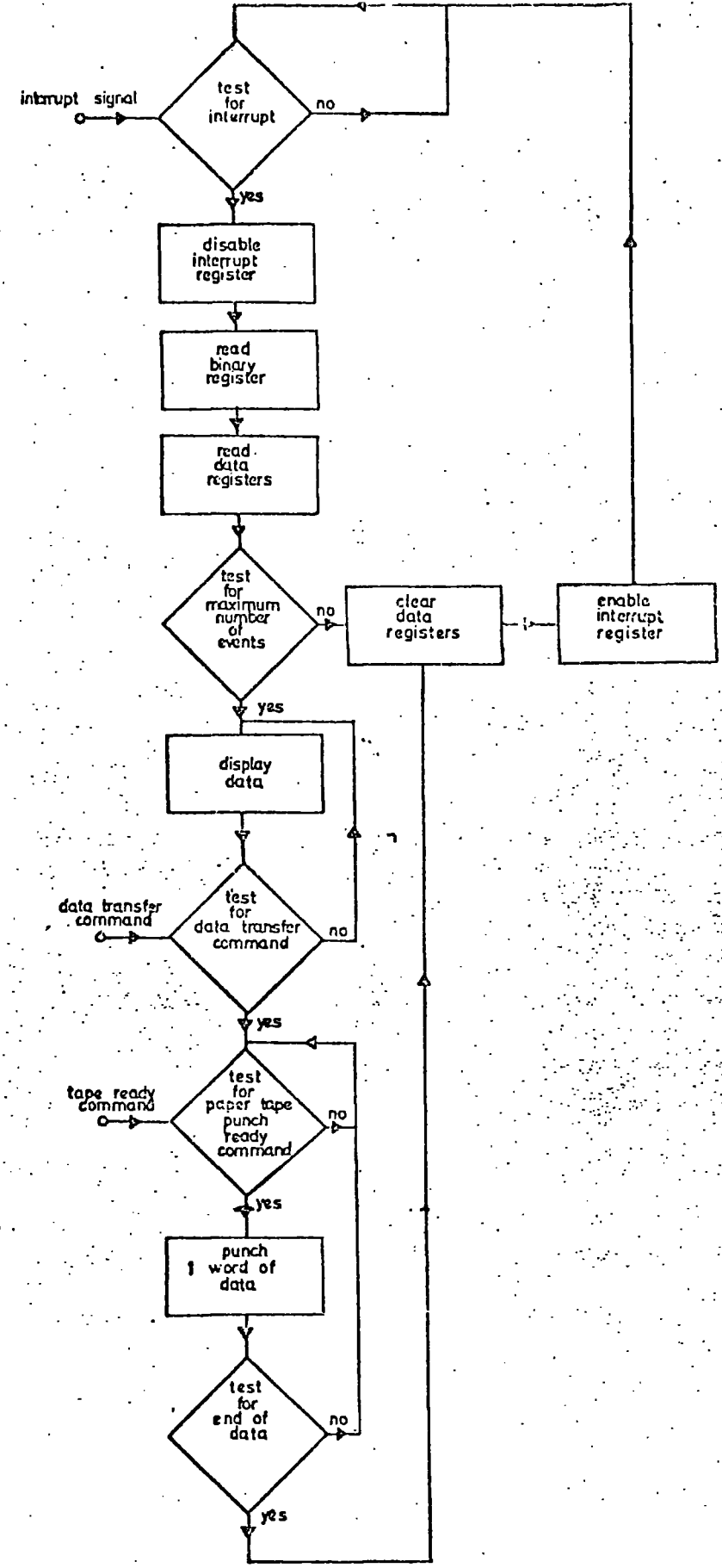

Fig. A6 the computer program flow diagram

ACKNOWLEDGEMENTS

The author would like to thank Professor G.D. Rochester FRS and Professor A.W. Wolfendale for their support of this work and use of the laboratory facilities.

He is indepted to his supervisor, Dr. J.M. Breare, for his continual guidance and assistance throughout the work, Mr. I.D. Tait for his help in analysing the data, Mr. W. el Disouki for his assistance with experimental work and Mr. J. Webster for building much of the experimental apparatus. The International Research and Development Company of Newcastle-upon-Tyne is acknowledged for manufacturing the flash tubes and the Daresbury Nuclear Physics Laboratory is thanked for providing experimental and computing facilities. In particular, Mr. M. Rousseau and Mr. A. Peatfield of the DNPL are thanked for their help and interest.

He would also like to thank Mr. R. Browell for his helpful criticisms of the script, Mrs. D.A. Anson for the typing and Mrs. A. Gregory for her help with the diagrams.

Finally, the Science Research Council is thanked for providing a Research Studentship.